Declassified in Part - Sanitized Copy Approved for Release @ 50-Yr 2014/03/07 : CIA-RDP81-01043R004200090004-8

STAT

TRANSLATION

GROWTH OF CRYSTALS
(Selected Articles)

By Various Authors

October 1959

282 Pages

STAT

PREPARED BY
LIAISON OFFICE
TECHNICAL INFORMATION CENTER
MCLTD
WRIGHT-PATTERSON AIR FORCE BASE, OHIO

STAT

Declassified in Part - Sanitized Copy Approved for Release @ 50-Yr 2014/03/07 : CIA-RDP81-01043R004200090004-8

Declassified in Part - Sanitized Copy Approved for Release @ 50-Yr 2014/03/07 : CIA-RDP81-01043R004200090004-8

STAT

Page Denied

Declassified in Part - Sanitized Copy Approved for Release @ 50-Yr 2014/03/07 : CIA-RDP81-01043R004200090004-8

Declassified in Part - Sanitized Copy Approved for Release @ 50-Yr 2014/03/07 : CIA-RDP81-01043R004200090004-8

Akademii Nauk SSSR
Institut Kristallograffii

Rost Kristallov

Doklady
Na Pervom Soveshchanii
Po Rostu Kristallov

(5-10 Marta 1956 G.)

Izdatel'stvo Akademii Nauk SSSR

Moskva - 1957

STAT

Declassified in Part - Sanitized Copy Approved for Release @ 50-Yr 2014/03/07 : CIA-RDP81-01043R004200090004-8

Declassified in Part - Sanitized Copy Approved for Release @ 50-Yr 2014/03/07 : CIA-RDP81-01043R004200090004-8

To the reader:

This translation is in two parts. Part I is a complete translation of twenty-one selected articles from the book. Part II is an abstract of six additional articles. A table of contents precede each part.

STAT

Declassified in Part - Sanitized Copy Approved for Release @ 50-Yr 2014/03/07 : CIA-RDP81-01043R004200090004-8

Declassified in Part - Sanitized Copy Approved for Release @ 50-Yr 2014/03/07 : CIA-RDP81-01043R004200090004-8

PART I

Complete Translation Of Foreign Pages

74-109

128-137

178-189

229-304

311-319

326-340

351-373

STAT

Declassified in Part - Sanitized Copy Approved for Release @ 50-Yr 2014/03/07 : CIA-RDP81-01043R004200090004-8

Declassified in Part - Sanitized Copy Approved for Release @ 50-Yr 2014/03/07 : CIA-RDP81-01043R004200090004-8

Table of Contents

	Page
Effect of Diffusion of Impurities in a Melt on their Distribution in the Crystal during Directed Crystallization, by A.I.Landau	1
On the Nucleation of Crystals in Binary Alloys, by Ya.V.Grechniy	13
A Contribution to the Question of the Formation and Growth of Negative Crystals (Pores) Arising from Supersaturated Solutions of Vacancies in the Crystal Lattice, by Ya.Ye.Geguzin	26
Thermal and Diffusional Processes during the Growth of Crystals, by G.P.Ivantsov	37
The Influence of Modifiers on the Process of Ingot Crystallization, by V.Ye.Neymark and A.I.Dukhin	55
Study of the Processes of Crystallization from a Melt, by I.N.Fridlyander	70
Artificial Fluorite, by I.V.Stepanov and P.P.Feofilov	88
The Growing of Single Crystals of Lithium Fluoride and Sodium Fluoride with a High Transparency in the Ultraviolet and Infrared Regions of the Spectrum, by M.A.Vasil'yeva	107
Methods of Growing Luminescent Crystals for Scintillation Counters, by L.M.Belyayev, B.V.Vitovskiy, and G.F.Dobrzhanskiy	118
Apparatus and Methods of Growing Single Crystals of Semiconductors, by D.A.Petrov and V.S.Zemskov	137
First Experiments in Growing Large Mica Crystals, by K.V.Kapralov, Yu.V.Koritskiy and N.N.Sheftal'	152
Synthetic Mica, its Properties and Application, by I.I.Yamzin and M.S.Leyzerzon	159
On the Growing of Single Crystals of Sorbitol Hexaacetate, by I.S.Rez and L.I.Tsinober	173
The Preparation, Dielectric and Optical Properties of Single Crystals of Solid Solutions (Ba - Sr)TiO_3, by A.L.Khodakov, M.L.Sholokhovich, Ye.G.Fesenko, and O.P.Kramarov	183

STAT

Declassified in Part - Sanitized Copy Approved for Release @ 50-Yr 2014/03/07 : CIA-RDP81-01043R004200090004-8

Declassified in Part - Sanitized Copy Approved for Release @ 50-Yr 2014/03/07 : CIA-RDP81-01043R004200090004-8

Page

A New Technique of Studying the Phase Transformations under High Pressures and Temperatures and its Application to the Study of the Polymorphism of Phosphorous, by V.P.Butuzov and S.S.Boksha 198

A New Type of Autoclave for Hydrothermal Synthesis, by V.P.Butuzov, G.P.Shakhovskoy and S.P.Smirnov 212

Technique of Synthesis of Refractory Crystals Insoluble in Water, by. I.N.Anikin 217

A Precision Method of Determining the Saturation Temperature of Transparent Solutions, by A.N.Kovalevskiy 228

Crystallization of Viruses, by V.L.Ryzhkov 234

Some Questions of the Kinetics of Crystal Growth, by V.A.Koptsik 247

Experience of the Work of the Student Practical Course in the Technology of Artificial Crystal Growing, by N.L.Pokrovskiy 258

STAT

Declassified in Part - Sanitized Copy Approved for Release @ 50-Yr 2014/03/07 : CIA-RDP81-01043R004200090004-8

Declassified in Part - Sanitized Copy Approved for Release @ 50-Yr 2014/03/07 : CIA-RDP81-01043R004200090004-8

EFFECT OF DIFFUSION OF IMPURITIES IN A MELT ON THEIR DISTRIBUTION IN THE CRYSTAL DURING DIRECTED CRYSTALLIZATION

by

A.I.Landau

Formulation of the Problem in Partial Derivatives, and Methods of Solution

The principle of directed crystallization from the melt is widely used today for artificially growing large single crystals, and also for the preparation of ultra-pure substances. There are a number of experimental methods based on this principle: those of Obreimov and Shubnikov, Bridgman, Kyropoulos, Stoeber, Stockbarger (Bibl.1, 2), the method of zone melting (Bibl.3), and others. Since, in the existing experimental methods of directed crystallization, the rate of advance of the interface between the liquid and solid phases is slight, the process of crystallization is quasi-stationary, and the liquid melt is always in equilibrium with the solid phase at their interface, i.e., at the front of crystallization. Here, as is well known, in accordance with the equilibrium diagram, the liquid melt will become enriched with the impurity, provided only that the solubility of that impurity in the solid phase is lower than in the melt (which is what is, for the most part, observed)*. The impurity driven into the melt will be distributed variously in it, depending on the rate of diffusion, on the convection currents, and on other factors. In many cases the natural convection in the liquid phase may be neglected. Thus, for example, in the Stockbarger method, the crystal grows in the vertical direction when there is a higher temperature toward the top and the lower temperature toward the bottom, the melt, enriched with the impurity, has a higher specific gravity than

*In the present work we are considering this case, but all the results obtained by us may be easily extended to the case where the solubility of the impurity in the solid phase is higher than in the melt.

STAT

Declassified in Part - Sanitized Copy Approved for Release @ 50-Yr 2014/03/07 : CIA-RDP81-01043R004200090004-8

Declassified in Part - Sanitized Copy Approved for Release @ 50-Yr 2014/03/07 : CIA-RDP81-01043R004200090004-8

the melt with the lower content of impurity, the interface between the phases is close to horizontal, the rate of crystal is low, etc. All these factors hinder natural convection. In this case, the distribution of the impurity in the melt, and consequently, in the single crystals as well, will depend primarily on its rate of diffusion in the liquid phase.

In connection with the fact that the diffusion coefficient D of impurities in liquid melts of salt or metals at temperatures close to the melting point is very low ($D \approx 10^{-4} - 10^{-5}$ cm^2/sec), the impurity driven into the liquid melt is irregularly distributed in it, accumulating at the boundary of crystallization. To find the distribution of the impurity along the length of the single crystal it is necessary, in this case, first to find the distribution of the impurity in the liquid phase at each given instant of time, i.e., to find the function $c_{liq} = c_{liq}(x, t)$, where c_{liq} is the concentration of the impurity in the melt*. Then the value of $c_{liq}(x, t_1)$, taken at time $t_1 = \frac{x}{v}$, will give us the relation $c_\alpha = c_\alpha(x) = \frac{c_{liq}(x, t_1)}{g}$. Here c_α is the concentration of the impurity of the solid phase, v the rate of growth of the crystal, and g is the purification factor, equal to the equilibrium ration c_α/c_{liq} on the boundary of crystallization. The calculation of the function $c_{liq} = c_{liq}(x, t)$ must be carried out by the aid of the diffusion equations

$$\frac{\partial c_{liq}}{\partial t} = D \frac{\partial^2 c_{liq}}{\partial x^2} \tag{1}$$

with a boundary condition on the boundary of crystallization of the following form (Bibl.4, 5):

$$(1-g)\, v c_{liq} + D \frac{\partial c_{liq}}{\partial x} = 0 \Big|_{x=vt}. \tag{2}$$

*Here x is the length of the single crystal in a fixed system of coordinates, rigidly bound to the container (the origin of coordinates being selected on the front wall of the container, at the initial point of crystallization). Hereafter we shall also use a moving system of coordinates Y, where the origin of coordinate will be selected on the moving boundary of crystallization. In both cases the coordinates will be measured in the direction toward the liquid phase. The statements here made about the moving and fixed coordinate systems relate to the figures in this paper.

STAT

Declassified in Part - Sanitized Copy Approved for Release @ 50-Yr 2014/03/07 : CIA-RDP81-01043R004200090004-8

Declassified in Part - Sanitized Copy Approved for Release @ 50-Yr 2014/03/07 : CIA-RDP81-01043R004200090004-8

The second boundary condition, on the opposite side of the column of the melt, and the initial condition, have the following forms:

$$\frac{\partial c_{liq}}{\partial x} = 0 \Big|_{x=L} \tag{3}$$

and

$$c_{liq}(x, 0) = c^{0}_{liq} \tag{4}$$

where L is the length of the container (i.e., the original length of the column of melt). Thus, in this case, one of the boundary conditions is assigned on the non-stationary (moving) boundary. This kind of problems, if they are solved in the general form, are among the most difficult in mathematical physics. It is most convenient of all to perform the numerical solution of the system (1) - (4) by the aid of the method of finite differences. Let us pass to the moving coordinates Y, the origin of which has been chosen on the boundary of crystallization. In this system of coordinates, eq.(1) will have the following form:

$$\frac{\partial c_{liq}}{\partial t} = D \frac{\partial^2 c_{liq}}{\partial y^2} + v \frac{\partial c_{liq}}{\partial y}. \tag{5}$$

The derivatives $\partial c_{liq}/\partial t$, $\partial c_{liq}/\partial y$ and $\partial^2 c_{liq}/\partial y^2$, written in finite differences, will be, respectively, of the following form:

$$\frac{\left(c^{i,\,k+1}_{liq} - c^{i,\,k}_{liq}\right)}{l}; \quad \frac{\left(c^{i+1,\,k}_{liq} - c^{i-1,\,k}_{liq}\right)}{2h}$$

and

$$\frac{c^{i+1,\,k}_{liq} - 2c^{i,\,k}_{liq} + c^{i-1,\,k}_{liq}}{h^2}.$$

Here l is the interval in time; h is the interval in length; k is the number of the cell along the t axis; i is the number of the cell along the y axis. Let us choose the following relation between the time and space interval:

$$l = \frac{h^2}{2D}. \tag{6}$$

With such a choice of the dependence between l and h, the error of the calculation is of the same order of magnitude as h^4 (Bibl.6, 7), while eq.(5), written in finite

STAT

Declassified in Part - Sanitized Copy Approved for Release @ 50-Yr 2014/03/07 : CIA-RDP81-01043R004200090004-8

Declassified in Part - Sanitized Copy Approved for Release @ 50-Yr 2014/03/07 : CIA-RDP81-01043R004200090004-8

differences, takes the following form:

$$c_{liq}^{i,k+1} = \left(\frac{1}{2} - \frac{hv}{4D}\right) c_{liq}^{i-1,k} + \left(\frac{1}{2} + \frac{hv}{4D}\right) c_{liq}^{i+1,k}. \quad (7)$$

The boundary conditions (2) and (3) and the initial condition (4) will then read respectively as follows:

$$c_{liq}^{0,k} = \frac{2h(1-g)v}{D} c_{liq}^{1,k} + c_{liq}^{2,k}, \quad (8)$$

$$c_{liq}^{(L-vlk-h)/h,k} = c_{liq}^{(L-vlk)/h,k} \quad (9)$$

$$c_{liq}^{i,0} = c_{liq}^{0} \quad \text{for all values of } i \quad (10)$$

Results of Solution and Fundamental Equations

Calculations performed by the method of finite differences by the aid of eqs.(7) - (10) yield the distribution of the impurity in the liquid phase which is shown by us in Fig.1.

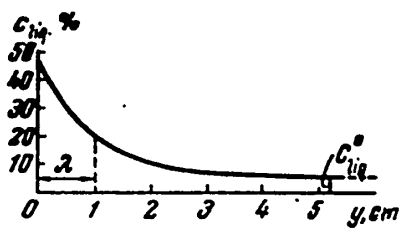

Fig.1 - Distribution of Impurity in a Melt Close to the Boundary of Crystallization, Calculated for $D = 10^{-4}$ cm^2/sec, $v = 3.6$ mm/hr, $c_{liq}^{0} = 5\%$ and $g = 0.1$ at time $t = 53$ hr after Beginning of the Growth of the Crystal; the Origin of Coordinates is Taken on the Boundary of Crystallization; λ is the Characteristic Thickness of the Concentration Barrier

These calculations also show that in the initial period of time the concentration barrier of the impurity in the melt rapidly increases. Then follows its gradual stabilization, and the distribution of the impurity in the liquid phase approaches a certain asymptotic curve resembling that shown in Fig.1. The equation describing this curve is easily found from the following considerations. First of all let us assume that the concentration barrier has already become completely stabilized and that the distribution of the impurity in the melt is described by eq.(5) at $\partial c_{liq}/\partial t = 0$, i.e., by the equation

$$D \frac{\partial^2 c_{liq}}{\partial y^2} + v \frac{\partial c_{liq}}{\partial y} = 0. \quad (11)$$

STAT

Declassified in Part - Sanitized Copy Approved for Release @ 50-Yr 2014/03/07 : CIA-RDP81-01043R004200090004-8

Declassified in Part - Sanitized Copy Approved for Release @ 50-Yr 2014/03/07 : CIA-RDP81-01043R004200090004-8

We note further that, as will be seen from Fig.1, the characteristic thickness λ of the concentration barrier of the mixture close to the boundary of crystallization is not great and is smaller by one order than the dimensions of the container (L ~ 10 – – 20 cm or more). For this reason we may consider the front of crystallization on the opposite side of the container as being at infinity. The boundary conditions in this case takes the following form (the origin of coordinates being chosen at the boundary of crystallization):

$$(1-g)vc_{liq} + D\frac{\partial c_{liq}}{\partial y} = 0\Big|_{y=0} \tag{12}$$

and

$$c_{liq}(y) \to c^{o}_{liq} \quad \text{at} \quad y \to \infty. \tag{13}$$

Solving the system (11) – (13) by the usual methods, we get:

$$c_{liq}(y) = c^{o}_{liq}\left[\frac{(1-g)}{g}\, e^{-\frac{v}{D}y} + 1\right]. \tag{14}$$

It follows from the asymptotic formula (14) that, in the stabilized concentration barrier, the concentration, c^{bo}_{liq}, of the impurity at the boundary of crystallization, is connected with the quantity c^{o}_{liq} by the following relation: $c^{bo}_{liq} = c^{o}_{liq}/g$*. In this case, the impurity will enter the crystal in the concentration $c_\alpha = gc^{bo}_{liq} = c^{o}_{liq}$, i.e., in a concentration equal to the initial concentration of the impurity in the melt (cf.Bibl.5). The characteristic thickness λ of the concentration barrier may also be evaluated from eq.(14):

$$\lambda = \frac{D}{v}. \tag{15}$$

At $D = 10^{-4}$ cm^2/sec and $v = 3.6$ mm/hr, we shall have $\lambda = 1$ cm (cf.Fig.1); at the

*Obviously, however $c^{o}_{liq} \leq gc^{S}_{liq} < g$ must obtain (or, expressed as a percentage $< g \cdot 100\%$), where c^{S}_{liq} is the eutectic or peritectic concentration. Otherwise, before the stabilization of the concentration barrier sets in, the eutectic will be thrown down or other processes substantially changing the physical picture under consideration will begin.

STAT

Declassified in Part - Sanitized Copy Approved for Release @ 50-Yr 2014/03/07 : CIA-RDP81-01043R004200090004-8

Declassified in Part - Sanitized Copy Approved for Release @ 50-Yr 2014/03/07 : CIA-RDP81-01043R004200090004-8

same rate of growth and $D = 10^{-5}$ cm^2/sec, we get $\lambda = 1$ mm. We note that eq.(15), expressing the evaluation of the characteristic thickness of the concentration barrier, found by us from eq.(14), agrees with the analogous formula found by different methods by other authors.

After finding the distribution of the impurity in the melt at each instant of time by the method of finite differences, we can construct a graph of the distribution of the impurity along the length of the single crystal, which is shown schematically in Fig.2.

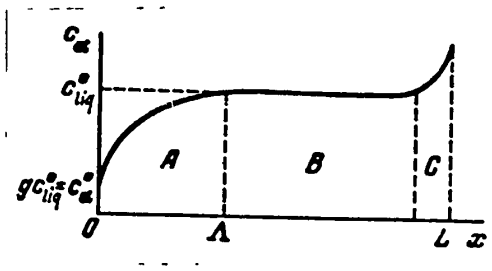

Fig.2 - Distribution of Impurity along Length of Single Crystal Grown by the Method of Directed Crystallization, Found Taking Account of the Finite Rate of Diffusion of the Impurity in the Liquid Phase; the Origin of Coordinates is Taken on the Front Wall of the Container

It will be easily seen that this distribution is substantially different from that obtained under the assumption of an infinite rate of diffusion of the impurity in the melt (cf.Bibl.3). The region A on Fig.2 corresponds to the appearance and stabilization of the concentration barrier. Region B corresponds to the position where the concentration barrier has already been stabilized, and is described by the asymptotic formula (14). In this case the impurity enters the crystal uniformly along its length. Finally, region C corresponds to the period when the concentration barrier moves up to the rear wall of the container, and the stability of the process is disturbed. Obviously region C has dimensions of the order of the characteristic thickness λ of the concentration barrier.

The evaluation of the linear dimensions of the region A is of the greatest interest. Figure 3 shows the curve of distribution of the impurity in the single crystal in the region of stabilization of the concentration barrier A, obtained by

STAT

Declassified in Part - Sanitized Copy Approved for Release @ 50-Yr 2014/03/07 : CIA-RDP81-01043R004200090004-8

Declassified in Part - Sanitized Copy Approved for Release @ 50-Yr 2014/03/07 : CIA-RDP81-01043R004200090004-8

the aid of calculations by the method of finite differences for $D = 10^{-4}$ cm^2/sec, $v = 3.6$ mm/hr, $g = 0.1$, and $c^o_{liq} = 5\%$.

It will be seen from Fig.3 that the characteristic length Λ of region A with the given choice of the parameters D, v, and g ≈ 20 cm. Let us find how Λ depends on the quantity D, v, and g (it is easy to convince oneself that Λ does not depend on c^o_{liq}).

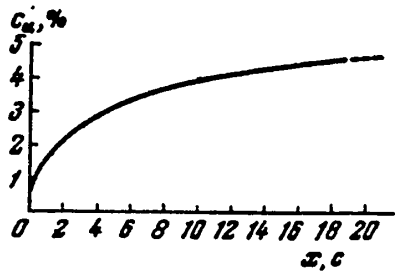

Fig.3 - Distribution of the Impurity along the Length of a Single Crystal in the Region A of Appearance and Stabilization of the Concentration Barrier Obtained by the Aid of Calculation by the Method of Finite Differences at $D = 10^{-4}$ cm^2/sec, $v = 3.6$ mm/hr, $c^o_{liq} = 5\%$ and $g = 0.1$; the Origin of Coordinates is Chosen on the Front Wall of the Container

Consider the case when the coefficient of diffusion D of the impurity in the melt has changed by a certain factor (for instance by a factor of a) with unchanged v and g, i.e., the new diffusion coefficient D' is connected with the previous relation: $D' = aD$. If in this case we select the new space interval $h' = ah$, then, as will be easily seen, the difference equations will undergo no change whatever and the numerical values of the computation net will remain the same as before. It follows from this that if in the previous calculation the stabilization of the concentration barrier took place in the computation net at intervals of a definite number of lines along the time axis, then in the calculation with the changed values of the quantities D and h, the stabilization will also take place after the same number of lines. But one of the same number of lines of the computation net along the time axis now corresponds to a different time interval, since the spacing of the net has changed in accordance with eq.(6). The new spacing

STAT

Declassified in Part - Sanitized Copy Approved for Release @ 50-Yr 2014/03/07 : CIA-RDP81-01043R004200090004-8

Declassified in Part - Sanitized Copy Approved for Release @ 50-Yr 2014/03/07 : CIA-RDP81-01043R004200090004-8

$$l' = \frac{h'^2}{2D'} = \frac{a^2h^2}{2aD} = \frac{ah^2}{2D} = al,$$

where l is the previous space interval. Consequently, the stabilization of the concentration barrier with time will now occur 1/a times more rapidly (more slowly). Since the rate of growth of the crystal v remains unchanged, the rate of stabilization of the concentration barrier with time is directly related to the rate of its stabilization along the length of the single crystal. Thus we reach the result:

$$\tau = f(g, v) \cdot D \text{ and } \Lambda = F(g, v) \cdot D,$$

where τ is the characteristic time of stabilization of the concentration barrier, and f(g, v) and F(g, v) are certain functions of g and v. We may consider by analogy the dependence of the quantities τ and Λ on the rate of growth v. Let the rate of growth vary by a factor of a: $v' = av$, with the quantities D and g remaining unchanged. If in this case we choose a new space interval: $h' = h/a$, then, as in the preceding case, the difference equations undergo no change whatever. The new time interval will be:

$$l' = \frac{h'^2}{2D} = \frac{h^2}{2a^2D} = l\frac{1}{a^2},$$

where l is the previous space interval. Hence, by analogy to the foregoing, we convince ourselves that the stabilization of the concentration barrier with time will now take place more rapidly by a factor of a^2 (more slowly), i.e., the relation $\tau = \varphi(g, D) \frac{1}{v^2}$ will hold. However, since the relation $\Lambda = v\tau$ holds, the characteristic length Λ of stabilization of the concentration barrier along the axis of the single crystal will be related to the velocity v, not by a quadratic dependence, but by the linear dependence:

$$\Lambda = \Phi(g, D) \frac{1}{v},$$

where the $\Phi(g, D)$, just like the $\varphi(g, D)$, represent certain functions of the quantities g and D. Combining the relations so obtained, we arrive at the following fundamental equations:

STAT

Declassified in Part - Sanitized Copy Approved for Release @ 50-Yr 2014/03/07 : CIA-RDP81-01043R004200090004-8

Declassified in Part - Sanitized Copy Approved for Release @ 50-Yr 2014/03/07 : CIA-RDP81-01043R004200090004-8

$$\Lambda = R(g)\frac{D}{v} = R(g)\lambda, \tag{16}$$

$$\tau = R(g)\frac{D}{v^2} = R(g)\frac{\lambda}{v}, \tag{17}$$

where R(g) is a certain dimensionless coefficient depending on g. By passing, at the limit, from eqs.(7) - (10) to eqs.(1) - (4), we may easily convince ourselves that the relations (16) and (17) obtain not only for the difference equations, but also for the exact equations (1) - (4).

The dependence of the coefficient R(g) on g may be determined with a sufficient degree of accuracy by the aid of the asymptotic formula (14). By its aid we may find the excess quantity of the impurity M which will be consumed in forming the stable concentration barrier:

$$M = \rho\int_0^\infty \left[c_{liq}(y) - c_{liq}^0\right] dy =$$

$$= \rho\int_0^\infty \frac{c_{liq}^0(1-g)}{g} e^{-\frac{v}{D}y} dy = \frac{\rho c_{liq}^0(1-g)}{g}\frac{D}{v}, \tag{18}$$

where ρ is the specific mass per percent of impurity.

We note for future use that the distribution of the impurity along the length of the single crystal (Fig.3) very exactly obeys the law $\beta(1 - e^{-\gamma x})$ where β and γ are certain constants. To verify this proposition, we calculated the function

$$W = \lg\frac{1}{g}\left[c_{liq}^0 - c_\alpha(x)\right],$$

whose graph (Fig.4) is almost a straight line, except for small values of x, where the difference equations permit of considerable errors.

Thus, for the region A (Fig.2) we shall have:

$$c_\alpha(x) \approx g c_{liq}^0 + c_{liq}^0(1-g)(1-e^{-\gamma x}). \tag{19}$$

Let us assume arbitrarily that the stabilization of the barrier takes place when the quantity $1 - e^{-\gamma x}$ reaches the value 0.9 at a certain $x = \Lambda$

$$1 - e^{-\gamma\Lambda} = 0{,}9, \tag{20}$$

STAT

Declassified in Part - Sanitized Copy Approved for Release @ 50-Yr 2014/03/07 : CIA-RDP81-01043R004200090004-8

Declassified in Part - Sanitized Copy Approved for Release @ 50-Yr 2014/03/07 : CIA-RDP81-01043R004200090004-8

$$\gamma\Lambda = \frac{1}{\lg e}. \tag{21}$$

During the period of growth and stabilization of the concentration barrier, the flow of impurity entering the boundary layer of the melt at each given instant of time t is of intensity equal to $\rho v[c^0_{liq} - c_\alpha(vt)]$. After the time τ, in which the crystallization boundary advances a distance equal to Λ in the fixed coordinates, the following quantity of impurity will be transported by this flow into the boundary layer of the melt:

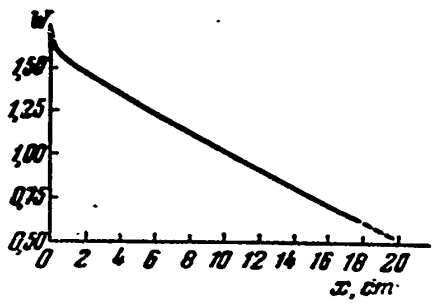

Fig.4 - Graph of Function $W = \log \frac{1}{g}[c^0_{liq} = c_\alpha(x)]$, where c (x) is the Distribution of the Impurity along the Length of the Single Crystal Calculated for $D = 10^{-4}$ cm^2/sec, v = 3.6 mm/hr, c^0_{liq} = 5% and g = 0.1 [Fig.3 gives a graph of the function $c_\alpha(x)$]

$$\int_0^{\tau=\Lambda/v} \rho v[c^0_{liq} - c_\alpha(vt)]\,dt = \int_0^{\tau=\Lambda/v} \rho v c^0_{liq}(1-g)e^{-\gamma vt}\,dt = \frac{\rho c^0_{liq}(1-g)}{\gamma}(1-e^{-\gamma\Lambda}) = 0{,}9\lg e\cdot\Lambda\rho c^0_{liq}(1-g). \tag{22}$$

On the other hand, up to the instant when the coefficient $1 - e^{-\gamma x}$ reaches the value 0.9 (at $x = \Lambda$), the concentration barrier reaches about 0.9 of its stable value. Thus:

$$0{,}9\lg e\cdot\Lambda\rho c^0_{liq}(1-g) \approx 0{,}9M = 0{,}9\frac{\rho c^0_{liq}(1-g)}{g}\frac{D}{v}. \tag{23}$$

Hence:

$$\Lambda \approx \frac{1}{g\cdot\lg e}\frac{D}{v}. \tag{24}$$

Equation (24) is true for all values of g except g = 1, since in the latter case the cancellation of the factor 1 - g from the right and left sides of eq.(23) is impossible. Obviously, at g = 1, Λ = 0. If we neglected the quantity $\rho v c_\alpha(vt)$ on integration of eq.(22), then after the necessary transformations we would obtain the

STAT

Declassified in Part - Sanitized Copy Approved for Release @ 50-Yr 2014/03/07 : CIA-RDP81-01043R004200090004-8

Declassified in Part - Sanitized Copy Approved for Release @ 50-Yr 2014/03/07 : CIA-RDP81-01043R004200090004-8

following evaluation of the minimum value of Λ:

$$\Lambda > \frac{1-g}{g}\frac{D}{v}. \tag{25}$$

From eqs.(24) and (25) and eq.(16), the following evaluation of the function $R = R(g)$ results:

$$\frac{1-g}{g} < R(g) \approx \frac{1}{g \cdot g^{\varepsilon}}. \tag{26}$$

By the aid of eqs.(21) and (24), we are also able to find the value of the constant γ, which has the dimension of cm^{-1}:

$$\gamma = g\frac{v}{D}. \tag{27}$$

Thus for the regions A and B of increase and stabilization of the concentration barrier (cf.Fig.2) we are finally able to write:

$$c_{\alpha}(x) \approx g c^{0}_{liq} + c^{0}_{liq}(1-g)(1-e^{-g\frac{v}{D}x}). \tag{28}$$

In conclusion, I avail myself of this opportunity of expressing my profound gratitude to Professor L.S.Palatkin, Instructor V.I.Startsev and Senior Scientist B.S.Aleksandrov for their joint discussion of the questions touched in the present paper.

Conclusions

1. The distribution of various small admixtures of impurities along the length of single crystals grown from the melt by the method of directed crystallization has been investigated as a function of their initial concentration, the value of the diffusion coefficient of these impurities in the melt, the rate of growth of the crystal and the value of the equilibrium purification factor has been investigated. We have written the partial differential equations (1) - (4), giving the distribution of the impurity in the melt at each given instant of time, and we have indicated a method of solving them.

2. The asymptotic formula (14) has been obtained, describing the stabilized

STAT

Declassified in Part - Sanitized Copy Approved for Release @ 50-Yr 2014/03/07 : CIA-RDP81-01043R004200090004-8

Declassified in Part - Sanitized Copy Approved for Release @ 50-Yr 2014/03/07 : CIA-RDP81-01043R004200090004-8

concentration barrier of impurity in the melt near the boundary of crystallization. By the aid of eq.(14) we have evaluated the characteristic thickness of the concentration barrier, and have found that in the case of formation of a stable concentration barrier, the impurity enters uniformly into the crystal in a concentration equal to the initial concentration of the impurity in the melt.

3. We have shown that the formation and stabilization of the concentration barrier does not take place at one time, but during a certain characteristic time, and that during this time the crystal is able to grow by the definite length Λ. When the crystal attains length Λ, the impurity enters uniformly into the crystal.

4. Equation (16) has been obtained, expressing the dependence of the value of Λ on the diffusion coefficient of the impurity in the melt, and on the rate of growth of the crystal. In addition, we have approximately evaluated the dependence of the length Λ on the equilibrium purification factor eqs.(24) and (25).

5. We have shown that the distribution of the impurity along the length of the single crystal very exactly obeys the law $\beta(1 - e^{-\gamma x})$, where β and γ are certain constants. As a result, eq.(28) has been obtained, which describes with a considerable degree of accuracy the required distribution of impurity in the region of growth and stabilization of the concentration barrier.

BIBLIOGRAPHY

1. Kuznetsov,V.D. - Crystals and Crystallization. Gostekhizdat (1954), pp.338 - 346
2. Bakli,G. (H.Buckley) - The Growth of Crystals. State Publishing House for Foreign Literature (1954), pp.62 - 78
3. Pfann,W.G. - Trans. AIMME, Vol.194 (1952), pp.747 - 753
4. Burton,J.A., Prim,R.G., and Slichter,W.P. - Journ.Chem.Phys., Vol.21, No.11 (1953), pp.1987 - 1991
5. Wagner,C. - Journ. of Metals, Vol.6, Sec.I, No.2 (1954), p.154
6. Mikeladze,Sh.Ye. - Numerical Methods of Integrating Partial Differential Equations. Publishing House, Academy of Sciences USSR, 1936
7. Panov,D.Yu. - Manual on Numerical Solution of Partial Differential Equations. Gostekhizdat,(1949)

STAT

Declassified in Part - Sanitized Copy Approved for Release @ 50-Yr 2014/03/07 : CIA-RDP81-01043R004200090004-8

Declassified in Part - Sanitized Copy Approved for Release @ 50-Yr 2014/03/07 : CIA-RDP81-01043R004200090004-8

ON THE NUCLEATION OF CRYSTALS IN BINARY ALLOYS

by

Ya.V.Grechniy

In this paper the results of a study of the formation of crystal nuclei in binary alloys of a number of transparent substances will be reported. All the starting substances are metalloid with respect to supercooling, i.e., at any attainable rates of cooling they crystallize, and cannot be converted into a glass. This is the consequence of the continuous increase in the rate of nucleation with increasing supercooling, and also of the higher velocity of growth of the crystals.

I have investigated the kinetics of formation of crystal nuclei in alloys forming either a continuous or a limited series of solid solutions, and likewise in alloys of the eutectic type with absence of mutual solubility of the original substances in the solid state. The original substances were purified from impurities by repeated recrystallization and distillation.

To find the rate of nucleation, we experimentally determined the "waiting time" to the appearance of the first nucleus at a given degree of supercooling. The technique developed by V.I.Danilov for pure substances (Bibl.1) was applied to this work. The melt investigated was placed in thin-walled glass capillaries sealed at both ends. The specimen was rapidly transferred from the thermostat to a temperature above the liquidus curve to another liquid thermostat, where a temperature below the liquidus curve had been established, and observations on the crystallization were made through a 12 × power lens. The appearance of the first crystal was also observed by the aid of a microscope provided with a heating or cooling stage and an attachment for measuring temperatures.

In this case the alloy under study was placed between glass plates (cover glasses). In determining the incubation period δ of crystallization from the "waiting time" τ, the thermal inertia t of the specimen and the time required for the

STAT

Declassified in Part - Sanitized Copy Approved for Release @ 50-Yr 2014/03/07 : CIA-RDP81-01043R004200090004-8

Declassified in Part - Sanitized Copy Approved for Release @ 50-Yr 2014/03/07 : CIA-RDP81-01043R004200090004-8

nucleus to grow to visible size was taken into account. That is:

$$\delta = \tau - \left(t - \frac{R}{v}\right),$$

where v is the velocity of growth of the crystals, and R the minimum size of a crystallite distinctly distinguishable under a lens or microscope. To determine the mean value of δ, a frequency curve of the values at a given isothermal holding time was constructed.

The rate of nucleation I was determined from the relation

$$I = \frac{1}{\delta W} cm^{-3} \, sec^{-1},$$

where W is the volume of the melt in the specimen.

Formation of Crystal Germs in Melts Forming a Continuous and Limited Series of Solid Solutions

a. Melts of camphor with borneol. The relation between the incubation period δ of crystallization for a series of melts of camphor with borneol and the supercooling ΔT is given in Fig.1. It follows from an analysis of the curves given in Fig.1 that the minimum tendency to supercooling is exhibited by pure camphor and the maximum tendency by borneol. The solid solutions possess an intermediate capacity for supercooling, which increases with the content of borneol in the melt. The tendency of the melts to supercooling largely depends on the content of borneol in melts with borneol content up to 20%. When the borneol content increases beyond 20%, the supercooling tendency increases slowly, but in melts containing 50 to 100% of borneol, the tendency to supercooling is no longer, in practice, dependent on the composition of the melt. Common to all the melts is the presence of a relatively narrow interval of temperatures (supercooling), within which the length of the incubation period rapidly decreases to zero.

The boundaries of this interval of supercooling are the upper (UBM) and lower (LBM) boundaries of metastability of the liquid.

The minimum degree of supercooling at which crystallization takes place without

STAT

Declassified in Part - Sanitized Copy Approved for Release @ 50-Yr 2014/03/07 : CIA-RDP81-01043R004200090004-8

Declassified in Part - Sanitized Copy Approved for Release @ 50-Yr 2014/03/07 : CIA-RDP81-01043R004200090004-8

incubation was taken as the LBM. The degree of supercooling at which the length of the incubation period of crystallization is great (the rate of nucleation being correspondingly low) was taken as the UBM. Thus, for instance, the supercooling at which nucleation begins in 30 min was taken arbitrarily as the UBM. It follows from what has been said above that melts of camphor with borneol are characterized by a narrow interval between the UBM and the LBM of the liquid; the width of this interval varies slightly with variation of the melt composition for melts containing less than 20% of borneol; at a higher borneol content, this width is already practically independent of the melt composition.

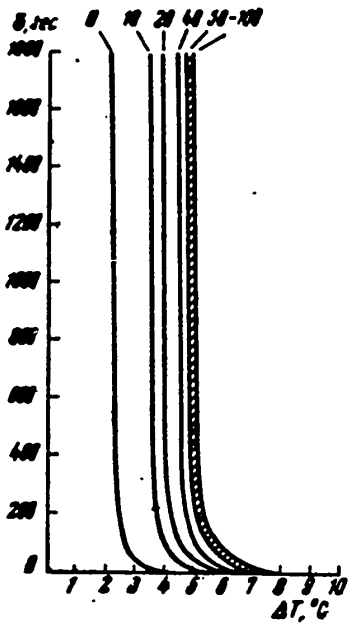

Fig.1 - Curves of Relation between Incubation Period and Supercooling for Melts of Camphor with Borneol (the Figures over the Curves Indicate the Content of Borneol in the Melt in %)

b. Melts of camphor and hydroquinone, and of parachloronitrobenzene with parabromonitrobenzene. In the former case I studied melts with a hydroquinone content up to 62.5%, in the latter case melts with up to 60% parabromonitrobenzene, i.e., melts within the limits of the region of formation of solid solutions. Figures 2 and 3 give the relation of the incubation period of crystallization and the supercooling for these melts.

The following results from an analysis of these curves (Fig.2): 1) the supercooling tendency of melts of camphor with hydroquinone, i.e., the interval between the temperatures corresponding to the liquidus and to the UBM increases with increasing camphor content (and the interval between the UBM and the LBM also increases in this case); 2) the supercooling tendency of melts of parachloronitrobenzene with parabromonitro-

STAT

Declassified in Part - Sanitized Copy Approved for Release @ 50-Yr 2014/03/07 : CIA-RDP81-01043R004200090004-8

Declassified in Part - Sanitized Copy Approved for Release @ 50-Yr 2014/03/07 : CIA-RDP81-01043R004200090004-8

benzene (Fig.3) increases with increasing content of parabromonitrobenzene in the melt, while the interval between the UBM and the LBM of the liquid in this case decreases; specific for the melts of this system is the change in the character of the

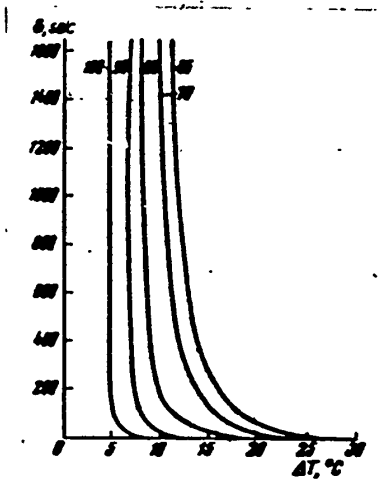

Fig.2 - Curves of the Relation between the Incubation Period and the Degree of Supercooling for Melts of Camphor and Hydroquinone (the Figures on the Curves Indicate the Hydroquinone Content of the Melt in %)

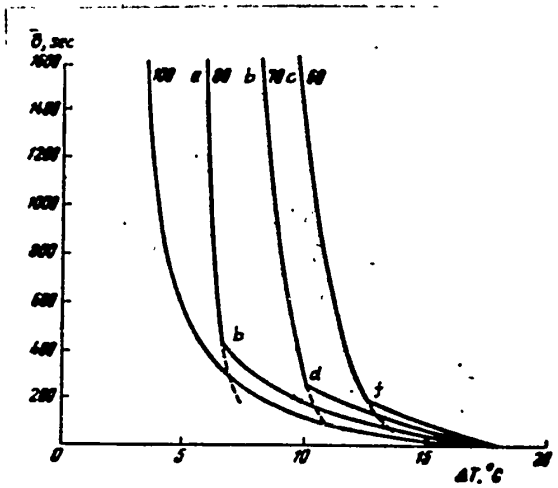

Fig.3 - Curves of the Dependence of the Incubation Period on the Supercooling for Melts of Parachloronitrobenzene and Parabromonitrobenzene (the Figures above the Curves Indicate the Content of Parabromonitrobenzene in the Melt, in %)

relation between δ and the supercooling ΔT in the range of temperatures between the UBM and the LBM.

Beginning with the UBM (with increasing supercooling), the duration of the incubation period falls rapidly until a certain value of the supercooling has been reached. This value is greater, the higher the parabromonitrobenzene content of the melt (the regions ab, cd, ef on the curves of Fig.3). With further increase of supercooling, the incubation period decreases at a lower rate than on the first regions.

STAT

Declassified in Part - Sanitized Copy Approved for Release @ 50-Yr 2014/03/07 : CIA-RDP81-01043R004200090004-8

Declassified in Part - Sanitized Copy Approved for Release @ 50-Yr 2014/03/07 : CIA-RDP81-01043R004200090004-8

These peculiarities in the character of the relation between the duration of the incubation period of crystallization and the degree of supercooling for each system may be explained if we use the diagrams of phase equilibrium and take account of the general propositions of the fluctuation theory of phase transformations.

Figures. 4 - 6 are diagrams of phase equilibrium for the systems under study, on

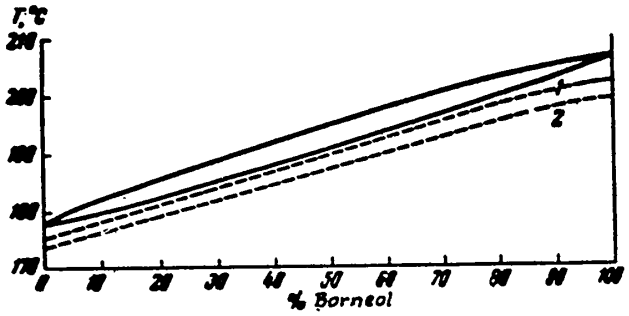

Fig.4 - Crystallization Diagram for Melts of Camphor with Borneol; Curve I - UBM of Liquid; 2 - Curve of LBM of Liquid

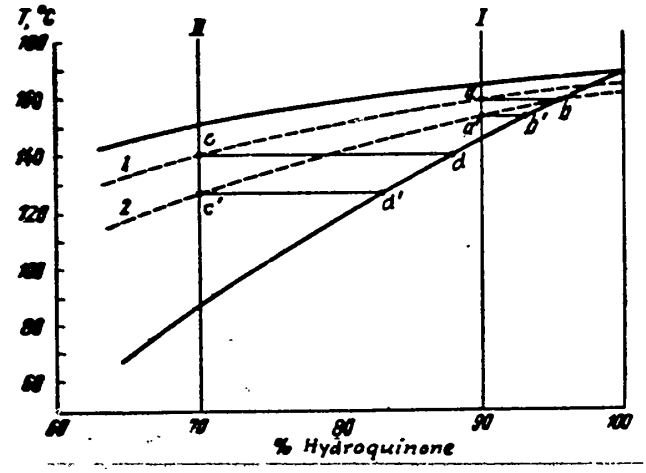

Fig.5 - Crystallization Diagram for Melts of Camphor with Hydroquinone; Curve - UBM of Liquid; 2 - LBM of Liquid

which the UBM and the LBM of the liquid have been plotted. As will be seen from Fig.4, the UBM and LBM of the liquid in the melts of camphor with borneol are located below the solidus. Naturally the formation of crystal nuclei in these melts

STAT

Declassified in Part - Sanitized Copy Approved for Release @ 50-Yr 2014/03/07 : CIA-RDP81-01043R004200090004-8

Declassified in Part - Sanitized Copy Approved for Release @ 50-Yr 2014/03/07 : CIA-RDP81-01043R004200090004-8

is possible on the basis of phase fluctuations, but the presence of concentration fluctuations is not necessary for the formation of crystal nuclei, since the composition of the nucleus may be the same as the composition of the original liquid.

The conditions of nucleation in the other two systems are different. In the melts of camphor with hydroquinone, beginning with the melt containing about 4% of camphor, the UBM and the LBM of the liquid on the diagram are located above the solidus (Fig.5). For this reason the formation of a crystal nucleus in these melts involves the formation of concentration and phase fluctuation, since the composition of the germ must differ from that of the liquid. It is obvious that the minimum quantity of hydroquinone in the composition of the germ is described by the points of the solidus. The degree of concentration fluctuation necessary for nucleation at the temperatures corresponding to the UBM and LBM of the liquid for melt I (Fig.5) are described respectively by the segments ab and a'b', and for melt II, containing more camphor than melt I, by the segments cd and c'd', i.e., the degree of concentration fluctuation necessary for the formation of a nucleus increases with increasing camphor content of the melt. It results from this that with increasing content of camphor in the melt, other conditions being equal, the probability of nucleation decreases. It is therefore clear that the supercooling tendencies of melts of camphor with hydroquinone, i.e., the distance of the UBM and LBM of the liquid from the temperature of the corresponding liquidus must increase with increasing camphor content, and this is in fact observed.

In melts of parachloronitrobenzene and parabromonitrobenzene containing over 90% of parabromonitrobenzene, the UBM is higher than the solidus on the diagram, while the LBM is lower than the solidus (Fig.6). With such a mutual position of the solidus line, the UBM and the LBM of the liquid, the rate of decrease of the incubation period with increasing degree of supercooling in the limits between the UBM and the LBM must vary. In the temperature region I (Fig.6) an increase in degree of supercooling leads to easier nucleation for two reasons: owing to the decrease in

STAT

Declassified in Part - Sanitized Copy Approved for Release @ 50-Yr 2014/03/07 : CIA-RDP81-01043R004200090004-8

Declassified in Part - Sanitized Copy Approved for Release @ 50-Yr 2014/03/07 : CIA-RDP81-01043R004200090004-8

the critical nuclear size, and owing to the decrease in the degree of necessary concentration fluctuation. In region II of temperatures (Fig.6), the increased ease of nucleation with increasing supercooling is due only to the former circumstance.

Apparently the change in the character of the dependence of δ on ΔT observed in

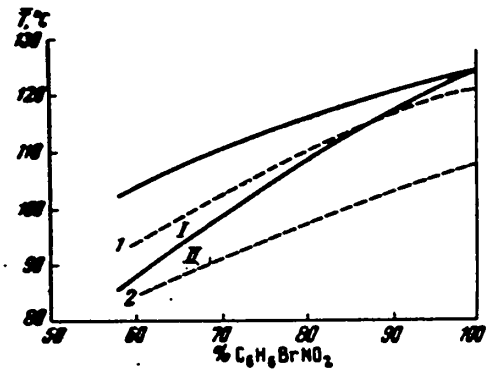

Fig.6 - Crystallization Diagram for Melts of Parachloronitrobenzene with Parabromonitrobenzene; Curve 1 - UBM of Liquid; 2 - LBM of Liquid

melts of parachloronitrobenzene with parabromonitrobenzene (Fig.3) is a consequence of the fact that the solidus in these melts is located between the UBM and the LBM of the liquid.

It is necessary to dwell on the peculiarities of structural formation during the crystallization of solid solutions - peculiarities due to the character of the mutual position of the solidus, the UBM and the LBM of the liquid.

In melts of camphor with borneol, regardless of the concentration of the initial melt and the conditions of its cooling, the phenomenon of intercrystalline liquation is not observed. This is due to the fact that the crystallization of melts begins and proceeds at temperatures below the solidus, at which the crystallization takes place without diffusion, i.e., without redistribution of the component between the liquid and crystalline phases. Crystallization takes place similarly in melts of camphor with hydroquinone if the composition of the melts is within the

STAT

Declassified in Part - Sanitized Copy Approved for Release @ 50-Yr 2014/03/07 : CIA-RDP81-01043R004200090004-8

Declassified in Part - Sanitized Copy Approved for Release @ 50-Yr 2014/03/07 : CIA-RDP81-01043R004200090004-8

limits in which the UBM and the LBM are below the solidus, and in melts of parachloronitrobenzene with parabromonitrobenzene if their crystallization begins and proceeds in region II of temperatures, i.e., below the solidus. In the other melts of camphor with hydroquinone, in which crystallization under any cooling conditions begins above the solidus and therefore takes place under conditions of diffusion redistribution of the components between the liquid and crystalline phases, the phe-

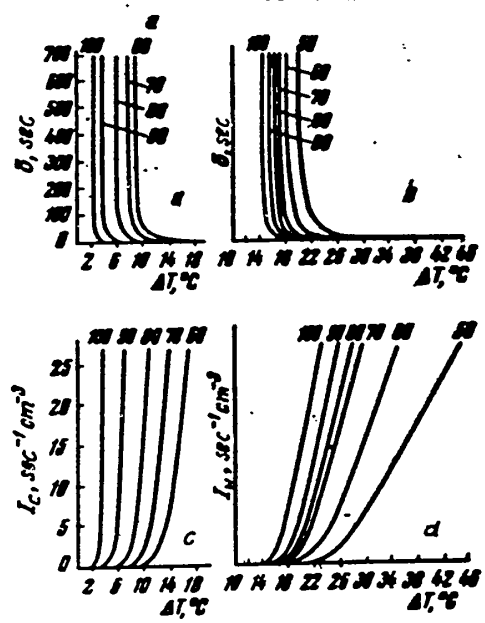

Fig.7 - Dependence of Incubation Period (a, b) and Rates of Nucleation (c, d) on the Degree of Supercooling for Melts of Camphor and Naphthalene. The figures on the curves correspond to the molar percentages of camphor (a, c) and of naphthalene (b, d)

nomenon of intracrystalline liquation is observed, and is the more distinct, the poorer the conditions for diffusion, i.e., the more rapidly the heat is removed during the crystallization of the melts.

In melts of parachloronitrobenzene with parabromonitrobenzene, the phenomenon of intracrystalline liquation is observed only in cases where the crystallization of

STAT

Declassified in Part - Sanitized Copy Approved for Release @ 50-Yr 2014/03/07 : CIA-RDP81-01043R004200090004-8

Declassified in Part - Sanitized Copy Approved for Release @ 50-Yr 2014/03/07 : CIA-RDP81-01043R004200090004-8

the melts begins in region I. For this reason, in these melts, an accelerated cooling, assuring the supercooling of the liquid in region II without nucleation, leads to the diffusionless crystallization of the melts to form a homogeneous solid solution, while, on the other hand, slow cooling, leading to nucleation in region I of

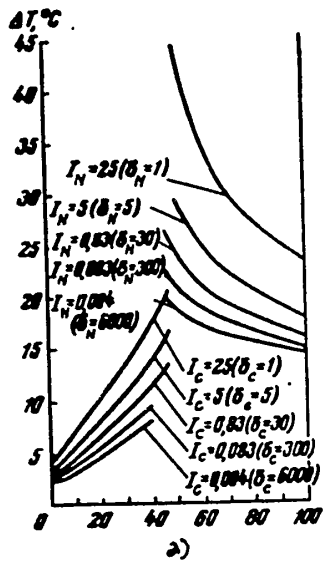

Fig.8 - Isoprobability Curves of Formation of Crystal Nuclei in Melts of Camphor with Naphthalene

a) Mole % of naphthalene

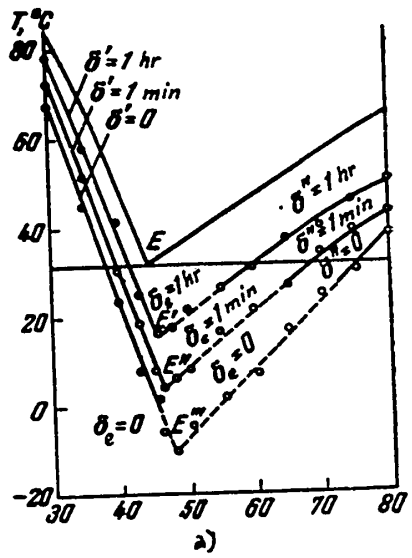

Fig.9 - Crystallization Diagram for Melts of Camphor with Naphthalene:

δ' - Incubation period of crystallization of camphor; δ'' - Of naphthalene; δ_e - Of eutectic

a) Mole % of naphthalene

temperatures, favors the formation of an inhomogeneous solid solution, that is, the formation of intracrystalline liquation.

Formation of Crystal Germs in Melts of Eutectic Type

Melts of camphor with benzoic acid, camphor with naphthalene, camphor with orthochloronitrobenzene, and camphor with paradibromobenzene, were investigated. All these substances are metalloid, and their crystals do not exert a mutually

STAT

Declassified in Part - Sanitized Copy Approved for Release @ 50-Yr 2014/03/07 : CIA-RDP81-01043R004200090004-8

Declassified in Part - Sanitized Copy Approved for Release @ 50-Yr 2014/03/07 : CIA-RDP81-01043R004200090004-8

nucleating influence during crystallization. The dependence of the incubation period of crystallization of the melts in these systems on the degree of supercooling is of the same character as for melts of camphor with hydroquinone (Fig. 2), which is entirely natural, since in eutectic type melts the nucleation of each of the components involves the formation of concentration fluctuations. As an example, Fig.7 gives the curves of the dependence of δ and I on ΔT for melts of camphor and naphthalene.

Figure 8 gives curves each of which corresponds to a single value of δ and to the crystallization of camphor (the curves on the left side of Fig.8; or of naphthalene, the curves on the right side). This curve may be regarded as a curve of isoprobability for the formation of nuclei of camphor or of naphthalene.

Figure 9 is a phase equilibrium diagram for the system camphor-naphthalene, on which the three isoprobability curves corresponding to $\delta = 1$ hr, $\delta = 1$ min and $\delta = 0$ have been plotted. Each curve, like the liquidus, consists of two branches. The left branches are the isoprobability curve for the crystallization of camphor, the right branches are the curves for the crystallization of naphthalene. It is obvious that the points of intersection of the branches of each isoprobability curve correspond to the conditions of equal probability of formation of nuclei of the two components. The curve E' E'' (Fig.9), which may be drawn through the points of intersection of the branches of the isoprobability curve, will be the equiprobability line. The points on this line describe the conditions corresponding to the equal probability of the formation of nuclei of the two components. The line of equal probability must begin at the eutectic point E (Fig.9), since the point E corresponds to the condition of equal probability (equal to zero) of nucleation of the two components.

It has been established experimentally that the line of equal probability of formation of the two components on the phase diagram is located in the region of hypereutectic concentrations (the systems camphor-naphthalene, camphor-benzoic acid)

STAT

Declassified in Part - Sanitized Copy Approved for Release @ 50-Yr 2014/03/07 : CIA-RDP81-01043R004200090004-8

Declassified in Part - Sanitized Copy Approved for Release @ 50-Yr 2014/03/07 : CIA-RDP81-01043R004200090004-8

or in the region of hypoeutectic concentrations (camphor-paradibromobenzene), or else this line is located both in the region of hypoeutectic concentrations and that of hypereutectic concentrations (camphor-orthochloronitrobenzene). All these cases are schematically represented in Fig.10.

In the former case (Fig.10b), nuclei of the second component appear first in the melt of eutectic composition, and these nuclei then initiate the eutectic transformation. In the second case (Fig.10a), camphor is the initiator of eutectic de-

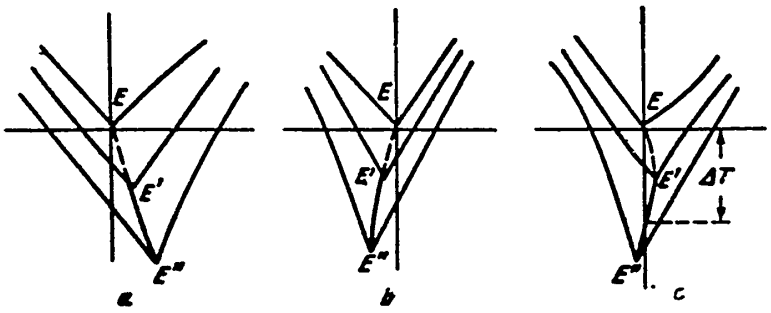

Fig.10 - Various Cases of Mutual Position of the Eutectic Point E and the Line of Equal Probability of Formation of Nuclei of the Two Components E', E''

composition. In the third case (Fig.10c) we observe equal probability of the formation of the germs of the two components in a melt of eutectic composition, but only at a definite supercooling ΔT (Fig.10c), corresponding to the point of intersection of the vertical passing through the point E with the "equiprobability" line. At degrees of supercooling less than ΔT, the eutectic transformation is initiated by camphor, and at supercoolings greater than ΔT, by orthochloronitrobenzene. From this it follows that the so-called principle of equal probability of formation of nuclei of each of the two phases during a eutectic transformation (Bibl.3) is unsound.

Conclusions

We have considered three cases of the formation of crystal nuclei during the

STAT

Declassified in Part - Sanitized Copy Approved for Release @ 50-Yr 2014/03/07 : CIA-RDP81-01043R004200090004-8

Declassified in Part - Sanitized Copy Approved for Release @ 50-Yr 2014/03/07 : CIA-RDP81-01043R004200090004-8

crystallization of solid solutions:

1) The upper (UBM) and lower (LBM) boundaries of metastability of the liquid are located below the solidus line; in this case, nucleation and crystallization proceed without diffusion, and without redistribution of the components among the liquid and solid phases. The phenomenon of intracrystalline liquation is not observed in these melts, under any cooling conditions whatsoever, during the period of crystallization.

2) The UBM and the LBM are located above the solidus line; in this case the formation of germs takes place on the basis of phase and concentration fluctuations; the degree of concentration fluctuation necessary for the formation of nuclei depends on the initial composition of the melt; intracrystalline liquation in these melts cannot be avoided by rapid cooling, since the formation of nuclei will unavoidably begin at temperatures above the solidus line, and during crystallization there will be redistribution of the components between the liquid and solid phases.

3) The solidus line is located between the UBM and the LBM; in this case, crystallization proceeds in the temperature range between the UBM and the solidus line, as in the second case, but in the range between the solidus and the LBM it proceeds as in the first case. The influence of intracrystalline liquation in these melts can be avoided by accelerated cooling of the liquid in the region of temperatures below the solidus.

Besides this, for a series of systems of eutectic type, we have established the conditions corresponding to equal probability of formation of the germs of the two components. The equiprobability line on the phase diagram is located either in the region of hypoeutectic or hypereutectic concentrations, or in both these regions. In a melt of eutectic composition, in the first case, the eutectic transformation is always initiated by the second component, and in the second case, by the first component; and it is only in the third case that equal probability of the formation of nuclei proved to be possible at a definite degree of supercooling, above which the

STAT

Declassified in Part - Sanitized Copy Approved for Release @ 50-Yr 2014/03/07 : CIA-RDP81-01043R004200090004-8

Declassified in Part - Sanitized Copy Approved for Release @ 50-Yr 2014/03/07 : CIA-RDP81-01043R004200090004-8

first component is the initiator of the eutectic transformation, and below which the second component is such initiator.

BIBLIOGRAPHY

1. Danilov,V.I. - Formation of Crystallization Centers in Supercooled Liquids. Zhur.Tekh.Fiz., No.3 (1949)
2. Grechniy,Ya.V. - Probability of Formation of Crystal Nuclei in Eutectic Type Binary Melts. Dok. AN USSR, Vol.84, No.1 (1952)
3. Avakyan,S.V. and Lashko,N.F. - The Nature of Eutectic Melts. Dok. AN USSR, Vol.65, No.1 (1949)

STAT

Declassified in Part - Sanitized Copy Approved for Release @ 50-Yr 2014/03/07 : CIA-RDP81-01043R004200090004-8

Declassified in Part - Sanitized Copy Approved for Release @ 50-Yr 2014/03/07 : CIA-RDP81-01043R004200090004-8

A CONTRIBUTION TO THE QUESTION OF THE FORMATION AND GROWTH OF NEGATIVE CRYSTALS (PORES) ARISING FROM SUPERSATURATED SOLUTIONS OF VACANCIES IN THE CRYSTAL LATTICE

by

Ya.Ye.Geguzin

It has been shown by many experimental works (Bibl.1, 2, 3, 4) that in mutual diffusion in substitution solid solutions, when the diffusion is primarily of unipolar character (the case of inequality of the partial coefficients of diffusion $D_{A \to B} > D_{B \to A}$, evaporation of volatile components from an alloy, etc.), the metal from which a larger number of atoms have been lost than have arrived in it, becomes enriched in vacancies. The concentration of vacancies in this case exceeds the equilibrium value, i.e., $\xi > \xi_0 = e^{-u/kT}$ (u being the activation energy of the process of hole formation), and the system so formed may be regarded as a supersaturated solution of vacancies in the metal (Bibl.3). Owing to the supersaturation of the solution, the phase corresponding to the vacancies "crystallizes out" of it, i.e., negative crystals or pores (Bibl.3, 5) appear, whose shape, according to the Curie-Wulff rule, is determined by the anisotropy of the coefficient of surface tension on the boundary metal-vacuum.

In this connection, the question naturally arises as to the mechanism of the formation and growth of negative crystals. Of interest, thus, are the questions of the existence of a "critical" nucleus of the negative crystallite, of the connection between the supersaturation of the solution of vacancies in the metal ($\Delta\xi = \xi - \xi_0$) with the kinetics of growth of the negative crystallite. Starting out from the analogy between the process of precipitation of a supersaturated phase in ordinary solutions, and the process of appearance of negative crystals, it is natural to address ourselves to the question of the effect of foreign "impurities" on the appearance of the nucleus of a negative crystal.

STAT

Declassified in Part - Sanitized Copy Approved for Release @ 50-Yr 2014/03/07 : CIA-RDP81-01043R004200090004-8

Declassified in Part - Sanitized Copy Approved for Release @ 50-Yr 2014/03/07 : CIA-RDP81-01043R004200090004-8

In this paper we shall consider some of the above-enumerated questions.

The Critical Nucleus of the Negative Crystal

Starting out from primitive model ideas, it may be postulated that the appearance of negative crystals does not involve the formation of a critical (viable) germ, which may become a center of crystallization, since even the coalescence of two vacancies, from among the excess vacancies, leads to an energy gain, due to the fact that the coalescence of a pair of vacancies leaves only 11 uncompensated bonds instead of the original 12 ($2 \times 6 = 12$ for the coordination number $z = 12$) since one bond is now saturated. It is easy, however, to show the existence of a critical nucleus, and estimate its size. Let us consider the question of the nucleus from the point of view of the kinetics of its appearance and growth. It is well known that, near the surface of a drop of radius of curvature r, the equilibrium vapor pressure P_0 is increased by

$$\Delta P = \frac{2\sigma}{r}\frac{a^3}{kT}P_0, \tag{1}$$

where a^3 is the volume of one molecule in the condensed phase (a is the lattice parameter), and σ is the surface tension. Since, in the case of dilute solutions,

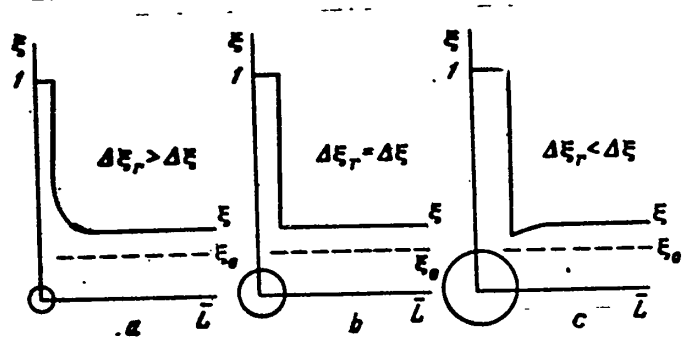

Fig.1 – Concentration of Vacancies as a Function of the Distance from the Surface of a Pore

ΔP and P_0 are proportional to the concentrations, and since eq.(1) does not contain the mass of the particles, this formula may be used to determine the equilibrium

STAT

Declassified in Part - Sanitized Copy Approved for Release @ 50-Yr 2014/03/07 : CIA-RDP81-01043R004200090004-8

Declassified in Part - Sanitized Copy Approved for Release @ 50-Yr 2014/03/07 : CIA-RDP81-01043R004200090004-8

concentration of vacancies near a pore of radius r (Bibl.6) which we shall hereafter denote by ξ_r

$$\Delta\xi_r = \frac{2\sigma}{r} \cdot \frac{a^3}{kT} \cdot \xi_0. \qquad (2)$$

In connection with the dependence of $\Delta\xi_r$ on r, the distribution of concentrations in the region adjoining a pore situated in a supersaturated solution of vacancies will differ substantially for different values of r. Indeed, when $\Delta\xi_r > \Delta\xi$ (Fig.1a), the distribution of the concentrations of vacancies will be such that there will be a flow of vacancies from the surface of the pore, which corresponds to the process of "sintering" the pore, or to a decrease in its size. When $\Delta\xi_r < \Delta\xi$ (Fig.1c), the distribution of the concentrations of vacancies near the pore will assure their flow to the pore, i.e., the pore will grow. Obviously the critical size of a viable nucleus will be determined by the condition (Fig.1b):

$$\Delta\xi_r = \Delta\xi, \qquad (3)$$

from which, taking eq.(2) into account, we can obtain the following expression for the radius of a critical nucleus:

$$r^* = \frac{\xi_0}{\Delta\xi} \cdot 2\sigma \frac{a^3}{kT}. \qquad (4)$$

The size of a critical nucleus has been determined by the ratio between two opposing tendencies: the tendency to "sintering" of the pore and the tendency toward its growth. We note that eq.(4) may be obtained by minimizing the value of the change of free energy of the supersaturated solution due to the appearance of a pore of radius r. Indeed, the change in the thermodynamic potential of the supersaturated solution in connection with the appearance of a nucleus of radius r will be equal to

$$\Delta\Phi = S \cdot \sigma - V\Delta\varphi, \qquad (5)$$

where $S = 4\pi r^2$ is the surface of the pore; $V = \frac{4}{3}\pi r^3$ is the volume of the pore; and $\Delta\varphi$ is the change in the thermodynamic potential of the system on the replacement of unit volume of the supersaturated solution by a pore. Obviously $\Delta\varphi = \frac{1}{a^3}(\mu'' - \mu')$,

STAT

Declassified in Part - Sanitized Copy Approved for Release @ 50-Yr 2014/03/07 : CIA-RDP81-01043R004200090004-8

Declassified in Part - Sanitized Copy Approved for Release @ 50-Yr 2014/03/07 : CIA-RDP81-01043R004200090004-8

where $\frac{1}{a^3}$ is the number of lattice sites in unit volume, μ'' and μ' are respectively the chemical potentials of the vacancies in solutions with the respective concentrations ξ and ξ_0. Since (Bibl.7), $\mu^i = kT \ln \xi^i + \psi(P; T)$, where $\psi(P; T)$ is a certain function of pressure and temperature, then:

$$\Delta\varphi = \frac{kT}{a^3} \ln \frac{\xi}{\xi_0} = \frac{kT}{a^3} \ln \left(1 + \frac{\Delta\xi}{\xi_0}\right) \simeq \frac{kT}{a^3} \frac{\Delta\xi}{\xi_0}. \qquad (6)$$

Substituting eq.(6) in eq.(5), it is easy from the condition $\frac{\partial}{\partial r}(\Delta\Phi) = 0$, to find an expression for the radius of the critical nucleus in agreement with that found previously [see eq.(2)].

The expression found for r differs from the well-known expression determining the radius of the critical nucleus in ordinary supersaturated solutions by the fact that the surface tension of the substance itself enters into eq.(4), a surface tension which is approximately two orders greater than the surface tension on the nucleus-matrix interface in ordinary solutions (Bibl.8). For this reason, at the same deviations from equilibrium (determined by the value of the supersaturation), the appearance of a nucleus of a negative crystallite presupposes a substantially greater fluctuation (cf.infra). It is easy to show that the work of formation of a negative crystallite in solution characterized by a given degree of supersaturation is written as follows:

$$\Delta\Phi_s = \frac{4}{3}\pi r^{*2}\sigma = \frac{16\pi\sigma^3 a^6 \xi_0^2}{3(kT)^2(\Delta\xi)^2}. \qquad (7)$$

Supersaturation of the Crystal Lattice with Vacancies

After observing the kinetics of growth of negative crystals, we may experimentally estimate the linear dimensions of the critical nucleus by determining the value of the supersaturation for this. Indeed, according to Zener (Bibl.9), the time dependence of the linear dimension of a precipitate growing out of a supersaturated solution (in the solid phase) is determined by the relation:

STAT

Declassified in Part - Sanitized Copy Approved for Release @ 50-Yr 2014/03/07 : CIA-RDP81-01043R004200090004-8

Declassified in Part - Sanitized Copy Approved for Release @ 50-Yr 2014/03/07 : CIA-RDP81-01043R004200090004-8

$$L(t) = k\left(\frac{n_\infty - n_r}{n_0 - n_r}\right)^{2/3}(D_v t)^{1/2}, \qquad (8)$$

where k = 1, n_∞ is the concentration of the supersaturated phase far from the precipitate, n_r is the concentration of the supersaturated phase close to the precipitate-matrix interface, and n_0 is the concentration of the supersaturated phase in the precipitate. Bearing in mind the existence of a critical nucleus of radius r* for the case of negative crystals, when $n_0 \gg n_r$; $n_\infty = \xi$; $n_r = \xi_r$, eq.(8) may be written in the form:

$$L(t) = 2r^* + (\Delta\xi)_z^{1/3}(D_v t)^{1/2}, \qquad (9)$$

where D_v is the diffusion coefficient of vacancies, $(\Delta\xi)_z = \xi - \xi_r$. It follows from eq.(9) that by extrapolating the experimentally found relation $L = \varphi(t^{1/2})$ to zero time, the dimension of the critical nucleus may be estimated. We note, however, that such an extrapolation is only legitimate if the value of $\Delta\xi_z$ is constant during the entire time of growth of the precipitate, or varies only slightly with time.

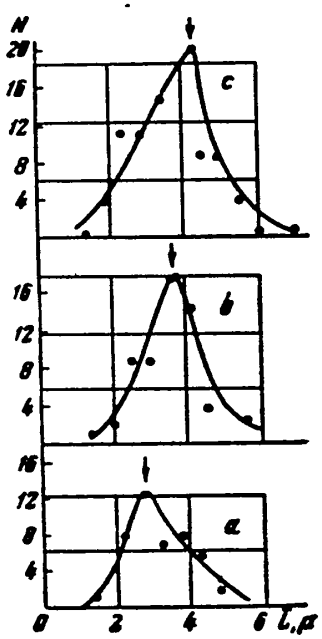

Fig.2 - Relation $N = \varphi(\bar{L})$ at 750°C:

a - t = 5 min; b - t = =20 min; c - t = 60 min

An alloy from which a volatile component is separated at high temperature might serve as an object for the study of the time dependence of the linear dimension of a negative crystallite. For the experimental determination of $L = \varphi(t^{1/2})$ we staged the following experiments. Plane-parallel strips of α-brass containing 30% of zinc and 1 mm thick, were annealed in a vacuum furnace at 650, 750 and 820°C for various periods, with the object of partially removing the zinc, which leads to the supersaturation of the brass with vacancies and, in consequence, the formation of negative crystals. After annealing, the

STAT

Declassified in Part - Sanitized Copy Approved for Release @ 50-Yr 2014/03/07 : CIA-RDP81-01043R004200090004-8

Declassified in Part - Sanitized Copy Approved for Release @ 50-Yr 2014/03/07 : CIA-RDP81-01043R004200090004-8

specimen was examined metallographically, as a result of which the distribution curve of the pores visible in the field of the polished section by linear dimension $\bar{L}$ was established. Figure 2 gives curves obtained in experiments run at 750°C. The value of $\bar{L}$ corresponding to the distribution of the maximum on the curve of $N(\bar{L})$ was taken as the mean size of the pores and the specimen given that particular anneal. In connection with the fact that the distribution of pores, not throughout the volume but on a plane polished surface is considered, the maximum on the curve will be somewhat shifted toward lower values of $\bar{L}$ (Bibl.10). Figure 3 gives data obtained by this method* in the form of graphs of $\bar{L} = \varphi(t^{1/2})$.

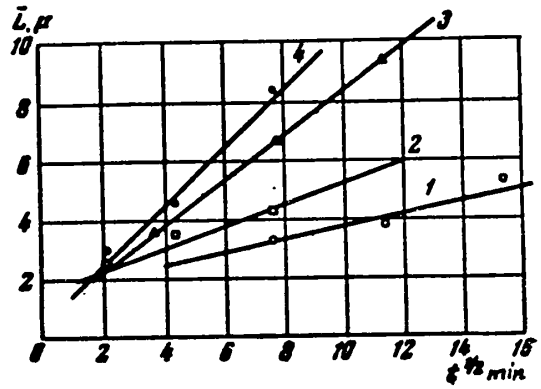

Fig.3 - Relation $\bar{L} = \varphi(t^{1/2})$:
1 - at 650°C; 2 - 750°C; 3 - 780°C (Bibl.11); 4 - 850°C

Strictly speaking, these graphs are not straight lines, since the quantity $\Delta\xi_z$ entering into eq.(9) likewise depends on the time, for in connection with the increase in the radius of the pore, the concentration of vacancies close to its surface (ξ_r) decreases. The deviation from linearity is substantial only at the beginning of the growth of the crystallite when $L \approx 2r$; at longer times, taking account of the errors of measurement, the relations $L = \varphi(t^{1/2})$ are well described by straight lines. The graphs of the relation obtained in experiments on evaporation of a volatile component must not (with the object of finding r*) be extrapolated to the region t = 0, since at such

*During the time this work was being performed, the paper of Accary (Bibl.11) appeared, reporting experiments similar to those described and run only at 780°C. The data given later, relating to the temperature 780°C, have been borrowed from that paper (Bibl.11).

STAT

Declassified in Part - Sanitized Copy Approved for Release @ 50-Yr 2014/03/07 : CIA-RDP81-01043R004200090004-8

Declassified in Part - Sanitized Copy Approved for Release @ 50-Yr 2014/03/07 : CIA-RDP81-01043R004200090004-8

a distance from the surface of the specimen, at different temperatures, supersaturation is established in different times. For this reason, in evaluating r*, we must first determine the value of the supersaturation from the slope of the straight line $L = \varphi(t^{1/2})$, and then estimate r* by eq.(4). According to eq.(9), we may write $\Delta\xi_z = \frac{\left[\frac{d}{dt^{1/2}} L(t)\right]^2}{D_v}$. Obviously $\Delta\xi_z = \xi - \xi_r = (\xi - \xi_o) - (\xi_r - \xi_o) = \Delta\xi - \Delta\xi_r$. Since $\Delta\xi \sim \frac{1}{r^*}$, while $\Delta\xi_r \sim \frac{1}{L(t)}$, we may put $\Delta\xi_z = \Delta\xi$ for $L > r^*$. Taking this into account, and bearing in mind that $D_a \approx \xi_o D_v$, where D_a is the coefficient of diffusion of atoms, we write

$$\frac{\Delta\xi}{\xi_o} = \frac{\left[\frac{d}{dt^{1/2}} L(t)\right]^2}{D_a}. \qquad (10)$$

In calculating $\frac{\Delta\xi}{\xi_o}$ by eq.(10) we use the well-known data (Bibl.14) on the temperature dependence of the coefficient of diffusion of α-brass, likewise found in experiments on the evaporation on the volatile component. Figure 4 gives data on the values of $\frac{\Delta\xi}{\xi_o}$. To find the absolute value of the supersaturation, it is necessary to know the equilibrium concentration of vacancies ξ_o. Since there are no direct measurements of the values of ξ_o or of the energy of vacancy formation in alloys, and especially, in α-brass, at the present time, the value of ξ_o cannot be reliably determined.

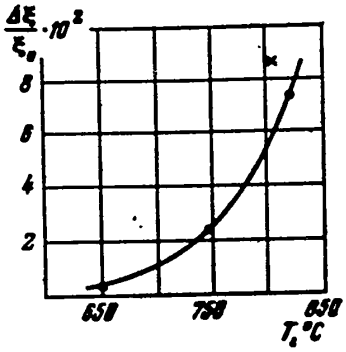

Fig.4 - Temperature Dependence of the Value of the Supersaturation

The Role of "Impurities" in the Formation of the Negative Crystal

The evaluation of the linear dimension of the critical nucleus, originating by fluctuation, based on experimental data on the value of $\frac{\Delta\xi}{\xi_o}$, indicates the necessity of very great fluctuation; a nucleus so appearing must consist of about 10^9 vacancies, which appears highly improbable. At supersaturations $\frac{\Delta\xi}{\xi_o} \approx 10$, nuclei consist-

STAT

Declassified in Part - Sanitized Copy Approved for Release @ 50-Yr 2014/03/07 : CIA-RDP81-01043R004200090004-8

Declassified in Part - Sanitized Copy Approved for Release @ 50-Yr 2014/03/07 : CIA-RDP81-01043R004200090004-8

ing of several vacancies would be viable, but, as shown by experience, in any case in an alloy from which a volatile component is evaporated, such supersaturations do not occur. It should be noted that, in general, supersaturations $\frac{\Delta\xi}{\xi_0} \approx 10$ at which excess vacancies are uniformly distributed through the entire volume of the specimen in the high-temperature region when r* is small, could hardly be realized, since such an excess of vacancies might lead to the destruction of the crystal lattice. Indeed, if we used the ratio established (Bibl.11, 12) between the energy of hole formation and the energy of activation for self-diffusion Q, according to which $u \approx \frac{1}{3} Q$, ξ_0 may be determined. Since for copper at a temperature of 1000°C, $\xi_0 = 2 \times 10^{-3}$, then for $\frac{\Delta\xi}{\xi_0} \approx 10$, $\Delta\xi = 2 \times 10^{-2}$, which leads to a relative change of volume of $\frac{\Delta v}{v} \approx 2 \times 10^{-2}$, a value close to that preceding melting.

In connection with the above it is natural to assume that the nucleation of negative crystals in a supersaturated solution of vacancies in a crystal lattice may take place, not on nuclei originating fluctuationally (which, in principle, speaking generally, is not excluded), but on various kinds of foreign "impurities", whose presence might substantially decrease the work of nucleation. Discussing the question of the possible effect of impurities on the formation of germs of negative crystals, two substantially different types of "impurities" must be kept in mind. Various kinds of interfaces between adjacent elements of metal structure (grains, mosaic blocks) characterized by the boundary surface tension σ_{ik}, might be included in the first type of "impurities". Speaking of the surfaces of separation between adjacent elements of the metal structure, we assume that they are free of discontinuities, which, for instance, in deformed objects, very often arise, and precisely between grains or mosaic blocks. In this case the surfaces of separation become "impurities" of the second type. The second type includes microscopic fissures, which may exist in the specimen either as a result of its earlier history (appearing during crystallization, or fissures originating in deformation), and also those appearing during the process of diffusion as a result of the stresses arising in the

STAT

Declassified in Part - Sanitized Copy Approved for Release @ 50-Yr 2014/03/07 : CIA-RDP81-01043R004200090004-8

Declassified in Part - Sanitized Copy Approved for Release @ 50-Yr 2014/03/07 : CIA-RDP81-01043R004200090004-8

diffusion zone. It is well known that these stresses are great and lead to the process of polygonization.

The influence of various "impurities" on the process of the nucleation of negative crystals may be evaluated by a comparison of the minimum work of formation of a nucleus under different conditions: spontaneously, and close to the interfaces between structural elements of the metal. It is obvious that the appearance of a nucleus of radius r^* on an interface characterized by an interfacial surface tension σ_{ik} is connected with the disappearance of an interface of area πr^{*2}, i.e., with a decrease in the work of nucleation by a quantity of the order of $\pi r^{*2}\sigma_{ik}$. Comparing the work of formation of a three-dimensional nucleus close to an interface [cf.eq.(7)] with the work of formation of a three-dimensional nucleus in the immediate proximity of the boundary, $\Delta\Phi_3^{*\prime} = \Delta\Phi_3^* - \pi r^{*2}\sigma_{ik}$, and considering the quantity $K = \frac{\Delta\Phi_3^*}{\Delta\Phi^{*\prime}} = \frac{\sigma}{\sigma - 3/4\sigma_{ik}}$, we convince ourselves that the existence of interblock boundaries ($\sigma_{ik} \sim 10^{-3} - 10^{-4}\sigma$) (Bibl.8) and of intergrain boundaries ($\sigma_{ik} \sim 10^{-1}\sigma$) (Bibl.8) cannot substantially affect the value of the probability of spontaneous nucleation.

Let us now consider the question of the role of microscopic fissures. For a fissure having a boundary characterized by the surface tension of the metal itself to be able to become the nucleus of a negative crystal, its area would have to exceed the area of that viable two-dimensional nucleus L^{*2}, which must be formed for the growth of the fissure to be possible. By minimizing the change of free energy connected with the appearance of a two-dimensional nucleus, we easily find its critical linear dimension: $L^* = \frac{\xi_0}{\Delta\xi} 2\sigma_L \frac{a^2}{kT}$, where σ_L is the "linear" tension. Taking account of the value previously found for the relative supersaturation, $\frac{\Delta\xi}{\xi_0} \approx 10^{-1}$, and putting $\sigma_L \sim a\sigma$, we get $L^* \sim 10^{-6}$. Thus, tiny fissures with a linear dimension of the order of $10^{-2}\mu$ may be nuclei of negative crystallites.

Indirect evidence of the important role of free boundaries possessing a great surface tension in the nucleation of negative crystals is furnished by the absence

STAT

Declassified in Part - Sanitized Copy Approved for Release @ 50-Yr 2014/03/07 : CIA-RDP81-01043R004200090004-8

Declassified in Part - Sanitized Copy Approved for Release @ 50-Yr 2014/03/07 : CIA-RDP81-01043R004200090004-8

of crystallites near the surface of the specimen, and near microscopic fissures arising in the surface layer at an early stage of evaporation of the zinc. The following observations are likewise evidence of this. Very often a group of pores oriented in the same way with respect to the polished surface [i.e., in the same grain (Bibl.5)], are regularly arranged, forming a certain chain along which, apparently, a fissure has extended (Fig.5). The position of the pores shown on Fig.5 would be very improbable if we consider their origin to be due to fluctuation.

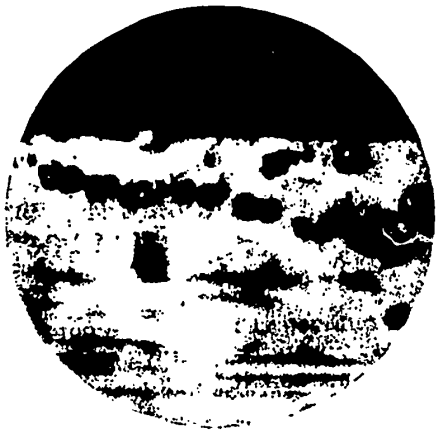

Fig.5 - Arrangement of Negative Crystallites in a Chain. 350 ×

Thus, on the basis of the experimental data obtained on the value of the supersaturation arising in brass on evaporation of the zinc, it may be assumed that the spontaneous nucleation of negative crystals is very improbable; the negative crystals observed are apparently the result of the development of microscopic fissures existing in the specimen.

In conclusion I express my thanks to Ye.S.Borovik for his valuable advice during the discussion of this paper, and to N.N.Ovcharenko for his help with the experiments.

BIBLIOGRAPHY

1. Smigelskas,A. and Kirkendall,E. - Met.Techn.T. P. No.2007.
2. Buekle,H. and Blin,J. - Journ.Inst.Metal, March 1952
3. Pines,B.Ya. and Geguzin,Ya.Ye. - Zhur.Tekh.Fiz., Vol.23, No.9 (1953)
4. Geguzin,Ya.Ye. and Pek Yen Gin - Zhur.Tekh.Fiz., Vol.24, No.9 (1954)
5. Geguzin,Ya.Ye. - Dok.AN SSSR, Vol.100, No.2 (1955)
6. Pines,B.Ya. - Zhur.Tekh.Fiz., Vol.16, No.6 (1946)

STAT

Declassified in Part - Sanitized Copy Approved for Release @ 50-Yr 2014/03/07 : CIA-RDP81-01043R004200090004-8

Declassified in Part - Sanitized Copy Approved for Release @ 50-Yr 2014/03/07 : CIA-RDP81-01043R004200090004-8

7. Landau,L.D. and Lifshits,Ye.M. - Statistical Physics. Gostekhizdat (1954)

8. Pines,Ya.Ye. - Zhur.Tekh.Fiz., Vol.23, No.12 (1953)

9. Zener,C. - Journ.Appl.Phys., Vol.20, No.10 (1949)

10. Saltykov,S.A. - Zavod.Lab., Vol.11 (1949), p.1317

11. Accary,A. - Comp.Rend., Vol.240, No.5 (1955), p.519

12. Lazarev,V.G. and Ovcharenko,O.N. - Dok. AN SSSR, Vol.100, No.5 (1955), p.875

13. Gertsriken,S.D. - Dok. AN SSSR, Vol.98, No.2 (1954), p.211

14. Gertsriken,S., Il'kevich,G., Sakharov,I., and Fayngol'd,M. - Zhur.Tekh.Fiz., Vol.10, No.10 (1940), p.286

STAT

Declassified in Part - Sanitized Copy Approved for Release @ 50-Yr 2014/03/07 : CIA-RDP81-01043R004200090004-8

Declassified in Part - Sanitized Copy Approved for Release @ 50-Yr 2014/03/07 : CIA-RDP81-01043R004200090004-8

THERMAL AND DIFFUSIONAL PROCESSES DURING THE GROWTH OF CRYSTALS

by

G.P.Ivantsov

The role of heat in the process of formation of a metal ingot is well known to metallurgists. By regulating the removal of heat from the molten metal, the metallurgist is able to obtain the desired ingot structure.

In an effort to formulate a more profound idea of the laws of formation of a metal ingot, I found myself forced to examine the role of heat removal during the growth of the individual crystals, as the elementary unit of the aggregate constituting the ingot itself. This study was initiated with an analysis of the growth of a single crystal of the simplest form in a supercooled melt of a pure substance.

A "viable" crystal nucleus arising in such a melt is somewhat larger than the equilibrium crystallite; as the nucleus grows, latent heat of crystallization is liberated on the phase interface. It is consumed in heating the crystallite and the melt adjoining it. A heat flow arises from the heated crystallite into the melt surrounding it. The rate of growth is determined both by the rate of removal of latent heat from it, as well as by the power of the given substance to crystallize at one linear velocity or another under the given conditions (at a given temperature and orientation of its surface).

For small sizes of the crystallite, and at very low rate of growth, the system will be almost isothermal, the influence of the irregular temperature field will be negligible, and the crystal will acquire a polyhedral form close to the equilibrium shape.

However, if the substance in question has a high linear rate of crystallization and there is intense heat removal from the crystal, then a temperature difference will appear, and the nonisothermicity of the system will exert substantial influence on the shape of the crystal formed - "irregular" forms of growth will appear -

STAT

Declassified in Part - Sanitized Copy Approved for Release @ 50-Yr 2014/03/07 : CIA-RDP81-01043R004200090004-8

Declassified in Part - Sanitized Copy Approved for Release @ 50-Yr 2014/03/07 : CIA-RDP81-01043R004200090004-8

needles, dendrites, etc.

Thus, in this case, the shape of the crystal will be determined both by the kinetic patterns (the dependence of the linear rate of crystallization on the temperature at the crystallization front and on the orientation of the crystal) and by the patterns of heat transfer, the role of the latter factors becoming very substantial, and often even decisive.

In investigating the formation of an alloy, the simplest schematized kinetic conditions have been assigned, but the phenomena of heat removal (and of diffusion in the analysis of the crystallization of two-component systems) have been fully taken into account.

1. The Growth of a Crystal of Spherical Form at Constant Surface Temperature

Formulation of the question: in a supercooled, motionless melt, a crystal of spherical form grows; the latent heat of crystallization liberated on the surface of the crystal is propagated into the surrounding melt. Required, to determine the temperature field of the system and the law of growth of such a crystal. An exact solution of this problem has been obtained (Bibl.1). It has been found that in this case, as in crystallization on a plane wall, the dimensions of the growing crystals are proportional to the square root of the time. For slight degrees of supercooling (in the case of a metallic melt, not over 5°C) the rather complex mathematical relations are replaced by the following formula:

$$r_c = \sqrt{2a\tau\frac{c(t_f - t_m)}{q_c}}, \qquad (1)$$

where r_c is the radius of the crystal;

c, a = the heat capacity and temperature conductivity of the melt;

q_c is the latent heat of crystallization;

t_f, t_m are the temperatures on the crystallization front and in the melt at a sufficient distance from the crystal;

STAT

Declassified in Part - Sanitized Copy Approved for Release @ 50-Yr 2014/03/07 : CIA-RDP81-01043R004200090004-8

Declassified in Part - Sanitized Copy Approved for Release @ 50-Yr 2014/03/07 : CIA-RDP81-01043R004200090004-8

τ is the time.

The following case is of considerably greater interest.

2. Growth of a Crystal of Spherical Form at Constant Rate

Formulation of question: in a supercooled motionless melt, a crystal grows at the constant velocity w; the latent heat of crystallization liberated on the surface of the crystal is propagated both inside the crystal and into the surrounding melt; the thermophysical constants of the crystal on the melt are the same, and both media are isotropic. Required, to determine the temperature field of the system. The exact solution of this problem is expressed by a very complicated formula. For the initial stage of growth, however, the very simple expression obtained is:

$$\theta \approx T. \tag{2}$$

Here $\theta = \frac{c(t_f - t_m)}{q_c}$ is the dimensionless temperature (in this expression the variable is t_f, while the other quantities are constants); $T = \frac{w^2\tau}{a}$ is the dimensionless time; and the other notation is as before.

Solving eq.(2) for the excess temperature of the crystal over that of the melt, we get

$$t_f - t_m \approx \frac{q_c w^2 \tau}{ca} \approx \frac{q_c \rho w^2 \tau}{\lambda}, \tag{3}$$

where λ is the coefficient of thermal conductivity.

It will be seen from eq.(3) that the temperature of the crystal likewise increases at a constant rate.

The problem then became more complicated.

3. Growth of a Crystal of Cubical Shape at Constant Velocity

The formulation of the question differs from the preceding by the assumption that the crystal grows at a very low velocity. The exact solution of this problem shows the following picture of the phenomenon: the surface of the crystal is non-

STAT

Declassified in Part - Sanitized Copy Approved for Release @ 50-Yr 2014/03/07 : CIA-RDP81-01043R004200090004-8

Declassified in Part - Sanitized Copy Approved for Release @ 50-Yr 2014/03/07 : CIA-RDP81-01043R004200090004-8

isothermal; the highest temperature is at the centers of the faces, and the lowest at the vertices, where the outflow of heat is greatest. The rate of increase of their temperatures is expressed by the following relations:

center of face

$$\theta \approx 1{,}5546\,T, \tag{4}$$

Vertex

$$\theta \approx 1{,}2204\,T, \tag{5}$$

where

$$\theta = \frac{c\,(t_f - t_m)}{q_c}, \quad T = \frac{w^2\tau}{a}.$$

The temperature difference between the center of the face and the vertex, being the maximum temperature difference on the surface of the crystal, is

$$\theta \approx 0{,}344\,T. \tag{6}$$

This expression, after transformations, takes the following form (the substitution b = wτ was performed, b being half of the transverse dimension of the crystal at the given instant):

$$t_{c.f.} - t_{vert.} \approx 0{,}344\,\frac{wbq_c\rho}{\lambda}. \tag{7}$$

The crystal evidently maintains its shape until the nonisothermicity of its surface becomes so small that it does not prevent the regular growth of the crystal by the formation of two-dimensional nuclei on its faces.

V.I.Danilov and V.I.Malkin have investigated the relation between the rate of growth of crystals of salol crystals of regular shape from supercooling at very low velocities of growth (Bibl.2). The salol crystal has the shape of a rhombic dipyramid, and therefore the application of the relations derived to this case is purely arbitrary, although the order of magnitudes yielded by calculation do, beyond all possible doubt, correspond to reality. The calculation of the temperature drop by eq.(7) for a rate of growth of 0.006 mm/min = 10^{-5} cm/sec for a crystal 0.2 mm in dimension (b = 0.01 cm) leads to the following value (here and below the dimensions of all quantities are expressed in the CGS system):

STAT

Declassified in Part - Sanitized Copy Approved for Release @ 50-Yr 2014/03/07 : CIA-RDP81-01043R004200090004-8

Declassified in Part - Sanitized Copy Approved for Release @ 50-Yr 2014/03/07 : CIA-RDP81-01043R004200090004-8

$$\Delta t = 0{,}344 \frac{10^{-6} \cdot 0{,}01 \cdot 21{,}7 \cdot 1{,}25}{3{,}6 \cdot 10^{-4}} = 0{,}026^\circ.$$

According to other data (Bibl.2), a temperature change of 0.026°C corresponds to a change of about 5% in the rate of growth, while the crystal maintains its shape during growth - this drop is "surmounted" by the crystal.

It would be a very interesting problem to determine the temperature drop at which the shape of the crystal begins to change.

Experimental studies of this question, coupled with the appropriate theoretical calculations, would permit one to find the quantitative laws of transition from regular to irregular crystal growth. It may be asserted that without analysis of the temperature field of a system, these laws cannot be established (for a crystal of a one-component system).

4. Acicular Crystal

At high velocities of growth, acicular, lamellar and dendritic forms of crystals are formed.

It has long been known that the acicular form of crystal facilitates the removal of heat from the vertex of the needle. This has now been confirmed by mathematical analysis as well (Bibl.1). An exact solution for the following problem was obtained: in a supercooled motionless melt, an acicular crystal, on the surface of which rules the constant temperature t_f, grows at constant velocity w. Required, to determine the shape of the crystal.

It was found that under these conditions the crystalline needle should have the shape of a paraboloid of revolution. The isothermal surfaces in the melt around the crystalline needle are a system of confocal paraboloids of revolution (Fig.1). The temperature field of the system is expressed by the following equation

$$\frac{t - t_m}{t_f - t_m} = \frac{Ei\left(-\frac{w\rho}{2a} z\right)}{Ei\left(-\frac{w\rho}{2a}\right)}, \qquad (8)$$

STAT

Declassified in Part - Sanitized Copy Approved for Release @ 50-Yr 2014/03/07 : CIA-RDP81-01043R004200090004-8

Declassified in Part - Sanitized Copy Approved for Release @ 50-Yr 2014/03/07 : CIA-RDP81-01043R004200090004-8

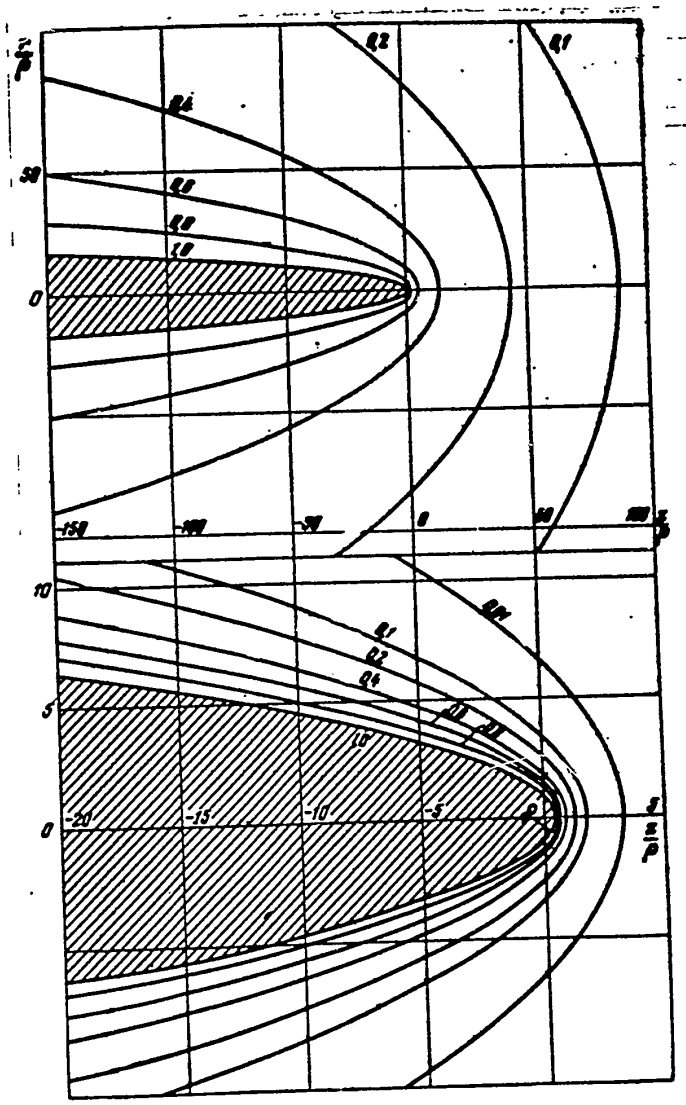

Fig.1 - Temperature Field around Acicular Crystal Growing at Constant Rate in a Supercooled Melt. The upper graph is for a slight degree of supercooling ($\Omega = \frac{c(t_f - t_m)}{q_c} = 0.0156$), the lower at a high degree of supercooling ($\Omega = 0.5$). z/ρ is plotted on the abscissa axis and r/ρ on the ordinate axis, ρ being the radius of curvature of the vertex of the crystal

STAT

Declassified in Part - Sanitized Copy Approved for Release @ 50-Yr 2014/03/07 : CIA-RDP81-01043R004200090004-8

Declassified in Part - Sanitized Copy Approved for Release @ 50-Yr 2014/03/07 : CIA-RDP81-01043R004200090004-8

where

$$\varepsilon = \frac{\zeta}{\rho} + \sqrt{\left(\frac{r}{\rho}\right)^2 + \left(\frac{\zeta}{\rho}\right)^2}, \tag{9}$$

where Ei is the tabular integral exponential function of the expression in the parentheses, w is the velocity of growth of the needle in the direction of its axis; ρ is the radius of curvature of the vertex of the needle; t is the current temperature; r, ζ are the cylindrical coordinates; and the other notation is as before.

The complex $\frac{w\rho}{2a}$ is connected by the following single-valued relation with the complex $\frac{c(t_f - t_m)}{q_c}$:

$$\frac{c(t_f - t_m)}{q_c} = -\frac{w\rho}{2a} e^{\frac{w\rho}{2a}} Ei\left(-\frac{w\rho}{2a}\right). \tag{10}$$

Consequently, in a melt with given physical properties and with a given degree of supercooling, either "blunt" needles may grow at a low velocity or "sharp" needles at a high velocity ($w\rho$ = const).

The actual velocity at which the needle grows will obviously be the maximum velocity peculiar to a crystal of the particular substance at the given temperature on a front of crystallization, and in the given direction.

The upper graph on Fig.1 relates to the case of a low-degree supercooling ($\Omega = \frac{c(t_f - t_m)}{q_c} = 0.0156$) and the lower graph to a high degree of supercooling ($\Omega = 0.5$). The numbers of the curve denote the relative temperature, i.e., the value of $\frac{t - t_m}{t_f - t_m}$. The graphs show that, the greater the supercooling, the thinner the layer of the melt in which a temperature change takes place (the higher the temperature gradients in the melt at the crystal surface). The expression for Ω is the same in outward form as the expression for θ in eq.(2), but its physical meaning is different. The quantity Ω is the parameter, the dimensionless supercooling, which remains constant during the time of the process, while θ is the dimensionless temperature of the crystal, varying with time. It may be asserted on the basis of the above that, if an acicular crystal has a shape differing from a paraboloid of revolution, then its surface is nonisothermal.

STAT

Declassified in Part - Sanitized Copy Approved for Release @ 50-Yr 2014/03/07 : CIA-RDP81-01043R004200090004-8

Declassified in Part - Sanitized Copy Approved for Release @ 50-Yr 2014/03/07 : CIA-RDP81-01043R004200090004-8

If the shape of the acicular crystal is known (for instance, by photographic recording), together with the rate of growth and the thermophysical parameters, then the temperature distribution on its surface may be found. Let the shape of the acicular crystal shown on Fig.2 be assigned by the empirical equation $R = f(\zeta)$. Then the temperature at the arbitrary point A(x, y, z) may be calculated by the aid of the following expression, derived under the assumption that the thermophysical parameters of both phases are the same and that these phases are isotropic:

$$t_A - t_m = \frac{w q_c \rho}{4\pi\lambda} \int_0^{2\pi} \int_{-\infty}^{0} \frac{R}{L}\left(-\frac{dR}{d\zeta}\right) e^{-\frac{w}{2a}[L+(z-\zeta)]} d\varphi\, d\zeta, \qquad (11)$$

where

$$L = \sqrt{(x-\xi)^2 + (y-\eta)^2 + (z-\zeta)^2}.$$

The calculation by the aid of eq.(11) requires a large amount of time, but with the appearance of computers, this problem has become solvable in practice.

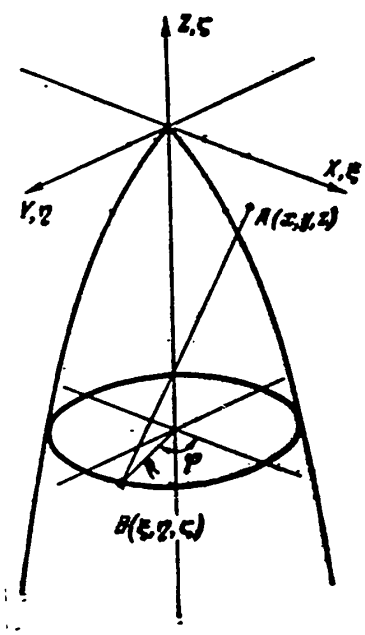

Fig.2 - Crystalline Needle of Arbitrary Shape

If the needle has the conical shape shown in Fig.3 (the dashed line showing the shape of the needle after a short time interval) then, putting $x = y = z = 0$ and $-\frac{dR}{d\zeta} = \tan\alpha = \text{const}$, eq.(11) may be integrated and the following equation obtained for the temperature of the point of the needle:

$$\frac{c(t_n - t_m)}{q_c} = (1-\cos\alpha)\left[1 - e^{-\frac{wl}{2a}\left(1+\frac{1}{\cos\alpha}\right)}\right]. \qquad (12)$$

If the growth velocity of the needle is high or the length of the conical portion is great, so that the exponent takes a value >4 and the expression in brackets becomes equal to unity, then this expression takes the following simple form, which no longer contains the velocity of growth of the needle:

STAT

Declassified in Part - Sanitized Copy Approved for Release @ 50-Yr 2014/03/07 : CIA-RDP81-01043R004200090004-8

Declassified in Part - Sanitized Copy Approved for Release @ 50-Yr 2014/03/07 : CIA-RDP81-01043R004200090004-8

$$\frac{c(t_n - t_m)}{q} = 1 - \cos\alpha. \tag{13}$$

The last expression may be put into the following form:

$$\frac{c(t_n - t_m)}{q_c} = \frac{\omega}{2\pi}, \tag{14}$$

where ω is the solid angle of the cone of the needle.

If in a supercooled melt there grows at constant velocity w a prismatic needle

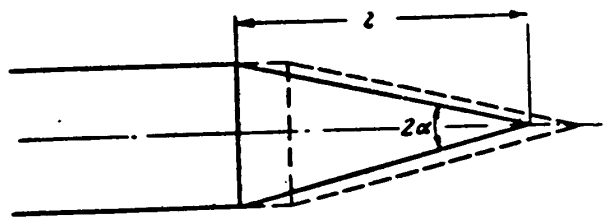

Fig.3 - Shape of Acicular Crystal Assumed in Calculating the Temperature of the Point

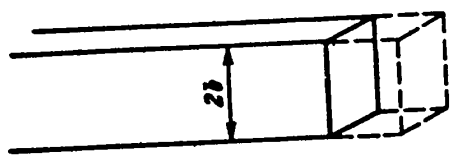

Fig.4 - Shape of Prismatic Crystal on which the Calculation was Based

of constant square section 2b × 2b (Fig.4), then at low velocities of growth we have the following temperature distributions on the front face:

center of face $$\theta = 2{,}244\frac{wb}{4a}, \tag{15}$$

vertex $$\theta = 1{,}122\frac{wb}{4a}, \tag{16}$$

temperature difference $$\Delta\theta = 1{,}122\frac{wb}{4a}, \tag{17}$$

or $$t_{c.f.} - t_{vert.} = 0{,}2805\frac{wbq_c\rho}{\lambda}. \tag{18}$$

STAT

Declassified in Part - Sanitized Copy Approved for Release @ 50-Yr 2014/03/07 : CIA-RDP81-01043R004200090004-8

Declassified in Part - Sanitized Copy Approved for Release @ 50-Yr 2014/03/07 : CIA-RDP81-01043R004200090004-8

The solutions for the simplest case of crystal growth have been obtained by the aid of the classical methods of mathematical physics. The application of modern methods of mathematical analysis, and the use of computers, which effect an extraordinary expansion in the field of practical application of analytical methods, will permit the solutions for more complex and interesting cases to be given.

5. Growth of a Crystal of Spherical Shape at Constant Surface Temperature in a Supercooled Melt of a Binary Alloy

The phenomenon of crystallization of alloys, it is well known, is determined by the combined action of the processes of diffusion and heat transfer. Since the regularities of the latter are expressed by the same differential equations, it has proved possible to apply the above regularities to the analysis of certain cases of crystallization of a binary alloy taking account of both the phenomena of heat transfer and of diffusion.

In an unbounded supercooled binary melt of a binary alloy, let one crystal of schematized, spherical shape grow. Let us assume that the melt and the crystallite in it are motionless, that the densities of both phases are the same, and that all thermophysical parameters are constants, and let us consider that the thermal and diffusion phenomena proceed independently (i.e., let us neglect the thermodiffusional phenomena). Assume that the process proceeds slowly, and that the concentrations on the phase boundaries correspond to the equilibrium diagram and remain constant during the course of the entire process, like the temperature on the surface of the crystal.

The state of the supersaturated melt at a sufficient distance from the crystal is assigned (point A on Fig.5).

In contrast to the case of crystallization of a pure substance, the value of the temperature on the phase boundary t_f cannot be assigned, but must be determined as a result of calculation.

Required, to determine the law of growth of the crystal, the temperature t_f and

STAT

Declassified in Part - Sanitized Copy Approved for Release @ 50-Yr 2014/03/07 : CIA-RDP81-01043R004200090004-8

Declassified in Part - Sanitized Copy Approved for Release @ 50-Yr 2014/03/07 : CIA-RDP81-01043R004200090004-8

the concentrations c_{lo} and c_{so} on the phase boundary, and the expressions for the temperature and concentration fields.

As result of an exact solution of this problem, the following picture of the

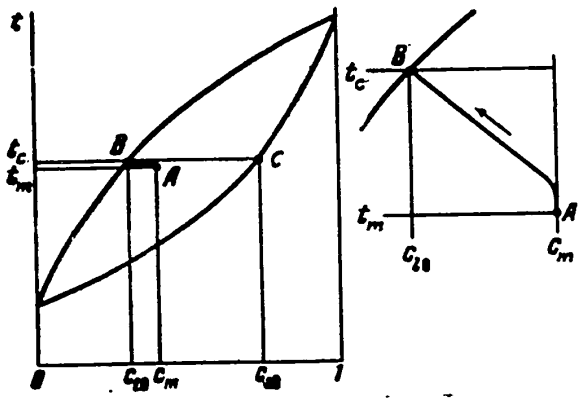

Fig.5 – Equilibrium Diagram of Binary Alloy and Path of the Figurative Point of the Melt (A – B) during the Growth of a Spherical or Acicular Crystal; the Figurative Point is Shown on the Right on an Enlarged Scale

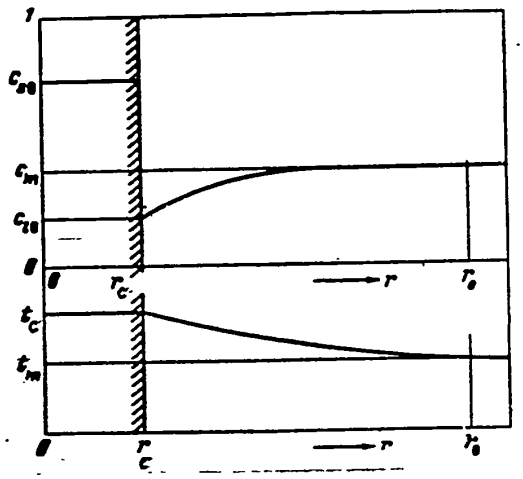

Fig.6 – Temperature and Concentration Fields during the Growth of a Spherical Crystal of a Binary Alloy

phenomenon was obtained (Bibl.3).

As in the case of crystallization on a plane wall, the law of crystal growth is

STAT

Declassified in Part - Sanitized Copy Approved for Release @ 50-Yr 2014/03/07 : CIA-RDP81-01043R004200090004-8

Declassified in Part - Sanitized Copy Approved for Release @ 50-Yr 2014/03/07 : CIA-RDP81-01043R004200090004-8

determined by the expression $r_c = \beta\sqrt{\tau}$. Figure 6 shows the temperature and concentration fields at a certain instant of time.

Let us trace the variation of temperature and concentration of the melt at a certain fixed point, for instance at distance $r = r_o$, as the crystallization front approaches it. At this point, at first, the temperature will increase at the same concentration, and, consequently, the figurative point of the alloy on the phase diagram will be displaced upward. In order to indicate clearly the path of the figurative point, a section of the phase diagram is shown on the right side of the figure with the temperature scale many times enlarged. As the front approaches the element of the melt under consideration, the concentration of the latter begins to change and the path is rotated leftward.

The relative temperature drop, i.e., the quantity $\frac{c(t_f - t_m)}{q_c}$, is thousands of times smaller than the concentration drop $\frac{c_m - c_{lo}}{c_{so} - c_{lo}}$, and their ratio is defined by the following relation (obtained from eq.(13) of reference (3) as $u \to 0$):

$$\frac{\dfrac{c(t_f - t_m)}{q_c}}{\dfrac{c_m - c_{lo}}{c_{so} - c_{lo}}} = \frac{D}{a}. \tag{19}$$

It follows that the process of growth is limited by diffusion. For small dimensions of the crystallite, the law of its growth is defined by the following expression, analogous to that previously given (it follows from eq.(6) of reference (3) as $\beta \to 0$):

$$r_c = \sqrt{2a\tau\frac{c_m - c_{lo}}{c_{so} - c_{lo}}}. \tag{20}$$

Owing to the high thermal conductivity of metals, a slight temperature drop $t_f - t_m$ is required to assure the necessary removal of the heat of crystallization (and can be determined from eq.(8) of the work cited).

6. Crystallization of a Binary Alloy on a Plane Wall

Let us consider the case of crystallization of a binary alloy under the condi-

STAT

Declassified in Part - Sanitized Copy Approved for Release @ 50-Yr 2014/03/07 : CIA-RDP81-01043R004200090004-8

Declassified in Part - Sanitized Copy Approved for Release @ 50-Yr 2014/03/07 : CIA-RDP81-01043R004200090004-8

tions of the famous classical problem of Stefan on the freezing through of the soil.

On a plane wall, a thin crust grows on a binary alloy. On its outer surface the constant temperature t_0 is maintained. The melt is motionless and superheated, and its initial temperature t_m is assigned (at a great distance from the front of crystallization - theoretically, at an infinite distance). The other general conditions of the problem and notation are the same as those in the problem discussed above.

The exact solution of this problem yielded the law of growth of the thin crust, the temperature and phase concentrations at the interface, and expressions for the temperature and concentration fields (Bibl.4).

The law for the growth of the fine crust remains the same as in the case of a single-component system:

$$\xi = \beta \sqrt{\tau}.$$

For a very slow process, β is defined by the following expression [obtained from eq.(6) (Bibl.4) as $u \to 0$]:

$$\beta = \frac{2\sqrt{D}}{\sqrt{\pi}} \frac{c_m - c_{l0}}{c_{s0} - c_{l0}}. \tag{21}$$

The variation of temperatures and concentrations at a certain instant of time are represented by the heavy line on the graph of Fig.7, while the lapse of a certain interval of time is represented by the dashed line.

Thus, the temperature and concentration curves are elongated in the positive direction of the abscissa axis.

The concentration of the high-melting component in the melt falls toward the front of crystallization. This takes place as a result of the fact that the crystal, as it were, sucks out of the melt the high melting component necessary for its own construction, as a result of which the concentration of the high melting component in the melt decreases in front of the crystallization front; this, in turn, causes diffusion of the high melting component from the deep layers of the melt toward the crystal.

STAT

Declassified in Part - Sanitized Copy Approved for Release @ 50-Yr 2014/03/07 : CIA-RDP81-01043R004200090004-8

Declassified in Part - Sanitized Copy Approved for Release @ 50-Yr 2014/03/07 : CIA-RDP81-01043R004200090004-8

At the same time the concentration of the low melting component at the front of crystallization increases, as a result of which it diffuses into the melt.

The layer of melt in which there is a temperature drop, ahead of the crystallization front, is many times as thick as the layer in which the concentration varies.

Let us consider the variation of temperature and concentration in a fixed ele-

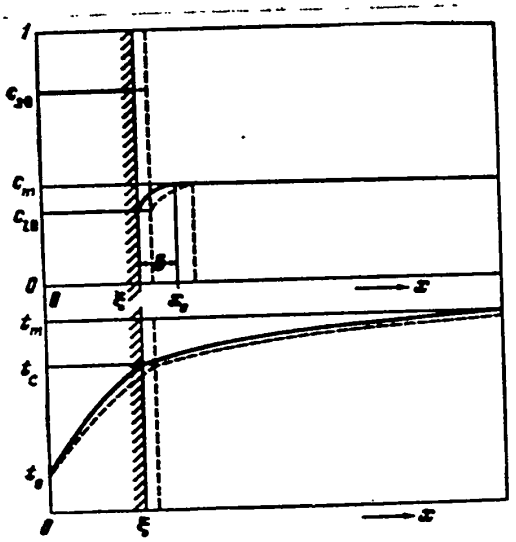

Fig.7 - Fields of Temperatures and Concentrations during Crystallization on a Plane Wall

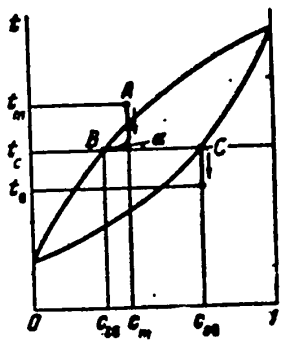

Fig.8 - Path of the Figurative Point of an Alloy on the Phase Diagram during Crystallization of a Binary Alloy on a Plane Wall

ment of the melt as the front of crystallization approaches it (Fig.8).

At first the temperature of the melt falls with its concentration remaining constant, and the figurative point is displaced downward along the vertical straight line, intersects the liquidus, and passes over into the region of supersaturation.

The variation of concentration begins in immediate proximity to the front of crystallization, and as a result the path of the figurative point sharply turns to the left and passes over into an almost horizontal straight line.

The slope of this straight line (more accurately the tangent) toward the path at the point of its encounter with the liquidus line (tan α on Figs.8 and 9) is defined by the following expressions for the extreme cases of the process:

STAT

Declassified in Part - Sanitized Copy Approved for Release @ 50-Yr 2014/03/07 : CIA-RDP81-01043R004200090004-8

Declassified in Part - Sanitized Copy Approved for Release @ 50-Yr 2014/03/07 : CIA-RDP81-01043R004200090004-8

infinitely slow process $\beta \to 0$: $\frac{dt_l}{dc_l} = \frac{t_m - t_f}{c_p - c_{l0}} \sqrt{\frac{D}{a}}$, (22)

infinitely rapid process $\beta \to 0$: $\frac{dt_l}{dc_l} = \frac{t_m - t_f}{c_m - c_{l0}} \frac{D}{a}$. (23)

For nonmetallic substances, $\frac{D}{a}$ is of the order of 10^{-2}, for metals 5×10^{-4}. Consequently, on the crystallization of binary systems of any substances, this part of the path of the figurative point is an almost horizontal straight line.

Thus, ahead of the front of crystallization, a layer of supersaturated melt

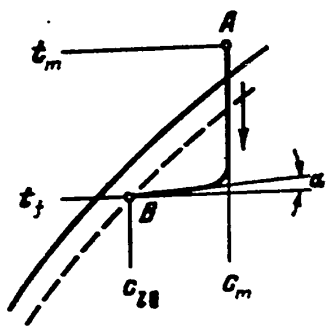

Fig.9 - Paths of Figurative Point of Melt in the Case of the Displacement of the Liquidus Line (Under Supercooling on the Front of Crystallization)

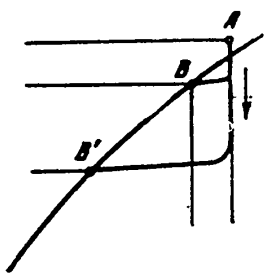

Fig.10 - Paths of Figurative Point of Melt during Relatively Rapid and Relatively Slow Process of Crystallization of a Binary Alloy on a Plane Wall

arises, in spite of the fact that the melt is superheated over a considerable distance from the front, and that the equilibrium state is assigned on the phase boundary.

The shape of the path of the figurative point of the melt, however, remains unchanged if supercooling of the phase boundary is assumed. Figure 9 shows such a case, the dashed line representing the liquidus under the conditions of a real process during supercooling on the phase boundary.

The value of the maximum supersaturation depends on the intensity of the pro-

STAT

Declassified in Part - Sanitized Copy Approved for Release @ 50-Yr 2014/03/07 : CIA-RDP81-01043R004200090004-8

Declassified in Part - Sanitized Copy Approved for Release @ 50-Yr 2014/03/07 : CIA-RDP81-01043R004200090004-8

cess. Figure 10 shows schematically the path of the figurative point of the melt for a relatively rapid and a relatively slow process.

With a rapid process, a plane front, of course, cannot exist, since the crystallites ahead of it are necessarily thrown down.

To solve this question with respect to the slow process, the time factor must also be taken into account. Considering the curves of temperatures in concentrations before the front of crystallization on Fig.7 and the paths of the figurative point on Fig.8, we see that its maximum departure from the line of the liquidus is observed where a change in the concentration begins in the melt ahead of the front (the coordinate x_0 on Fig.7).

The boundary of this layer in which a variation of the concentration takes place is easily determined from eq.(6) (Bibl.4); as $\beta \to 0$ we get the following expression

$$x_0 = \xi \frac{4\sqrt{D}}{\beta}. \qquad (24)$$

The value of the maximum supersaturation $c_m - c_{l0}$ which is attained in the cross section x_0 is easily found from eq.(21):

$$c_m - c_{l0} = \frac{\sqrt{\pi}}{2\sqrt{D}} (c_{s0} - c_{l0}) \beta.$$

Thus the value of the maximum supersaturation $c_m - c_{l0}$ is directly proportional to β, i.e., it decreases with decreasing intensity of the process, while the distance x_0 at which this occurs is inversely proportional to β, i.e., it increases without limit as β decreases. At the same time the duration of this process sharply increases, and consequently, the probability of the precipitation of crystals even in a slightly supersaturated melt also increases.

Consequently there are still no grounds for holding that on a sharp slowing of the process, it is possible to obtain a stable plane front of crystallization. This question may be answered if we know the rates of nucleation of centers of crystallization for binary systems as a function of the degree of supersaturation.

STAT

Declassified in Part - Sanitized Copy Approved for Release @ 50-Yr 2014/03/07 : CIA-RDP81-01043R004200090004-8

Declassified in Part - Sanitized Copy Approved for Release @ 50-Yr 2014/03/07 : CIA-RDP81-01043R004200090004-8

We note once again that all that has been set forth above relates to the case of crystallization with removal of heat across the crystallization front.

Such a pattern of temperature and concentration fields, however, will also be observed in the case where the formation of a crystal surrounded by melt on all sides is accompanied by a slight rise in the temperature of the melt. In consequence of this a heat flow toward the crystal arises, and the region of greatest supersaturation is shifted toward the crystal surface.

The phenomenon of the precipitation of crystals ahead of the crystallization front has long been known, but up to now there was no satisfactory explanation for it.

Modern researches show that the crystallites arising at a certain distance from the front of crystallization sometimes even cover a layer of the matrix ahead of the front, as a result of which a layer of matrix is formed in the crystal. This is observed with the relatively rapid growth of the crystals from the solution in the absence of mixing of the solution [see reference (5), pp.135, 163, and also reference (6), pp.180 and 372].

And, finally, the unusually extensive occurrence in nature of globular crystallization, by which the crystals are formed ahead of the front, shows that under real conditions the formation of crystals ahead of the front is more probable than the growth of crystals on the front of crystallization itself.

Conclusions

1. The surface of a crystal of polyhedral shape, growing in a motionless, supercooled melt, is nonisothermal; the temperature drop at the surface of a crystal of cubic shape is determined by eq.(7).

2. A crystalline needle grown at constant rate in a motionless supercooled melt at constant temperature has the shape of a paraboloid of a revolution; if it does not have this shape, then its surface is nonisothermal.

STAT

Declassified in Part - Sanitized Copy Approved for Release @ 50-Yr 2014/03/07 : CIA-RDP81-01043R004200090004-8

Declassified in Part - Sanitized Copy Approved for Release @ 50-Yr 2014/03/07 : CIA-RDP81-01043R004200090004-8

3. On crystallization of a binary alloy on a plane wall, a layer of supersaturated melt appears before the front of crystallization, even if the melt is superheated at a sufficient distance from the front, while equilibrium concentrations are realized on the phase boundary.

BIBLIOGRAPHY

1. Ivantsov,G.P. - Dok. AN SSSR, Vol.58 (1947), p.567

2. Danilov,V.I., and Malkin,V.I. - On the Experimental Verification of the Theory of Crystal Growth. Problems of Metal Science and Physics of Metals. Collected Papers of Institute of Metals and Physics of Metals, TsNIIChM. Collection 2. Metallurgizdat, Moscow (1951)

3. Ivantsov,G.P. - Dok. AN SSSR, Vol.83 (1952), p.573

4. Ivantsov,G.P. - Dok. AN SSSR, Vol.81, No.2 (1951), p.172

5. Kuznetsov,V.D. - Crystals and Crystallization. Gostekhizdat, Moscow (1953), State Publishing House for Foreign Literature, p.411

6. Bakli,G. (Buckley,H.) - The Growth of Crystals. State Publishing House for Foreign Literature (1954), p.406

STAT

Declassified in Part - Sanitized Copy Approved for Release @ 50-Yr 2014/03/07 : CIA-RDP81-01043R004200090004-8

Declassified in Part - Sanitized Copy Approved for Release @ 50-Yr 2014/03/07 : CIA-RDP81-01043R004200090004-8

THE INFLUENCE OF MODIFIERS ON THE PROCESS OF INGOT CRYSTALLIZATION

by

V.Ye.Neymark and A.I.Dukhin

One of the principal problems of metallurgical production is improving ingot quality. Investigators are faced by the problem of decreasing surface defects and shrinkage holes in an ingot and increasing its uniformity in both structure and composition. The existence of surface defects, shrinkage holes and chemical inhomogeneity, as well as inhomogeneity of structure, are connected with the rate of formation in growth of crystals. By changing the rate of solidification, one may influence the deformation of the crust formed, which, to a considerable degree determines the quality of the ingot surface. By varying the direction of the heat removal along the height of the ingot, the depths at which the shrinkage holes lie may be reduced. By increasing the rate of crystallization, the chemical inhomogeneity of the ingot may be decreased.

In plant practice one must often find ways to eliminate the coarse structure during crystallization of an ingot. It is particularly desirable to avoid the appearance of a columnar zone, whose presence leads to the formation of cracks during the rolling of the ingots. The thicker a columnar crystal, the larger the quantity of impurities that are forced out by the crystallization front towards its boundaries, and the greater the danger of the occurrence of cracks along the boundaries between the crystals. In this connection, the work in search of methods of producing ingots with a finely crystalline and uniform structure is very timely and urgent.

The ingot quality may be improved by various influences on the crystallization process. The modification of the melt with small amounts of additives has a substantial effect on the parameters of crystallization.

Four kinds of modifiers are distinguished: 1) insoluble additives, activated in the solid metal; 2) insoluble isomorphic additives activated in the liquid metal;

STAT

Declassified in Part - Sanitized Copy Approved for Release @ 50-Yr 2014/03/07 : CIA-RDP81-01043R004200090004-8

Declassified in Part - Sanitized Copy Approved for Release @ 50-Yr 2014/03/07 : CIA-RDP81-01043R004200090004-8

3) additives soluble in the liquid metal and insoluble in the solid metal; 4) additives soluble in both the liquid and the solid metal. All these types of modifiers should decrease the work of formation of the crystal nuclei, which will help to increase the number of centers of crystallization in the supercooled melt, to limit crystal growth and refine ingot structure.

V.I.Danilov and V.Ye.Neymark (Bibl.2) have shown that insoluble additives, for example lead oxides, increase the rate of formation of centers of crystallization in bismuth and tin. On superheating a melt, oxides of lead are deactivated and the rate of nucleation in these metals decreases. The purification of bismuth and tin from the active additives by filtration of the melt in vacuo leads to the same results as deactivation does.

Lead oxides that had not been in contact with the solid phase of bismuth and tin were not active with respect to the process of crystal nucleation. When incorporated in a melt, they do not decrease the capacity of the melt for supercooling. It is only after bismuth and tin containing lead oxides have commenced to crystallize that the additive is "activated" and on remelting can decrease, tens of times, the region of metastable existence of the melt.

After the metal has begun to crystallize, the additive "grows into" the solid phase, and on the boundary between the crystals of the principal substance and of the additive, "molecular contact" arises, accompanied by "overpacking" of the molecules in accordance with the interaction between the molecules of additive and the solidified material. In the boundary crystalline layer, during its formation, elements of structural correspondence with the crystal of the principal substance must be present. It is also possible for such a crystalline layer to fail to melt above the melting point of the base metal, as a result of the great molecular interaction between the additive and the substance being crystallized.

A melt containing activated insoluble additives does not begin to crystallize at the equilibrium temperature, since in this case the thermodynamic potentials of

STAT

Declassified in Part - Sanitized Copy Approved for Release @ 50-Yr 2014/03/07 : CIA-RDP81-01043R004200090004-8

Declassified in Part - Sanitized Copy Approved for Release @ 50-Yr 2014/03/07 : CIA-RDP81-01043R004200090004-8

the two phases are equal. The rate of growth of one phase at the expense of the other will be zero. In order for crystallization to begin, the system must be brought out of equilibrium: the temperature of the melt must be lowered, i.e., the liquid must be supercooled. Since in the supercooled melt, the thermodynamic potential of the crystalline layer on the activated additive is less than the thermodynamic potential of the liquid, centers of crystallization will be formed on these crystallites, if they are larger than the critical nucleus. The rate of their formation, in spite of low degrees of supercooling of the melt containing activated additives, must likewise depend on the degree of supercooling, as in the case of an unmodified melt.

Danilov and Neymark (Bibl.3) have proposed the introduction of a "seed" in a melt that is not strongly superheated, in order to decrease the work of nucleation. Activated insoluble additives are used in the seed. On these additives, in the supercooled melt, a large number of centers of crystallization are formed, leading to refinement of the ingot structure.

Danilov, Kazachkovskiy and Lobkovskiy (see Bibl.4) investigated the activation of insoluble impurities in salol. These authors have established the following regularities: the activation of impurities proceeds in contact with the crystals of salol in a definite temperature range and increases with increasing time of this contact.

Lesnik and Danilov (Bibl.5) have found that an insoluble additive, rock salt, is isomorphic with β-salol. The activation of rock salt takes place in liquid β-salol. The superheating of salol 70°C above its melting point does not decrease the rate of formation of crystallization centers in the supercooled melt, but, on the contrary, increases it.

Danilov and Kamenetskaya (Bibl.6) have established that the modifier potassium, which is soluble in liquid mercury and insoluble in solid mercury, increases the rate of formation of centers of crystallization at optimum concentration of the

STAT

Declassified in Part - Sanitized Copy Approved for Release @ 50-Yr 2014/03/07 : CIA-RDP81-01043R004200090004-8

Declassified in Part - Sanitized Copy Approved for Release @ 50-Yr 2014/03/07 : CIA-RDP81-01043R004200090004-8

additive.

Kogan, Neymark, Piletskaya and Entin (Bibl.7) have studied the influence of the soluble modifiers boron, titanium, aluminum, vanadium and zirconium on the processes of crystallization and recrystallization of steel. These studies have shown that ingots without additives, 50 mm in diameter, are of columnar structure. Additions of boron in an amount of 0.003 - 0.004% refine the structure of the ingot. With increasing boron concentration in the steel, the columnar crystals again appear, and

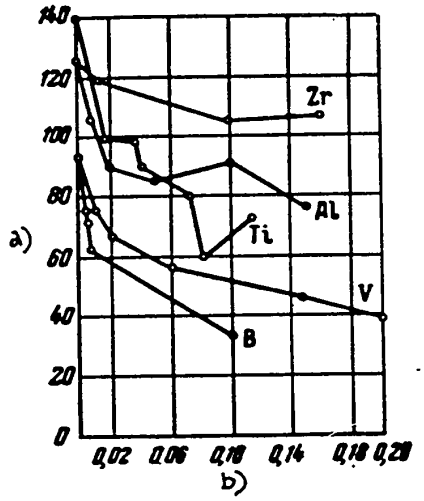

Fig.1 - Size of Austenite Grain of Primary Crystallization of Steel as a Function of the Content of Boron, Vanadium, Titanium, Aluminum and Zirconium in the Cast (Unworked) Steel

a) Size of austenite grain of primary crystallization, μ; b) Concentration of additive, %

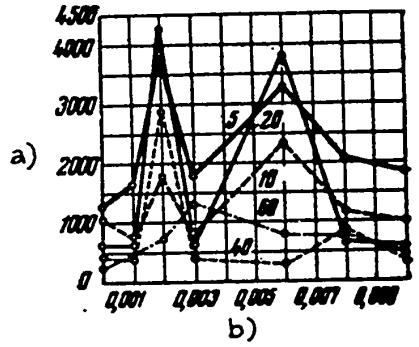

Fig.2 - Relation between Rate of Formation of Centers of Crystallization of Ferrite Grains and the Boron Content (the Figures Near the Curves Indicate the Holding Time in sec)

a) Rate of formation of centers of crystallization of ferrite grains, $1/mm^3$ sec; b) Boron concentration, %

at concentration 0.05 - 0.08%, the columnar crystals become thicker than in ingots without additives. Aluminum and vanadium have the same action, but at concentrations about 10 times as high as boron. The effect of additions of titanium on ingot

STAT

Declassified in Part - Sanitized Copy Approved for Release @ 50-Yr 2014/03/07 : CIA-RDP81-01043R004200090004-8

Declassified in Part - Sanitized Copy Approved for Release @ 50-Yr 2014/03/07 : CIA-RDP81-01043R004200090004-8

structure is somewhat different. On addition of up to 0.3% of titanium, there is a gradual structural refinement of the ingot. Additions of zirconium in the same concentrations as aluminum have no effect on the primary structure of the ingot.

The modifiers boron, vanadium titanium, aluminum and zirconium refine the austenite grain of primary crystallization, boron showing the greatest refinement, and zirconium the least (Fig.1). Aluminum, titanium and vanadium, restrain the growth of the secondary austenite grain, while small additions of boron increase its growth. The additions of boron at optimum concentrations (Bibl.8) at the same time increase both the rate of nucleation and the rate of growth of ferrite grains on their segregation from austenite (Figs.2 and 3). On recrystallization of steel in

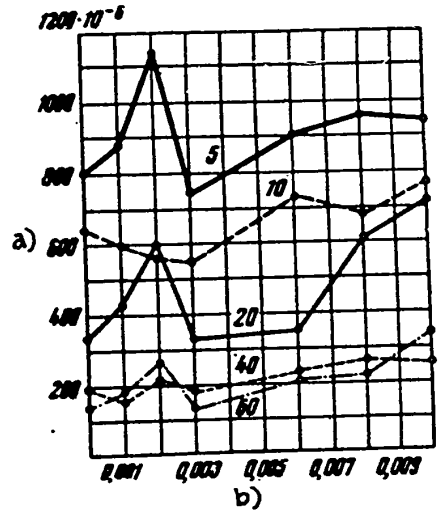

Fig.3 - Relation of Rate of Growth of Ferrite Grains to the Boron Content (the Figures Near the Curves Show the Holding Time in sec)

a) Rate of grain growth, mm/sec; b) Boron concentration, %

the temperature range 600 - 400°C, small additions of boron decrease the rate of formation of pearlite grains.

Since boron, even at very low concentrations, exerts a considerable influence

STAT

Declassified in Part - Sanitized Copy Approved for Release @ 50-Yr 2014/03/07 : CIA-RDP81-01043R004200090004-8

Declassified in Part - Sanitized Copy Approved for Release @ 50-Yr 2014/03/07 : CIA-RDP81-01043R004200090004-8

on the parameters of crystallization, studies were made to elucidate the question of the state in which boron is present in steel, whether as a soluble or insoluble impurity. By measuring the microhardness of the ferrite segregated from austenite, it was found that boron lowers the hardness of steel. The fact that boron increases the growth of ferrite and austenite crystals, decreases the rate of formation of pearlite grains, and decreases the hardness of the ferrite, shows that the boron is in solid solution. Measurements of the diffusion of boron in steel show it to be soluble up to 0.01% in the solid steel. At higher boron concentrations, a boron-containing phase is precipitated along the primary crystallization austenite grain boundaries, and it is this that probably retards its growth. Chemical analysis also proved boron to be present in solid solution.

These studies indicate that boron is a modifier soluble in both liquid and solid steel, and that it must affect the surface tension between the old phase and the new one being formed. The formation of a critical nucleus R_c strongly depends on the surface tension σ between the old phase and the new phase, since R_c is directly proportional to σ^3. When boron decreases the σ, the rate of formation of centers of crystallization of the new phase in the old phase is increased (transition from liquid to solid state, formation of grains of ferrite in the austenite). When, however, the boron increases the value of σ, then the rate of formation of centers of crystallization decreases (the formation of pearlite grains in austenite, and of austenite grains in pearlite).

The case when boron, at concentrations higher than optimum, decreases the rate of formation of centers of crystallization, is probably connected with the tendency of boron to increase the energy of activation during the transition of the steel atoms from the liquid state to the solid (Bibl.5). Small additions of boron show a favorable effect on the properties of steel as well. 0.003% of boron increases the hardenability of the steel. The relative influence of such an addition is about 100 - 150 times as great as the action of the same quantity of manganese or

STAT

Declassified in Part - Sanitized Copy Approved for Release @ 50-Yr 2014/03/07 : CIA-RDP81-01043R004200090004-8

Declassified in Part - Sanitized Copy Approved for Release @ 50-Yr 2014/03/07 : CIA-RDP81-01043R004200090004-8

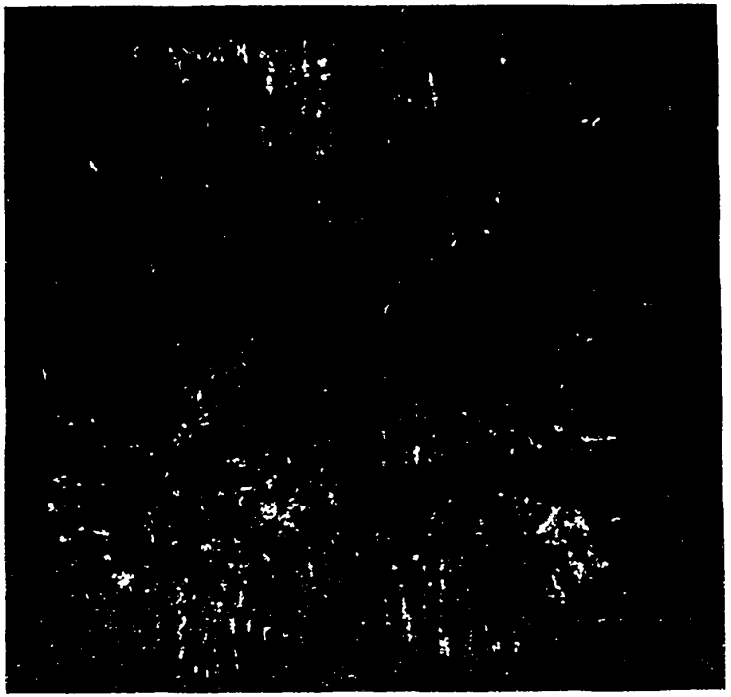

Fig.4 - Macrostructure of St.3 Ingot

Without Additives

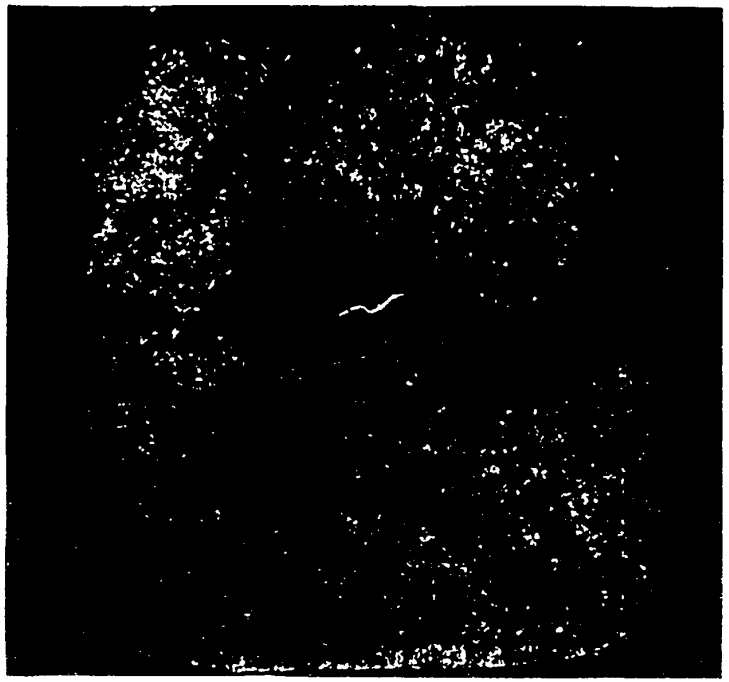

Fig.5 - Macrostructure of Ingot of

St.3 with 0.005% of Boron

STAT

Declassified in Part - Sanitized Copy Approved for Release @ 50-Yr 2014/03/07 : CIA-RDP81-01043R004200090004-8

Declassified in Part - Sanitized Copy Approved for Release @ 50-Yr 2014/03/07 : CIA-RDP81-01043R004200090004-8

nickel.

In connection with the results obtained on the influence of boron, titanium and aluminum on the growth of columnar crystals in an ingot 50 mm in diameter, it appears to be of practical interest to investigate the effect of these modifiers on the structure of a larger ingot (120 × 120 mm), approaching the cross section of the

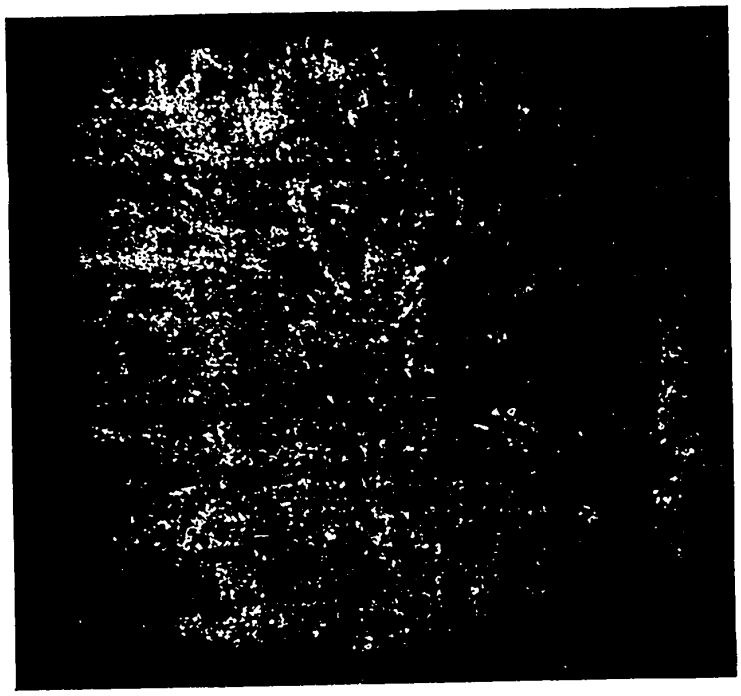

Fig.6 - Macrostructure of Ingot of St.3 with 0.1% of Titanium

ingots produced on continuous casting machines.

Neymark and Dukhin studied the influence of modifiers on the structure of carbon, ferrite and austenite steels. In an St.3 ingot without additives, three zones were found: on the periphery, a finely crystalline zone; then a columnar zone; and at the center, an equiaxial zone (Fig.4). Additions of 0.003 - 0.005% of boron sharply refine the structure of the ingot (Fig.5). On introduction of 0.02% of boron into steel, the structure obtained was inhomogeneous and somewhat coarser than in an ingot with lower concentrations of the additive. In larger ingots modified

STAT

Declassified in Part - Sanitized Copy Approved for Release @ 50-Yr 2014/03/07 : CIA-RDP81-01043R004200090004-8

Declassified in Part - Sanitized Copy Approved for Release @ 50-Yr 2014/03/07 : CIA-RDP81-01043R004200090004-8

with titanium, the structure is entirely different. The addition of titanium yielded a homogeneous structure with fine crystals (Fig.6). This characteristic structure is obtained on incorporation of 0.08 to 0.3% of titanium with the steel. The addition of aluminum in quantities from 0.03 to 0.1% results in no appreciable ingot structure refinement. Larger additions (up to 0.2%) even increase the width of the columnar crystals.

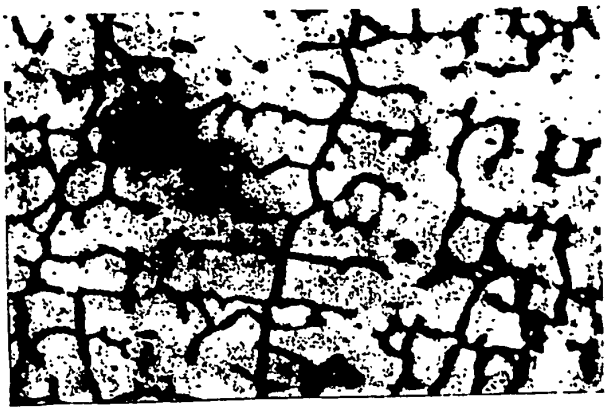

Fig.7 - Dendritic Structure of Ingot (Diameter 90 mm) of Austenite Steel 1Kh18N9T. 200 ×

The influence of boron and titanium on the structure of ferrite and austenite steels was also investigated. The addition of boron and titanium limits the growth of columnar crystals in ferrite steel on casting the melt at a temperature close to the temperature corresponding to the liquidus line. By heating the modified melt 100°C above the temperature corresponding to the liquidus line, columnar crystals are obtained in the ingot. The structure of an ingot of austenite steel 1Kh18N9T could not be refined either by addition of boron, or by seeding; only finer columnar crystals were obtained.

Measurements of supercooling showed that the modifiers exert a slight influence on the boundary of metastability of Kh18N9 austenite steel. This is evidence that the work of formation of the critical nuclei, even in modified steel Kh18N9, is very great, and that deep supercooling is required for its appearance. But ingots of austenite steel Kh23N18 may be refined by modification with boron or titanium, followed by low-temperature pouring of the melt. The dendritic structure in the ingot so obtained was investigated. In the austenite steel the dendrites are easily detected. In ferrite steel, however, the dendrites are not revealed by electrolytic

STAT

Declassified in Part - Sanitized Copy Approved for Release @ 50-Yr 2014/03/07 : CIA-RDP81-01043R004200090004-8

Declassified in Part - Sanitized Copy Approved for Release @ 50-Yr 2014/03/07 : CIA-RDP81-01043R004200090004-8

action. The modifiers boron and titanium show no appreciable effect on the dendritic structure of ingots of steel 1Kh18N9T (Fig.7) and steel Kh23N18 (Fig.8) crystallized in a chill mold 90 mm in diameter.

To increase the supercooling on the front of crystallization, we employed a technique permitting the casting of specimens in copper tubes 3 mm in diameter. The steel was drawn, by the aid of a rubber bulb, into a tube with its lower end submerged in the melt (Fig.9). This technique was used to prepare specimens of austenite steels Kh18N9 and Kh23N18 with additions of boron and titanium.

Fig.8 - Dendritic Structure of Ingot (Diameter 90 mm) of Kh23N18 Austenite Steel with 0.5% of Titanium. 200 ×

In the specimens of Kh18N9 austenite steel, a narrow zone of small unoriented dendrites was formed on the periphery. When the heat removal is so rapid, the branches of the dendrite become finer and change their shape. The addition of 0.01% of boron to steel Kh18N9 refines the dendrites in the central zone of the specimen as well (Fig.9). The refinement of the dendritic structure in the specimen is also obtained by the introduction of 0.5% of titanium into the steel. An increase in the rate of crystallization of Kh23N18 austenite steel leads to a strong structural refinement. The addition of 0.005% of boron produces a still greater refinement of the dendritic structure of this steel (Fig.10). The photograph presented, shows that the modifiers have a more effective influence on the rate of nucleation of centers with increasing supercooling on the front of crystallization.

The influence of the modifiers boron and titanium on the size of the austenite grain revealed in the specimens by destruction of the liquation during diffusion

STAT

Declassified in Part - Sanitized Copy Approved for Release @ 50-Yr 2014/03/07 : CIA-RDP81-01043R004200090004-8

Declassified in Part - Sanitized Copy Approved for Release @ 50-Yr 2014/03/07 : CIA-RDP81-01043R004200090004-8

annealing, was less than it was on the size of the dendrites. The refinement of the dendrites by modification and by increasing the heat removal, may lead to a decrease in the chemical inhomogeneity of the ingot, since with decreasing dendrite size, the diffusion paths of the liquated elements during diffusion annealing are shortened.

The modifiers boron and titanium have less of an effect on the ingot structure when the steel is cast at high temperatures. The fact that the temperature of the melt does have an influence on the structure of an ingot modified by soluble additives speaks for the view that this phenomenon is due to the deactivation of the insoluble additives and the change in the degree of supercooling on the front of crystallization.

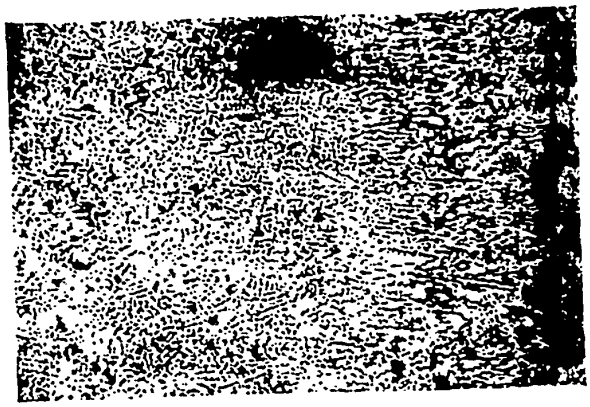

Fig.9 - Dendritic Structure of Kh18N9 Steel with 0.01% of Boron Crystallized in a Copper Tube (3 mm in Diameter). 200 ×

We have established that if one first superheats aluminum, 5% aluminum bronze, or Kh-27 ferrite steel, thus deactivating the insoluble impurities, and pours them at low temperatures through a stopper, a columnar ingot structure will result. If, however, the melt was not superheated above the deactivation point for the insoluble additives, then a finely crystalline structure is always obtained on low-temperature casting.

The same phenomenon is also observed in a modified metal. The modifiers only increase the superheat temperature at which deactivation of the insoluble additives does not take place (Bibl.10).

In casting the superheated melt into a chill mold, the supercooling on the front of crystallization will be low until the heat of superheat has been removed from the melt. A decrease in the supercooling on the front of crystallization leads

STAT

Declassified in Part - Sanitized Copy Approved for Release @ 50-Yr 2014/03/07 : CIA-RDP81-01043R004200090004-8

Declassified in Part - Sanitized Copy Approved for Release @ 50-Yr 2014/03/07 : CIA-RDP81-01043R004200090004-8

to a decrease in the rate of formation of critical three-dimensional nuclei, and in this connection the probability of the growth of columnar crystals due to the appearance of two-dimensional nuclei will be increased, since the work of formation of two-dimensional nuclei is far less than that of three-dimensional nuclei, and the columnar crystals can grow even at a slight supercooling on the front of crystallization.

Danilov and Neymark (Bibl.2) have proposed a technique of determining the deactivation of insoluble additives. The technique of deactivating insoluble additives is based on the determination of the relation between the original structure of the finely crystalline cast specimen and the final structure after its melting and beginning of crystallization in one and the same crucible. The study of deactivation is conducted on the original finely crystalline small ingots, and it determines the superheat temperature at which all relation between the original and final structures disappears. The study of the activation of insoluble additives is conducted on the original coarsely crystalline specimens. If the structure after melting, and a certain superheating is refined, then this is evidence that activation of the additives in the solid state took place. If, however, the structure is refined after a high degree of superheat, then there are grounds for considering that the isomorphic insoluble additives in the melt were activated.

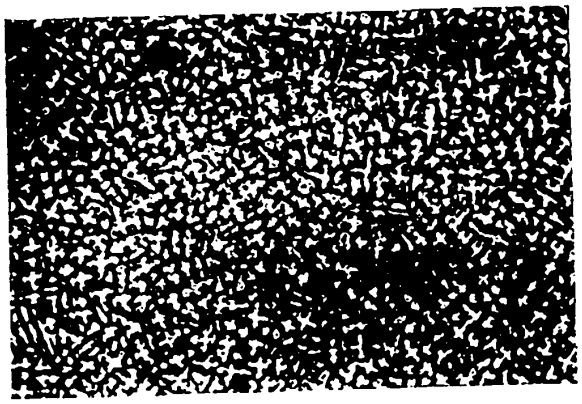

Fig.10 - Dendritic Structure of Kh23N18 Steel with 0.005% of Boron, Crystallized in a Copper Tube (3 mm in Diameter). 200 ×

On melting and superheating a finely crystalline small ingot of Kh27 steel without an additive, to a temperature 5 - 10°C above the liquidus, the relation be-

STAT

Declassified in Part - Sanitized Copy Approved for Release @ 50-Yr 2014/03/07 : CIA-RDP81-01043R004200090004-8

Declassified in Part - Sanitized Copy Approved for Release @ 50-Yr 2014/03/07 : CIA-RDP81-01043R004200090004-8

tween the original and final structures is maintained. On a superheat of 30 - 40°C, this relation is lost, and a partial deactivation of the insoluble additives takes place. A superheat of 100°C leads to almost complete deactivation of the insoluble additives. The addition of 0.25% of titanium to steel Kh27 increases the temperature of the activation of the additive, and the heating of the melt to 40°C above the liquidus does not lead to the disappearance of the relation between the original and final structures.

A finely crystalline small ingot of Kh23N18 steel after melting and slight superheat (2 - 3°C) above the liquidus, becomes coarsely crystalline, and a deactivation of the insoluble additive takes place. If 0.5% of titanium is present in Kh23N18 steel, the deactivation temperature is raised by about 100°C. The heating of the original finely crystalline small ingots of Kh18N9 steel 5 - 10°C above the liquidus led to almost total deactivation of the insoluble additives.

The increase in the deactivation temperature of Kh27 steel with 0.25% of titanium added, and of Kh23N18 steel with 0.5% of titanium added, may be explained by the formation of insoluble impurities in the steel, which, after solidification of the melt, become activated in the solid steel. When steel is melted together with titanium, the activated insoluble impurities, even on superheating of the liquid 100°C above the liquidus, still do not lose their activity and serve as centers of crystallization in the supercooled melt.

The activation of impurities was observed on melting a small ingot of Kh18N9 steel with a columnar structure, and superheating the melt 150°C above the temperature corresponding to the liquidus line. The structure in the solidified specimen was finely crystalline. This phenomenon is evidence that isomorphic impurities, on which additional centers of crystallization were formed, were activated in the superheated melt.

These results show that by modification of a melt with small amounts of additives, the structural and chemical inhomogeneity of the ingot may be decreased. A

STAT

Declassified in Part - Sanitized Copy Approved for Release @ 50-Yr 2014/03/07 : CIA-RDP81-01043R004200090004-8

Declassified in Part - Sanitized Copy Approved for Release @ 50-Yr 2014/03/07 : CIA-RDP81-01043R004200090004-8

further investigation of the mechanism of modification by measuring the supercooling of the steel, the linear rate of crystallization, and the surface tension on the interface between melt and inert gas, will provide an opportunity for scientific approach to the problem of selecting the optimum modifier concentration for one steel or another.

Conclusions

1. The modifiers boron and titanium differently affect crystal growth in an ingot of carbon steel: additions of boron limit the growth of columnar crystals, while additions of titanium encourage the growth of very fine columnar crystals.

2. On crystallization of the melt in chill molds 50 mm in diameter, the modifiers boron and titanium retard the growth of columnar crystals of Kh27 ferrite steel and show no substantial effect on the growth of crystals of Kh18N9 austenite steel.

3. The increase of heat removal, i.e., the increase in the degree of supercooling on the crystallization front, leads to a more effective influence of the modifiers on the rate of formation of centers of crystallization in austenite steel.

4. On increasing the temperature of a melt modified with soluble additives, the growth of columnar crystals is increased. This phenomenon may be explained by two causes: the presence in ferroboron and ferrotitanium, of active insoluble impurities that are deactivated on superheating of the liquid steel; and by the decrease in the supercooling on the crystallization front.

5. The modifier titanium increases the temperature of deactivation of insoluble impurities in Kh27 steel. This is evidence that the ferrotitanium contains activated insoluble impurities encouraging the formation of centers of crystallization.

BIBLIOGRAPHY

1. Neymark, V.Ye. - The Influence of Modifiers and of the Crystallization Conditions

STAT

Declassified in Part - Sanitized Copy Approved for Release @ 50-Yr 2014/03/07 : CIA-RDP81-01043R004200090004-8

Declassified in Part - Sanitized Copy Approved for Release @ 50-Yr 2014/03/07 : CIA-RDP81-01043R004200090004-8

on the Quality of the Ingot Crust. Continuous Casting of Steel. Pub.Dept., Academy of Sciences USSR, (1956)

2. Danilov,V.I., and Neymark,V.Ye. - Zhur.Teor.Eksp.Fiz., Vol.10, No.8 (1940), p.942

3. Danilov,V.I., and Neymark,V.Ye. - Metallurg, Vol.10 (1936), p.34

4. Danilov,V.I., Kazachovskiy,O.D., and Lobkovskiy,Ya.M. - Problems of Metal Science and the Physics of Metals. Metallurgizdat (1949)

5. Lesniki,A.G., and Danilov,V.I. - Questions of Physics of Metals and of Metal Science. Izv.AN UkrSSR, Vol.2 (1950), p.80

6. Danilov,V.I., and Kamenetskaya,D.S. - Problems of Metal Science and of the Physics of Metals (1951)

7. Kogan,V.I., Neymark,V.Ye., Piletskaya,I.B., and Entin,R.I. - Problems of Metal Science and of the Physics of Metals (1949)

8. Neymark,V.Ye., and Peletskaya,I.B. - Problems of Metal Science and of the Physics of Metals (1952)

9. Neymark,V.Ye. - Zavod.Lab., No.12 (1948), p.1445

10. Neymark,V.Ye. - The Influence of Impurities on the Crystallization of Metals and Alloys. Collected Papers, III Conference on Physicochemical Principles of Steel Production (in press)

STAT

Declassified in Part - Sanitized Copy Approved for Release @ 50-Yr 2014/03/07 : CIA-RDP81-01043R004200090004-8

Declassified in Part - Sanitized Copy Approved for Release @ 50-Yr 2014/03/07 : CIA-RDP81-01043R004200090004-8

STUDY OF THE PROCESSES OF CRYSTALLIZATION FROM A MELT

by

I.N.Fridlyander

In the post-war years, the continuous casting of ingots, with the intense cooling of the crystallized metal characteristic of that process, has become widespread. In this connection, the study of the effect of the rate of cooling on the process of crystallization from a melt acquires not only theoretical significance but also great practical importance. In particular, it must be more precisely determined what properties can be obtained by the aid of continuous methods of casting, the possibilities of the new casting methods must be studied, and the mechanism of action of high rates of crystallization on the structure of the metal must be investigated.

For this purpose , we staged the investigation on aluminum alloys, and, in a number of cases, on organic transparent substances as models.

1. The Influence of the Rate of Crystallization on the Structure and Properties of Aluminum Alloys

D.K.Chernov (Bibl.1) noted the substantial influence of the rate of crystallization on the structure and properties of ingots. The influence of supercooling on the form of crystal growth is discussed in the works of A.A.Bochvar (Bibl.2), A.V.Shubnikov (Bibl.3), in the work by H.Buckley (Bibl.4), in the works of D.A.Petrov (Bibl.5), D.D.Saratovkin (Bibl.6), and by others. A.G.Spasskiy (Bibl.7), V.A.Livanov (Bibl.8), V.I.Dobatkin (Bibl.9), and V.V.Gulyayev (Bibl.10) call attention to the fact that with increasing rate of crystallization, the internal structure of the grains is refined and the strength and plasticity of the metal are increased.

Various rates of crystallization had been previously obtained by me (Bibl.11): in one case by using a thin-walled copper chill mold bathed with water, and in the

STAT

Declassified in Part - Sanitized Copy Approved for Release @ 50-Yr 2014/03/07 : CIA-RDP81-01043R004200090004-8

Declassified in Part - Sanitized Copy Approved for Release @ 50-Yr 2014/03/07 : CIA-RDP81-01043R004200090004-8

other case, a mold inserted in hollowed chamotte brick. The rate of cooling of the metal crystallizing in the copper chill mold, as shown by measurements with the aid of a string galvanometer, was 70°/sec.

The properties of rapidly and slowly crystallized aluminum alloys differ substantially, whether in the as-cast or heat-treated states. The slowly crystallized alloys have a decreased tensile strength and zero plasticity in the as-cast state. After heat treatment, the yield point and the ultimate strength of these alloys increase considerably, but in absolute value still remain very low, even after prolonged holding at high quenching temperatures.

Fig.1 - Aluminum Alloy D16, Casting in Chamotte. 115 ×

The yield point rises more rapidly than the ultimate strength, so that, as a result of heat treatment, these quantities approach each other almost to coincidence. Consequently, slowly cooled alloys are not capable of taking even a very small plastic deformation (over 0.2% of the elongation set) and fail prematurely.

From the extension curves of specimens of alloy Al + 4% Cu, likewise, the immense difference in the work of deformation during the tests of rapidly and slowly crystallized alloys will be clear. The fractures of slowly cooled castings are brittle and coarse, with accumulation of gas bubbles, shrinkage holes, inclusions of intermetallides and nonmetallic films. During the process of quench heating, the fractures blacken and show clear signs of burning.

Alloys crystallized at high rates of cooling have, even in the as-cast state, a relatively high resistance to deformation and a higher plasticity. Heat treatment STAT

Declassified in Part - Sanitized Copy Approved for Release @ 50-Yr 2014/03/07 : CIA-RDP81-01043R004200090004-8

Declassified in Part - Sanitized Copy Approved for Release @ 50-Yr 2014/03/07 : CIA-RDP81-01043R004200090004-8

shows an exceptionally favorable influence on these alloys. The general improvement of properties is such that the ingots after heat treatment approach the deformation strength of heat-treated alloys. The principal strengthening of water-cooled ingots after heat treatment is attained after a relatively short (1 hr) quench heating. After heat treatment, specimens cut out of water-cooled ingots preserve a bright surface. The burning temperature of these specimens rises 15 - 20°C above that of the slowly crystallized alloys.

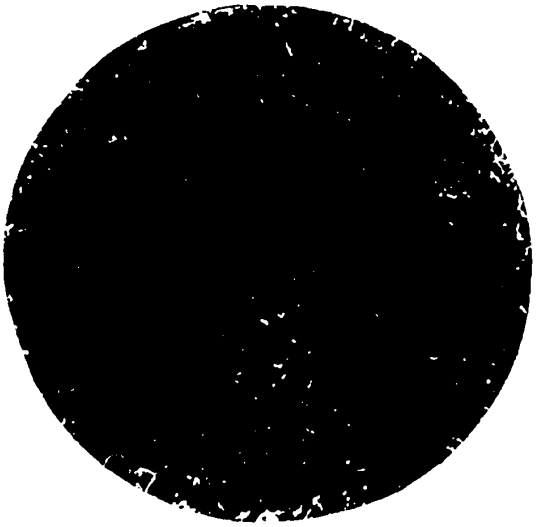

Fig.2 - Alloy Al + 10% Mg; Casting in Water-Cooled Chill Mold. 115 ×

The differences in the mechanical properties of castings, the type of fractures, and the burning temperature for rapidly and slowly crystallized alloys are due directly to the change in character of the grains and dendrites (Fig.1 and 2). With increasing rate of cooling, the number of secondary dendrites strongly increases, and the principal and secondary axes of the dendrites become thinner; the distance between the secondary dendrites and the individual primary dendrites decreases; the impurities (soluble and insoluble) have no time to be driven toward the grain boundaries and are deposited between the secondary dendrites in the form of small segregated round inclusions; the dendrites become elongated. During heat treatment, the impurities disseminated through the solid solution do not come in contact with the air, and are not oxidized, but are rapidly dissolved. The composition of the grain becomes equalized, the dendrites are converted into grains in close contact with each other, and with narrow boundaries.

During slow cooling, equiaxial dendrites are formed, with wide cavities appear- STAT

Declassified in Part - Sanitized Copy Approved for Release @ 50-Yr 2014/03/07 : CIA-RDP81-01043R004200090004-8

Declassified in Part - Sanitized Copy Approved for Release @ 50-Yr 2014/03/07 : CIA-RDP81-01043R004200090004-8

ing between them. The impurities (soluble and insoluble) are almost completely displaced toward the grain boundaries, and are deposited there in the form of coarse inclusions. Alternating with the intradendritic cavities, they form a continuous fringe, making the metal brittle. The structure of the alloy after heat treatment is little changed, and only the grain boundaries are appreciably oxidized.

The general increase in the density of the metal, and especially the disperse-

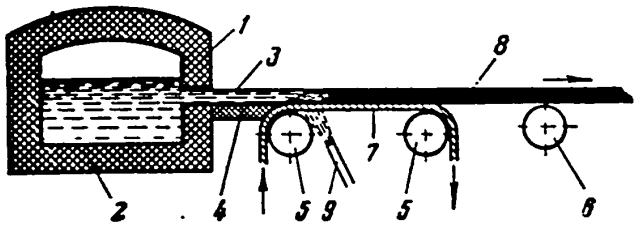

Fig.3 - Continuous Casting of Thin Sheet Workpiece of Aluminum Alloys by the Method of I.N.Fridlyander and V.G.Golovkin

1 - Furnace; 2 - Liquid metal in furnace; 3 - Liquid metal; 4 - Notch of furnace; 5, 6 - Rollers; 7 - Screen; 8 - Solidified metal; 9 - Water cooling

ness of the structure at high rates of cooling, favors the radical improvement of the properties of the alloy. Thus, high rates of cooling during crystallization exert an influence which to a certain extent is analogous to the influence of deformation. From this point of view, D.K.Chernov's forecast that high casting skill would be able to make fundamental improvements in the properties of the casting, and lead to the replacement of forging by casting, has been justified. It must, however, be noted that the plasticity of cast metals after heat treatment is still below the values characteristic of these same alloys in the deformed and heat treated states.

STAT

Declassified in Part - Sanitized Copy Approved for Release @ 50-Yr 2014/03/07 : CIA-RDP81-01043R004200090004-8

Declassified in Part - Sanitized Copy Approved for Release @ 50-Yr 2014/03/07 : CIA-RDP81-01043R004200090004-8

2. Continuous Casting of a Thin Sheet Work Piece of Aluminum Alloys

The maximum improvement of cast metal is attained on continuous casting of thin strips or wire, when a high rate of cooling can be realized.

Let us consider, as an example, the continuous casting of a thin sheet work piece of aluminum alloys according to the system proposed by the author and V.G.Golovkin (Fig.3).

Fig.4 - Fibrous Crystals in Upper Part of Strip; View from Top (Natural Size)

The liquid metal is delivered in a smooth flat jet, through a notch having the form of a thin slit, onto a moving screen, washed from below with a vigorous stream of water passing through the screen. The solidification of a thin layer of liquid metal (6 - 10 mm) in direct contact with the water when it reaches the screen, takes

STAT

Declassified in Part - Sanitized Copy Approved for Release @ 50-Yr 2014/03/07 : CIA-RDP81-01043R004200090004-8

Declassified in Part - Sanitized Copy Approved for Release @ 50-Yr 2014/03/07 : CIA-RDP81-01043R004200090004-8

place at extremely high speed. Two zones are clearly found in the cast strip through its thickness (Bibl.12): in the lower part, small vertical crystals grow upward from below; in the upper half, fibrous crystals are formed, growing in a horizontal plane with the strip moving at 12 - 15 m/hr. The fibrous crystals may have a length measured in meters. As they develop they gradually widen and occupy a considerable part of the surface of the strip, which confirms A.V.Shubnikov's idea of geometrical selection during the process of appearance of a columnar zone (Fig.4). The fibrous crystals are formed by individual fibers in more or less linear arrangement (Fig.5). The impurities are drawn out in short lines along the

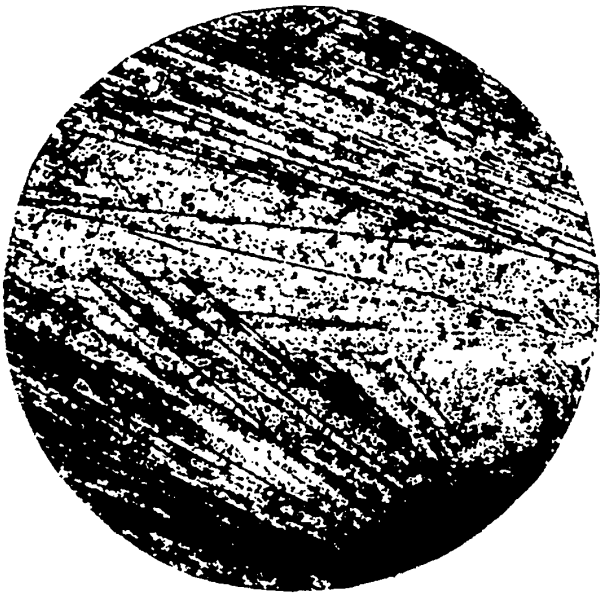

Fig.5 - Fibrous Crystals, 200 ×

fibers. The crystals grow from a common center; after long annealing the fibers merge with each other. But the impurities maintain their short-line arrangement, evidencing the forms of crystal growth and resulting in a difference of properties in different directions.

On the surface of the strip, ahead of the main crystallization front, small equiaxial crystals are sometimes formed, and are rapidly surrounded by better ori- STAT

Declassified in Part - Sanitized Copy Approved for Release @ 50-Yr 2014/03/07 : CIA-RDP81-01043R004200090004-8

Declassified in Part - Sanitized Copy Approved for Release @ 50-Yr 2014/03/07 : CIA-RDP81-01043R004200090004-8

ented fibrous crystals. But, as the temperature of the casting decreases, the number of small equiaxial crystals increases, and may become predominant. The transition from one form of crystal growth (and from grains of immense size) to the other form (and to small crystals) is accomplished over a relatively small fall in temperature. This temperature threshold has different values for different alloys. The transition from equiaxed dendrites to fibrous crystals is, in all probability, due to the increase of the temperature gradient in the zone of the liquid adjacent to the crystallization front (and perhaps, to a certain extent, also to the deactivation of the impurities during superheating).

The strength of the zones of fibrous and equiaxial crystals of a thin cast strip in the longitudinal and transverse directions reaches high values, even in the as-cast state, and increases still more after heat treatment (Table 1).

The direction of cut of the specimen in the zone of equiaxial crystals has no effect on the value of the elongation. In the zone of the fibrous crystals, the longitudinal specimens have elongations of 12 and 19%, and the transverse specimens 5 and 8%, respectively, in the as-cast and heat-treated states. While the cast metal is not inferior in strength to heat-treated rolled sheet, its plasticity in the cross direction is insufficient. The elongation depends to a greater degree on the disperseness and character of distribution of the second phases and impurities than does the strength. After the imposition of a certain deformation, however, the plasticity of the metal does improve to a sufficient extent. In exactly the same way, cast wire of very high strength and elongation in the longitudinal direction will not rivet if it is not subjected to drawing. In this case, as well, the dashed arrangement of the impurities adversely affects the transverse plasticity. It is understandable that in the case of pure aluminum, or of very soft alloys, the plasticity in the cross direction will be adequate even in the as-cast strip or cast wire.

The method of casting a thin sheet work piece (Fig.3) may be used to produce

STAT

Declassified in Part - Sanitized Copy Approved for Release @ 50-Yr 2014/03/07 : CIA-RDP81-01043R004200090004-8

Declassified in Part - Sanitized Copy Approved for Release @ 50-Yr 2014/03/07 : CIA-RDP81-01043R004200090004-8

sheet, skipping the ingot stage.

It is well known that the method of direct slabless rolling of sheet, proposed by H.Bessemer, and extensively tested in practice by Hazelett (Bibl.13), in spite of

Table 1

Mechanical Properties of Zones of Fibrous and Equiaxial Crystals of Cast Strip and Rolled Sheet of Aluminum Alloy D1

Condition of Material	Type of Crystals	Direction of Specimen Cut	Tensile Strength, kg/mm2	Elongation, %
Cast strip	Fibrous Fibrous	Longitudinal Transverse	31,8 31,2	12,1 5,0
	Equiaxed Equiaxed	Longitudinal Transverse	32,1 29,7	7,7 7,1
Cast strip after quenching and aging	Fibrous Fibrous	Longitudinal Transverse	39,8 37,7	18,9 8,3
	Equiaxed	Longitudinal Transverse	40,3 40,1	9,2 8,4
Rolled sheet after quenching and aging		Longitudinal Transverse	40,1 40,6	19,4 16,1

its outward simplicity, proved to be unsuccessful. The metal is poured between two rotating rollers, and during crystallization is subjected to pressure; squeezing out the low-melting components and leading to extremely strong reverse liquation. The irregular arrival of the solidifying metal at the jaw of the rollers causes excessive pressure, and in combination with the high temperature and the direct action of the liquid metal on the surface of the rolls, leads to the rapid wear of the equipment.

The method of the thin sheet workpiece is more promising, especially in cases where it is possible by its aid to obtain essentially new properties. Thus, in casting strip of aluminum-manganese alloy (Al + 2.0 – 3.0% Mn) it is possible to ob-

STAT

Declassified in Part - Sanitized Copy Approved for Release @ 50-Yr 2014/03/07 : CIA-RDP81-01043R004200090004-8

Declassified in Part - Sanitized Copy Approved for Release @ 50-Yr 2014/03/07 : CIA-RDP81-01043R004200090004-8

tain an unusually low temperature coefficient of electrical resistivity (with a high electrical resistivity). After such a material is annealed or quenched, its electrical resistivity falls, while the temperature coefficient of electrical resistivity increases considerably. A study of the lattice parameter of the alloy (staged by the present author in collaboration with V.A.Konstantinov and N.I.Zaytseva) shows (Fig.6) that in the cast specimens (curve a) the manganese content of the solid solution reaches 3% by weight, i.e., considerably higher than the maximum equilibrium solubility. The concentration of the solid solution does not increase under our conditions of casting when the total manganese content in the alloy is increased up to 9%. For alloys of the compositions studied, quenched in the solid phase from a temperature close to the melting point (curve b), one and the same parameter, corresponding to about 1.4% Mn in the solid solution, is maintained, indicating the segregation of a supersaturated solid solution from the liquid state during the process of quench heating.

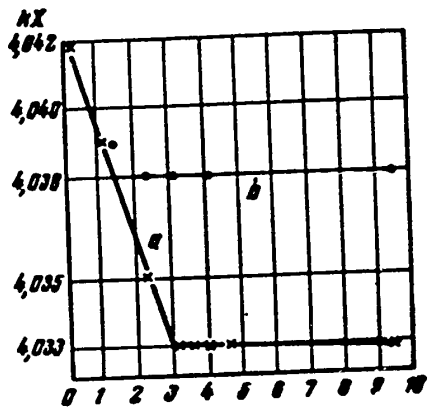

Fig.6 - Variation in the Crystal Lattice Parameter of Alloys After Various Forms of Heat Treatment (I.N.Fridlyander, V.A.Constantinov, and N.I.Zaytseva)

a - As-cast state; b - Quenched in water after heating to 650°C

a) Weight % Mn

The formation from the liquid state of a supersaturated solid solution with a concentration of the second element exceeding the maximum equilibrium concentration should in our opinion be treated as an effect of quenching from the liquid state (Bibl.14), i.e., the fixation in the solid state of that concentration that is characteristic of the liquid solution, or as a retardation of the decomposition of

STAT

Declassified in Part - Sanitized Copy Approved for Release @ 50-Yr 2014/03/07 : CIA-RDP81-01043R004200090004-8

Declassified in Part - Sanitized Copy Approved for Release @ 50-Yr 2014/03/07 : CIA-RDP81-01043R004200090004-8

the solution during the process of crystallization. The effect of quenching from the liquid state may be obtained on intense cooling of the crystallizing metal, for example, during continuous casting of a thin sheet workpiece.

3. Study of the Forms of Crystal Growth Depending on the Rate of Cooling

As a result of the opacity of metals, it is inconvenient to study the mechanism of crystallization in them.

For this reason, in work performed by the author in collaboration with N.B.Kondrat'yeva and S.A.Yudina (Bibl.15), we used a transparent substance, camphene, in our observations on the growth of crystals at various rates of cooling (Bibl.16).

The processes of crystallization was studied by the aid of motion-picture photography under a microscope. This technique was first applied in the USSR by G.B.Ravich and V.A.Vol'nova. Camphene, which always contains a certain quantity of impurities, was placed in a thin layer of the order of 0.1 mm thickness, between object and cover glasses. With the very slowest cooling, when the temperature of the heating stage was maintained close to the melting point of camphene, small round crystals are formed. The small crystals are spherical, but as they grow they lose their shape, still keeping their round outlines. At the same time as large crystals grow, the small crystals may melt. The roundness of the crystals and the melting of the small crystals is probably connected with the action of surface tension.

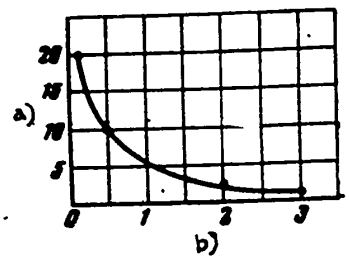

Fig.7 - Displacement of Sphere by Growing Crystals Depending on the Rate of Cooling

a) Displacement; b) Rate of water flow, ltr/min

If air bubbles are present in the melt, the crystals shift them during very slow growth, and flow around them at accelerated growth.

An increase in the cooling rate leads to the elongation of round grains, and to

STAT

Declassified in Part - Sanitized Copy Approved for Release @ 50-Yr 2014/03/07 : CIA-RDP81-01043R004200090004-8

Declassified in Part - Sanitized Copy Approved for Release @ 50-Yr 2014/03/07 : CIA-RDP81-01043R004200090004-8

the appearance of the first branches. The crystals, on approaching impurities, branch without intergrowing. The change in the ability of the crystals to displace impurities suspended in the melt, depending on their rate of growth, has been quantitatively shown in our experiments with N.A.Vysotskaya (Bibl.17) (Fig.7) and in the works of A.G.Spasskiy and associates.

A.A.Baykov (Bibl.18) has found that every molten metal contains a mass of suspended insoluble particles. At low rates of growth, the crystal displaces these particles. During the process of displacement, or further diffusion, the particles

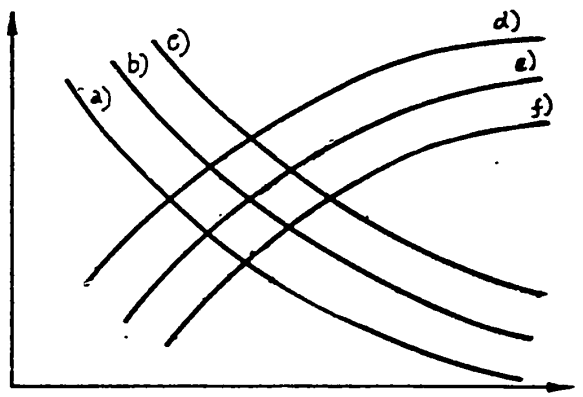

Fig.8 - Diagram of Influence of Rate of Cooling During Crystallization (Velocity of Crystal Growth) on the Structure and Properties of the Metals

a) Diameter of impurity particles; b) Distance between secondary branches of dendrites; c) Thickness of branches of dendrites; d) Strength of metal; e) Elongation of metal; f) Density of metal; g) Velocity of crystal growth

coalesce, intergrow with each other, and become consolidated. With increasing rate of growth, the crystal is more and more often compelled to flow around the particles, retreating from the secondary branches, which become finer and finer, and more and more numerous. In this case, the disperseness and distribution of the

STAT

Declassified in Part - Sanitized Copy Approved for Release @ 50-Yr 2014/03/07 : CIA-RDP81-01043R004200090004-8

Declassified in Part - Sanitized Copy Approved for Release @ 50-Yr 2014/03/07 : CIA-RDP81-01043R004200090004-8

particles in the solid metal approaches more and more closely to their disperseness in the liquid metal.

It is therefore incorrect to say that the impurities are refined with increasing rate of cooling. In reality, they do not become consolidated during rapid crystallization, and do become consolidated during slow crystal growth.

Naturally, there is a definite relation between the velocity of crystallization, the size of the particles, the thickness of the secondary branches of the dendrites, the distance between them, and the mechanical properties of the cast metal (Fig.8).

When solidified camphene is held close to the melting point, the dendrites are converted into grains, one grain being formed from each dendrite. The process of conversion of a dendrite into a grain reduces down to the equalization of the chemical composition within the boundaries of the same crystal, and to the homogenization of the grains. The distribution of the insoluble impurities within and along the grain boundaries is completely determined by the initial forms of growth of the crystals.

The same phenomena, as during the crystallization of camphene, take place in all likelihood, in the crystallization of aluminum alloys as well. When cooling becomes more rapid, the crystals go around the impurities more and more, without displacing them, and the branches are put out more and more often; the distribution of the impurities acquires a more and more disperse character; and the branches of the dendrites become finer and finer. During the process of homogenization, the branches of the dendrites become intergrown; the chemical composition of the crystals become equalized; and the dendrites are transformed into grains, which inherit from the dendrites the character of the distribution of the impurities, one density or another, and one level of properties or another.

4. Study of the Dependence of the Temperature on the Crystallization Front on the Degree of Supercooling

In this work we repeatedly noted the dependence of the structure of the metal

STAT

Declassified in Part - Sanitized Copy Approved for Release @ 50-Yr 2014/03/07 : CIA-RDP81-01043R004200090004-8

Declassified in Part - Sanitized Copy Approved for Release @ 50-Yr 2014/03/07 : CIA-RDP81-01043R004200090004-8

and of its properties on the velocity of crystal growth, but not on the supercooling. In metallurgical practice, the increase in the velocity of crystal growth and the corresponding improvement of the structure is obtained precisely by accelerating the heat removal from metal superheated above its melting point (for example, by transi-

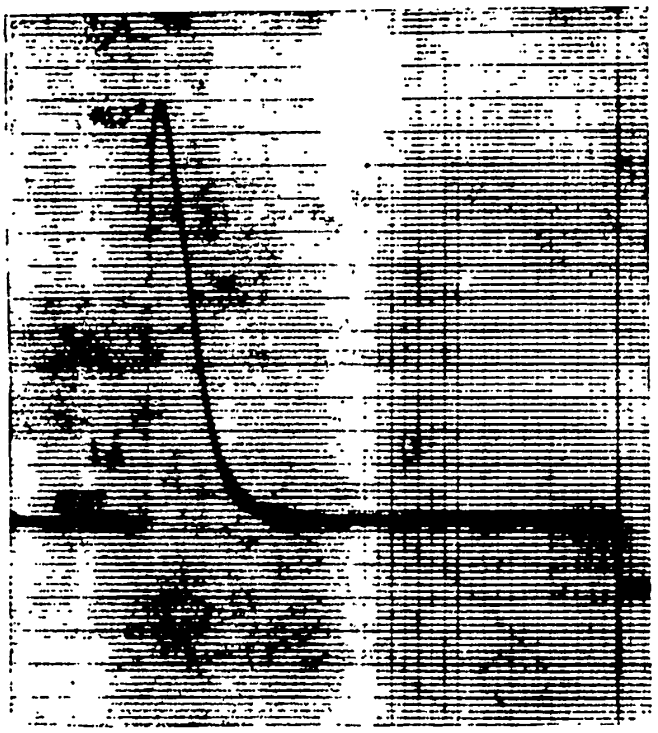

Fig.9 - Variation of Temperature on the Crystallization Front of Benzophenone, First Supercooled to 13.2°C

tion from the cast-iron chill mold to the copper water-cooled chill mold, and then still further to the continuous casting of ingots with water supplied directly onto the crystallizing metal). Tamman's experiments determined the dependence of the linear crystallization velocity on the supercooling of the melt. It still remains unclear, however, how the degree of supercooling of the metal varies during the process of crystallization.

Attempts have been repeatedly made (Bibl.19 - 23) to establish the relations of

STAT

Declassified in Part - Sanitized Copy Approved for Release @ 50-Yr 2014/03/07 : CIA-RDP81-01043R004200090004-8

Declassified in Part - Sanitized Copy Approved for Release @ 50-Yr 2014/03/07 : CIA-RDP81-01043R004200090004-8

the temperature on the crystallization front to the initial supercooling.

All investigators who have ever worked with salol have reached the conclusion that when the crystallization front passes across a thermocouple junction there is an actual rise of temperature, which rise increases with the preliminary supercooling of the melt, reaches a certain maximum value, and does not thereafter increase. The temperature on the crystallization front over the entire range of supercooling investigated, remains considerably below the melting point of the substance. In this case (Bibl.22, 23), the excess temperature of the crystallization front above the temperature of the thermostat remains constant over the entire range of supercoolings corresponding to a constant linear crystallization velocity. In collaboration with Z.G.Filippova and M.S.Model' (Bibl.24), I have investigated the temperature conditions on the crystallization front of salol, which has a relatively low linear crystallization velocity (maximum value 3.46 mm/min) and of benzophenone, which has a relatively high linear crystallization velocity (maximum 55.5 mm/min). The principal difficulty was to obtain a considerable supercooling of the melt with the hollow-junction thermocouple introduced into it.

After numerous experiments, we succeeded in supercooling benzophenone with the thermocouple junction by 35.3°C (down to a temperature of 13.2°C). On passing the crystallization front, we noted a sharp local temperature rise, approaching the melting point of the substance, 48.5°C, and then a more or less rapid fall in temperature (Fig.9). This rise is considerably higher with benzophenone than with salol. The rise increases proportionally to the degree of initial supercooling (Fig.10) while the temperature on the crystallization front of the benzophenone over a wide initial supercooling range remains constant, close to the melting point, even in the region with constant linear crystallization velocity. It is necessary also to take into account the purely methodological causes responsible for a certain lowering of the upper point of the temperature peak, that is, the consumption of heat in warming up the thermocouple junction, and the inertia of the recording sys-

STAT

Declassified in Part - Sanitized Copy Approved for Release @ 50-Yr 2014/03/07 : CIA-RDP81-01043R004200090004-8

Declassified in Part - Sanitized Copy Approved for Release @ 50-Yr 2014/03/07 : CIA-RDP81-01043R004200090004-8

tem. Consequently, the true supercooling on the crystallization front, over a very wide initial supercooling range, varies only little, and is very small. It does, however, constantly fluctuate, decreasing on the formation of a regular crystalline

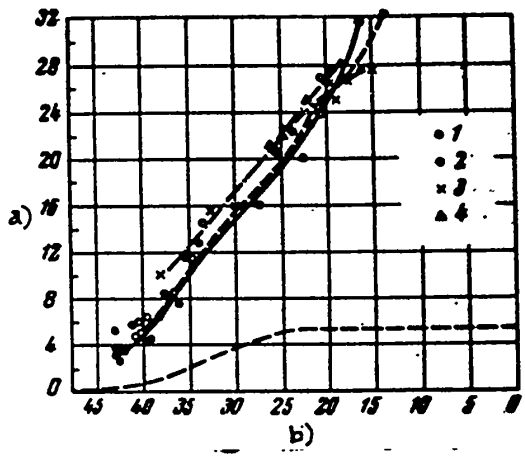

Fig.10 - Rise of Temperature on the Crystallization Front of Benzophenone as a Function of the Thermostat Temperature for Four Series of Experiments with Different Diameters of the Thermocouple Wires

Diameter of thermocouple wire was: 1 - 0.1 mm; 2 - 0.1 mm; 3 - 0.05 mm; 4 - 0.045 mm. The dashed lines show the variation of the linear crystallization velocity as a function of the thermostat temperature

a) Temperature rise, °C; b) Thermostat temperature, °C

layer, and increasing with the decrease of the local temperature rise that takes place in this case.

Analogous phenomena are also observed on crystallization of pure aluminum at both low and high velocity ratio of cooling (casting into a heated chamotte chill mold and onto a screen washed from below with water). After a certain supercooling preceding the beginning of crystallization, the temperature of crystallization of

STAT

Declassified in Part - Sanitized Copy Approved for Release @ 50-Yr 2014/03/07 : CIA-RDP81-01043R004200090004-8

Declassified in Part - Sanitized Copy Approved for Release @ 50-Yr 2014/03/07 : CIA-RDP81-01043R004200090004-8

pure aluminum in both cases remains one and the same, practically equal to the melting point. Naturally enough, there is some supercooling, but it is within the limits of the accuracy of measurement.

Consequently, crystal growth requires a very small degree of supercooling, often within the range of errors of measurement. The velocity of crystal growth is regulated by the intensity of heat removal from the crystallized layer, in particular by the temperature gradient in the solidified layer.

A decrease in the temperature of the thermostat accelerates the lowering of the local temperature rises and intensifies the heat removal from the crystallized substances, i.e., it acts just like a change from a cast-iron chill mold to a copper, water-cooled chill mold. For this reason, the form of crystal growth may be connected, with sufficient grounds, with the rate of cooling of the crystallized substance, or with the velocity of crystal growth.

In those cases where the true supercooling on the crystallization front reaches considerable levels, the crystal growth proceeds under hindered conditions, and the effect of a quenching from the liquid state is possible, as has been described above for rapidly cooled Al - Mn alloys.

Conclusions

1. With increased rate of cooling during the process of crystallization of aluminum alloys, the branches of the dendrites become finer, the spaces between the branches decrease, and the inclusions of the second phases are segregated, taking positions mainly between the dendrite branches. The refining of the impurities and of the secondary dendrite branches may be connected with the decreased power of the crystals to displace the impurities suspended in the melt, as the velocity of crystal growth increases.

2. Corresponding to these changes in structure, the strength of cast alloys increases, and in the heat-treated state reaches the level of strength of forged alloys. The elongation also increases, but remains below the values characteristic

STAT

Declassified in Part - Sanitized Copy Approved for Release @ 50-Yr 2014/03/07 : CIA-RDP81-01043R004200090004-8

Declassified in Part - Sanitized Copy Approved for Release @ 50-Yr 2014/03/07 : CIA-RDP81-01043R004200090004-8

of forged heat-treated alloys.

3. The maximum improvement of the properties of the cast metal is achieved by continuous casting of a thin layer of liquid metal on a moving screen washed with water. This method may be used for the direct slabless rolling of metals into sheet.

4. Over a wide range of initial supercooling range, the temperature on the front of crystallization, within the limits of accuracy of the ordinary methods of measurement, approaches close to the melting point. With a substantial decrease in the true temperature on the crystallization front, one may expect the appearance of a metastable structure and of new properties.

5. By means of continuous casting of a thin sheet work piece of an aluminum-manganese alloy, it is possible to obtain an unusually low temperature coefficient of electrical resistivity.

BIBLIOGRAPHY

1. Chernov,D.K. - Structure of Cast Steel Ingots (1879)
2. Bochvar,A.A. - Study of the Mechanism and Kinetics of Crystallization of Eutectic-Type Alloys. ONTI (1935)
3. Shubnikov,A.V. - The Formation of Crystals. Pub.Dept., Academy of Sciences USSR (1947)
4. Bakli,G. - Crystal Growth. State Pub.House for Foreign Lit. (1954)
5. Petrov,D.A., and Bukhanova,A.A. - Study of the Forms of Primary Crystallization of Metals. Trudy Mosk.Inst.Aviats.Tekh., No.7 (1949)
6. Saratovkin,D.D. - Dendritic Crystallization. Metallurgizdat (1953)
7. Spasskiy,A.G. - Principles of Industrial Casting. Metallurgizdat (1950)
8. Livanov,V.A. - Tr.Pervoy Tekh.Konf.Metallurg.Zavodov (1945)
9. Dobatkin,V.I. - Continuous Casting and the Casting Properties of Alloys. Oborongiz (1948)

STAT

Declassified in Part - Sanitized Copy Approved for Release @ 50-Yr 2014/03/07 : CIA-RDP81-01043R004200090004-8

Declassified in Part - Sanitized Copy Approved for Release @ 50-Yr 2014/03/07 : CIA-RDP81-01043R004200090004-8

10. Gulyayev,B.V. - Solidification and Inhomogeneity of Steel. Metallurgizdat (1950)

11. Fridlyander,I.N. - Effect of Increased Rate of Cooling During Crystallization on the Structure and Properties of Aluminum Alloys. Tr.Pervoy Tekh.Konf. Metallurg.Zavodov (1945)

12. Fridlyander,I.N., and Kondrat'yeva,N.B. - Structure and Properties of Ingots of D1 Alloy Crystallized under Conditions of Rapid Cooling. Oborongiz (1952)

13. Lippert,T.W. - The Iron Age., Vol.21 (1935); Vol.13 (1940), p.14

14. Fridlyander,I.N. - Dok.AN SSSR, Vol.104 (1955), p.3

15. Fridlyander,I.N. - Study of the Forms of Crystal Growth Depending on the Rate of Cooling. Oborongiz (1949)

16. Yefremov,N.N. - Izv.Ross.Akad.Nauk. Vol.23 (1915), p.529

17. Fridlyander,I.N., and Vysotskaya,N.A. - Dok.AN SSSR, Vol.62 (1948), p.1

18. Baykov,A.A. - Collected Works. Vol.11 (1948), p.213

19. Wilson,H.A. - Phyl.Mag., Vol.50 (1900), p.238

20. Burger,H. - Proc.Sect.Sci., Vol.23 (1920)

21. Pollatschek,H. - Zeits.Phys.Chem., Vol.142 (1929), p.289

22. Mosing,G., and Reinbach,R. - Atti X Cong.In.Chem.Roma., Vol.3 (1938), p.594

23. Danilova,A.I., and Danilov,V.I. - Problems of Metallography and Physics of Metals. Metallurgizdat (1948), p.80

24. Fridlyander,I.N., Filippova,Z.G., and Model',M.S. - Izv.Sekt.Fiz.-Khim.Anal. Vol.22 (1953)

STAT

Declassified in Part - Sanitized Copy Approved for Release @ 50-Yr 2014/03/07 : CIA-RDP81-01043R004200090004-8

Declassified in Part - Sanitized Copy Approved for Release @ 50-Yr 2014/03/07 : CIA-RDP81-01043R004200090004-8

ARTIFICIAL FLUORITE

by

I.V.Stepanov and P.P.Feofilov

The optical glasses that are widely used in instrument building, have a substantial shortcoming: their insignificant transparency for rays lying beyond the visible region of the spectrum. The working region of the most widely used grades of optical glass is confined to a narrow range of wavelengths (from about 0.33 to 2 μ), and therefore their use in instruments working in the ultraviolet/infrared regions of the spectrum is practically impossible.

Very pure crystals of certain natural minerals, as well as artificially grown crystals of a number of substances, are used as optical media for both the invisible regions of the spectrum. The total number of such crystalline materials is exceedingly small (apparently not over twenty), and this fact greatly restricts the widespread use of a very important group of optical instruments designed to operate in the ultraviolet and infrared regions of the spectrum.

A particularly acute shortage is felt in the optical media for the region of wavelength shorter than 0.2 μ (the Schumann region). Only three optical materials with a sufficiently high and uniform transmission in the shortwave ultraviolet part of the spectrum are known: crystals of sodium fluoride, lithium fluoride and fluorite. The first of these substances is inadequately water-resistant and therefore it can be used in optical instruments only in special cases. Lithium fluoride, owing to a group of optical, mechanical and other properties, is a very valuable optical material.

And finally, fluorite is an exceedingly valuable optical material that is difficult to replace. Only lithium fluoride can compete with it.

The peculiar properties of fluorite include , above all, its high and uniform transparency in a wide range of wavelengths, from 0.125 μ in the Schumann region of

STAT

Declassified in Part - Sanitized Copy Approved for Release @ 50-Yr 2014/03/07 : CIA-RDP81-01043R004200090004-8

Declassified in Part - Sanitized Copy Approved for Release @ 50-Yr 2014/03/07 : CIA-RDP81-01043R004200090004-8

the spectrum to 9.5 - 10 μ in the infrared, i.e., over a range of 6.5 octaves. For the ultraviolet rays, fluorite has a rather great dispersion and a rather high transparency in this region, which permits its use for building prisms for vacuum spectral instruments (spectrographs, monochromators, etc.). In the visible region of the spectrum, the dispersion of fluorite is very small. This property offers wide possibilities for the design of achromatic systems. Fluorite also possesses greater hardness and moisture resistance than many other crystals, except quartz.

The almost total lack of natural resources of colorless and uniform crystals of large size has prevented the widespread use of fluorite in optical instrument building. Crystals of natural optical fluorite, from which plates or lenses 25 mm in diameter could be made, are already a great rarity today.

In this connection the urgency and great current interest of the problem of preparing artificial crystals of optical fluorite becomes obvious.

1. Main Prerequisites for Choice of Method

In its chemical and physical properties, fluorite differs sharply from all the materials for which the methods of growing crystals were previously developed (for instance, from rock salt, sylvine, soda saltpeter, and many others). Its high melting point (1378°C), the high chemical aggressiveness of fluorine at these temperatures, and finally, the relatively low chemical stability of fluorite itself at high temperatures, require the establishment of special physicochemical conditions, using other apparatus, very greatly differing from those previously employed, for growing crystals of optical fluorite.

The attempt of many investigators to grow single crystals of fluorite by the generally known methods of Kyropoulos, Stockbarger or Tamman, inevitably led to failure. In all cases, white porcelain-like, completely opaque, finely crystalline conglomerates were grown, and were strongly contaminated with unknown foreign substances.

Certain investigators, including D.Stockbarger (Bibl.1) established the fact

STAT

Declassified in Part - Sanitized Copy Approved for Release @ 50-Yr 2014/03/07 : CIA-RDP81-01043R004200090004-8

Declassified in Part - Sanitized Copy Approved for Release @ 50-Yr 2014/03/07 : CIA-RDP81-01043R004200090004-8

that when fluorite is melted in the ordinary atmosphere, it becomes partially hydrolyzed under the action of atmospheric and adsorbed moisture. This process is accompanied by loss of fluorine and enrichment of the melt with calcium oxide:

$$CaF_2 + H_2O = CaO + 2HF\uparrow.$$

Calcium oxide is not isomorphous with the principal substance being crystallized, CaF_2, and during crystallization it is precipitated in the form of a separate, finely crystalline phase, differing sharply in refractive index from fluorite (for CaO, N_D = 1.837; for CaF_2, N_D = 1.434). As a result, the crystals that are grown show high internal scattering of light.

The practical possibility of growing optically perfect single crystals of fluorite depends primarily on the possibility of carrying out the process of growing the crystals in a space free from water vapor. In practice, such conditions can be attained if the process is conducted in a vacuum. Experience shows that at high rate of exhaustion of the gases liberated during heating, it is possible to melt fluorite and subsequently grow the crystal without appreciable decomposition of the material.

By growing the crystal in a vacuum at high temperatures, it is not possible to accomplish the usual visual observation of the growing crystal from outside, nor to correct the process of growth. It is necessary for the very method of growing selected, to permit the automation of all the separate operations. For this, first of all, the number of such operations must be extremely small.

Among the well-known classical methods of growing crystals, these conditions are best met by the method of I.V.Obreimov and L.V.Shubnikov (Bibl.2), or, more accurately, by its improved version described by Bridgman (Bibl.3). It was this version, used later by D.Stockbarger (Bibl.1), that was used by us as the basis for developing an apparatus for growing fluorite crystals.

STAT

Declassified in Part - Sanitized Copy Approved for Release @ 50-Yr 2014/03/07 : CIA-RDP81-01043R004200090004-8

Declassified in Part - Sanitized Copy Approved for Release @ 50-Yr 2014/03/07 : CIA-RDP81-01043R004200090004-8

2. The Vacuum Apparatus for Growing Single Crystals

The primary requirement that apparatus for growing crystals of fluorite (and a number of other crystals) in vacuo must meet is the possibility of obtaining, and stably maintaining a temperature in the range of 800 - 1500°C in a vacuum of the order of $2 - 5 \times 10^{-4}$ mm Hg. The simultaneous satisfaction of these two conditions, so difficult to reconcile, gives considerable trouble in the design and practical operation of such a plant.

When fluorite is melted in a vacuum, there is an appreciable evaporation of that substance, accompanied by the simultaneous dissociation of certain impurities accompanying the fluorite. The presence of chemically aggressive vapors of fluorine compounds at high temperatures in the vacuum space still further complicates the solution of this problem, since it greatly limits the range of materials suitable for building the parts of the high-temperature vacuum unit.

The production of high temperatures and a high vacuum was accomplished by us, by means of the simultaneous:

1) extreme decrease of the entire vacuum space, by placing outside of it all the auxiliary units or parts whose presence in the vacuum space is not strictly necessary;

2) removal from the vacuum space, as far as possible, of all forms of materials with a hindered liberation of gas: ceramics, mica, fibrous and powdered heat insulating materials, as well as all materials with a vapor pressure over 10^{-5} mm Hg at their working temperature;

3) bringing outside the vacuum space all units or parts of units with semi-closed cavities, hindering the exhaustion of the gases (for example, threaded connections, deep openings, slits, etc.); all surfaces in the vacuum space must have, as far as possible, a simple "streamline" shape;

4) the application of intense water cooling of all parts, whose normal functioning does not demand elevated temperatures (for example, the vacuum cap, plate,

STAT

Declassified in Part - Sanitized Copy Approved for Release @ 50-Yr 2014/03/07 : CIA-RDP81-01043R004200090004-8

Declassified in Part - Sanitized Copy Approved for Release @ 50-Yr 2014/03/07 : CIA-RDP81-01043R004200090004-8

etc.), to eliminate the liberation of gas by large masses of metal when heated.

Without going into details relating directly to the work of finding heat-resistant and, at the same time, fluorine-resistant materials, we note that tungsten, tantalum, molybdenum, iron and nickel prove to be the best. All these metals, under the conditions of vacuum and high temperatures, are entirely resistant to the action of vapors of fluorides and melts of fluorine salts. The upper temperature limit for the use of one metal or the other is determined, not by its melting point, but by the lower temperature at which its vapor pressure does not exceed 10^{-5} mm Hg. Thus, for example, tungsten and tantalum may be used up to temperatures of 2500 - 2600°C, molybdenum up to 1700°C, iron and nickel, up to 1050°C.

It may seem unexpected, that, for example, such a generally recognized heat- and fluorine-resistant material as platinum should prove unsuitable for vacuum work. At 1650°C, the vapor pressure of platinum is close to 5×10^{-4} mm Hg, and it is only at 1500°C that it approaches 10^{-5} mm Hg. Obviously, as a result of the intense vaporization, the service life of the platinum crucible (for crystallization), and in particular, of the platinum heater, would be measured only in several hours.

In the experiments on growing fluorite crystals in a vacuum, we used crucibles built of thin sheet molybdenum (0.15 - 0.2 mm thick). When this was done, no corrosion of the inner surfaces of the crucible could be detected, even after melts of pure calcium fluorite had remained for 70 - 80 hrs in them.

Figure 1 gives a general view of the design of the high-temperature apparatus for growing crystals out of a melt, developed by I.V.Stepanov and M.A.Vasil'yeva:

1 - Steel water-cooled vacuum plate; for cooling, a copper tube lined with lead, is placed in circular grooves bored in the lower side of the plate, and cold water is passed through this tube (shown separately on Fig.1 in the upper right-hand corner);

2 - Steel vacuum cap with a cooler, soldered onto it with tin solder, in the form of a spiral copper tube (the upper part of a steel cylinder for storage and

STAT

Declassified in Part - Sanitized Copy Approved for Release @ 50-Yr 2014/03/07 : CIA-RDP81-01043R004200090004-8

Declassified in Part - Sanitized Copy Approved for Release @ 50-Yr 2014/03/07 : CIA-RDP81-01043R004200090004-8

transportation of compressed gases being used as the cap);

3 - High-temperature non-ceramic electric furnace with molybdenum heater wound in the form of a bifilar spiral and mounted on three corundized supports (A - the upper "hot" chamber of the furnace, B - the lower "cold" chamber, and D - the diaphragm separating them); in its electrical characteristics, this furnace is of the type of low-voltage furnaces designed to take heavy currents. For example, at a working power of 3 kw, the furnace draws a current of about 120 amp at 25 v. At higher feed voltages for the furnace, and on an accidental vacuum breaking, a voltaic arc self-ignites in it, leading to serious damage.

The heat-insulating baffle screens, made of sheet molybdenum 4, and sheet nickel 5, polished on both sides; these baffle screens are assembled in the form of two separate multilayer blocks;

6 - Electric terminals (two of them) water-cooled from inside, serving to supply current to the heater of the furnace;

7 - Lead-in ducts for the electrical terminals of the furnace with removable airtight packings, electrically insulated from the plate (their arrangement is shown separately on the right side of the figure);

8 - Oil-vapor diffusion pump (type MM-40A); the forevacuum pump (type RVN-20) is not shown in the figure.

Crucible with conical bottom 9, placed in the holder 10, which is water-cooled from inside;

11 - Sylphon (metal bellows) to transmit, from outside, into the vacuum space, the vertical displacement of the crucible in the furnace for crystal growing;

12 - Screw of automatic device rigidly attached to the crucible holder 10; the automatic device (not shown on the figure) serves for the automatic lowering of the crucible from the upper "hot" chamber of the furnace into the lower "cold" chamber through the molybdenum diaphragm D, while the crystal is being grown.

The glass tube 13, with sealed upper end, and a millimeter scale engraved on

STAT

Declassified in Part - Sanitized Copy Approved for Release @ 50-Yr 2014/03/07 : CIA-RDP81-01043R004200090004-8

Declassified in Part - Sanitized Copy Approved for Release @ 50-Yr 2014/03/07 : CIA-RDP81-01043R004200090004-8

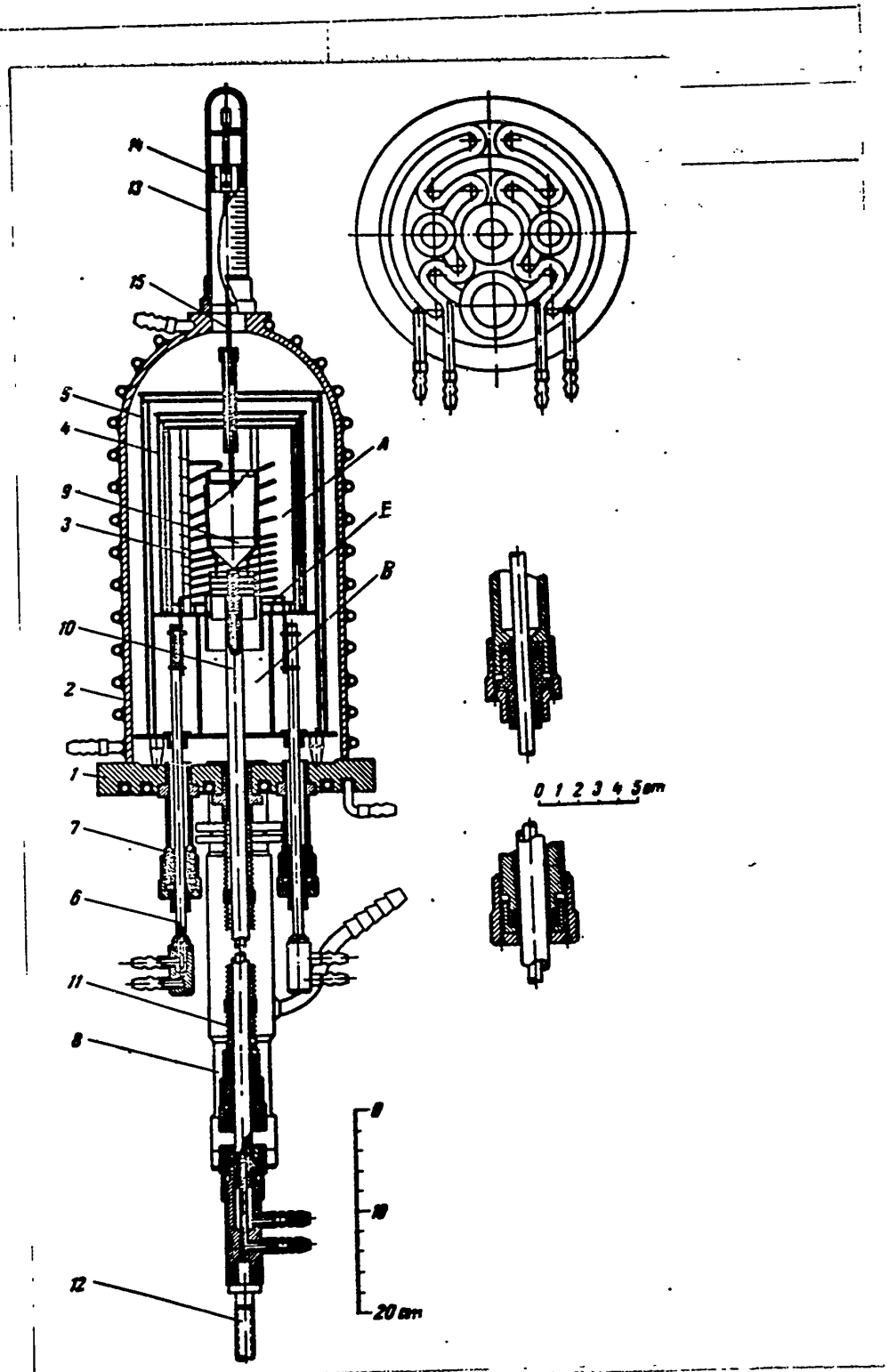

Fig.1 - High-Temperature Vacuum Apparatus for Growing Crystals

STAT

Declassified in Part - Sanitized Copy Approved for Release @ 50-Yr 2014/03/07 : CIA-RDP81-01043R004200090004-8

Declassified in Part - Sanitized Copy Approved for Release @ 50-Yr 2014/03/07 : CIA-RDP81-01043R004200090004-8

it; the iron armature 14, can be displaced freely in the glass tube in the vertical direction; the molybdenum rod 15, at the upper end of which is attached the iron armature 14. The lower end of the rod passes into the crucible through a small opening in the crucible cover. By the aid of a powerful electromagnet seated on the glass tube, the iron armature may be released and the molybdenum rod lowered with the crucible until it meets the stop. From the scale divisions on the glass tube, it is possible to determine what is happening in the crucible: melting of the material, growth of the crystal, etc.

3. Starting Materials for Growing Fluorite Single Crystals

Two materials have found use as the raw material for growing optical fluorite: technical fluorspars from certain deposits of the Soviet Union, and also artificially synthesized calcium fluoride of a very high degree of purity, produced by a special method.

The use of natural fluorspar became possible only after methods were found for removing contaminations of foreign minerals from it, not only those on the surface, but also those present in the form of minute internal inclusions.

The surface contaminations may be removed either chemically, by dissolving them in various acids (hydrofluoric, hydrochloric, nitric) or mechanically, by removing the upper layer from the lumps of fluorspar in revolving drums.

The removal of the internal inclusions involves first of all the possibility of detecting them and making them accessible for subsequent removal by chemical treatment. Simple mechanical crushing of the fluorspar does not attain this aim, since the destruction of the crystal takes place not at the site of the inclusions, but along the planes of cleavage. For the most part, however, the inclusions, as before, remain concealed inside the fluorspar grains. Almost complete detection can be accomplished by using thermal crushing. It is well known when natural fluorite is heated (at 300 - 350°C) there is an intense disintegration (splitting) of these crystals into small fragments. It has been found on specimens with vary-

STAT

Declassified in Part - Sanitized Copy Approved for Release @ 50-Yr 2014/03/07 : CIA-RDP81-01043R004200090004-8

Declassified in Part - Sanitized Copy Approved for Release @ 50-Yr 2014/03/07 : CIA-RDP81-01043R004200090004-8

ing degrees of growth that owing to the difference in the coefficients of expansion, the crystals fracture first of all at the site of the inclusions, and not along the planes of cleavage.

Subsequent chemical treatment of the thermally comminuted material may be brought to a high degree of purity. The best single crystals of artificial fluorite are grown from natural materials treated by this method.

The use of artificially synthesized preparations of calcium fluoride as the raw

Fig.2 - Finely Crystalline Calcium Fluorite (the Rolled Shape of the Crystals is Due to Dissolving During Subsequent Chemical Treatment). 600 ×

material has its own peculiar features. As far back as 1949, D.Stockbarger reported (Bibl.1) the complete unsuitability of synthetic preparations of CaF_2 for growing pure single crystals of fluorite. A little later we also ran experiments in growing crystals from reagent CaF_2 (both USSR produced and that of the best foreign companies) of the grades "pure", "purissimum", etc. These experiments invariably gave the worst possible results. As a whole, we grew porcelain-like white or colored blocks, which were opaque even in thin fragments (1 - 2 mm).

STAT

Declassified in Part - Sanitized Copy Approved for Release @ 50-Yr 2014/03/07 : CIA-RDP81-01043R004200090004-8

Declassified in Part - Sanitized Copy Approved for Release @ 50-Yr 2014/03/07 : CIA-RDP81-01043R004200090004-8

A characteristic feature of reagent calcium fluoride is its exceedingly high disperseness. Under the microscope at 600 × magnification, the particles composing the preparation cannot be detected. The high disperseness, and the greatly developed surface of the particles of the material, may explain its strong contamination, and as a result, the failures of attempts to grow pure crystals from it.

The use of a special method of synthesizing CaF_2 permitted us to obtain this preparation in the form of fine (0.1 - 0.3 mm) and very pure crystallites. The peculiarity of this method is that the CaF_2 is precipitated, not from solutions of the starting salts, as it usually is, but from their melts. Figure 2 is a photomicrograph of the finely crystalline calcium fluoride obtained by this method. Pure single crystals of fluorite were grown without trouble from such preparations.

4. The Growing and Annealing of the Crystals

If the apparatus is in good adjustment, the process of growing, itself, is extremely simple.

The finely crystalline starting calcium fluoride, with an addition of 0.25% by weight of lead fluoride, is charged into the crucible. Experience shows that even under intense exhaustion of the gas and slow heating of the original material, an insignificant part of the CaF_2 is still hydrolyzed under the action of the small quantities of water adsorbed by the grains of the material, and the fluorite crystals ultimately obtained, as a result, grow slightly turbid. The lead fluoride is introduced in order to saturate with fluorine the small quantity of calcium oxide that is formed:

$$CaO + PbF_2 = CaF_2 + PbO\uparrow.$$

The PbO formed, and the excess PbF_2 at the melting points of fluorite, are completely distilled off, and even lead cannot be detected, even in traces, in the crystals grown.

The crucible with the starting material is placed in the stand 10 (see Fig. 1)

STAT

Declassified in Part - Sanitized Copy Approved for Release @ 50-Yr 2014/03/07 : CIA-RDP81-01043R004200090004-8

Declassified in Part - Sanitized Copy Approved for Release @ 50-Yr 2014/03/07 : CIA-RDP81-01043R004200090004-8

in the upper chamber of the furnace, in such a way that the cone of its bottom shall be 20 – 25 mm above the diaphragm. The apparatus is then assembled, and the gas is pumped out. The furnace is slowly heated, making sure by the manometer that the pressure does not rise above 10^{-3} mm Hg, and the material is then brought into the completely melted state. Varying the heating of the furnace, the power applied is so selected that the crystal begins to grow very slowly in the cone of the crucible. As already mentioned, this instant is determined by a magnetic probe. The crystal is grown at a furnace power level 100 – 120 watts above the value so found.

To grow the crystal, the crucible with the melt is slowly lowered by the aid of the automatic feed (at a lowering speed of 10 mm/hr) from the upper "hot" chamber of the furnace into the "cold" chamber. When fluorite crystals are grown at higher velocities than this, single crystals often do not result. At velocities of 10mm/hr, nonsingle crystals grow very rarely. The crystal after growing is cooled just as slowly in the upper chamber of the furnace.

The crystal is removed with relative ease from the crucible after growing, by means of gently tapping the inverted crucible on the table.

The crystals of fluorite so grown, have very high internal tensions, which are manifested in the form of anomalous refraction. To eliminate these tensions, the crystals are finely annealed in a special gradient-free annealing furnace. The annealing is conducted at 1100°C, followed by very slow cooling to room temperature. In order to prevent the crystals from clouding owing to hydrolysis during the process of annealing, they are placed in a large platinum crucible, and covered with powdered fluorite barely moistened with hydrofluoric acid. The crucible is then tightly closed with a platinum cover. When heating in the annealing furnace, the hydrofluoric acid is almost completely volatilized, but the very small amount of HF still remaining in the crucible is sufficient to prevent the crystals from clouding.

By this method, we have grown many thousands of single crystals of optical fluorite of two sizes: one 40 mm in diameter, weighing 200 gm, and the other 60 mm

STAT

Declassified in Part - Sanitized Copy Approved for Release @ 50-Yr 2014/03/07 : CIA-RDP81-01043R004200090004-8

Declassified in Part - Sanitized Copy Approved for Release @ 50-Yr 2014/03/07 : CIA-RDP81-01043R004200090004-8

in diameter and weighing about 800 gm.

5. Physical Properties of the Artificial Fluorite Crystals

In a number of principal physical properties (refractive index, dispersion, mechanical properties), the artificial fluorite crystals show practically no difference from the natural crystals. The heat resistance of artificial fluorite is considerably higher than that of the natural substance. While natural crystals disintegrate into small fragments when heated to 300 - 350°C (apparently on account of the presence of liquid inclusions), artificial fluorite withstands heating up to the melting point.

A substantial difference between the artificial and natural fluorite crystals is observed in the magnitude and character of internal scattering of light. In natural crystals, scattering is due to the relatively large foreign inclusions (solid, liquid and gaseous), to microfissures, etc. In good natural crystals the scattering in the spaces between the defects is negligible. In artificial fluorite, internal scattering of light of two types takes place: 1) isotropic scattering due to the extremely minute particles which fill in disorder the entire volume of the crystal; and 2) anisotropic scattering, due to the finely crystalline particles about 10 - 20 μ in size, in the form of hexagonal platelets, which are regularly oriented with their base in the (111) planes. The regular orientation of these particles may be easily observed from the periodic appearance of light refracted by these particles when the crystal is rotated about the axis of the cylinder.

Scattering of the first type is naturally connected with various nonisomorphic particles, including CaO, which is formed, as already mentioned, as a result of the hydrolysis of CaF_2. The crystal particles causing scattering of the second type are apparently formed as a result of the decomposition of the solid solution during the process of slow cooling of the single crystal. The chemical nature of the microcrystals so thrown down, still remains unelucidated.

The greatest difference was observed in the spectral transmission of natural

STAT

Declassified in Part - Sanitized Copy Approved for Release @ 50-Yr 2014/03/07 : CIA-RDP81-01043R004200090004-8

Declassified in Part - Sanitized Copy Approved for Release @ 50-Yr 2014/03/07 : CIA-RDP81-01043R004200090004-8

and artificial fluorite. The best natural crystals are transparent down to 125 mμ in the ultraviolet region, and up to 10 μ in the infrared part of the spectrum. The artificial fluorite crystals were completely transparent in the infrared region, having the same longwave boundary of transmission as the natural crystals, and differed, advantageously, from the natural crystals, in the absence of the absorption

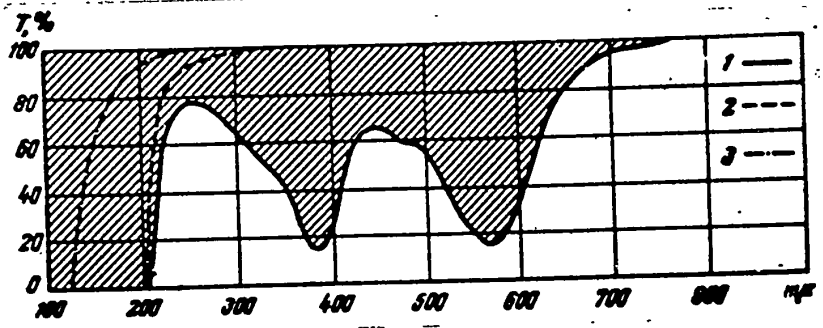

Fig.3 - Spectral Transmission of Fluorite Crystals in the Visible and Ultraviolet Parts of the Spectrum (Schematic)

1 - Artificial fluorites with visible color centers; 2 - Artificial fluorite with centers of shortwave absorption; 3 - Natural fluorite

bands of water and hydroxyl at around 2.8 and 6.0 μ. In their transmission in the shortwave part of the spectrum, however, they were substantially inferior to the natural crystals, since the boundary of transmission in them was located as a rule, around 210 mμ. In the vacuum ultraviolet (Schumann) region, the crystals were completely opaque. Moreover, the crystals often had an intense red-violet color, which made them unsuitable not only for the ultraviolet, but even for the visible part of the spectrum (Fig.3).

Another distinctive feature of these crystals was their high photochemical sensitivity. They became colored under the action of short-wave ultraviolet radiation, and also under the action of X-rays and radioactive radiations.

STAT

Declassified in Part - Sanitized Copy Approved for Release @ 50-Yr 2014/03/07 : CIA-RDP81-01043R004200090004-8

Declassified in Part - Sanitized Copy Approved for Release @ 50-Yr 2014/03/07 : CIA-RDP81-01043R004200090004-8

This difference in the properties of natural and artificial crystals of fluorite is connected with the complex physicochemical processes that take place when the crystals are grown under the conditions of vacuum and high temperatures. As a result of these processes, structural defects arise in the crystal lattice, which are connected with the deviations from stoichiometric composition and cause the coloring of the crystals, their opacity in the shortwave part of the ultraviolet spectrum, and their photochemical sensitivity.

A study of the properties of the centers causing visible coloration of the crystals show that these centers are close in nature to the electronic color centers which have been well studied in crystals of alkali halides. A study of the polarized luminescence found by us in crystals containing color centers (Bibl.4) permitted us to identify these centers with the so-called F_2-centers, i.e., with electron pairs localized in adjacent anionic vacancies. In this way we established that the absorption of light by artificial fluorite crystals is connected, not with the presence of foreign impurities in them but with structural defects, whose formation is entirely natural if we bear in mind the immense difference in the velocity of growth of artificial and natural crystals.

The establishment of the electronic nature of the absorption centers permitted us to assume that, to reduce the possibility of formation of these centers when growing crystals, foreign impurities should be introduced into the melt, which, remaining in the crystals, could serve as electron acceptors. Trivalent ions of the rare earths, which are capable of entering the fluorite lattice and isomorphically substituting calcium ions, might serve as such acceptors in the crystal lattice of fluorite, which contains divalent calcium ions. The closeness of the ionic radii of Ca^{++} (1.04) and RE^{+++} (1.04 - 0.80), which are in the same isomorphic heterovalent series, favors the isomorphic introduction of rare-earth ions (RE) into the crystal lattice. The hypothesis of the possible influence on the process of color-center formation that might be exerted by the introduction of electron-acceptor ad-

STAT

Declassified in Part - Sanitized Copy Approved for Release @ 50-Yr 2014/03/07 : CIA-RDP81-01043R004200090004-8

Declassified in Part - Sanitized Copy Approved for Release @ 50-Yr 2014/03/07 : CIA-RDP81-01043R004200090004-8

ditives was based not only on general considerations, but also on the work of Schulmann et alias (Bibl.5), who have established the desensibilizing action of additions of trivalent cations on the photochemical sensitivity of salts of the divalent metals.

In this connection we staged experiments in growing crystals of fluorite with the addition of small amounts (~10^{-2}%) of rare earth fluorides (La, Ce, Pr, Nd, Sm, Eu, Gd, Tb, Dy, Ho, Er, Tu, Yb). A study of the properties of the crystals so obtained confirm the correctness of our hypothesis. The crystals, as a rule, grew colorless and photochemically insensitive, with a higher transparency in the short-wave part of the spectrum than the crystals grown without additions of the rare earth elements*. There were, however, exceptions to this rule. Individual crystals or parts of crystals still remained photochemically sensitive and of low transparency, in spite of the presence of rare-earth ions in the crystal lattice.

We attained understanding of this difference in the behavior of the crystals as a result of a study of the luminescence spectra of the rare earths in the artificial fluorite crystals. This study showed that each rare earth element, capable of yielding a line spectrum of luminescence (element from praseodymium to thulium), display luminescence spectra of two sharply different types in artificial fluorite crystals (Bibl.6). The existence of two types of luminescence spectra (and accordingly, of absorption spectra) indicates that the nearest-neighborhood structure of the luminescent ion may vary. It was found here that there is a one-to-one correspondence between the type of luminescent spectrum and the photochemical sensitivity, and consequently, also with the transparency of the crystals. The rare earth ions may manifest their electron-acceptor properties only with an entirely definite nearest-neighborhood structure. To obtain this structure stably, it proved necessary to grow the crystals in a strongly reducing atmosphere, by adding powdered graphite to

*The absorption of the rare-earth ions themselves at these concentrations is negligible, since the corresponding transitions are forbidden.

STAT

Declassified in Part - Sanitized Copy Approved for Release @ 50-Yr 2014/03/07 : CIA-RDP81-01043R004200090004-8

Declassified in Part - Sanitized Copy Approved for Release @ 50-Yr 2014/03/07 : CIA-RDP81-01043R004200090004-8

the charge in an amount of about 0.1% of the weight of the crystal to be grown. It was found here that if the growing is conducted under these conditions, then, to create electron-acceptor centers preventing the formation of color centers, it is, in most cases, sufficient to have the same content of rare earths that is usually found in natural fluorite. It is only in individual cases, when the growing is from synthetic calcium fluorite or from natural fluorite originating in deposits very poor in rare earths, that the addition of graphite does not give favorable results, and the introduction of the rare earths themselves is required to obtain photochemically insensitive and transparent crystals.

When roasted in air at 900 - 1000°C, the crystals lose their transparency in

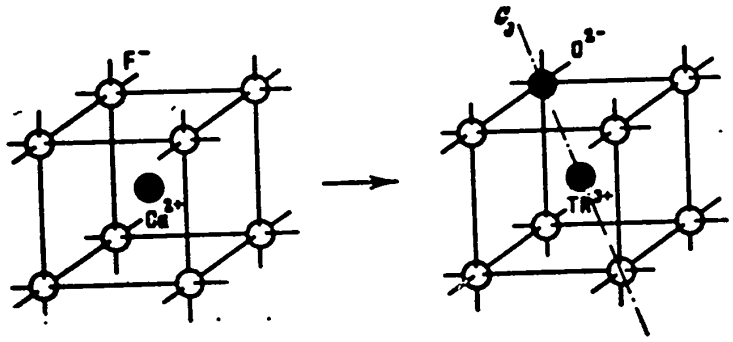

Fig.4 - Structure of Luminescence Center (Right) in the Case of Compensation of the Excess Charge by an Oxygen Ion (Center, Unable to Capture an Electron); the Segregation Direction (-·-·-) Coincides with the Third-Order Symmetry Axis; Left - Unactivated Crystal

the shortwave part of the spectrum and become photochemically sensitive. In this case, the structure of the spectrum of rare-earth luminescence changes sharply.

The difference in the structure of the luminescence centers is evidently due to the difference in the method of compensation of the excess positive charge introduced into the crystal by the isomorphic substitution of the bivalent Ca^{++} ions by the

STAT

Declassified in Part - Sanitized Copy Approved for Release @ 50-Yr 2014/03/07 : CIA-RDP81-01043R004200090004-8

Declassified in Part - Sanitized Copy Approved for Release @ 50-Yr 2014/03/07 : CIA-RDP81-01043R004200090004-8

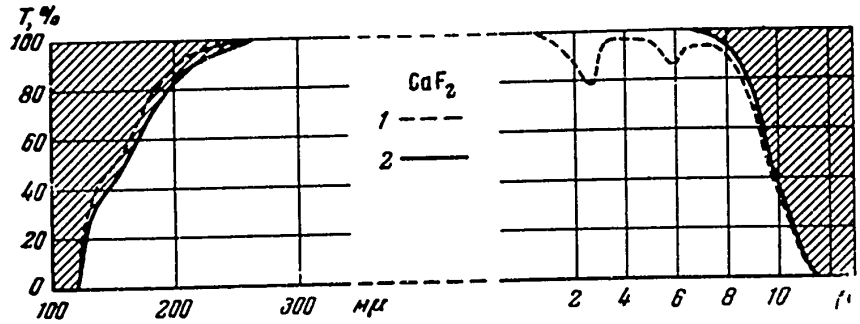

Fig.5 - Spectral Transmission of Natural (1) and Artificial (2) Fluorite (d = 5 mm) in the Ultraviolet and Infrared Parts of the Spectrum

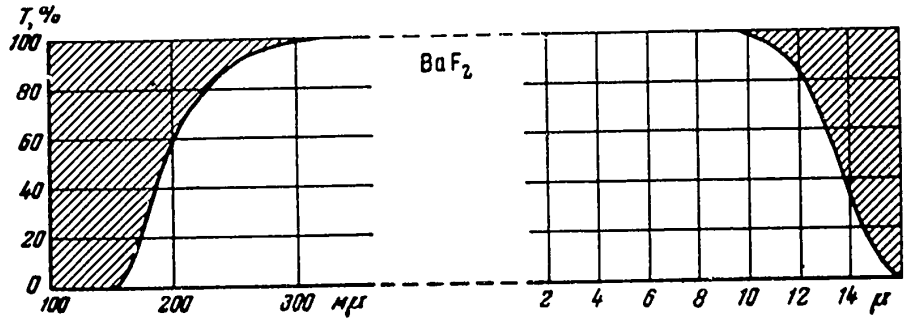

Fig.6 - Spectral Transmission of Crystals of Barium Fluoride (d = 5 mm) in the Ultraviolet and Infrared Parts of the Spectrum

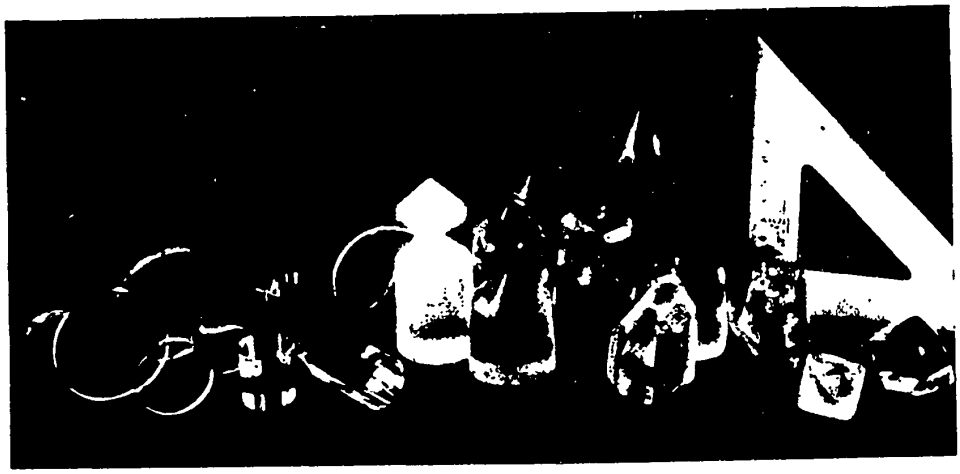

Fig.7 - Artificial Crystals of Optical Fluorite (Right) and Optical Parts Made of Artificial Fluorite (Left)

STAT

Declassified in Part - Sanitized Copy Approved for Release @ 50-Yr 2014/03/07 : CIA-RDP81-01043R004200090004-8

Declassified in Part - Sanitized Copy Approved for Release @ 50-Yr 2014/03/07 : CIA-RDP81-01043R004200090004-8

trivalent RE^{+++} ions. It is natural to assume that, in crystals roasted in air, or grown under insufficiently reducing conditions, this compensation is effected by the isomorphic substitution of one of the F^- ions (ionic radius 1.33) in the first coordination sphere surrounding the RE^{+++} ion by an O^{--} ion (1.36) (Fig.4).

This idea of the structure of the luminescent centers in crystals roasted in air is in complete agreement with the data on the orientation of rare-earth ions in the crystal lattice of fluorite, obtained from studies of the polarization of the luminescence (Bibl.7). It follows from these data that in the fluorite lattice these ions are subjected to the action of fields directed along the third-order symmetry axis. As will be seen from Fig.4, in the case of compensation of the charge by oxygen ions, the segregation direction in the nearest neighborhood of the RE^{+++} ions likewise coincides with the third-order symmetry axis.

Thus, in the case of compensation of an excess charge by an oxygen ion, the structure of the luminescence center proves stable, and the rare-earth ion cannot manifest its electron-acceptor properties. On the other hand, in crystals grown under strongly reducing conditions, compensation on account of the oxygen is impossible, and the electron-acceptor levels that can be formed in the crystal are deeper than the levels of the F- and F_2-centers. In this case, the electrons with the F-levels will migrate to the RE^{+++} ions, thus compensating the excess charge. This may prevent the localization of the electrons on levels where their presence causes the appearance of relatively long-wave absorption.

A study of the mechanism of electron processes that take place during the growing of artificial fluorite crystals has thus permitted a conscious direction of these processes, and has yielded crystals approaching, in their most valuable properties (transparency in the far ultraviolet part of the spectrum), the best specimens of natural fluorite (Fig.5).

Single crystals of barium fluoride, which also has a fluorite-type cubic lattice, may be grown in the same way. In the spectral transmission in the ultraviolet

STAT

Declassified in Part - Sanitized Copy Approved for Release @ 50-Yr 2014/03/07 : CIA-RDP81-01043R004200090004-8

Declassified in Part - Sanitized Copy Approved for Release @ 50-Yr 2014/03/07 : CIA-RDP81-01043R004200090004-8

region, BaF_2 crystals are somewhat inferior to fluorite, but they have a longer wave boundary in the infrared region of the spectrum (Fig.6). The lack of any corresponding natural mineral makes it necessary to use specially prepared synthetic preparations as the starting material for growing barium fluoride.

The technique of growing single crystals of optical fluorite developed by us is used in industry, and the optical parts of many instruments being produced today are made of artificial fluorite (Fig.7).

BIBLIOGRAPHY

1. Stockbarger,D. - Journ.Opt.Soc.Am., Vol.39 (1949), p.731
2. Obreimov,I.V., and Shubnikov,L.V. - Trudy Len.Fiz.Tekh.Lab., No.1 (1925), p.21
3. Bridgman,P.W. - Proc.Am.Acad.Sci., Vol.60 (1925), p.306
4. Feyolov,P.P. - Dok.AN SSSR Vol.92 (1953), p.545; Zhur.Eksp.Teor.Fiz., Vol.26 (1954), p.609; Izv.AN SSSR, Ser.Fizich., Vol.18 (1954), p.688
5. Schulman,J.H., Cinther,R.J., and Kirk,R.D. - Journ.Chem.Phys., Vol.20 (1952), p.1966
6. Stepanov,I.V., and Feyofilov,P.P. - Dok.AN SSSR, Vol.108 (1956)
7. Feyofilov,P.P. - Dok.AN SSSR, Vol.99 (1954), p.731

STAT

Declassified in Part - Sanitized Copy Approved for Release @ 50-Yr 2014/03/07 : CIA-RDP81-01043R004200090004-8

Declassified in Part - Sanitized Copy Approved for Release @ 50-Yr 2014/03/07 : CIA-RDP81-01043R004200090004-8

THE GROWING OF SINGLE CRYSTALS OF LITHIUM FLUORIDE AND SODIUM FLUORIDE WITH A HIGH TRANSPARENCY IN THE ULTRAVIOLET AND INFRARED REGIONS OF THE SPECTRUM

by

M.A.Vasil'yeva

In the USSR and foreign literature, there are references to the very valuable properties of single crystals of lithium fluoride as an optical material. Such properties include its high transparency in a wide range of wavelengths, which goes far beyond the limits of the visible regions of the spectrum, more specifically, from 110 mμ in the ultraviolet, to 6.5 - 7 μ in the infrared regions of the spectrum. In the shortwave ultraviolet region, lithium fluoride transmits further than any other known optical material, not excepting even fluorite, which is transparent down to 130 mμ. It may be thought that lithium fluoride in general has the furthest transmission boundary of all possible ionic crystals, since it contains the lightest of the alkali and halogen elements.

In the longwave region below 300 mμ, the dispersion in lithium fluoride crystals increases strongly. This property, together with its high transparency in the entire ultraviolet region of the spectrum, and especially in the shortwave ultraviolet, puts lithium fluoride crystals in the category of the best optical material for vacuum spectral instruments with a working range in the far ultraviolet (shorter than 250 - 200 mμ).

Lithium fluoride crystals also possess other valuable properties. Thus, for example, they are rather resistant to the action of atmospheric reagents (and consequently, optical parts made of such crystals do not require special protection), they are very heat resistant, and in hardness they are only slightly inferior to fluorite.

STAT

Declassified in Part - Sanitized Copy Approved for Release @ 50-Yr 2014/03/07 : CIA-RDP81-01043R004200090004-8

Declassified in Part - Sanitized Copy Approved for Release @ 50-Yr 2014/03/07 : CIA-RDP81-01043R004200090004-8

Crystals of lithium fluoride are not encountered among the natural minerals. They can be obtained only artificially. With a well adjusted procedure for growing, single crystals of lithium fluoride may be produced in large sizes, weighing several kilograms (Bibl.1, 2).

In the Soviet Union, the growing of lithium fluoride crystals has long been mastered (in the years from 1937 to 1939). Since then, i.e., during almost 20 years, our laboratories and industry have produced a large number of such crystals, of rather large sizes. But the quality of the crystals that have been grown has proved in most cases to be unsatisfactory.

The Stockbarger and Kyropoulos methods, which have been utilized and considerably improved by us, have permitted the growing of entirely satisfactory crystals of rock salt, sylvine, and several other alkali halides. However, until recently, we have not succeeded in growing good lithium fluoride crystals by the same methods. They were opaque in the Schumann region of the spectrum, that is, for wavelengths shorter than 200 mμ, frequently colored yellow, and had several deep absorption bands in the infrared region of the spectrum.

The suspicion arose, already in the initial stages of the work, that the poor quality of lithium fluoride crystals was primarily related to the insufficient purity of the raw material. This assumption was subsequently completely confirmed. It was found that to obtain pure lithium fluoride crystals requires a considerably higher degree of chemical purity of the starting material than in growing crystals of rock salt, sylvine, etc.

The attempts of various laboratories and plants to prepare the reagent grade of the high degree of purity required by us were unsuccessful for many years. The specimens of lithium fluoride at our disposition, produced by the best foreign companies (Merck, Riedel de Haen, grades "rein", "reinst") likewise proved to be unsuitable for the preparation of high-grade lithium fluoride crystals.

The question arose whether the procedure for growing crystals could not be

STAT

Declassified in Part - Sanitized Copy Approved for Release @ 50-Yr 2014/03/07 : CIA-RDP81-01043R004200090004-8

Declassified in Part - Sanitized Copy Approved for Release @ 50-Yr 2014/03/07 : CIA-RDP81-01043R004200090004-8

modified so as to grow optically perfect lithium fluoride crystals from the available starting material of average quality.

A regularly conducted chemical and spectral control of the starting lithium fluoride showed that, regardless of the origin of the preparation, the principal contaminations were Si, Al, Ca, Mg, Pb, Na. Certain other impurities were also present, for example, Mn, Zn, Ag, Cu, Tl, etc., but either in insignificant quantities, or as an exception.

It was of interest to trace the distribution of the impurities, during the growing of the crystals, between the pure parts of the crystal, its strongly contaminated parts, and the residue of the melt in the crucible after the crystal had been grown.

The following table, compiled on the basis of many analyses, gives the answer to this question.

Table

Specimen	Si	Al	Ca	Mg	Pb	Na
Original LiF	++	++	++	++	++	++
Transparent part of crystal	++	+	+	++	+	+
Cloudy part of crystal	++++	+++	+++	++	+++	++

As will be seen from the Table, the purest and the most contaminated parts of the crystal contain about the same impurities that were present in the original preparation. Their quantitative content in the pure and contaminated parts of the crystal, however, differed sharply. As a rule, the contaminated parts of the crystal proved to be particularly enriched in Si, Al, very often Ca, Mg, and Pb, and sometimes with small quantities of Mn, Zn, etc.

The presence of these contaminations in the starting lithium fluoride made it very difficult to grow single crystals, and when their content was very high, it was

STAT

Declassified in Part - Sanitized Copy Approved for Release @ 50-Yr 2014/03/07 : CIA-RDP81-01043R004200090004-8

Declassified in Part - Sanitized Copy Approved for Release @ 50-Yr 2014/03/07 : CIA-RDP81-01043R004200090004-8

not possible to grow single crystals at all. Single crystals of lithium fluoride grown from not very badly contaminated material, proved to be more or less cloudy and colored. Moreover, the presence of impurities spoiled the spectral transmission of the crystals, as a rule, completely cutting off all the shortwave, and part of the longwave ultraviolet region of the spectrum, and badly affected the transmission in the visible and infrared regions of the spectrum, constant absorption bands being observed in the infrared region at about 2.7 μ, coinciding with the absorption band of OH^- ions (Fig.1).

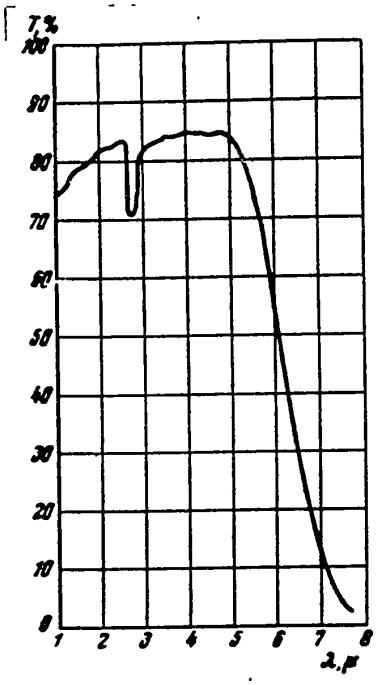

Fig.1 - Transmission (T) of Lithium Fluoride in Infrared Region of the Spectrum; This Crystal was Grown in Air

It was found that the presence of hydroxyl absorption bands in the infrared region was due to the presence of small quantities of free alkali in the starting lithium fluoride (about 0.5%) and to its presence in considerably greater quantities (about 5 - 6%) in the badly contaminated parts of the crystal, and especially in the residue of the melt after growing the crystal. And, finally, aqueous extracts of the finely ground pure parts of the crystals likewise showed an alkaline reaction.

Neutralization of the original preparation with HF yielded no appreciable improvement - the contents of free alkali in the crystals and residue of the melts remained approximately the same.

The appearance of large quantities of free alkali in the melt, in quantities many times greater than its content in the original preparation, is explained by the

STAT

Declassified in Part - Sanitized Copy Approved for Release @ 50-Yr 2014/03/07 : CIA-RDP81-01043R004200090004-8

Declassified in Part - Sanitized Copy Approved for Release @ 50-Yr 2014/03/07 : CIA-RDP81-01043R004200090004-8

ready hydrolysis of LiF during its heating for melting as a result of the interaction of LiF with the atmospheric moisture. The loss of fluorine and the enrichment of the melt with OH^- ions proceeds according to the equation:

$$LiF + H_2O = LiOH + HF \uparrow.$$

This reaction becomes marked at 350 - 400°C, and its velocity strongly increases with increasing temperature and with increasing concentration of water vapor over the surface of the lithium fluoride.

During the time of growth of an LiF crystal, the hydroxyl ion isomorphously substitutes the fluorine ion in the crystal lattice of lithium fluoride, yielding as a result, an entirely homogeneous mixed crystal containing LiF and LiOH.

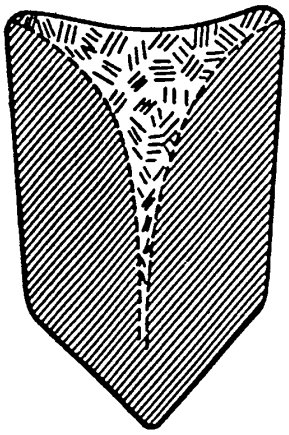

Fig.2 - Distribution of Contaminations in Lithium Fluoride Crystal Grown in a Vacuum

It does not appear possible to prevent hydrolysis when the crystals are grown in ordinary air. It has been found by experience, however, that the process of hydrolysis proceeds most intensely not in the melted material, but at temperatures somewhat below the melting point, when the surface of the powder grains is still rather great. It has also been established that if, after melting the material, it is saturated with hydrogen fluoride, then lithium fluoride crystals, without appreciable absorption bands of water in the 2.7 μ region can be grown from such a melt. We accomplished the saturation of the melt with hydrogen fluoride in a very simple way - at the end of the melting of the lithium fluoride, the last additions were made with powder slightly moistened with hydrofluoric acid.

STAT

Declassified in Part - Sanitized Copy Approved for Release @ 50-Yr 2014/03/07 : CIA-RDP81-01043R004200090004-8

Declassified in Part - Sanitized Copy Approved for Release @ 50-Yr 2014/03/07 : CIA-RDP81-01043R004200090004-8

This procedure permitted us to grow lithium fluoride crystals with improved transmission in the infrared region of the spectrum, but it showed no appreciable effect on the transmission of the crystals in the visible and ultraviolet regions. As before, the crystals were colored, and were transparent in the ultraviolet region only down to 200 mμ.

A 1955 experimental project on growing lithium fluoride crystals in a vacuum was staged on apparatus developed by us for growing crystals of optical fluorite (Bibl.3). The process of growing lithium fluoride differed only in the temperature range in which the operations of melting, growing, etc. were conducted.

Let us attempt to explain the principal processes taking place during the melting and crystallization of lithium fluoride in a vacuum during continuous and intense exhaustion of the gases.

In the initial stage of the heating up to 150 - 200°C, there is intense elimination of the adsorbed water and other gases. This process is accompanied by a strong but temporary breaking of the vacuum. On further heating, the pressure of the gases remains almost constant up to 400 - 450°C. Near these temperatures a second decline in the vacuum is observed, apparently connected with the dehydration of LiOH and its conversion into Li_2O, as well as to the conversion of the other hydrated compounds in the material.

The process of decomposing the hydrates proceeds in a wide temperature range, and ends only after the entire mass of lithium fluoride has been melted. From this moment, the gas pressure falls to $2 - 6 \times 10^{-4}$ mm Hg, and remains approximately constant until the end of the growing process. Parallel to these chemical processes, there also proceed processes of simple distillation of a number of substances with high vapor pressure. Such substances include, first of all, a group of fluorine compounds, for instance, the fluorides of Si, Al, Mn, etc. Their vapor pressure at temperatures as low as 100 - 200°C ranges from several mm Hg up to many atmospheres (for instance, the vapor pressure of SiF_4 is about 2 atm at a temperature as low

STAT

Declassified in Part - Sanitized Copy Approved for Release @ 50-Yr 2014/03/07 : CIA-RDP81-01043R004200090004-8

Declassified in Part - Sanitized Copy Approved for Release @ 50-Yr 2014/03/07 : CIA-RDP81-01043R004200090004-8

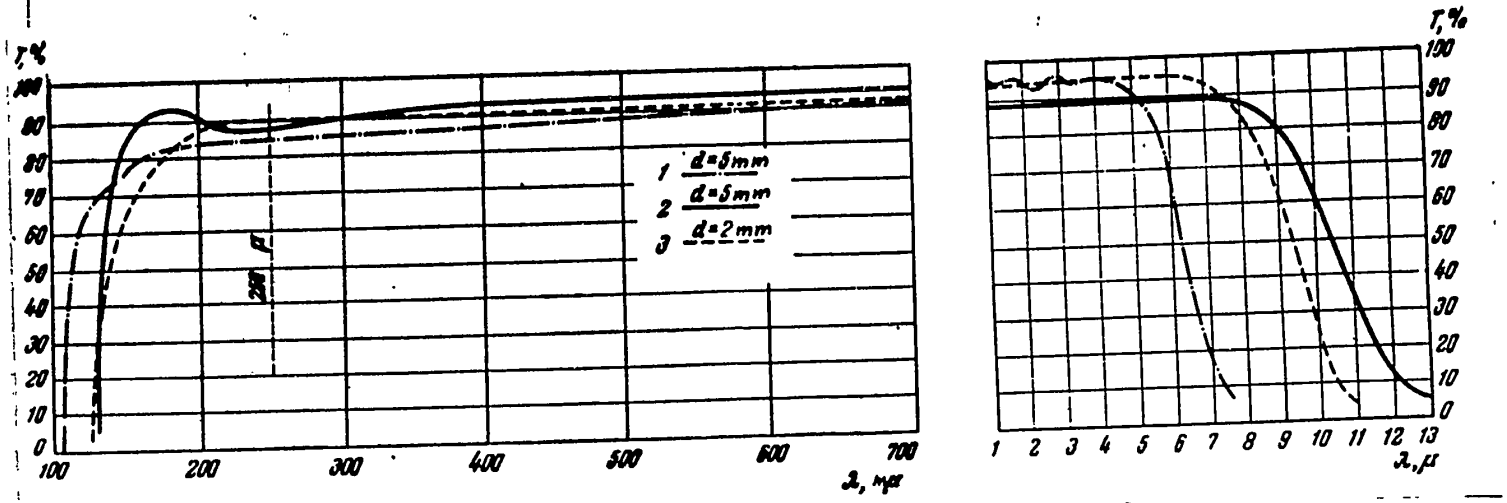

Fig.3 - Curves of Spectral Transmission (T) of Artificial Single Crystals

1 - Lithium fluoride; 2 - Sodium fluoride; and 3 - Fluorite

STAT

Declassified in Part - Sanitized Copy Approved for Release @ 50-Yr 2014/03/07 : CIA-RDP81-01043R004200090004-8

Declassified in Part - Sanitized Copy Approved for Release @ 50-Yr 2014/03/07 : CIA-RDP81-01043R004200090004-8

as 80°C).

As a result of this distillation, a considerable part of the impurities in the lithium fluoride is removed from the melt.

Even when lithium fluoride crystals are grown in vacuo, it is still not possible to obtain a high-grade crystal from poor raw material in a single step. Cloudy regions, in which the contaminations are concentrated, are likewise formed in them. These regions usually occupy a volume in the crystal in the form of an inverted cone, with the vertex at the bottom (Fig.2). Most of the crystal, however, grows without color, but with a faint opalescence, and of moderate transparency in the shortwave part of the spectrum.

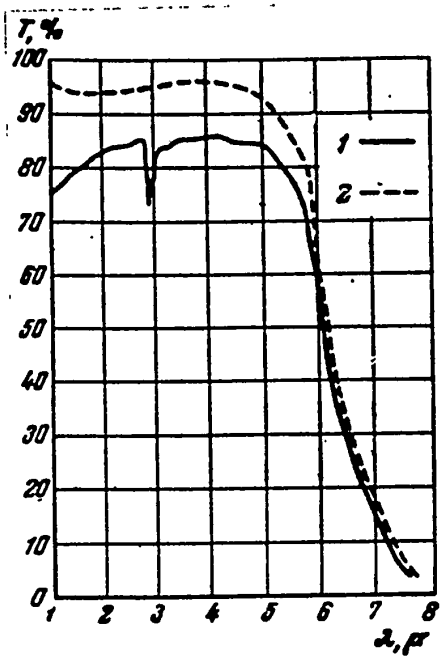

Fig.4 - Transmission (T) of Lithium Fluoride Crystals

The crystals were grown: 1 - In the air; and 2 - In vacuo

It was found during the work that the contaminated parts of vacuum-grown crystals do not contain silicon nor aluminum, as is the case in crystals grown in the ordinary atmosphere. This is explained by the ease of distillation of their fluorine compounds in the vacuum. The principal contaminant of such parts is Li_2O, a compound which is nonisomorphic with LiF. In crystals grown in the atmosphere, however, Li_2O cannot be detected. They do, however, contain a certain quantity of LiOH, which does enter isomorphously into the LiF crystal lattice. Thus, on heating and melting lithium fluoride in vacuo, it is freed from the principal isomorphous impurity (LiOH) and becomes genuinely pure.

The crystals so grown were broken up into large lumps, from which the cloudy

STAT

Declassified in Part - Sanitized Copy Approved for Release @ 50-Yr 2014/03/07 : CIA-RDP81-01043R004200090004-8

Declassified in Part - Sanitized Copy Approved for Release @ 50-Yr 2014/03/07 : CIA-RDP81-01043R004200090004-8

parts were carefully removed. The transparent parts, however, were then utilized as raw material for regrowing.

The regrown crystals already differ markedly in their optical indices from the crystals grown in vacuo after the first crystallization, and still more from crystals grown from the same raw materials under ordinary atmospheric conditions (by the Kyropoulos or Stockbarger method).

Figure 3 gives the curves of spectral transmission of lithium fluoride crystals twice grown in vacuo, and of sodium fluoride, also grown in vacuo.

For a final conclusion as to the quality of lithium fluoride crystals grown in vacuo, we give in Fig.3 a transmission curve of a good specimen of optical fluorite. It will be seen that lithium fluoride transmits further in the shortwave ultraviolet region than the best specimens of fluorite, namely down to 105 mμ, while the best fluorite specimens are transparent only down to 125 - 130 mμ. Figure 4 shows the transmission of lithium fluoride crystals in the infrared regions, grown in the atmosphere and in vacuo. The vacuum-grown crystals have a higher total transmission (almost 10% higher); and also have no absorption bands of water in the 2.7 μ region.

Another practically important result of this work is the possibility, demonstrated by us, of using certain base metals as a material for crucibles employed for growing lithium fluoride and sodium fluoride crystals. The following base metals with a high melting point were tried: Fe, Ni, Mo, W, Tl. Experience showed that all these materials are entirely resistant to the action of melts of lithium and Na fluoride, and also of calcium fluoride (fluorite), provided water vapor and oxygen are absent from the surrounding medium. The single crystals of lithium fluoride and sodium fluoride that are vacuum-grown in crucibles of these materials have no specific tinge due to the presence of these metals. More precise spectrophotometric studies likewise failed to reveal their presence in the crystals grown.

It should be noted that the upper limit of the temperatures at which the utilization of one base metal or another is possible, lies below its melting point, and is

STAT

Declassified in Part - Sanitized Copy Approved for Release @ 50-Yr 2014/03/07 : CIA-RDP81-01043R004200090004-8

Declassified in Part - Sanitized Copy Approved for Release @ 50-Yr 2014/03/07 : CIA-RDP81-01043R004200090004-8

determined by the beginning of its intense vaporization in vacuo.

Another remarkable property of the metals so tested was the unwettability of their surfaces by melts of fluorides (except for tantalum). The crystals grown do not intergrow with the walls of the crucibles, and are removed from them with perfect freedom. This property advantageously distinguishes these metals even from platinum, so widely used, which is very difficult to separate from the crystal: the crucible

Fig.5 - Lithium Fluoride Crystals

must be broken and the crystal removed from it in small parts. By comparison with metal crucibles (iron, nickel, and molybdenum), crucibles made of the pure grades of artificial graphite have great advantages. Their shape does not change under thermal and mechanical influences taking place during the growth of the crystals. Many tens of lithium fluoride or sodium fluoride crystals can be grown in a single graphite crucible. The manufacture of graphite crucibles is considerably simpler than that of metal crucibles, especially those of molybdenum.

The possibility of replacing platinum by base metals opens up wide possibilities of industrial manufacture of lithium fluoride crystals of large sizes and high quality, using vacuum technology.

Thus, we consider the possibility of growing lithium fluoride crystals with the

STAT

Declassified in Part - Sanitized Copy Approved for Release @ 50-Yr 2014/03/07 : CIA-RDP81-01043R004200090004-8

Declassified in Part - Sanitized Copy Approved for Release @ 50-Yr 2014/03/07 : CIA-RDP81-01043R004200090004-8

widest transmission in the Schumann region of the spectrum, and without selective absorption bands in the infrared region, to have been established. For growing high-grade lithium fluoride crystals (Fig.5), starting material of average quality may be used.

The possibility of avoiding the use of the noble metals considerably simplifies the problem of industrial preparation of these crystals.

BIBLIOGRAPHY

1. Stockbarger,D. - Preparation of Large Single Crystals of Lithium Fluoride. Rev.Sci.Inst., Vol.7 (1936), pp.133 - 136

2. Cramers, - Synthetic Optical Crystals. Ind.Eng.Chem. (Industrial Ed.) Vol.32, No.11 (1940), pp.1478 - 1483

3. Stepanov,I.V., and Feofilov,P.P. - Artificial Fluorite. This Symposium, p.229

STAT

Declassified in Part - Sanitized Copy Approved for Release @ 50-Yr 2014/03/07 : CIA-RDP81-01043R004200090004-8

Declassified in Part - Sanitized Copy Approved for Release @ 50-Yr 2014/03/07 : CIA-RDP81-01043R004200090004-8

METHODS OF GROWING LUMINESCENT CRYSTALS FOR SCINTILLATION COUNTERS

by

L.M.Belyayev, B.V.Vitovskiy, and G.F.Dobrzhanskiy

The use of crystals of a number of luminescent substances in physical instrument building began in 1947 - 1948. The widely known method of registration of nuclear radiation by the aid of scintillations (Bibl.1) has been considerably improved in recent years. The visual method of counting the scintillations has been replaced by photoelectric registration by the aid of what are called electron multipliers (Bibl.2). A zinc sulfide screen, and a considerable number of crystalline, plastic and liquid phosphors are being used. The combination of a photoelectronic multiplier, a crystalline, plastic or liquid scintillator, and a special radiocircuit counting device has received the name of scintillation counter (Bibl.3). Such a scintillation counter is finding wider and wider application for the registration of nuclear radiation and in studies of the radiations emitted during operation of various particle accelerators. The scintillator (crystalline, plastic or liquid phosphor) plays an important role in such instruments, for it serves as a peculiar transducer of the invisible nuclear radiation into visible radiation. This transformation takes place at the instant of interaction of the radiation with matter. The character of the interaction of various forms of radiation with matter varies. Taking these differences into account, the requirements for scintillators are now formulated, and a rather broad class of substances used for these purposes has been found. We shall discuss only the crystalline scintillators.

For crystalline scintillators to meet the demands made on them, the crystals must possess:

1) Rather high density, and the presence of chemical elements and isotopes which are most reactive for the given form of radiation;

STAT

Declassified in Part - Sanitized Copy Approved for Release @ 50-Yr 2014/03/07 : CIA-RDP81-01043R004200090004-8

Declassified in Part - Sanitized Copy Approved for Release @ 50-Yr 2014/03/07 : CIA-RDP81-01043R004200090004-8

2) High physical effectiveness (the proportion of the absorbed energy converting into light must be high) and low transparency for its own radiation; the region of its own radiation must, to the maximum degree, correspond to the region of spectral sensitivity of the photocathode of the electron multiplier;

3) Short quenching time, i.e., low inertness;

4) Good mechanical properties, good heat and moisture resistance, so that they can be used under various conditions.

We present a list of the crystals used in practice as the most effective scintillators. These substances are conveniently divided into two groups, organic and inorganic. The two groups differ not only in chemical composition, but also in the mechanism of the luminescent processes that take place in them (Bibl.4). Table 1 is a list of the most effective organic substances, and their physical and chemical characteristics.

Table 1

Name	Melting Point °C	Density, gm/cm³	Maximum of Radiation Spectrum, Å	Characteristic Absorption Maximum, Å	Luminescence Decay, sec
Naphthalene $C_{10}H_8$	80	1,15	3450		$6 \cdot 10^{-8}$
Anthracene $C_{14}H_{10}$	216	1,28	4400	4050	$3 \cdot 10^{-8}$
Phenanthrene $C_{14}H_{10}$	101	1,03	4100 4300		$8 \cdot 10^{-9}$
Chrysene $C_{18}H_{12}$	254		4190 3520		$4 \cdot 10^{-8}$
Dibenzyl $C_{14}H_{14}$	52	1,0	3950		$1,5 \cdot 10^{-8}$
Stilbene $C_{14}H_{12}$	124	1,16	4200 4080		$8 \cdot 10^{-9}$
Tolane $C_{14}H_{10}$	62,5	1,18	3900		$6 \cdot 10^{-9}$
Terphenyl $C_{18}H_{14}$	213	1,23	4000		$1,2 \cdot 10^{-8}$
Quaterphenyl $C_{24}H_{18}$	318		4200		$8 \cdot 10^{-9}$

Table 2 lists the inorganic substances, and gives their physical and chemical

STAT

Declassified in Part - Sanitized Copy Approved for Release @ 50-Yr 2014/03/07 : CIA-RDP81-01043R004200090004-8

Declassified in Part - Sanitized Copy Approved for Release @ 50-Yr 2014/03/07 : CIA-RDP81-01043R004200090004-8

characteristics.

It will be seen from Tables 1 and 2 that the use of various methods is required for growing crystals of these substances. It must be added that the specific nature

Table 2

Substance	Melting Point °C	Density, gm/cm³	Refractive Index	Maximum of Emission Spectrum, Å	Characteristic Absorption Maximum, Å	Luminescence Decay, sec
LiBr(Tl)	547	3,464	1,784			
LiI(Tl)	446	4,06	1,955	4500		$>10^{-6}$
KI(Tl)	682	3,13	1,677	4100	2870	
					2360	$>10^{-6}$
NaI(Tl)	651	3,67	1,770	4100	2930	$2\cdot10^{-7}\div3\cdot10^{-7}$
			1,48		2340	$2,5\cdot10^{-7}$
CsF	684	3,59	1,578	4000		$5\cdot10^{-9}$
			1,582			
CsBr(Tl)	636	4,44	1,698		ultraviolet	
CsI(Tl)	621	4,51	1,787	2410		
				2190	»	$5\cdot10^{-7}\div11,1\cdot10^{-6}$
				2990		
				4350		
RbI(Tl)	642	3,55	1,648	4800		$\sim10^{-6}$
$CaWO_4$	1535	6,10	1,920	4300	<3800	$6\cdot10^{-6}$
$CdWO_4$	1325	7,90	2,20	5200	<4500	$8\cdot10^{-6}$

of the application of crystalline scintillators demands crystals of rather large size. To solve certain problems, single crystals of diameter up to 250 mm, and height up to 100 mm, must be used in scintillation counters. In other cases, very thin plates (down to 0.1 mm thick), but of large area, are used. Taking account of these demands, the methods of growing crystals were, in fact, worked out.

1. Growing Organic Crystals

Naphthalene has a melting point of 80.2°C, and crystallizes in the prismatic class of the monoclinic system. Tolane, or diphenylacetylene, has a melting point

STAT

Declassified in Part - Sanitized Copy Approved for Release @ 50-Yr 2014/03/07 : CIA-RDP81-01043R004200090004-8

Declassified in Part - Sanitized Copy Approved for Release @ 50-Yr 2014/03/07 : CIA-RDP81-01043R004200090004-8

of 62.5°C, and crystallizes in the same class as naphthalene. The distinctive feature of these substances, from the point of view of the production of single crystals, is their high volatility, which prevents the use of the well-known methods of crystallization. The methods of crystallization of naphthalene described in the literature (Bibl.5, 6, 7, 8) make it possible to obtain only crystals of small size. Taking account of the physical and chemical peculiarities of these substances, we have proposed the method and apparatus that is being used at the Kharkov chemical reagent plant. The crystals are grown in crystallizers that can be taken apart, and have a cooled bottom. The crystal seed is mounted on a special stage, and the growing crystal is withdrawn from the crystallizer by the aid of the same stage.

We give a description of the apparatus below. For convenience of production, three crystallizers are installed together (Fig.1).

The three-unit crystallization apparatus consists of:

a) A water bath (1), in the form of a rectangular copper tank 730 × 270 × 140 mm in size;

b) The two heaters (2), located at the bottom of the copper tank, one of them designed for continuous operation, while the second (emergency) heater is turned on only if the first one goes out of commission; each heater draws about 2 kw; the heaters consist of a nichrome spiral enclosed in a copper tube and insulated from it by special insulators and a filling of alumina; the ends of the spirals are connected to the terminals (4) mounted on the block (3);

c) The three cylindrical brass crystallizers (5), 145 - 150 mm in diameter, soldered into the bottom of the water bath (1); the cooler (6), with the two copper tubes (7) for supplying and withdrawing cold water, is soldered to the bottom of each crystallizer;

d) The three stages (8) which are placed in the crystallizers, and on which, properly speaking, the growth of the crystals really takes place; by the aid of these stages the grown crystal is withdrawn from the crystallizer;

STAT

Declassified in Part - Sanitized Copy Approved for Release @ 50-Yr 2014/03/07 : CIA-RDP81-01043R004200090004-8

Declassified in Part - Sanitized Copy Approved for Release @ 50-Yr 2014/03/07 : CIA-RDP81-01043R004200090004-8

e) The three heated covers (9), covering the crystallizer; in these covers is installed the nichrome spiral (10), the ends of which are attached to the terminals (11) on the block (12), which is fastened to the cover; the power of each heater is about 40 - 50 watts; the heated covers are necessary because the heating of the melt from above, provided by these covers, prevents parasitic crystallization on the surface;

f) The wooden case (13), in which the bath is installed;

g) The heat insulation (14), of asbestos shreds;

h) The getinax cover (15) for the entire apparatus, on which are mounted: 1) the type DT-75 motor (16) (2100 rpm, 220 v, clockwise rotation). Through a pair of conical gears, the motor is connected with the turbine-type stirrer attached to the same cover for mixing the water in the bath. The stirrer is so designed that the water collects in a single space and is distributed in three directions, thereby assuring thorough mixing of the water through the entire bath; (this stirrer is not shown in the Fig.); 2) The contact thermometer (17); the control thermometer (18); the float level indicator (19) for the water in the bath; the opening for filling the water bath, closed by the plug (20);

i) A rotameter which registers the amount of water arriving in the cooler; (in this way the process of crystal growing is standardized); depending on the water temperature, its consumption is determined individually for each substance.

The crystallization apparatus is designed for operation from a 220 v two-phase electric line. It draws about 3 - 3.5 kw. The overall dimensions of the apparatus are 860 × 450 × 300 mm^3. The water consumption does not exceed 20 ltr/hr.

A manufacturing process was worked out for this apparatus. We present the sequence of the main operations of the process of growing mixed crystals of naphthalene and anthracene.

1. The bath is filled with distilled water through a special opening in the cover, and is heated to 85°C.

STAT

Declassified in Part - Sanitized Copy Approved for Release @ 50-Yr 2014/03/07 : CIA-RDP81-01043R004200090004-8

Declassified in Part - Sanitized Copy Approved for Release @ 50-Yr 2014/03/07 : CIA-RDP81-01043R004200090004-8

2. A single crystal seed about 10 mm thick, oriented along the (001) face, and filling the entire surface of the stage, is placed on the stage and, together with the stage, is heated in a drying cabinet to 70 - 75°C.

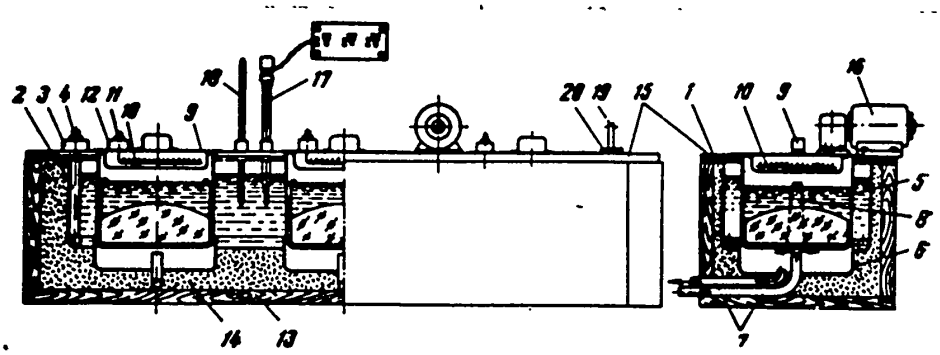

Fig.1 - Schematic Diagram of Apparatus for Growing Naphthalene and Tolane

1 - Water bath; 2 - Heater; 5 - Crystallizer; 6 - Cooler; 8 - Stage; 9 - Cover with heating device (detailed description given in text)

3. A melt of naphthalene heated to 85°C is poured into the crystallizer, and 0.5 weight % of activator (anthracene) is added.

4. The platform with the seed is placed in the crystallizer; in a few minutes the seed is slightly melted and lies tightly against the platform.

5. The cover of the crystallizer is closed, and at the same time the water cooling is turned on; the bath temperature is somewhat decreased.

6. The growth of the crystal begins and proceeds at the approximate velocity of 0.5 mm/hr (perpendicular to the surface of the seed)*.

7. After the crystal has reached the necessary size, the cooling is stopped, and as a result a certain melting of the crystal takes place at the side walls and at the bottom of the crystallizer, and the stage with the crystal lying on it is

*As the thickness of the crystal increases, the cooling must be intensified, i.e., the quantity of running water must be increased.

STAT

Declassified in Part - Sanitized Copy Approved for Release @ 50-Yr 2014/03/07 : CIA-RDP81-01043R004200090004-8

Declassified in Part - Sanitized Copy Approved for Release @ 50-Yr 2014/03/07 : CIA-RDP81-01043R004200090004-8

withdrawn from the crystallizer.

8. The crystal is transferred to the thermostatic cabinet for slow cooling.

The industrial process of growing mixed crystals of naphthalene and anthracene has been described above only in outline. And, of course, in cases where crystals of pure naphthalene, tolane or dibenzyl are grown on this apparatus instead, the principal temperature points in the rate of growing will be different.

This crystallizing apparatus may be used to crystallize, not only highly volatile substances, large crystals of which cannot be grown by other methods, but also a number of other substances. By replacing the water in the bath with some other liquid having a higher boiling point, crystals of substances with a melting point exceeding 100°C may be grown. The apparatus is also convenient because it permits the growing crystal to be kept under observation. The removal of the cover from the crystallizer, for a time that is not very long, does not disturb the processes of crystallization. This fact is of very substantial importance, since in some cases, one can intervene in the process of crystallization. In crystallizing volatile substances, especially with a high velocity of growth, a gas bubble may appear on the surface of the crystal. Adhering to the surface, this bubble will move together with it during the period of crystallization, leaving a space beneath it unfilled with solid substance. For this reason, if such a bubble is detected on the crystal surface during the process of growth, it is necessary not only to remove it, but to proceed so the cavity formed shall be filled by the growth. For this purpose, some thin pointed object is introduced for an instant to a certain depth, thus helping to fill the channel with melt.

The shortcomings of this melt include the fact that owing to the low thermal conductivity of crystals, they grow with high internal stresses, which cannot always be removed by annealing.

We have developed a procedure for crystallizing stilbene. Stilbene, or diphenylethylene, likewise belongs, with respect to its symmetry, to the prismatic class

STAT

Declassified in Part - Sanitized Copy Approved for Release @ 50-Yr 2014/03/07 : CIA-RDP81-01043R004200090004-8

Declassified in Part - Sanitized Copy Approved for Release @ 50-Yr 2014/03/07 : CIA-RDP81-01043R004200090004-8

of the monoclinic family (its melting point is 124°C). The procedure for producing stilbene-crystals was based on two methods: the Obreimov-Shubnikov method (Bibl.9), and the Bridgmann method (Bibl.10). Of the modern methods of crystallization, this technique comes closest to the method proposed by B.V.Vitovskiy and A.B.Zemtsov (Bibl.11), crystallization from a melt with an isothermal surface of crystallization withdrawn from the zone of heating.

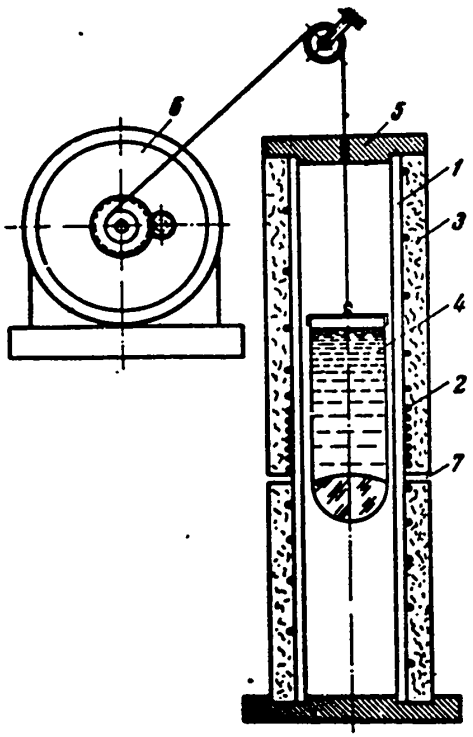

Fig.2 - Furnace for Growing Stilbene:

1 - Quartz tube; 2 - Heater winding; 3 - Heat insulation; 4 - Test tube with melt; 5 - Cover; 6 - Clockwork mechanism; 7 - Peep hole

The furnace built for this work consists of a quartz tube 55 mm in diameter, and 700 mm high, with an outside winding of nichrome wire 0.5 mm in diameter (Fig.2).

The corners of the winding are distributed irregularly along the entire tube, producing a certain temperature gradient assuring the necessary conditions for crystal growth. The turns of their maximum density in the middle part of the tube produce a zone of maximum heating in this place; above and below this zone, the spacing of the turns is considerably less, and consequently, the heating is also substantially less.

For thermal insulation, the furnace is wrapped with asbestos fabric on the outside, and is tightly closed with covers on the top and bottom. At the lower level of the maximum temperature zone there is a small peep window in the asbestos fabric for placing a test tube with melt at the

STAT

Declassified in Part - Sanitized Copy Approved for Release @ 50-Yr 2014/03/07 : CIA-RDP81-01043R004200090004-8

Declassified in Part - Sanitized Copy Approved for Release @ 50-Yr 2014/03/07 : CIA-RDP81-01043R004200090004-8

beginning of crystallization and observing the quality of the crystal during the process of growth.

The power drawn by such a furnace is only 47 watts. To avoid sharp temperature jumps inside the furnace, which might result from line voltage fluctuations, the current is supplied through a voltage stabilizer. In addition, an LATR-2 autotransformer is connected in series with the stabilizer, making it possible not only to adjust the furnace at the beginning, but also to use the furnace for crystallizing substances with other melting points.

The operating conditions for the furnace are so set as to bring the isothermal surface of crystallization outside the zone of maximum heating (Fig.3). Owing to this fact, the substance in the test tube is in the molten state over a wide range of test tube heights. Close to the isothermal surface of crystallization, a temperature drop of 10 - 15°C is observed. This both encourages deformation of the crystals and at the same time protects the crystal already formed from disintegration.

Owing to such a design of the furnace, we succeeded in growing crystals at a high velocity, without very carefully maintaining temperature stability throughout the process.

When the conditions in the furnace have already been established, and the position of the zone has been noted, the preparation for crystallization begins. To obtain stilbene crystals, one uses pyrex glass test tubes with a hemispherical bottom. The stilbene is grown on a seed. The seed is so prepared that its lower part has the same shape as the bottom of the test tube, and its upper part has the same diameter as the test tube. The seed is first oriented. The most successful orientation for stilbene is attained when the upper surface of the seed coincides with the plane of cleavage.

The test tubes in which crystallization is to be performed, are preheated and filled with the substance, already melted, which permits effective utilization of their volume. A preheated seed is next lowered into the test tube. In this case,

STAT

Declassified in Part - Sanitized Copy Approved for Release @ 50-Yr 2014/03/07 : CIA-RDP81-01043R004200090004-8

Declassified in Part - Sanitized Copy Approved for Release @ 50-Yr 2014/03/07 : CIA-RDP81-01043R004200090004-8

it is necessary to have the seed lie regularly against the test tube bottom. The test tube is then closed with the moving cover, suspended on a thin string with a hook, and lowered into the furnace. The other end of the cord is attached to the shaft of a clockwork mechanism making one revolution a day. The test tube is so placed in the furnace that the upper surface of the seed shall be above the isotherm of crystallization. It is very important to put the test tube at the center of the furnace. The furnace is then closed by means of the cover, and the crystallization begins.

The crystallization proceeds during the process of lowering the test tube with

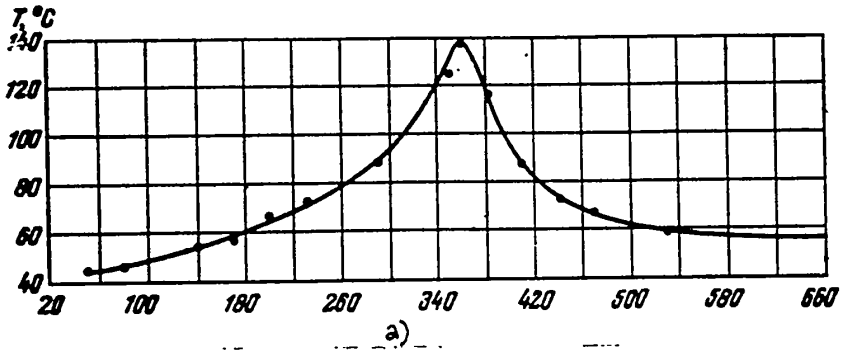

Fig.3 - Graph of Temperature Distribution in Furnace for Growing Stilbene

a) Distance from copper furnace, mm

the melt in the furnace space. In this case, the test tube is gradually lowered from the hotter furnace space into a less heated space, passing through the zone of maximum heating and the isothermal surface of crystallization, at which the melt crystallizes out. It has been experimentally found that to obtain a high-grade stilbene crystal 38 mm in diameter, the optimum velocity of growth must be 36 mm/day. Such a rate of crystallization likewise encourages the additional purification of the substance, since the impurities it contains are displaced to the upper part of the test tube.

STAT

Declassified in Part - Sanitized Copy Approved for Release @ 50-Yr 2014/03/07 : CIA-RDP81-01043R004200090004-8

Declassified in Part - Sanitized Copy Approved for Release @ 50-Yr 2014/03/07 : CIA-RDP81-01043R004200090004-8

On completion of crystallization, the crystal remains for a day in the lower part of the furnace for annealing, after which the furnace is shut off. The test tube with the crystal, cooled in the furnace, is taken out, inverted and wrapped in cloth for slow cooling to room temperature. After cooling, the test tube is broken by cautiously tapping it with a hammer on the bottom, and the crystal is then removed.

It is harder to grow large crystals of anthracene. One of the causes of this difficulty is the difficulty of preparing anthracene of the necessary degree of purity. Anthracene, obtained from coal tar, is difficult to purify from such hydrocarbons as naphthacene, tetracene, carbazole, etc. Even the chromatographic method does not always permit it to be freed from the impurities. Anthracene prepared synthetically from anthraquinone, likewise contains various intermediate products of photochemical reactions. The presence of impurities in anthracene not only hinders the process of crystal growing but also modifies the physical properties of the crystal: the crystals obtained have a yellowish tinge and the luminescence spectrum is modified. The second cause which badly complicates the growing of anthracene crystals is that additional products of the decomposition and oxidation of anthracene are formed during the process of growing crystals in the melt. Insufficient study has been devoted to the chemism of this process.

In the absence of light, anthracene crystallizes out of freshly distilled benzene, and the moist benzene product is charged into a vessel for crystallization.

The vessel for crystallization is a wide-necked Wurtz flask of fire-resistant glass, 50 - 100 ml in volume. The wide neck of the flask is necessary for more convenient charging of the product. An S-shaped capillary, 1.5 - 2 mm in diameter, and 15 mm long, or a capillary terminating in a ball, is sealed to the lower part of the flask. The function of this capillary is to initiate crystallization at its end, as far as possible, in a single point. As a consequence of the law of geometrical selection, out of the several crystallites formed, only one, with the orienta-

STAT

Declassified in Part - Sanitized Copy Approved for Release @ 50-Yr 2014/03/07 : CIA-RDP81-01043R004200090004-8

Declassified in Part - Sanitized Copy Approved for Release @ 50-Yr 2014/03/07 : CIA-RDP81-01043R004200090004-8

tion most favorable to growth, will survive.

After filling the flask, the substance is cooled until the benzene is completely solidified, the wide mouth is closed by sealing, the flask is exhausted, and when a vacuum of about 10^{-4} mm Hg has been reached, it is sealed off. The vacuum system has a trap with paraffin.

Anthracene is crystallized in a tube furnace. The furnace is provided with a contact thermometer and a control thermometer, a relay, and a clockwork mechanism for lowering the flask. The flask is lowered at the rate of 15 mm/day, and the growth of the crystal then takes place during such lowering. The presence of impurities and the progress of chemical reactions in the melt makes the single crystal growing out of the capillary "split up" and do its further growth in the form of a clump.

As a result of the crystallization of all the specimen on hand, clumps consisting of several transparent yellowish or almost colorless crystals were formed. It was noted that the purer the original product, the weaker the phenomenon of "splitting" was.

2. Growing Inorganic Crystals

Crystals of lithium bromide and iodide, with relatively low melting points, are grown in sealed quartz ampules by the Obreimov-Shubnikov method (Bibl.9). The complexity of preparing highly effective crystals from these compounds is explained by the difficulties of obtaining original reagents, and of the selection and dosage of the activator.

Crystals of the iodides of potassium, sodium and cesium may be grown by the Kyropoulos method (Bibl.12), but with the introduction of certain modifications which are necessary because the crystals of potassium, sodium and cesium iodides are grown for scintillation counters with the addition of an activator. Thalium iodide, usually used for that purpose, has a lower melting point, and a higher vapor pres-

STAT

Declassified in Part - Sanitized Copy Approved for Release @ 50-Yr 2014/03/07 : CIA-RDP81-01043R004200090004-8

Declassified in Part - Sanitized Copy Approved for Release @ 50-Yr 2014/03/07 : CIA-RDP81-01043R004200090004-8

sure, and as a result, it volatilizes out of the melt during the process of crystallization.

Taking account of this fact, we have introduced design modifications in the apparatus for growing crystals by the Kyropoulos method. Figure 4 shows this apparatus. It consists of the airtight furnace (1), the cooler (2), and a lifting mechanism consisting of two independent parts, the guiding mechanism (3) and a reducer with motor (5). The guiding mechanism serves to raise and lower the cooler. These operations may be handled either mechanically or manually. The mechanical lift is accomplished by a 15-watt motor through a reducer. The mechanism allows the rate of lift to be uniformly varied from 0.5 to 40 mm/min, which is particularly important for experimental work. The guide mechanism is connected with the reducer of the Cardan telescopic shaft (4). The lifting mechanism is mounted on a bracket which is attached to the wall on wall brackets* and may be rotated about its vertical axis.

The cooler of this apparatus is shown in Fig.5. It consists of a shell on which a 15-watt electric motor is installed, and rotates the crystal holder through a worm reducer at the rate of 2 rpm. The crystal holder is cooled with water, which is fed to the feed tube and is drawn off through the drain pipe. The crystal holder has interchangeable tips of various sizes made of copper or nickel, which are connected with threaded connections using tin solder. The dimensions of the end pieces depend on the volume of the crystal being prepared. The part of the crystal holder and the end piece in the furnace space are subject to the action of iodine and thallium vapor, which is highly destructive and partially contaminates the melt. In the cooler design proposed by us, the crystal holder and the end piece terminate in a quartz tube. The air barrier between the cold crystal holder and the quartz tube is so calculated that the tube shall be heated in the furnace space over the level of the melt, to above the vapor condensation temperature. The furnace has also been

*The bracket shown in Fig.1 is mounted on a stand.

STAT

Declassified in Part - Sanitized Copy Approved for Release @ 50-Yr 2014/03/07 : CIA-RDP81-01043R004200090004-8

Declassified in Part - Sanitized Copy Approved for Release @ 50-Yr 2014/03/07 : CIA-RDP81-01043R004200090004-8

substantially modified (Fig.6). The working space, 2900 cm^3 in volume, is formed by a fused quartz crucible mounted in the stop plate. The heater is made of nichrome wire 1.2 mm in diameter, wound directly on the crucible, thus decreasing the temperature inertia of the furnace. The heater takes 1250 watts. It is fed from an A.C. line with stabilized voltage. The voltage across the furnace terminals is measured by an astatic voltmeter.

Fig.4 - Apparatus for Growing Alkali Halide Crystals

Such a circuit diagram with a steady state made it possible to dispense with the observation of the temperature by the aid of a thermocouple. Thereby, we eliminated an additional source of damage, and increased the accuracy of the temperature adjustment.

The working space of the furnace is covered by two half-covers; on the left half-cover there is an illuminator, and on the right a peep hole. To supply the neutral gas to the furnace space, the covers have two connecting pipes, a feed pipe and an exhaust pipe. A high-speed seal presses the half-cover tightly against the support plate, assuring adequate sealing of the furnace. The clearance between the cover and the quartz shell of the cooler is closed by a packing washer cooled with water. The washer is first lined with asbestos or mica shreds. Cooling is necessary to condense the vapor of the volatile substances, thus favoring reliable self-sealing. The furnace is mounted on legs, and rotates around a horizontal shaft to drain the melt out of the crucible.

The furnace design so proposed permits direct observation of the crystal growth

STAT

Declassified in Part - Sanitized Copy Approved for Release @ 50-Yr 2014/03/07 : CIA-RDP81-01043R004200090004-8

Declassified in Part - Sanitized Copy Approved for Release @ 50-Yr 2014/03/07 : CIA-RDP81-01043R004200090004-8

without disturbing the crystallization conditions. The airtight seal of the furnace makes it possible to maintain constant temperature conditions and vapor pressure, makes it possible to conduct the processes in an inert gas atmosphere, etc.

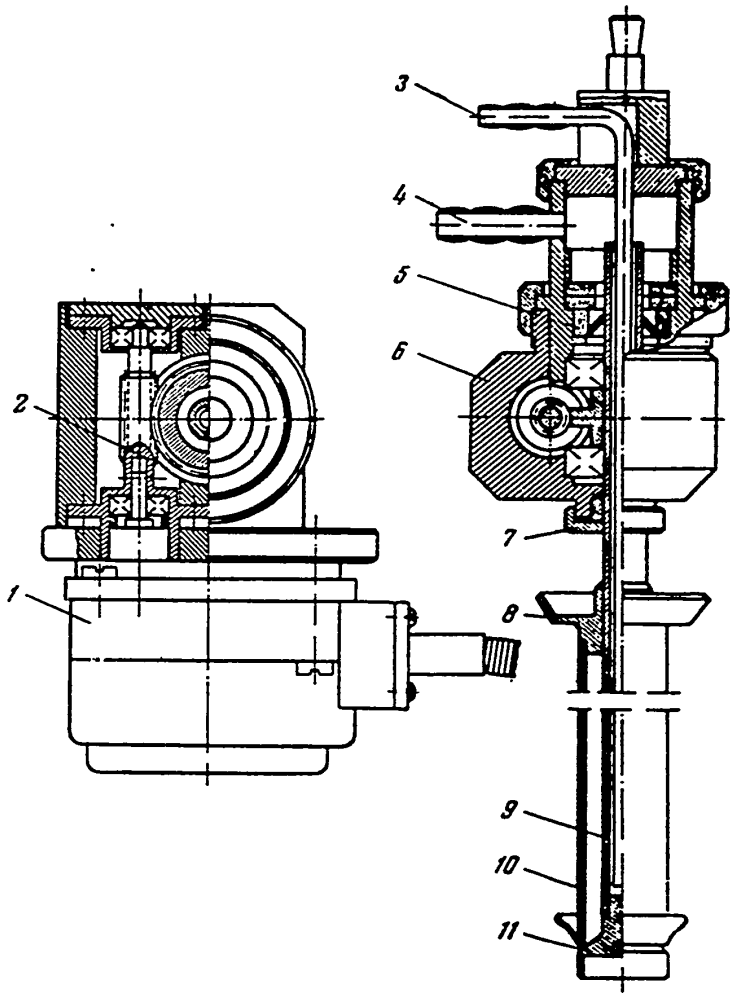

Fig.5 - Schematic Diagram of Cooler

1 - Motor; 2 - Worm reducer; 3 - Water feed tube; 4 - Connecting pipe for discharge of water; 5 - Packing ring; 6 - Barrel of cooler; 7 - Stuffing box; 8 - Oil collector; 9 - Crystal holder; 10 - Tube of quartz; 11 - Replaceable end piece

The technique of crystal growing on this apparatus is not basically modified.

STAT

Declassified in Part - Sanitized Copy Approved for Release @ 50-Yr 2014/03/07 : CIA-RDP81-01043R004200090004-8

Declassified in Part - Sanitized Copy Approved for Release @ 50-Yr 2014/03/07 : CIA-RDP81-01043R004200090004-8

On such an apparatus it is possible, in 6 - 12 hrs, to grow crystals of up to 100 mm in diameter, and up to 60 mm in height. The rotating cooler with the growing crystal agitates the melt and assures more uniform distribution of the activator along the

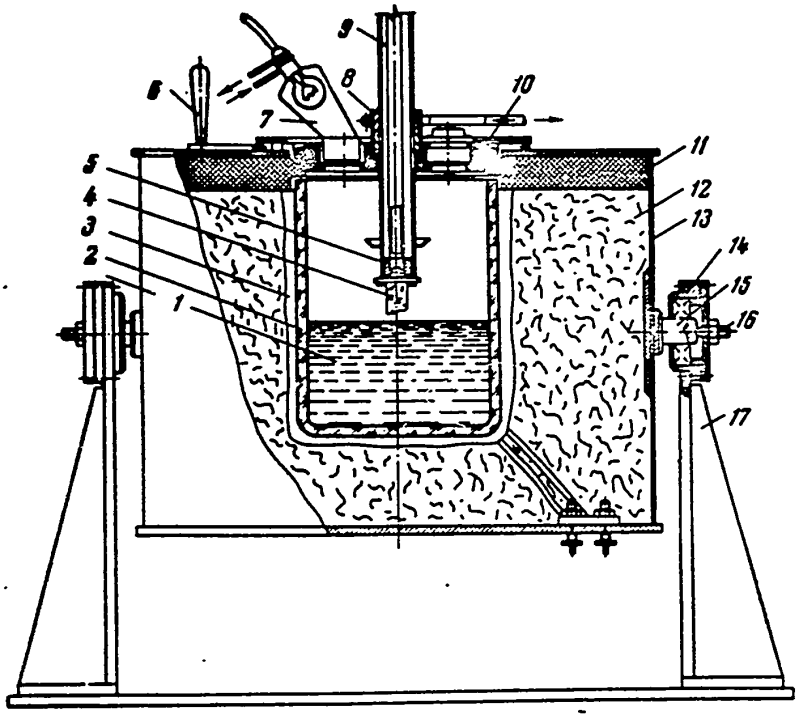

Fig.6 - Airtight Furnace:

1 - Melt; 2 - Fused quartz crucible; 3 - Heater; 4 - Seed crystal; 5 - Quartz tube; 6 - Gate handle; 7 - Illuminator; 8 - Bushing with washer; 9 - Crystal holder of cooler; 10 - Cover; 11 - Support plate; 12 - Thermal insulating powder; 13 - Furnace barrel; 14 - Cylinder; 15 - Split shaft; 16 - Adjusting screw; 17 - Stop post

crystal length, which, in turn, assures the high effectiveness of the crystals.

For growing calcium tungstate crystals, one uses a high-temperature vacuum furnace, equipped with a special mechanism for lowering the crucible with the growing crystal at an adjustable speed.

The crystallization was conducted in a conical molybdenum crucible 45 × 95 mm

STAT

Declassified in Part - Sanitized Copy Approved for Release @ 50-Yr 2014/03/07 : CIA-RDP81-01043R004200090004-8

Declassified in Part - Sanitized Copy Approved for Release @ 50-Yr 2014/03/07 : CIA-RDP81-01043R004200090004-8

in diameter. Before the beginning of the crystallization, the furnace is exhausted down to 10^{-4} mm Hg. The crucible, filled with substance, is placed on the stand attached to the apparatus for shifting the crucible. Then the furnace is heated to 1700°C. After all the reagent has been melted, the crucible is set at such a height in the furnace space that its lower part is at the level of the zone with

Fig.7 - Crystals and Mosaic of Calcium Tungstate (Natural Size)

temperature 1625°C (the melting point of the given reagent) while the upper part of the crucible with the melt is in the super-heated state. Crystallization takes place during the process of lowering the crucible at a rate of 3 mm/hr. Cooling is effected by reducing the temperature about 25 - 40°C/hr. Faster cooling would lead to strong disintegration of the calcium tungstate crystals. Our experiments yielded a slightly colored crystal up to 8 × 11 × 14 mm^3 in size. The single crystal regions of smaller sizes were used in preparing the mosaic. Figure 7 shows the crystals and mosaics in their natural size.

During the process of growth, the impurities are forced out into the upper part of the crystal boule. A spectral analysis of the upper part of the boule showed the

STAT

Declassified in Part - Sanitized Copy Approved for Release @ 50-Yr 2014/03/07 : CIA-RDP81-01043R004200090004-8

Declassified in Part - Sanitized Copy Approved for Release @ 50-Yr 2014/03/07 : CIA-RDP81-01043R004200090004-8

concentration of the impurities in it to have risen strongly.

Repeated crystallization permitted pure crystals of calcium tungstate to be obtained. A spectral analysis run after this recrystallization showed that the quantity of the impurities Mg, Al, Pb was decreased by a factor of 10, while Cu, Sr, Fe and Ba disappear entirely.

Studies on the scintillation properties of the crystal so obtained showed sub-

Fig.8 - Luminescent Crystals and Scintillators Manufactured from Them

stantial improvement in the crystal properties. The effectiveness of registration of γ-rays by crystals obtained after recrystallization is 10% higher than in crystals of the first crystallization.

During the development of the crystallization methods, a large number of experiments were run in connection with the working out of methods of purifying the original reagents and of selecting the materials for the crystallizers. The methods of treating the crystals and the methods of protecting them are the subject of a special paper. The methods proposed by the Crystallographic Institute were tested under pilot-plant conditions, and only then were introduced at the Kharkov Chemical Reagent Plant. Figure 8 is a photograph of luminescent crystals and the crystal

STAT

Declassified in Part - Sanitized Copy Approved for Release @ 50-Yr 2014/03/07 : CIA-RDP81-01043R004200090004-8

Declassified in Part - Sanitized Copy Approved for Release @ 50-Yr 2014/03/07 : CIA-RDP81-01043R004200090004-8

scintillators manufactured from them. The crystalline scintillators obtained were used in scintillation counters for different purposes and have permitted Soviet physicists to solve entirely new problems (Bibl.13) and to develop a new method of registration of nuclear radiations (Bibl.14).

The authors express their thanks to the laboratory staff members Z.B.Perekalina, G.S.Belikova, V.V.Chadayeva, K.S.Chernyshev, M.V.Koshuashvili, and V.A.Perl'shteyn, for their participation in developing the crystallization methods, and also to I.N.Tsigler for working out the design of the apparatus for growing crystals by the Kyropoulos method.

BIBLIOGRAPHY

1. Rezerford,E. - The Structure of the Atom and the Artificial Disintegration of Elements. GIZ (1923)
2. Chechik,N.O., Faynshteyn,S.M., and Lifshits,T.M. - Electron Multipliers. Gostekhizdat, IL (1955)
3. Birks,Dzh. - Scintillation Counters. State Pub.House for Foreign Lit. (1955)
4. Levshin,V.L. - Photoluminescent Liquids and Solids. Gostekhizdat (1951)
5. Hendricks,S.V. and Jefferson,M.E. - JOSA, Vol.23, No.9 (1933), pp.299 - 307
6. Kochendoerfer,A. - Zeits.Krist., Vol.97 (1937), p.263
7. Ronsett, Lochet. - Journ.Phys., III (1942), p.146
8. Feasel,C.E. and Smith,D. - Rev.Sci.Inst., Vol.19, No.11 (1948), p.817
9. Obreimov,I.V. and Shubnikov,L.V. - Zeits.Phys., Vol.25 (1924), p.31
10. Bridgmann,P.W. - Proc.Am.Acad.Sci., Vol.60 (1925), p.303
11. Vitovskiy,B.V. and Zemtsov,A.B. - Trudy Inst.Kristallogr., 9 (1954)
12. Kyropolous, - Zeits.Anorg.und Allg.Chem., Vol.154 (1925), p.303
13. Dzhelepov,V.P., Golovin,B.M., and Satarov,V.I. - Dok.AN SSSR Vol.99, No.6 (1954)
14. Zavoyskiy,Ye.K., Smolkin,G.Ye., Plakhov,A.G., and Butslov,M.M. - Dok.AN SSSR Vol.100, No.2 (1954)

STAT

Declassified in Part - Sanitized Copy Approved for Release @ 50-Yr 2014/03/07 : CIA-RDP81-01043R004200090004-8

Declassified in Part - Sanitized Copy Approved for Release @ 50-Yr 2014/03/07 : CIA-RDP81-01043R004200090004-8

APPARATUS AND METHODS OF GROWING SINGLE CRYSTALS OF SEMICONDUCTORS

by

D.A.Petrov and V.S.Zemskov

In connection with the development of semiconductor technology, the quality of semiconductor crystalline materials becomes more and more important. Properties assigned in advance are demanded of these materials, for the crystals decisively determine the characteristics and quality of the work of semiconductor instruments. The degree of spread of the parameters of the instrument depends on the degree of uniformity of the properties of the crystals.

The electrical properties of semiconductors are determined by the nature, content and distribution of the impurities existing or intentionally introduced into the material, and by the perfection of the crystal structure. It is important to know the laws that determine the distribution of impurities in the interior of the material, and to know how to control these laws.

The grain boundaries cause uncontrollable variations of the electrical properties of the material, disturbing the electronic processes in the instrument, and therefore the semiconductor materials used in technology must be manufactured in the form of single crystals.

Production of Single Crystals. Germanium is the best studied semiconductor material, and is already in widespread use. From its example we shall consider the questions to be expounded below.

Germanium, like many other semiconductors, expands appreciably during solidifi-

STAT

Declassified in Part - Sanitized Copy Approved for Release @ 50-Yr 2014/03/07 : CIA-RDP81-01043R004200090004-8

Declassified in Part - Sanitized Copy Approved for Release @ 50-Yr 2014/03/07 : CIA-RDP81-01043R004200090004-8

cation, and is extremely sensitive to all types of stresses. The volume of germanium increases by 5.5 ± 0.5% on solidification (Bibl.1). Stresses lead to twinning, and cause other undesirable disturbances of the crystal structure.

Stresses unavoidably arise during the solidification of germanium in the crucible, for instance in the preparation of single crystals by the Bridgman method (Bibl.2, 3).

The most suitable methods of growing germanium single crystals are the method of withdrawing from the melt, after Czochralski (Bibl.1), and the method of zone recrystallization proposed in 1949 by V.I.Likhtman and B.M.Maslennikov (Bibl.4) for growing single crystals of tin, and developed in the United States by Pfann for purifying crystals to remove the impurities (Bibl.1). The Czochralski method (Bibl.2,3) is most widely used at the present time.

Description of Equipment. The preparation of single crystals of germanium by the Czochralski method must be conducted in vacuo or in an atmosphere of inert gas, owing to the high affinity of germanium for oxygen (Bibl.5). Figure 1 is a schematic diagram of the apparatus.

The apparatus consists of three main parts: 1) the vacuum transit chamber 13 with the electric lead-in 4 and the mechanism for rotating the crucible 9; 2) the working chamber 1; 3) the cover 18 with the mechanism for rotating and growing the crystal (for more details see Fig.2).

The vacuum transit chamber (Fig.1) consists of a cylinder, to which the pipe 6, leading to the diffusion pump, has been welded. The bottom of the chamber has two openings for the electric leads 4. The leads are sealed in by the aid of the rubber ring 7, compressed by the nut 8. The electric leads are made in the form of hollow cylinders, cooled by water supplied through the pipe 10. The semicylindrical copper electrode 15, providing terminals for the heating element 16, are welded to the leads. The heating element used is a slit graphite heater. To decrease the radiation of heat, the heater is screened by the two baffles 17. The door of the transit

STAT

Declassified in Part - Sanitized Copy Approved for Release @ 50-Yr 2014/03/07 : CIA-RDP81-01043R004200090004-8

Declassified in Part - Sanitized Copy Approved for Release @ 50-Yr 2014/03/07 : CIA-RDP81-01043R004200090004-8

chamber has an entrance to admit the plunger 5, transmitting rotation to the crucible. The plunger is set in rotary motion by the iron armature 12, which is caused

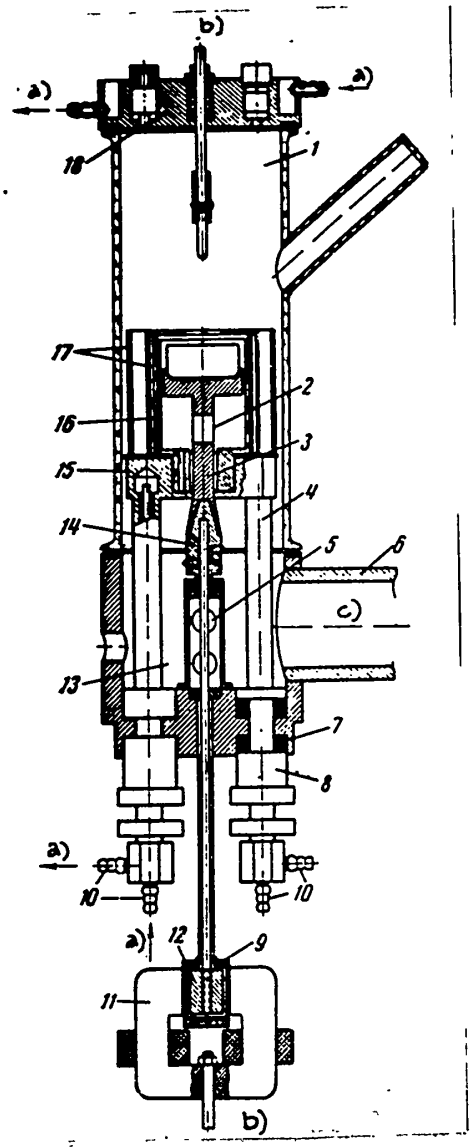

Fig.1 - Schematic Diagram of Apparatus for Preparing Single Crystals

a) Water; b) To reducer; c) To diffusion pump

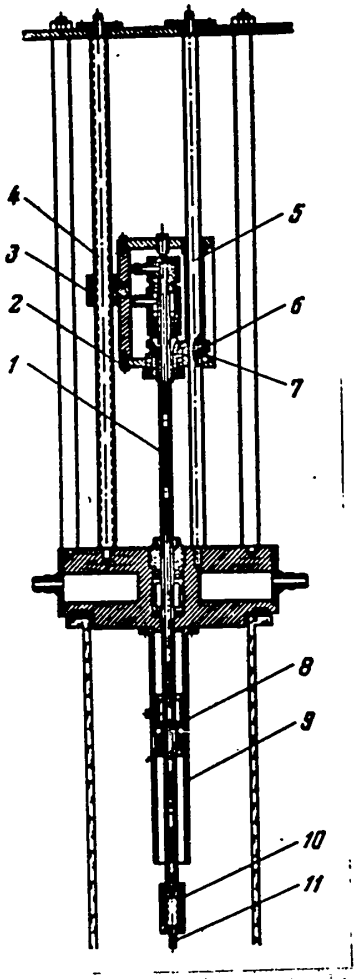

Fig.2 - Cover with Mechanism for Withdrawing and Rotating the Crystal

to rotate by the electromagnet 11. The plunger and armature are placed in the vac-

STAT

Declassified in Part - Sanitized Copy Approved for Release @ 50-Yr 2014/03/07 : CIA-RDP81-01043R004200090004-8

Declassified in Part - Sanitized Copy Approved for Release @ 50-Yr 2014/03/07 : CIA-RDP81-01043R004200090004-8

uum sleeve 9, soldered to the bottom of the transit vacuum chamber. The rotation of the plunger is transmitted through the steel cone 14, the graphite saddle 3 and the quartz tube 2, to the crucible.

Figure 2 is a diagram of the withdrawing mechanism. The entire mechanism is assembled on a water-cooled cover. At the center of the cover, the plunger 1 for raising and lowering the seed, passes through a vacuum seal. The displacement of the plunger is accomplished by the screw-nut pair 4, 3. The rotation of the plunger is transmitted from the shaft 5 through the two gears 2 and 6. The gear 2 is rigidly attached to the plunger, while the gear 6 is attached to the shaft 5 by the sliding key 7, providing for the translational and rotary motion of the plunger. The plunger 1 is cooled with water. The seed 11 is attached on the plunger by the graphite holder 10. To eliminate the vibration of the rotating plunger, an additional support is provided by the movable bearing 8, which is displaced in the rigidly attached guide tube 9.

The vacuum is measured by the aid of a thermocouple vacuum meter and an ionization vacuum meter. The vacuum attained in the apparatus in the working state is not less than 10^{-4} mm Hg.

The apparatus permits the melting to be done in an atmosphere of inert gas under excess pressure. In this case, the upper cover is drawn away from the transit chamber by special posts, thanks to which an adequate seal of the apparatus is maintained under excess pressure within it.

Phenomena Observed in the Production of Single Crystals. In growing single crystals out of a melt by the Czochralski method, the single-crystal seed attached to the plunger is lowered into the melt, whose temperature is held slightly over the melting point. After the seed has melted and proper contact with the melt has been established, the lifting mechanism comes into action.

The forces of cohesion on the crystallization front beyond the seed lift a liquid column of melt, whose height above the level of the melt in the crucible is en-

STAT

Declassified in Part - Sanitized Copy Approved for Release @ 50-Yr 2014/03/07 : CIA-RDP81-01043R004200090004-8

Declassified in Part - Sanitized Copy Approved for Release @ 50-Yr 2014/03/07 : CIA-RDP81-01043R004200090004-8

tirely definite under given steady withdrawal conditions (Fig.3). The height of the liquid column determines the diameter of the crystal grown.

To obtain a single crystal, it is necessary to produce conditions preventing the possible formation of parasite crystals on the front of crystallization or the spontaneous appearance of crystals in the bulk of the melt (Bibl.6). With this object, the distribution of temperature in the melt must correspond to the scheme (Fig.4) according to which the temperature gradually falls from the walls and bottom of the crucible toward its central part. To assure more reliable heat removal from the crystallization front, the seed is cooled. The conditions are similar to those that favor the appearance of columnar crystals in castings: a cold chill mold and a somewhat superheated melt.

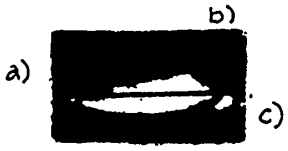

Fig.3 - Radiogram Illustrating the Position of the Crystallization Front Above the Level of the Melt in the Crucible (Natural Size)
a) Front of crystallization; b) Crystal being withdrawn; c) Level of melt in crucible

The seeds used is a single crystal with a definite orientation. The most desirable directions of growth are [111], [110], and [100].

As already stated, reliable contact between the seed and the melt must be provided. If the seed has not melted along the entire front of its contact with the melt, it is possible, as shown on Fig.5, that only an outer single crystal layer will be formed, and that the interior structure of the ingot will be polycrystalline.

The withdrawal must be accomplished at a definite rate under constant temperature conditions in the melt. It is observed that single crystals are more reliably obtained if the metal is somewhat superheated, when the possibility of the formation of crystallization centers in the melt, and particularly on its surface, is excluded.

The rotation of the crucible and of the growing crystal favor the symmetrical

STAT

Declassified in Part - Sanitized Copy Approved for Release @ 50-Yr 2014/03/07 : CIA-RDP81-01043R004200090004-8

Declassified in Part - Sanitized Copy Approved for Release @ 50-Yr 2014/03/07 : CIA-RDP81-01043R004200090004-8

growth of the crystal, since in this case the possible irregularities of the temperature field of the furnace are smoothed out. If there is no rotation, the crystal is usually curved, as will be seen from Fig.6 (case where the lower part of the crystal was grown without rotation). The contrary rotation of the crucible and crystal favors the uniform distribution of the impurities displaced from the crystallization front throughout the entire bulk of the melt. The rotation of the crystal at excessively high speeds is inadvisable. With a speed of the order of 350 rpm, the formation of a helical crystal shape is noted. The crystal in this case is curved toward the side opposite its rotation (Fig.7). At still higher rotary speeds on this apparatus, a crystal can be grown to only a short length, after which it breaks off. Figure 8 shows a crystal of which the upper part has been withdrawn at 90 rpm, and the lower part at 1400 rpm. The limit of the rate of rotation of the crucible is determined by the centrifugal forces by which the metal can be thrown out of the crucible.

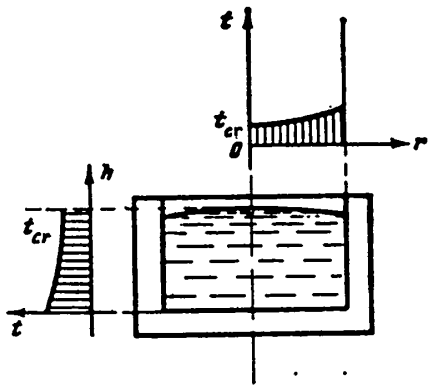

Fig.4 - Diagram of Temperature Distribution in Crucible

t_{cr} - Crystallization temperature

Distribution of Impurities during Crystallization. In preparing single crystals, the impurities present in the melt are irregularly distributed along the length of the ingot unless special measures are taken (Bibl.1,7,8). The cause of this phenomenon lies in the difference of composition between the liquid and solid phases of the substance in contact during crystallization (Fig.9). If we assume that during crystallization the diffusion in the liquid phase is total, but is practically absent in the solid phase, which under certain conditions may in fact be true during withdrawal (Bibl.7, 8), then the distribution of the impurities along

STAT

Declassified in Part - Sanitized Copy Approved for Release @ 50-Yr 2014/03/07 : CIA-RDP81-01043R004200090004-8

Declassified in Part - Sanitized Copy Approved for Release @ 50-Yr 2014/03/07 : CIA-RDP81-01043R004200090004-8

the length of the ingot may be found from the relation

$$\ln \frac{m_0}{m} = \int_x^{x_0} \frac{1}{x-y}\, dx,$$

where m_0 is the mass of the melt before the beginning of the withdrawal, x_0 the impurity content of the melt at the initial instant of withdrawal, y, x the impurity content of the solid phase and the melt, respectively, at any instant during the process of withdrawal, and m the mass of the melt at any instant during the process of withdrawal.

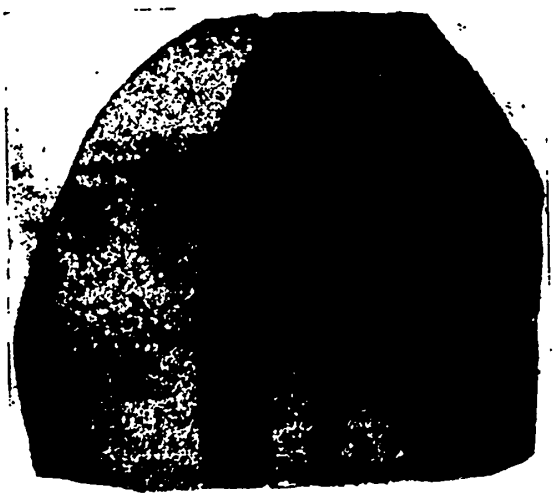

Fig.5 - Photograph of Macropolished Section of Single Crystal Obtained with Incomplete Fusion of the Seed 3 ×

Fig.6 - Photograph of Crystal Whose Lower Part Has Been Grown without Rotation 2 ×

The function y = f(x) is determined from the equilibrium phase diagram. If the concentration of impurities in the principal substance is slight and the Raoult law for dilute solutions holds (Bibl.1, 9), then the relation between x and y is linear, i.e., $y = k_0 x$ (Fig.10). In this case, the distribution of the impurity along the length of a single crystal may be calculated from the formula

$$y = x_0 k_0 (1 - m_{rel})^{k_0 - 1},$$

STAT

Declassified in Part - Sanitized Copy Approved for Release @ 50-Yr 2014/03/07 : CIA-RDP81-01043R004200090004-8

Declassified in Part - Sanitized Copy Approved for Release @ 50-Yr 2014/03/07 : CIA-RDP81-01043R004200090004-8

where m_{solid} is the crystallized part of the melt, and k_o the equilibrium coefficient of distribution, whose value depends on the form of the impurity.

Fig.7 - Photograph of Crystal of Helical Shape, 2 ×

For impurities depressing the melting point, $k_o < 1$ (Fig.10a). Such an impurity is displaced by the growing crystal. The melt is gradually enriched in the impurity, so that its content in the growing crystal likewise increases continuously.

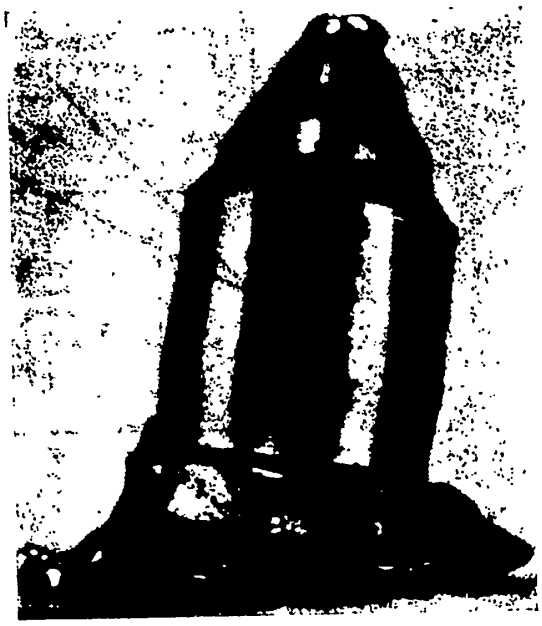

Fig.8 - Photograph of Crystal whose Lower Part Has Been Grown during Rotation of the Crystal at 1400 rpm, 2.6 ×

For an impurity increasing the melting point, $k_o > 1$ (Fig.10b). The content of such an impurity in the crystal decreases continuously as the crystal is withdrawn. At

STAT

Declassified in Part - Sanitized Copy Approved for Release @ 50-Yr 2014/03/07 : CIA-RDP81-01043R004200090004-8

Declassified in Part - Sanitized Copy Approved for Release @ 50-Yr 2014/03/07 : CIA-RDP81-01043R004200090004-8

a value of k_o close to unity, the impurity is distributed practically uniformly along the length of the ingots.

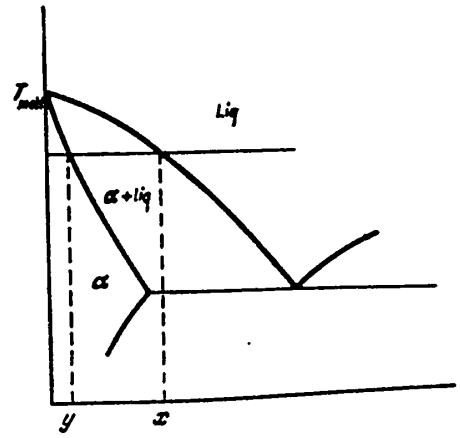

Fig.9

Irregular distribution of the impurity is associated with irregularity of the electrical properties along the length of the single crystal, for example the resistivity (Bibl.1).

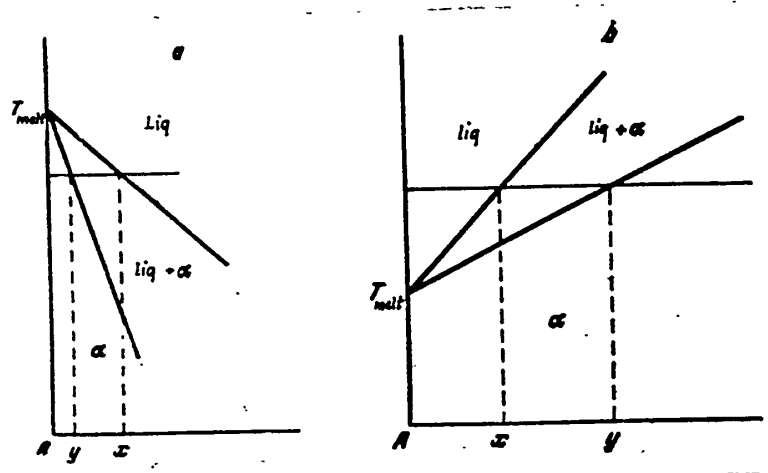

Fig.10

To reduce this irregularity, what is called programmed withdrawal is used. This method is based on the utilization of the relation that exists between the quantity of impurity captured by a growing crystal and the rate of withdrawal. For the case

STAT

Declassified in Part - Sanitized Copy Approved for Release @ 50-Yr 2014/03/07 : CIA-RDP81-01043R004200090004-8

Declassified in Part - Sanitized Copy Approved for Release @ 50-Yr 2014/03/07 : CIA-RDP81-01043R004200090004-8

$k_o < 1$, the rate of withdrawal is decreased as the melt becomes enriched in the impurity, so that the impurity is uniformly distributed along the length of the crystal (Bibl.1). For the same purpose, the following method may also be used (Bibl.10). To a melt of composition x, from which a single crystal of composition y is being grown, a melt of the same composition y, and in the same quantity as the withdrawn single crystal, is continuously added (Fig.10). The composition of the melt in this case remains constant, since the crystal being withdrawn will have a constant composition along its length. This method may be accomplished in a version in which an ingot of the same composition as that of the single crystals being withdrawn is introduced into the melt. This ingot must be lowered into the melt, and must melt away at the same rate with which the single crystal is being withdrawn, if its cross section is the same (Fig.11).

In the general case, the areas of the crystal being withdrawn and of the feed ingot will depend on the ratio between the rate of withdrawal and the rate of melting of the feed ingot; on the relation of the impurity content of the feed ingot and of the single crystal being withdrawn. The feed ingot need not necessarily contain the impurity, but its area Δ must be $(1 - k_o)$ times smaller than the area of the crystal being withdrawn, i.e., $\Delta = \Delta_o (1 - k_o)$; and in this case the rate of withdrawal and the rate of lowering of the feed ingot will be equal.

Apparatus for Preparing Single Crystals with Constant Feed of Melt

Figure 12 is a schematic diagram of the apparatus. The difference of this apparatus from that described above is that now the transitional disc 1 is introduced, assuring the eccentric displacement of the ingot 5 and the crystal 7, which permits minimizing the size of the crucible, so that the size of the apparatus need not be increased.

In order to accomplish the simultaneous melting of the ingot being lowered and the withdrawal of the single crystals of one and the same melt, the cooler 8 and the

STAT

Declassified in Part - Sanitized Copy Approved for Release @ 50-Yr 2014/03/07 : CIA-RDP81-01043R004200090004-8

Declassified in Part - Sanitized Copy Approved for Release @ 50-Yr 2014/03/07 : CIA-RDP81-01043R004200090004-8

heater 6 have been added. The heater produces the proper melting conditions for the ingot being lowered, while the cooler produces conditions of directed growth of the crystal being withdrawn.

The mechanism of simultaneous withdrawal of the crystal and lowering the ingot may be understood from the schematic diagram of the apparatus. To the sliding guide bearing 9 of the lifting plunger 10 is attached one of the ends of the flexible drive 3 by means of the screw 4. The drive is bent over the block 2. At the other end of the drive is attached the

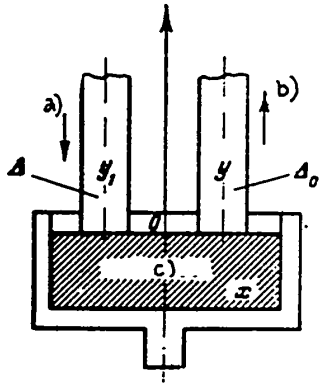

Fig.11 - Diagram of Feed of the Melt

a) Feed ingot; b) Single crystal being withdrawn; c) Melt

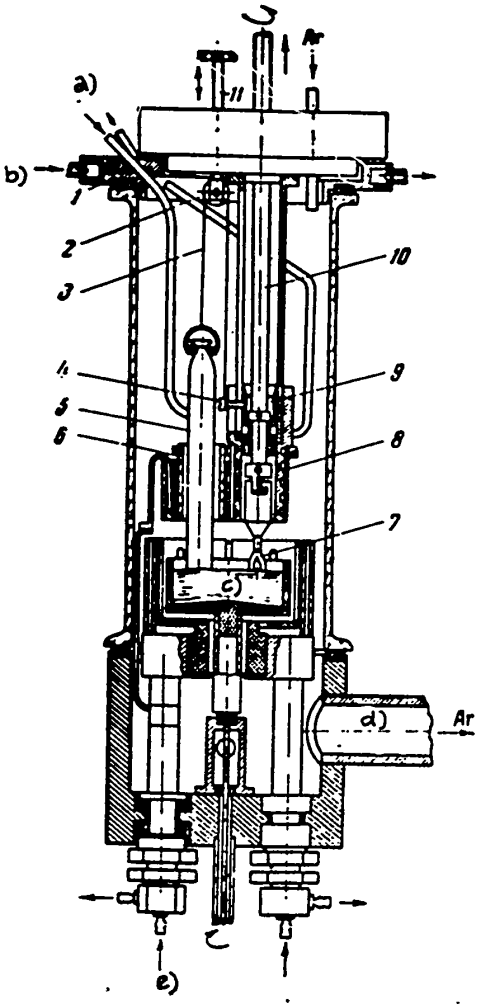

Fig.12 - Schematic Diagram of Apparatus for Preparing Single Crystals with Constant Feed of Melt

a) Cooling of cap; b) Cooling of disc; c) Melt; d) To air pump; e) Cooling of electrodes

feed ingot 5. Thus, on lifting the plunger 10 the feed ingot will be lowered. The instant of contact between the feed ingot 5 and the melt is adjusted by displacing

STAT

Declassified in Part - Sanitized Copy Approved for Release @ 50-Yr 2014/03/07 : CIA-RDP81-01043R004200090004-8

Declassified in Part - Sanitized Copy Approved for Release @ 50-Yr 2014/03/07 : CIA-RDP81-01043R004200090004-8

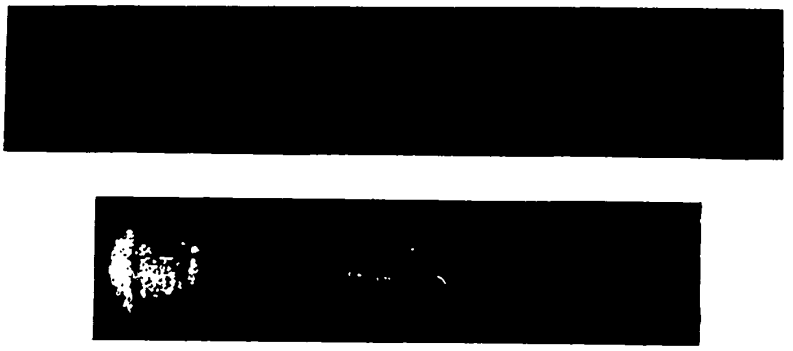

Fig.13 - Negative Prints of Radiograms of Single Crystals.

The crystals were prepared:

top - with feed of melt; bottom - without feed of melt. (Natural size)

a

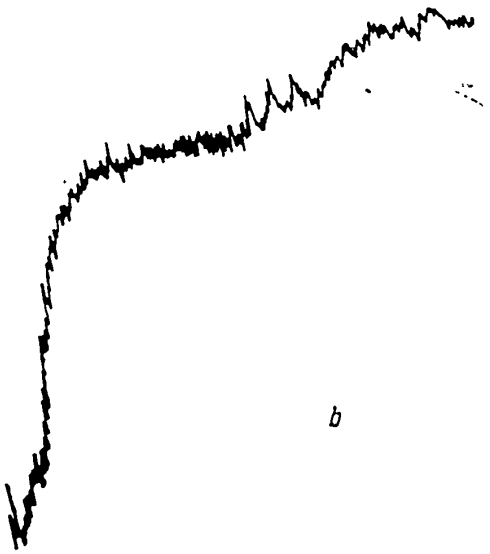

b

Fig.14 - Photometric Curves of Radiograms of Single Crystals.

The crystals were prepared:

a - With feed of melt; b - Without feed of melt

STAT

Declassified in Part - Sanitized Copy Approved for Release @ 50-Yr 2014/03/07 : CIA-RDP81-01043R004200090004-8

Declassified in Part - Sanitized Copy Approved for Release @ 50-Yr 2014/03/07 : CIA-RDP81-01043R004200090004-8

the block 2 attached to the movable plunger 11.

Results of Experiments in Growing Single Crystals of Constant Composition

The preparation of single crystals with uniform distribution of impurity lengthwise during constant feed of the melt was studied on germanium alloys with the radioactive isotope of indium In^{114}. The conditions of the preparation of a single crystal on this equipment were the same as on the preceding one. Figure 13 shows negative prints of radio-

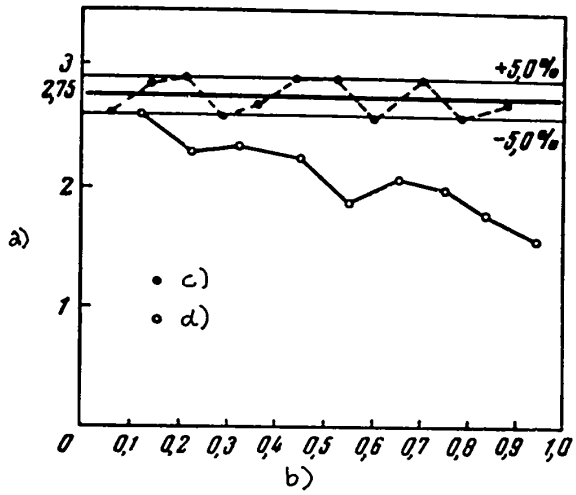

Fig.15 - Variation of Resistivity along the Length of Single Crystal. The single crystal 24 μ was prepared with constant feed of the melt; the single crystal 26 μ was prepared without feeding the melt

a) Resistivity, ohm-cm; b) Length of crystal in fractions of unity; c) Single crystal 24 μ; d) Single crystal 26 μ

Fig.16 - Negative of Radiogram of Part of a Single Crystal Withdrawn during Gentle Agitation of the Melt

grams of germanium single crystals produced with and without feeding the melt. The fluctuations in the concentration of the impurity (layered distribution) which are disclosed on the radiogram (Fig.13b) are connected with the instability of the conditions of growth of the single crystal: variation of the velocity of growth, fluctuation of the temperature of the melt. The photometric curves (Fig.14) of the

STAT

Declassified in Part - Sanitized Copy Approved for Release @ 50-Yr 2014/03/07 : CIA-RDP81-01043R004200090004-8

Declassified in Part - Sanitized Copy Approved for Release @ 50-Yr 2014/03/07 : CIA-RDP81-01043R004200090004-8

radiograms indicate uniform distribution of the impurities along the ingot when the melt is replenished, and irregular distribution when the crystal is withdrawn without replenishing the melt.

The measurement of the electrical resistivity (Fig.15) confirms this. The scatter of the resistivity values lies within the range of about ± 5%. In the case of withdrawal with replenished melt, mixing is particularly important, since the content of the impurity on the crystallization front is higher, but is lower on the melting front, than in the interior of the melt. Figure 16 shows a negative of the radiogram of part of a single crystal prepared with insufficient mixing of the melt. It is very clear that the crystal withdrawn is of irregular composition.

Conclusion

1. Apparatus for growing germanium single crystals by the Czochralski method has been described, and the principal conditions of preparation of single crystals have been considered.

2. The possibility of preparing single crystals with a uniform distribution of impurities along the length of the crystal has been shown, and the results of experimental work in this direction have been presented.

BIBLIOGRAPHY

1. - Collection of Translated Papers. D.L.Petrov,Editor. "Germanium", State Publishing House for Foreign Literature, 1955
2. Kuznetsov,V.D. - Crystals and Crystallography. Gostekhizdat (1954),p.381
3. Bakli,G. (H.Buckley) - Crystal Growth. State Publ.House for Foreign Lit. (1954), p.406
4. Likhtman,V.I. and Maslennikov,B.M. - Dok.AN SSSR. Vol.67,No.1 (1949),pp.93-95
5. Slavinskiy,M.P. - Physical and Chemical Properties of the Elements. Metallurgizdat (1952),p.763

STAT

Declassified in Part - Sanitized Copy Approved for Release @ 50-Yr 2014/03/07 : CIA-RDP81-01043R004200090004-8

Declassified in Part - Sanitized Copy Approved for Release @ 50-Yr 2014/03/07 : CIA-RDP81-01043R004200090004-8

6. Umanskiy,Ya.S. - Physical Principles of Metallurgy. Metallurgizdat (1954),p.724

7. Petrov,D.A. - Zhur.Fiz.Khim., Vol.21,No.12 (1947),pp.1449-1450

8. Petrov,D.A. - Zhur.Fiz.Khim., Vol.23,No.1 (1954),pp.161-174

9. Kubashevskiy,O. and Evans,E. - Thermochemistry in Metallurgy. State Publ.House for Foreign Lit. (1954),p.421

10. - Questions of Semiconductor Theory and Research and of the Processes of Semiconductor Metallurgy. (Trudy Soveshch.v Inst.Metallurg.im.Baykov, Academy of Sciences USSR), Publ.Dept. Academy of Sciences USSR (1955), pp.53-92

STAT

Declassified in Part - Sanitized Copy Approved for Release @ 50-Yr 2014/03/07 : CIA-RDP81-01043R004200090004-8

Declassified in Part - Sanitized Copy Approved for Release @ 50-Yr 2014/03/07 : CIA-RDP81-01043R004200090004-8

FIRST EXPERIMENTS IN GROWING LARGE MICA CRYSTALS*

by

K.V.Kapralov, Yu.V.Koritskiy and N.N.Sheftal'

Work on the creation of industrial methods of synthesizing mica was first initiated in Germany by Siemens & Halske in 1918 - 1919, since mica is a valuable strategic raw material. The method developed by that company did not assure the production of industrially suitable crystals. The patents (Bibl.1) relate primarily to the composition of the charge (the mica used was in all cases fluorophlogopite and was obtained from a melt) and to the attempt to produce crystals by the electrolytic method. This work, continued down to 1945, and described in detail by H.Buckley (Bibl.2), took on particular importance in connection with the Second World War.

The synthesis of mica was conducted in graphite crucibles and also in ceramic crucibles of clay and kieselguhr in two-chamber gas-electric furnaces. A charge of the following composition, for instance, was used, consisting of the pure components, (in %):

Al_2O_3	41.6	SiO_2 (diatomite)	30.7
MgO	32.6	K_2SiF_6	25.1

* This work was performed in 1947 - 1949 at the Mica Insulation Laboratory, All-Union Institute of Electrical Engineering (K.V.Kapralov and Yu.V.Koritskiy) in consultation with the Institute of Crystallography, Academy of Sciences USSR (N.N.Sheftal').

STAT

Declassified in Part - Sanitized Copy Approved for Release @ 50-Yr 2014/03/07 : CIA-RDP81-01043R004200090004-8

Declassified in Part - Sanitized Copy Approved for Release @ 50-Yr 2014/03/07 : CIA-RDP81-01043R004200090004-8

In order to eliminate the need for mixing the hot melt, thus making the composition of the melt of the mass uniform, which is difficult at temperature of 1400 - 1450°C, the charge in finely ground state was well mixed, and small tablets were

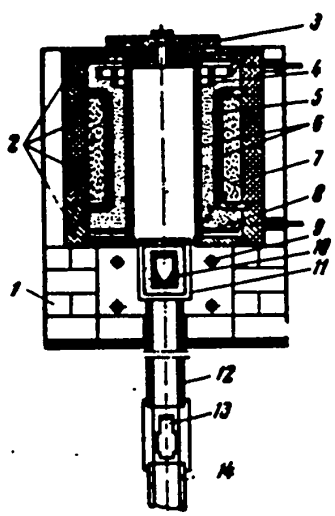

Fig.1 - Two-Chamber Electric Furnace with Kryptol and Silite Heater

1 - Masonry of chamotte brick; 2 - Heat insulating blocks; 3 - Furnace cover; 4 - Upper electrode; 5 - Kryptol cover; 6 - Refractory cylinders; 7 - Chamotte cover; 8 - Lower electrode; 9 - Silite heaters; 10 - Graphite crucible; 11 - Refractory capsule; 12 - Refractory stand for capsule; 13 - Optical pyrometer; 14 - Plunger of hydraulic lift. All packings between the refractory cylinders are made of chamotte flour

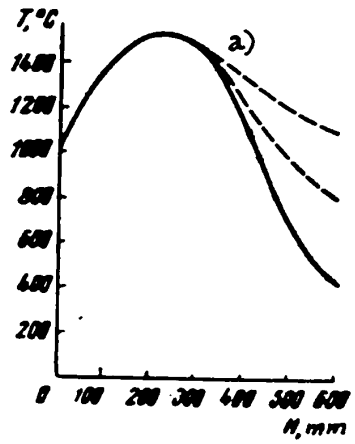

Fig.2 - Distribution of Temperatures over the Height of the Working Zone of the Two-Chamber Furnace

a) Working zone of furnace

then pressed out of it; and it was with these tablets that the crucible was filled. The very slow cooling in the crystallization range was the principal condition assuring directed crystallization. In addition attempts were made to use a magnetic field, or a bath of molten fluorides, in which the crucible was placed to reduce the losses of fluorine by the mica melt during crystallization.

In laboratory heats in crucibles of 200 gm capacity, plates of mica crystals up to 9 cm^2 in size were obtained.

STAT

Declassified in Part - Sanitized Copy Approved for Release @ 50-Yr 2014/03/07 : CIA-RDP81-01043R004200090004-8

Declassified in Part - Sanitized Copy Approved for Release @ 50-Yr 2014/03/07 : CIA-RDP81-01043R004200090004-8

As a result of these studies, an industrial method had not yet been worked out. The state of the work, however, was apparently close to the final pilot-plant stage. The Siemens Co. produced mica books of diameter up to 15 cm, and successfully employed synthetic mica instead of the natural substance.

The authors of the present paper, using the scanty literature information, have attempted to accumulate their own experimental material to solve the problem of the industrial synthesis of mica.

In 1947 heats were run on unspecialized equipment with the object of checking the materials. The best material for the crucible was found to be graphite (porcelain crucibles melt, and corundum crucibles crack). The graphite, used in an atmosphere of CO at 1400°C was found to be resistant to the destructive properties of the melt. The methods of mixing and briquetting were found to be justified, although even the briqueted charge shrank to half its volume during melting.

Up to 50% of a vitreous mass was observed in the products of the heats between the crystals.

In 1948 and the beginning of 1949, assembled laboratory furnaces meeting the requirements of the synthesis were designed and built. As a result of the experiments, mica was obtained in small pieces with a high content of glass (16 - 50%) and two generations of mica were often observed in the product of the heats, while crossed twin crystals were often formed. Analyses showed considerable losses of fluorine.

In 1949 a two-chamber electric furnace with kryptol and silite heaters was built (Fig.1). Its design features assured stable heat conditions in the furnace, and a low temperature gradient. The lower chamber was heated by silite rods and the upper by kryptol. The heater was separately fed from a special autotransformer, which permitted a specified temperature drop with height to be established in the working zone of the furnace (Fig.2).

The movable furnace sole, installed on a special hydraulic lift, made it pos-

STAT

Declassified in Part - Sanitized Copy Approved for Release @ 50-Yr 2014/03/07 : CIA-RDP81-01043R004200090004-8

Declassified in Part - Sanitized Copy Approved for Release @ 50-Yr 2014/03/07 : CIA-RDP81-01043R004200090004-8

sible to place the crucible in a definite temperature zone of the furnace, or slowly to lower it during the process of crystallization of the melt. A channel, provided in the furnace sole, permitted continuous observation of the temperature of the crucible bottom or of the bottom of the capsule in which the crucible was placed, by means of an optical pyrometer placed in the lower part of the channel. The furnace

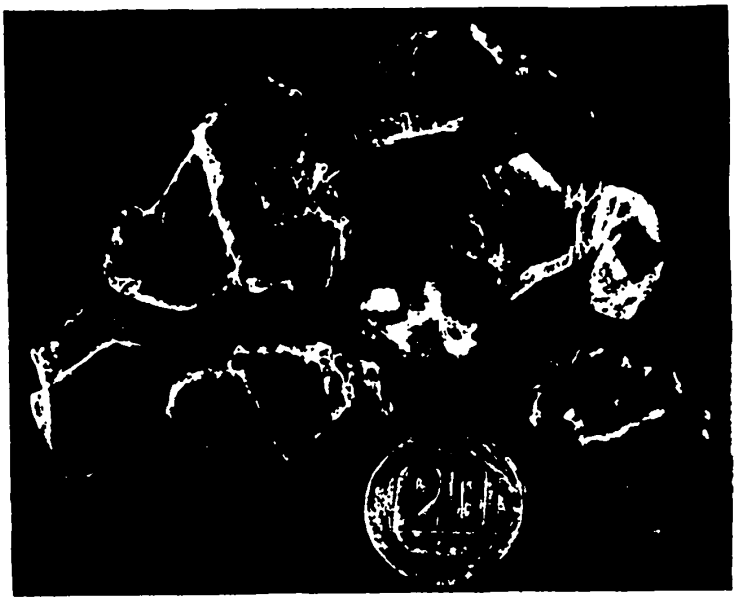

Fig.3 - Crystals of Synthetic Mica Prepared in the Mica Insulation Laboratory, of the VEI

had a removable metal framework, and its lining was made of separate refractory and heat-insulating blocks, the gaps between which were not closed with clay but were filled instead with chamotte flour. This assured a more reliable seal, permitted rapid checking of the furnace, as required after every heat or two, and favored the slower burning out of the kryptol and the establishment of a stable reducing medium in the working zone of the furnace, which is very important for the preservation of the graphite crucible.

The products of the first heats in the two-chamber furnace show a loss of weight (of as much as 46%) on account of the fluorine, potassium, and, obviously, the sil-

STAT

Declassified in Part - Sanitized Copy Approved for Release @ 50-Yr 2014/03/07 : CIA-RDP81-01043R004200090004-8

Declassified in Part - Sanitized Copy Approved for Release @ 50-Yr 2014/03/07 : CIA-RDP81-01043R004200090004-8

icon. The mica flakes were arranged vertically, especially during retarded cooling.

The composition of the charge used varied: quartz made up about 40%, potassium fluoride from 16 to 29%, magnesia from 18 to 32%, and clay from 11.5 to 22%. Natural mica was also taken, 71% of phlogopite with 29% of potassium fluoride added, and in addition a charge was made up based on the calculated formula of phlogopite.

Positive results were obtained in the two-chamber furnace after use of a bath with fluorides. The weighed portion was increased to 133.5 gm and the crucible with the mixture was placed in another crucible with the potassium fluoride and was covered with sand. The experiments took about a day. As a result, the entire melt crystallized into coarsely crystalline mica. The quantity of the vitreous phase was insignificant.

The crystals, oriented along the vertical axis of the crucibles, were easily cleaved into separate flakes. In this heat the flakes were strongly cruved. In the following experiments, the content of potassium fluoride in the charge was increased by 12% over the calculated amount. In these experiments the product of the melt consisted entirely of mica. The crystals were oriented vertically. The flakes reached 45 mm in length, and 4 cm^2 in area. The thickness of the mica packets was from 0.8 to 2.5 mm. The flakes were flat and elastic.

In one of the experiments the crystals attained a size of 4 × 2.5 cm^2 (Fig.3). The thickness of the large packets was about 0.8 mm. The size of the flakes was limited by the dimensions of the crucible. These favorable experimental results showed good reproducibility. The best results were obtained under the following conditions:

a) Composition of charge in %:

SiO_2	41,0	Al_2O_3	14,0
MgO	25,0	KF	20,0

b) Temperature conditions: superheating to 1400 - 1450°C for 2 - 3 hr, rapid cooling to 1300 - 1295°C, slow cooling at 3 - 5 degree/hr to 1200 - 1220°C.

STAT

Declassified in Part - Sanitized Copy Approved for Release @ 50-Yr 2014/03/07 : CIA-RDP81-01043R004200090004-8

Declassified in Part - Sanitized Copy Approved for Release @ 50-Yr 2014/03/07 : CIA-RDP81-01043R004200090004-8

Thirty-nine heats in all were run in 1947 - 1949.

It was proposed to use the mica so obtained for the production of micalex in connection with the existing data to the effect that micalex prepared from synthetic mica has considerably better electrical and thermal properties than that made from natural mica.

Subsequent work on growing mica was performed at the Institute of Crystallography (Bibl.3).

BIBLIOGRAPHY

1. - Patents on Mica Synthesis (Germany). Class 12,Group 37,No.367537, 22 January 1923; Class 12,Group 37,No.97924, 25 September 1924; Class 12, Group 38,No.458475, 11 April 1928.

2. Bakli,G. [H.Buckley] - The Growth of Crystals. State Publ.House for Foreign Lit., pp.77-78

3. Yamzin,I.I. and Leyzerzon,M.S. - The Present Symposium. p.277

Note. Investigators concerned at the present time with the synthesis of mica, indicate the difficulty of growing a single crystal in a crucible, since many intersecting vertical flakes are formed in this case. This difficulty may apparently be eliminated by starting out from the following considerations.

1. In the paper by N.N.Sheftal', N.P.Kokorish and S.K.Mukhonkin entitled "The advantage of growing single crystals with a flat crystallization isotherm" (not in this symposium) it was reported that the study of single crystals of silicon and germanium grown with a curved isotherm, disclosed a well expressed laminar growth, parallel to the planes of the principal faces. For this reason it may be assumed that the crystal must grow more uniformly in cross section in the case of a flat isotherm, parallel to the close-packed smoothly growing face of the crystal.

2. V.Ya.Khaimov-Mal'kov (Institute of Crystallography) has found that considerably purer crystals are obtained with a high temperature gradient and slow advance

STAT

Declassified in Part - Sanitized Copy Approved for Release @ 50-Yr 2014/03/07 : CIA-RDP81-01043R004200090004-8

Declassified in Part - Sanitized Copy Approved for Release @ 50-Yr 2014/03/07 : CIA-RDP81-01043R004200090004-8

of the crystallization isotherm.

3. For this reason one may recommend conducting the crystallization of mica with a very sharp temperature gradient (strong heating on top, strong cooling from below) with a flat isotherm. The sharp temperature gradient will permit placing the mica seed in the lower conical part of the crucible (the part cooled to below the melting point of mica). The plane of cleavage of the crystal must be established parallel to the isotherm. The slow upward advance of the crystallization isotherm should assure uniform growth of a single mica crystal, which might in that case gradually fill the entire crucible.

N.N.Sheftal'

STAT

Declassified in Part - Sanitized Copy Approved for Release @ 50-Yr 2014/03/07 : CIA-RDP81-01043R004200090004-8

Declassified in Part - Sanitized Copy Approved for Release @ 50-Yr 2014/03/07 : CIA-RDP81-01043R004200090004-8

SYNTHETIC MICA, ITS PROPERTIES AND APPLICATION

by

I.I.Yamzin and M.S.Leyzerzon

In this paper we shall state certain results of studies on the crystallization of fluorophlogopite and teniolite, staged at the Laboratory of Crystal Morphology, Institute of Crystallography (using small masses of melt, 50 - 100 gm), and the results of analogous studies staged at the Laboratory of Natural and Artificial Mica, All-Union Institute of Asbestos and Cement (with larger masses of melt, up to 5 kg). The latter work was staged in 1955 with the methodological assistance of the Institute of Crystallography*. In this paper we also report the first results of the work at the All-Union Research Institute for Asbestos and Cement in the preparation and study of new insulating materials based on synthetic mica.

1. The Components of the Charge, the Optimum Composition of the Fluorophlogopite Charge and the Method of Preparing It

The composition of the original charge, as well as the method of its preparation determines to a considerable extent the loss of volatiles during the process of mica synthesis. The literature gives the compositions of the original charge and

* The following also took part in the work: At the Institute of Crystallography, G.G.Lemmleyn, V.A.Timofeyeva, V.V.Vernikovskiy, T.I.Shashkina, Ye.N.Belova, and N.V.Gliki; at the All-Union Research Institute for Asbestos and Cement, Yu.N.Ul'ko, S.I.Sokol'skiy, O.L.Feofilova, A.S.Naletov, and I.M.Gol'dman.

STAT

Declassified in Part - Sanitized Copy Approved for Release @ 50-Yr 2014/03/07 : CIA-RDP81-01043R004200090004-8

Declassified in Part - Sanitized Copy Approved for Release @ 50-Yr 2014/03/07 : CIA-RDP81-01043R004200090004-8

indicates various starting products (Bibl.1-3), but there have been no data permitting the selection of the optimum composition. We therefore had to determine the relative volatility of a number of fluorine compounds, and the loss of volatiles during the synthesis of mica from various starting charges.

We established, that for example, fluorites that could be used in the synthesis of fluorophlogopite may be arranged in order of decreasing thermal stability as follows:

$$MgF_2,\ KF,\ K_2SiF_6,\ AlF_3.$$

As a rule, the smallest loss of volatiles during the synthesis of mica took place when a charge using the most stable fluorides was made up. For the preparation of fluorophlogopite, the best composition of those tested is

$$KF \cdot 0{,}5\,MgF_2 \cdot 2{,}5\,MgO \cdot 3\,SiO_2 \cdot 0{,}5\,Al_2O_3. \qquad (1)$$

The optimum composition of the charge for the synthesis of teniolite, $KMg_2Li[Si_4O_{10}]F_2$, was found to be

$$KF \cdot LiF \cdot 2\,MgO \cdot 4SiO_2 \qquad (2)$$

A microscopic study of the synthetic product was made. It was found that with a small deficit of fluorine (losses of volatiles not over 6 - 8%), the product of crystallization is pure mica. The admixture of a vitreous phase, forsterite, mullite and other minerals is negligible.

With increasing loss of volatiles, the quantity of impurities increases rapidly. Cross sections of crystalline slabs obtained under the conditions of high loss of volatiles, are characterized by small rosettes of crystals of synthetic mica (see Fig.1). Under a microscope, a crystallite of forsterite or mullite can often be detected at the center of such a rosette.

On the other hand, if the fluorine content of the melt is increased, when the composition of the original charge deviates from the stoichiometric ratio of the com-

STAT

Declassified in Part - Sanitized Copy Approved for Release @ 50-Yr 2014/03/07 : CIA-RDP81-01043R004200090004-8

Declassified in Part - Sanitized Copy Approved for Release @ 50-Yr 2014/03/07 : CIA-RDP81-01043R004200090004-8

ponents, or when an additional quantity of fluoride is introduced in the melt, the quantity of impurities in the final product is likewise increased. The purest syn-

Fig.1 - Rosettes of Fluorophlogopite Crystals after High Loss of Volatiles

thetic mica is formed in cases where the components of the charge are taken in stoichiometric proportions.

2. The Crystallization Temperature of Fluorine Micas

Besides the synthesis of fluorophlogopite, the principal objects of all preceding research, we synthesized about 30 other fluorine micas crystallizing at a lower temperature.

Table 1 gives the crystallization points of some of the micas synthesized, measured by the aid of a Kurnakov pyrometer (errors of measurement $\pm$ 10°C). For fluorophlogopite and teniolite, the crystallization temperatures were measured on an instrument for differential thermal analysis with an error of $\pm$ 5°C. The table also gives the values of the refractive index $N_g \approx N_m$ (Bibl.4).

STAT

Declassified in Part - Sanitized Copy Approved for Release @ 50-Yr 2014/03/07 : CIA-RDP81-01043R004200090004-8

Declassified in Part - Sanitized Copy Approved for Release @ 50-Yr 2014/03/07 : CIA-RDP81-01043R004200090004-8

As will be seen from the table, the substitution of part of the magnesium in the fluorophlogopite by lithium, keeping the sum of the charges of the cations constant, yields a series of micas whose last member is teniolite. The crystallization point and the refractive index $N_g \approx N_m$ of the micas of this series decrease with increasing lithium content by a linear law (taking account of the errors of measurement), which permits us to speak of the existence of a continuous series of fluorophlogopite-teniolite solid solutions.

Table 1

Temperature of Crystallization of Fluorine Micas

a)	b)	c)	d)	e)
$KMg_3[Si_3AlO_{10}]F_2$	1380	1340	1,547	f)
$KMg_{2,75}Li_{0,25}[Si_{3,25}Al_{0,75}O_{10}]F_2$	1360	1325	1,543	
$KMg_{2,5}Li_{0,50}[Si_{3,5}Al_{0,5}O_{10}]F_2$	1270	1260	1,543	
$KMg_{2,25}Li_{0,75}[Si_{3,75}Al_{0,25}O_{10}]F_2$	1260	1240	1,540	
$KMg_2Li[Si_4O_{10}]F_2$	1210	1185	1,540	g)
$KMg_{2,5}Mn_{0,5}[Si_3AlO_{10}]F_2$	1310	1275	1,555	
$KMg_2Mn[Si_3AlO_{10}]F_2$	1310	1260	1,558	
$KMg_3[Si_3BO_{10}]F_2$	1110	1090	1,537	

a) Composition; b) Melting point of charge, °C; c) Crystallization temperature, °C; d) Refractive index; e) Remarks; f) Fluorophlogopite; g) Teniolite

Further, the substitution in fluorophlogopite of up to one third of its magnesium ions by divalent manganese is possible, and leads to a depression of the crystallization temperature to 1260°C.

Phlogopites in which the magnesium has been partially replaced by lithium or manganese form considerably larger crystals than all other micas of the compositions given. There are no differences whatever between the micas of the fluorophlogopite-teniolite series with respect to the size of the crystals, their cleavage and uniformity. In the manganese-substituted phlogopites, the crystal size

STAT

Declassified in Part - Sanitized Copy Approved for Release @ 50-Yr 2014/03/07 : CIA-RDP81-01043R004200090004-8

Declassified in Part - Sanitized Copy Approved for Release @ 50-Yr 2014/03/07 : CIA-RDP81-01043R004200090004-8

decreases with increasing manganese content.

The existence of lithium-substituted phlogopites, crystallizing just as well as fluorophlogopite, but at lower temperatures, is very convenient. In the synthesis of teniolite, certain technical questions are solved with considerably greater ease than in the synthesis of fluorophlogopite. The new synthetic micas include some compositions with a very low crystallization temperature, which may make them promising for the protection of mica-ceramics by a method of hot pressing (Bibl.5).

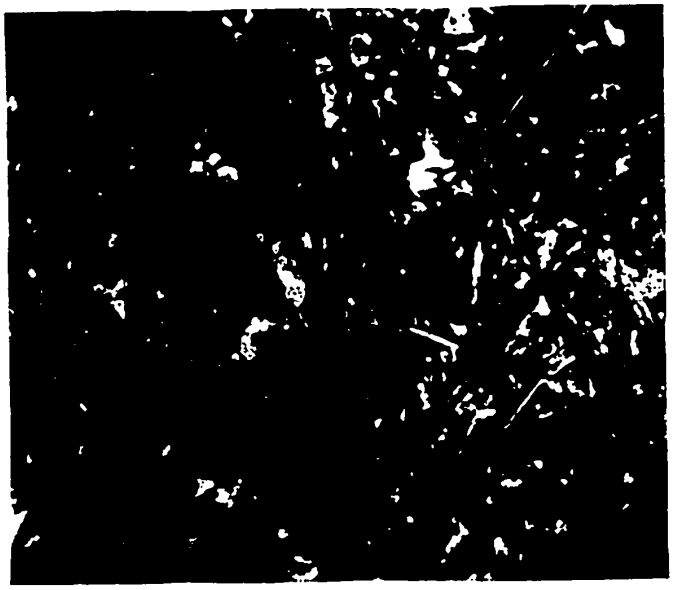

Fig.2 - Synthetic Mica - Fluorophlogopite - with Inclusions of Other Minerals Obtained at a Particularly High Loss of Volatiles

The determination of the crystallization temperature of fluorophlogopite and of the melting point of the fluorophlogopite charge (Bibl.4) permitted refinement of the temperature conditions of synthesis, about which very contradictory reports will be found in the literature (Bibl.1-3, 6). We also found that superheating a fluorophlogopite melt to 1450°C and over, which is recommended in the literature to accelerate the reactions between the components (Bibl.2, 3, 6-8) leads to a considerable loss of volatiles, and consequently to the formation of finely crystalline mica.

STAT

Declassified in Part - Sanitized Copy Approved for Release @ 50-Yr 2014/03/07 : CIA-RDP81-01043R004200090004-8

Declassified in Part - Sanitized Copy Approved for Release @ 50-Yr 2014/03/07 : CIA-RDP81-01043R004200090004-8

The holding of the melt at 1450°C for 2 - 3 hrs (weighed portion of charge 50 gm) led to such a substantial loss of volatiles that the product of crystallization consisted mainly not of mica but of a mixture of forsterite, mullite, andalusite, chondrodite, spinel, and other minerals.

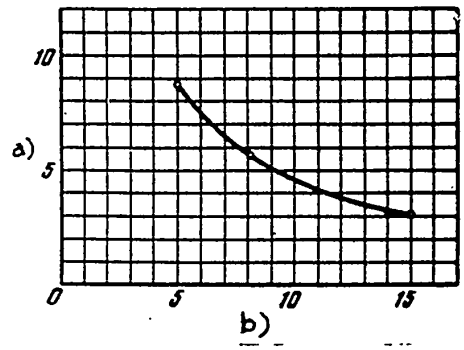

Fig.3 - Relation between the Size of Crystals of Synthetic Mica (Teniolite) and the Rate of Cooling of the Melt

a) Area of crystal, cm^2; b) Rate of cooling, degree/hr

Figure 2 is a photomicrograph of a polished section prepared from such a product. The long gray bands are sections of the fluorophlogopite flakes; the thin white streaks are crystals of forsterite and mullite; the small crystallites of isometric shape consist mainly of magnesia spinel.

With a decrease of the temperature of initial heating of the fluorophlogopite melt to 1380°C, the quantity of impurities in the crystallization product could be considerably reduced. Thus the optimum temperature conditions for the synthesis of fluorophlogopite were found to be as follows: heating to 1380°C as rapidly as possible, holding at this temperature for the time necessary to melt the charge, and then gradual cooling to a temperature somewhat below the crystallization point. These conditions differ substantially from those described in the literature (Bibl.1 - 3, 6 - 8).

Appropriate temperature conditions for the synthesis of teniolite are a temperature rise to 1210°C as rapidly as possible, holding at that temperature, followed

STAT

Declassified in Part - Sanitized Copy Approved for Release @ 50-Yr 2014/03/07 : CIA-RDP81-01043R004200090004-8

Declassified in Part - Sanitized Copy Approved for Release @ 50-Yr 2014/03/07 : CIA-RDP81-01043R004200090004-8

by slow cooling.

The size of the crystals of synthetic mica obtained depend substantially on the rate and uniformity of the temperature fall in the furnace during the time of crystallization.

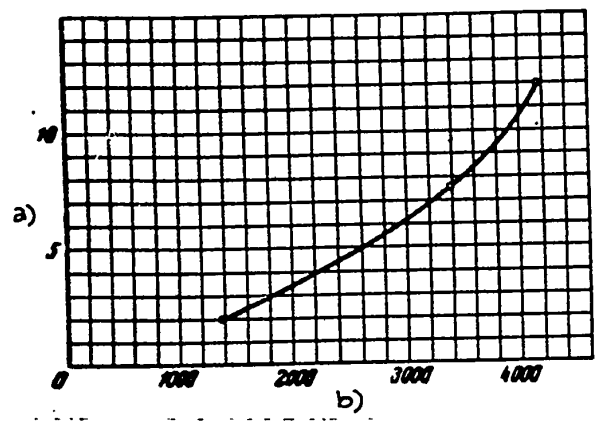

Fig.4 - Relation between the Size of Crystals of Synthetic Mica (Teniolite) and the Mass of the Melt

a) Area of face, cm^2; b) Mass of melt, gm

The more slowly the programmed lowering of the temperature proceeds, the larger the crystals (Fig.3). It must, however, be borne in mind that, with small masses of melt and very prolonged process time, there may be considerable losses of volatiles, leading to the formation of a finely crystalline product. With increasing uniformity of cooling, or, what is the same thing, with increasing mass of the melt, the size of the crystals is also increased, as will be seen from the graph of Fig.4.

3. Orientation of the Crystals Arising in the Surface Layer of the Melt

On crystallization of synthetic mica, the upper layer of the slab obtained sometimes consists of rather coarse mica flakes parallel to the surface of the melt. Such a position of the crystals is obviously due to the forces of surface tension on the melt-air interface, orienting the crystal seeds parallel to this surface.

STAT

Declassified in Part - Sanitized Copy Approved for Release @ 50-Yr 2014/03/07 : CIA-RDP81-01043R004200090004-8

Declassified in Part - Sanitized Copy Approved for Release @ 50-Yr 2014/03/07 : CIA-RDP81-01043R004200090004-8

On crystallization of teniolite in small platinum dishes (Nos.3, 4, and 5; weighed charge 60 - 70 gm), the surface layer of the slab obtained consisted of a mosaic of a small number of platelets of teniolite (Fig.5); some of them had an area up to 4 cm^2 and a thickness of 0.5 - 0.8 mm.

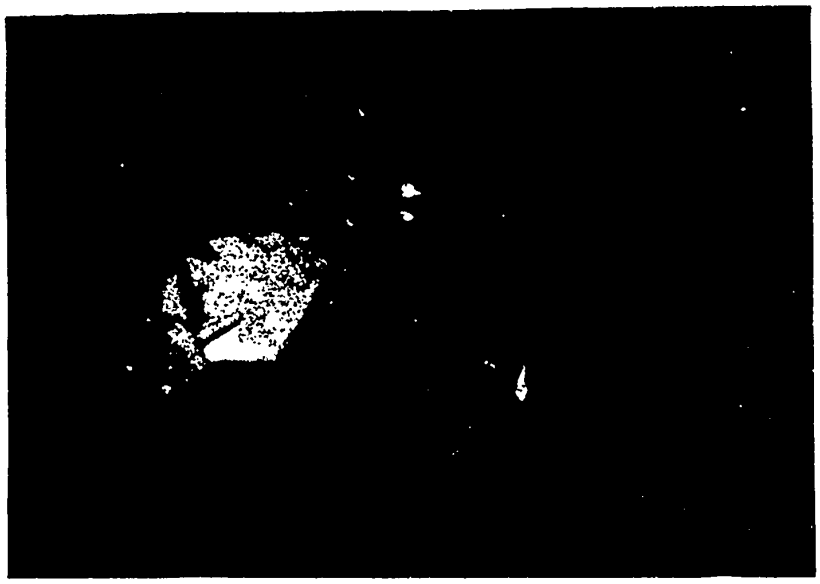

Fig.5 - Mosaics of Teniolite Crystals in Surface Layer of Crystallization Product

Crystals that were thickest and most uniform internally were obtained during the slow cooling of the melt. Some of the experiments were run with graphite crucibles internally lined with sheet molybdenum (weighed charges somewhat over 1 kg). In spite of the contamination of the melt surface by graphite particles, the size of the crystals in the surface layer reach 10 cm^2, with a thickness of up to 1.5 mm. It must be noted that the rate of cooling in both cases was apparently too high: 3 - 5 degree/hr. There are data according to which the rate of cooling in growing crystals of synthetic mica in thickness should not exceed 0.2 degree/hr (Bibl.6).

4. Preparation of Materials Based on Synthetic Mica

For the rapid preparation of large quantities of finely crystalline mica nec-

STAT

Declassified in Part - Sanitized Copy Approved for Release @ 50-Yr 2014/03/07 : CIA-RDP81-01043R004200090004-8

Declassified in Part - Sanitized Copy Approved for Release @ 50-Yr 2014/03/07 : CIA-RDP81-01043R004200090004-8

Fig.6 - Finely Crystalline Slab Obtained by Melting without a Crucible

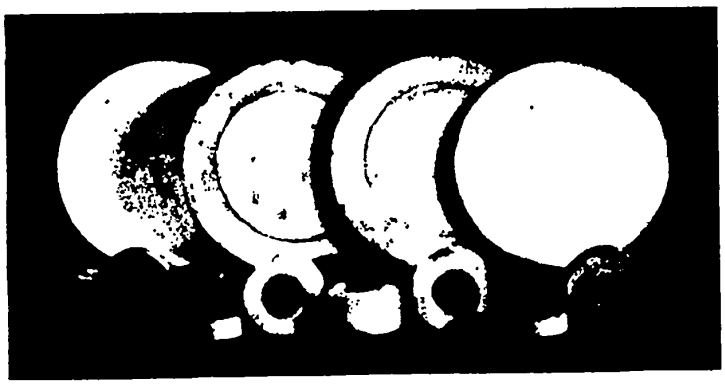

Fig.7 - Specimens of Ceramic from Synthetic Mica

STAT

Declassified in Part - Sanitized Copy Approved for Release @ 50-Yr 2014/03/07 : CIA-RDP81-01043R004200090004-8

Declassified in Part - Sanitized Copy Approved for Release @ 50-Yr 2014/03/07 : CIA-RDP81-01043R004200090004-8

essary for the manufacture of mica-ceramic, the process of crucibleless melting was employed. In the charge, placed in a thick layer in a refractory container, two massive electrodes are submerged. The ends of these electrodes are connected by a thin jumper. When current passes through the electrodes, the charge will melt around the incandescent jumper, after which the jumper burns away and the subsequent heating is assured by the passage of the current through the melt.

Figure 9 is a photograph of a crystal slab prepared in a small model furnace for crucibleless melting (1/3 natural size).

The crystalline slab obtained after melting (with or without a crucible) was next ground in a ball mill. A binder consisting of 85% of orthophosphoric acid was added to the powder so obtained in an amount of 10 - 15% the weight of the powder. Out of this mass, under pressure of 700 kg/cm^2, specimens were pressed. They were fired in an electric furnace for one and a half hours at 950 - 1000°C. Figure 7 presents photographs of specimens prepared from synthetic mica with a phosphate binder. With slight modifications, this process may be used in industrial production.

For the production of articles from synthetic mica using a glass binder, the sequence of operations corresponding to the manufacturing process for the production of ordinary micalex may be employed.

The production of sheet electrical insulating materials by the technology of paper and cardboard production is also possible based on synthetic mica. The required articles may be produced from the sheet material so obtained by means of punching on presses.

5. Properties of Synthetic Mica and the Materials Manufactured with It as a Base

In a recent paper (Bibl.4) we reported the results of measurements of the elementary cell periods of fluorophlogopite and teniolite, the refractive indices and the coefficients of absorption for the optical and ultraviolet parts of the spectrum.

STAT

Declassified in Part - Sanitized Copy Approved for Release @ 50-Yr 2014/03/07 : CIA-RDP81-01043R004200090004-8

Declassified in Part - Sanitized Copy Approved for Release @ 50-Yr 2014/03/07 : CIA-RDP81-01043R004200090004-8

Table 2 gives the results of a determination of certain mechanical and electrical properties of fluorophlogopite and teniolite, compared with the properties of the best specimens of natural micas.

Table 2

Electrical and Mechanical Properties of Fluorophlogopite and Teniolite

a)	b)	c)	d)	e)
f)				
$f = 10^2$ cycles	—	6,24	6,0	7,0
$f = 10^6$ cycles	6,7	6,0	—	
g)				
20 μ	3,5*	10,3**	—	5,7
50 μ	6,5	13,0	—	$3-5 \cdot 10^{-4}$
h)	3,1	$1 \cdot 10^{-4}$	—	
i)	61—65	2,65	20—120	65—150
j)		51—61		
k)	—	0,13	0,10—0,77	0,02—0,65
l)	—	0,40	1,5—5,2	1.3+4.5

* Synthetic mica prepared in graphite crucible.

** Synthetic mica prepared in platinum dish.

a) Characteristic; b) Fluorophlogopite; c) Teniolite; d) Natural phlogopite (Bibl.10); e) Muscovite (Bibl.10); f) Dielectric constant at: ; g) Breakdown voltage in kv at thickness: ; h) tan δ at 20°C; i) Density, gm/cm^3; j) Hardness, sec (by Kuznetsov method); k) Hygroscopicity, %; l) Water absorption, %

As will be seen from Table 2, fluorophlogopite and teniolite have better electrical insulating properties than natural micas; in combination with their high heat resistance (Bibl.4, 5), this makes the use of synthetic micas very promising for many fields of radio and electrical engineering.

The properties of materials manufactured with a synthetic mica base are of very great interest.

STAT

Declassified in Part - Sanitized Copy Approved for Release @ 50-Yr 2014/03/07 : CIA-RDP81-01043R004200090004-8

Declassified in Part - Sanitized Copy Approved for Release @ 50-Yr 2014/03/07 : CIA-RDP81-01043R004200090004-8

Materials of synthetic mica manufactured by the method of hot pressing have very low dielectric losses and are in this respect among the best dielectrics. The tangent of the dielectric loss angle ($f = 10^6$ cycles) of hot-pressed synthetic mica at 20°C is $3 - 7 \times 10^{-4}$, and at 300°C it does not exceed 4×10^{-4}. The bulk resistivity at 300°C, $\rho_v = 10^{12} - 10^{13}$ ohm-cm, i.e., is one order higher than that of the best ceramic dielectrics. If we bear in mind that all other high-frequency dielectrics are practically unsuitable at temperatures over 200°C, owing to the sharp rise in the dielectric losses, the advantages of hot-pressed synthetic mica become obvious. Ceramics of synthetic mica with a phosphate binder have somewhat poorer electrical properties, but they are easily machined by the ordinary cutting tool, which sharply distinguishes them from all ceramic materials.

A remarkable property of ceramics of synthetic mica is their exceptional resistance to thermal shock. An article of synthetic mica with a phosphate base may be repeatedly heated to 1000°C and sharply cooled, by being thrown into cold water, after which no traces of disintegration of the material can be detected.

A possible field of application of synthetic mica ceramic, where it cannot be replaced by any other ceramic material, is the manufacture of insulators designed for use under conditions of sharp temperature changes (for example in aircraft and ship apparatus). With a proper choice of the composition of the synthetic mica and the binder, it is possible to obtain materials with coefficients of expansion close to those of the metals and alloys used in structures operating under alternating thermal loads. Such materials may be used, for example, in gas turbines and jet engines. There is information on the use of coatings of such materials on the exhaust of supersonic jet aircraft (Bibl.9).

Polycrystalline sheet materials of synthetic mica may find wide application. For example, they could be successfully used in radio tube production instead of strips of monocrystalline mica, in the production of printed circuits designed for work at elevated temperatures, and also of insulation, in various electrical ma-

STAT

Declassified in Part - Sanitized Copy Approved for Release @ 50-Yr 2014/03/07 : CIA-RDP81-01043R004200090004-8

Declassified in Part - Sanitized Copy Approved for Release @ 50-Yr 2014/03/07 : CIA-RDP81-01043R004200090004-8

chines and apparatus.

Conclusions

1. A series of fluorine micas of varying chemical compositions has been synthesized. The optimum compositions have been found for the starting charges yielding the best results in the synthesis of fluorophlogopite and teniolite. Methods have been worked out for decreasing the losses of volatile components during the synthesis of mica, which has assured a practically 100% yield of mica from the product of the heat. The principles of the technological process of preparing synthetic mica so developed have been successfully used in experimental heats with increased masses of melt.

2. Crystals of fluorophlogopite and teniolite, large enough and of high enough grade for determination of their physical properties, have been prepared. The dielectric constants, the electrical breakdown strength, the bulk and surface resistivity, and the tangent of loss angle have been measured.

3. The principles of an approximate technology for the preparation of new electrical insulating materials based on synthetic mica have been formulated. The first specimens of electrical insulating materials based on fluorophlogopite and teniolite have been manufactured and certain of their properties investigated: electrical breakdown strength, bulk resistivity, tangent of loss angle, density, hygroscopicity, etc.

4. The first experimental melts have been made by the no-crucible method, which is very economical and promising for the production of the starting products in the manufacture of various electrical insulating materials based on synthetic mica.

5. Synthetic mica and materials based on it may find wide application in the electrical engineering, radio engineering and aviation industries.

STAT

Declassified in Part - Sanitized Copy Approved for Release @ 50-Yr 2014/03/07 : CIA-RDP81-01043R004200090004-8

Declassified in Part - Sanitized Copy Approved for Release @ 50-Yr 2014/03/07 : CIA-RDP81-01043R004200090004-8

BIBLIOGRAPHY

1. Tyler,P.M. - Synthetic Mica Research. FIAT, Final Report, No.746
2. Kendall,J.T. and Varley,E.R. - The German Mica Industry. BIOS, Final Report, No.785
3. Middel,V. - Technical Report. Experiments on the Preparation of Synthetic Mica in a Pilot Plant. PB, 32546
4. Yamzin,I.I., Imofeyeva,V.A., Shashkina,T.I., Belova,Ye.N., and Gliki,N.V. - Structure and Morphological Features of Fluorophlogopite and Teniolite. Zap.Vses.Mineralog.Obsh., Ch.83,No.4 (1955),pp.415-424
5. Comeforo,J.E., Hatch,R.A., Humphrey,R.A., and Eitel,W. - Journ.Amer.Ceram.Soc., Vol.36,No.9 (1953),pp.286-294
6. VanValkengurg,A. and Pike,R.G. - Journ.Res.Natl.Bur.Stand., Vol.48,No.5 (1952), pp.360-369
7. Jackel,R.D. - Electr.Manufacturing, No.3 (1950),pp.99-103, 190
8. - Mining. World., Vol.12,No.12 (1950),pp.33 and 35
9. - Bull.Amer.Ceram.Soc., No.1 (1955),pp.15-17
10. Lashev,Ye.K. - Mica. I. Properties of Micas. Promstroyizdat (1948)

STAT

Declassified in Part - Sanitized Copy Approved for Release @ 50-Yr 2014/03/07 : CIA-RDP81-01043R004200090004-8

Declassified in Part - Sanitized Copy Approved for Release @ 50-Yr 2014/03/07 : CIA-RDP81-01043R004200090004-8

ON THE GROWING OF SINGLE CRYSTALS OF SORBITOL HEXAACETATE

by

I.S.Rez and L.I.Tsinober

Investigators in the field of piezoelectric technology are continuing their searches for new materials. The specifications of two patents on the application of plates cut out of a new piezoelectiic crystal, sorbitol hexaacetate (SHA), published in 1954, are of considerable interest (Bibl.1).

Sorbitol hexaacetate is the acetic acid ester of the hexahydric alcohol d-sorbitol, [with the chemical formula $C_6H_8O_6(COCH_3)_6$] the molecular weight of 434.39, and the melting point of 99 - 100°C (Bibl.2). It crystallizes in colorless crystals (there are no crystallographic data in the literature) of specific gravity 1.34 (at 25°C), and a solubility in water of 2.7 gm/ltr at 25°C and 30 gm/ltr at 100°C (Bibl.2). Sorbitol hexaacetate is used industrially in the United States as a plasticizer and in intermediate inorganic synthesis.

Sorbitol hexaacetate was first prepared by Vincent (Bibl.3) by boiling sorbitol for 2 hrs with an excess of acetic anhydride in presence of a small quantity of zinc chloride. This mixture is then poured into water, and the precipitated sorbitol hexaacetate is washed with water, dissolved in ether, purified by filtration through charcoal, and after distilling off the ether, sorbitol hexaacetate is obtained in the form of a vitreous mass. According to later data (Bibl.4), it is obtained in good yield on acetylation of sorbitol in the cold by a mixture of acetic anhydride and acetic acid in presence of perchloric acid as a catalyst. It is separated from

STAT

Declassified in Part - Sanitized Copy Approved for Release @ 50-Yr 2014/03/07 : CIA-RDP81-01043R004200090004-8

Declassified in Part - Sanitized Copy Approved for Release @ 50-Yr 2014/03/07 : CIA-RDP81-01043R004200090004-8

the reaction mixture by pouring into water, followed by washing the precipitated product with water. The procedure for the industrial synthesis of sorbitol hexaacetate has not been published.

We used a typical technique of acetylation of sorbite by an excess boiling acetic anhydride without a catalyst. The acetylation was run for 3 - 5 hrs at 135°C. On completion of their reaction, the excess of acetic anhydride and the acetic acid formed were distilled off in vacuo, the residue was dissolved in hot 20% acetic acid, filtered and recrystallized from 40% ethyl alcohol. To clarify the solution before filtration, it was heated with 2% of fine activated charcoal. The product recrystallized in the cold was washed to remove the mother liquor with fresh 40% alcohol and then dried. The yield of a product with m.p. 98 - 99°C was 78 - 80% of the theoretical (based on the sorbitol). A larger amount of sorbitol hexaacetate was prepared from technical products, with an average yield of 74% of the theoretical.

A visual examination of fine crystallites of sorbitol hexaacetate showed that they belong more probably to the dihedral axial class of the monoclinic system. Four crystallites of sorbitol hexaacetate (0.5 - 1 mm in size) were measured on the goniometer.

Table 1 gives the results of the measurements.

The data of the measurement and the existence of piezoelectric properties show that the crystals actually belong to the dihedral axial class of the monoclinic system.

The monoclinic angle $\beta = 95°58' \approx 96°$, which is indirectly confirmed by the data (Bibl.3). Figure 1 is a drawing of a crystal of sorbitol hexaacetate indicating the direction of the axes.

A crystallite of sorbitol hexaacetate was subjected to X-ray study. Under Cu K_α-radiation 12 diffraction patterns were taken in an RKOP chamber without a filter. Of them, five Laue patterns were taken with the object of establishing the crystal

STAT

Declassified in Part - Sanitized Copy Approved for Release @ 50-Yr 2014/03/07 : CIA-RDP81-01043R004200090004-8

Declassified in Part - Sanitized Copy Approved for Release @ 50-Yr 2014/03/07 : CIA-RDP81-01043R004200090004-8

structure. On one of them (the primary beam being perpendicular to the second-order axis of the crystal), six thermal diffusion maxima are clearly revealed. Their study might be of interest in establishing the structure of sorbitol hexaacetate crystals.

Table 1

Data of Goniometric Measurement of Crystals of Sorbitol Hexaacetate

Face No.	ρ	φ	hkl
1	90°00′	130°35′	$(10\bar{1})$
2	90 00	76 16	$(\bar{1}00)$
3	90 00	352 14	$(00\bar{1})$
4	90 00	310 38	$(\bar{1}01)$
5	90 00	256 16	(100)
6	90 00	172 14	(001)
7	33 55	76 18	(110)
8	33 50	76 18	$(1\bar{1}0)$

Seven diffraction patterns were taken by the rocking method (rocking interval 15°) to determine the elementary cell parameters and the Bravais lattice type. The approximate values of the elementary cell periods were as follows: $a = 12.7_2$Å; $b = 9.4_3$Å; $c = 10.1_5$Å.

The taking of four rocking diffraction patterns around the directions of the three diagonals of the faces and the space diagonal showed that the crystals of sorbitol hexaacetate possess a primitive monoclinic Bravais lattice. Knowing the lattice parameters, the density and the molecular weight of sorbitol hexaacetate, from the relations

$$V = a \cdot b \cdot c \cdot \sin\beta \text{ and } n = \frac{V\rho}{M \cdot 1{,}66}$$

we determine the number of molecules in the elementary cell:

$$n = \frac{1470}{720} \approx 2.$$

STAT

Declassified in Part - Sanitized Copy Approved for Release @ 50-Yr 2014/03/07 : CIA-RDP81-01043R004200090004-8

Declassified in Part - Sanitized Copy Approved for Release @ 50-Yr 2014/03/07 : CIA-RDP81-01043R004200090004-8

Kforos patterns were taken of the planes (h0l) and (0kl) which unambiguously [from the extinctions of (0k0) with odd k] indicate that the crystals belong to the group $R2_1$.

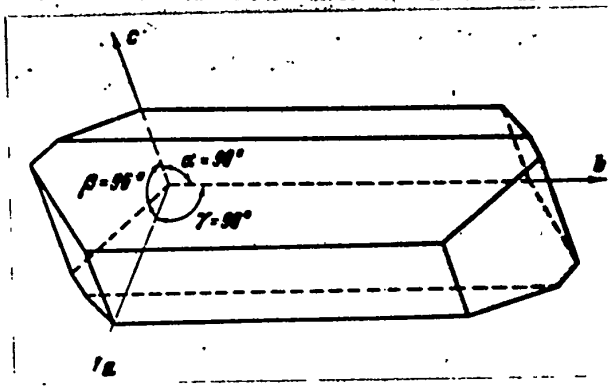

Fig.1 - Ideal Form of Crystal of Sorbitol Hexaacetate from Goniometric Data

The extremely low solubility of sorbitol hexaacetate in water made it necessary to select a different solvent. From the results of a qualitative evaluation of the

Table 2

Solubility of Sorbitol Hexaacetate in 96% Ethyl Alcohol

a)	b)	a)	b)
27,0	17,4	54,3	312
34,7	35,6	55,0	352
42,5	75,6	56,0	402
47,0	124,0	56,5	442
49,5	175	57,5	470
52,0	220	58,0	502
53,5	270		

a) Temperature, °C; b) Solubility, gm/ltr

solubility, we selected ethyl alcohol. Owing to the fact that the amount of preparation was insufficient for a solubility study, we used the classical method of Alekseyev (Bibl.5) in modified form, permitting a considerable acceleration of the

STAT

Declassified in Part - Sanitized Copy Approved for Release @ 50-Yr 2014/03/07 : CIA-RDP81-01043R004200090004-8

Declassified in Part - Sanitized Copy Approved for Release @ 50-Yr 2014/03/07 : CIA-RDP81-01043R004200090004-8

work.

This technique is essentially as follows.

We determine the approximate value of the solubility of the substance under study in the given solvent for two extreme temperatures; then in 10 - 12 or more numbered ampules, by the aid of a microburette, a standard quantity of the solvent was

Table 3

Solubility of Sorbitol Hexaacetate

in 40% Ethyl Alcohol

a)	b)	a)	b)
23	1,5	45	39,8
23	2,7	49	54
24	4,4	52,5	81,3
32	10,4	53	86,7
38	18,5	58,5	179
44	33,9	61	249

a) Temperature, °C; b) Solubility, gm/ltr

introduced (for the case of sorbitol hexaacetate, 2 ml of alcohol, etc.) and various quantities of the substance under study, so selected that the range of concentrations obtained covered the temperature range under study on the solubility curve. After filling, the ampules are sealed and placed in the holder of a shaking machine, loaded into a water thermostatic cabinet. The shaker provides the prescribed shaking cycle. The temperature was lowered manually every half hour by 0.2 - 0.25°C. To determine the solubility it is rational to use the finely dispersed solid phase.

On successive temperature rises, we note the time of complete disappearance of the solid phase in each ampule, a subsequent conversion of the results into gm/ltr gives the values of the solubility. The data obtained by this method are presented in Tables 2 - 4. The relative accuracy of the determination is about 0.5%. To increase the accuracy it is advisable to weigh the solvent.

Starting out from what has been said, it was of interest to elucidate the de-

STAT

Declassified in Part - Sanitized Copy Approved for Release @ 50-Yr 2014/03/07 : CIA-RDP81-01043R004200090004-8

Declassified in Part - Sanitized Copy Approved for Release @ 50-Yr 2014/03/07 : CIA-RDP81-01043R004200090004-8

pendence of the yield of sorbitol hexaacetate crystals on various additives. The corresponding experiments were run for solutions in 96% and in 40% alcohol. Tables 5 and 6 gives the results.

Table 4

Solubility of Sorbitol Hexaacetate in Water

a)	b)	a)	b)
33	1,3	69	10,6
36	1,6	71	12,4
45	2,2	75	15,5
51	3,8	78	22,4
58	4,7	82	27,0
64	7,7		

a) Temperature, °C; b) Solubility, gm/ltr

It follows from an analysis of these data that crystals of sorbitol hexaacetate are exceedingly sensitive to additives. In particular, for solutions in 96% alcohol, the addition of alkali lowers the yield of crystals far more sharply (to 0.3 - 0.03 of the yield without additives) than the addition even of relatively large quantities of acids. The addition of an organic acid (tartaric acid) has a weaker effect than the addition of small quantities of sulfuric acid. The solution of sorbitol hexaacetate in alcohol has a pronounced buffering action. It is characteristic that additions both of acids and, especially, of alkalies, should raise the interval of metastable saturation of solutions of sorbitol hexaacetate in 96% of alcohol, in individual cases, with the maximum addition of alkali, depressing the temperature of the beginning of spontaneous crystallization by almost 40°C below the saturation temperature. In habit, the addition of tartaric acid causes crystallization in the form of platelets, the addition of sulfuric acid, of relatively the best formed crystals, the addition of alkali, of elongated crystals; in the control boxes, without additions, turbid clumps of crystallites of the usual type are formed.

For solutions in 40% alcohol we observed a still greater delay of the beginning

STAT

Declassified in Part - Sanitized Copy Approved for Release @ 50-Yr 2014/03/07 : CIA-RDP81-01043R004200090004-8

Declassified in Part - Sanitized Copy Approved for Release @ 50-Yr 2014/03/07 : CIA-RDP81-01043R004200090004-8

of crystallization for both acid and alkaline additives. The retarding action of sulfuric acid on the yield of crystals in this case, as well, is stronger than that of acetic acid, and increases with increasing dosage of the additives. The buffer action of the systems is very pronounced. The allowable supercooling of the solutions under the influence of additives is likewise substantially increased, practically leading to the total inhibition of spontaneous formation of crystals of sorbitol hexaacetate without the introduction of seed crystals.

Table 5

Influence of Additives on Character of Crystallization of Sorbitol Hexaacetate from 96% Alcohol*

a)	b)	c)	d)	e)	f)	g)
h)	0,4 gm	0,2 N	23,5	3,0—3,1	1,612	0,93
i)	0,2 »	0,1 N	23,5	3,0—3,2	1,677	0,96
0,1 N H_2SO_4	0,5 ml	0,002 N	27	2,6—2,7	1,489	0,85
0,1 N H_2SO_4	2,0 »	0,008 N	24,5	3,1	1,209	0,69
3,7% NaOH	2,0 »	0,08 N	0	7,7	0,053	0,03
3,7% NaOH	1,0 »	0,04 N	23	8,1	0,504	0,29
3,7% NaOH	0,1 »	0,004 N	29	8,2	1,504	0,85
—	—	—	38—38	7,5	1,741	1,0
—	—	—	37—38	7,5	1,770	1,0

* In all cases the addition was made to 25 ml of solution of sorbitol hexaacetate, saturated at 40°C.

a) Added; b) Quantity; c) Calculated normality of solution after addition; d) Initial crystallization point, °C; e) pH of solution after crystallization; f) Quantity of sorbitol hexaacetate precipitated, gm; g) Relative quantity in precipitate; h) Tartaric acid; i) The same.

The crystals obtained in the presence of acetic acid are characterized by a somewhat greater degree of perfection. The control crystals proved defective.

It follows from the above that sorbitol hexaacetate is more sensitive to

STAT

Declassified in Part - Sanitized Copy Approved for Release @ 50-Yr 2014/03/07 : CIA-RDP81-01043R004200090004-8

Declassified in Part - Sanitized Copy Approved for Release @ 50-Yr 2014/03/07 : CIA-RDP81-01043R004200090004-8

impurities than the industrially grown piezo-crystals.

As follows from the above solubility data, sorbitol hexaacetate has a relatively

Table 6

Effect of Additives on Character of Crystallization of Sorbitol Hexaacetate from 40% Alcohol*

a)	b)	c)	d)	e)	f)	g)	h)
1	0,1 N H_2SO_4	2,5 ml	0,01 N	—	2,5	0,350	0,22
2	0,1 N H_2SO_4	0,25 »	0,001 N	—	2,75	0,652	0,41
3	CH_3COOH 100%	1,5 gm	0,1 N	—	2,68	0,422	0,26
4	CH_3COOH 10%	1,43 ml	0,01 N	—	3,18	0,715	0,45
5	CH_3COOH 10%	0,14 »	0,001 N	45	3,65	1,377	0,86
6	—	—	—	45	4,88	1,594	1,00
7	i)	0,1 ml	—	—	4,98	0,703	0,44
8		0,5 »	—	—	5,01	0,630	0,40
9		1,0 »	—	—	5,02	0,708	0.44
10		2,0 »	—	—	5,10	0,617	0,39
11		0,4 »	0,001 N	—	5,5	0,654	0,44
12	2,66% NaOH	0,4 »	0,01 N	—	4,5	0,554	0.35
13		4,0 »	0,1 N	—	6	0,212	0,13

* In all cases the addition was made to 25 ml of sorbitol hexaacetate solution in 40% alcohol, saturated at 45°C. In all cases except Nos.5 and 6, precipitate was thrown down after introduction of seed crystals of sorbitol hexaacetate at room temperature. The seeds were introduced on the third day.

a) Sample No.; b) Substance added; c) Quantity; d) Calculated normality of solution after addition; e) Initial crystallization point, °C; f) pH of solution after crystallization; g) Quantity of sorbitol hexaacetate added, gm; h) Relative quantity in precipitate; i) Control solution of sorbitol in 40% alcohol (20 gm/ltr)

high solubility in 96% alcohol. Starting out from this, experiments on growing single crystals of sorbitol hexaacetate were staged with solutions in 96% alcohol. In these experiments, the solution, saturated, according to calculations, at 45 - 50°C,

STAT

Declassified in Part - Sanitized Copy Approved for Release @ 50-Yr 2014/03/07 : CIA-RDP81-01043R004200090004-8

Declassified in Part - Sanitized Copy Approved for Release @ 50-Yr 2014/03/07 : CIA-RDP81-01043R004200090004-8

was poured into a half-liter chemical cylinder, placed in the standard externally heated eight-liter water thermostat. The seed crystal was attached to a glass rod with a rubber ring; a glass stirrer was used for mixing. The thermometer was placed inside the cylinder with the solution of sorbitol hexaacetate, and the thermoregulator in the outer vessel. The crystallizing cylinder was covered with a cover held against the upper edge by a system of spring holders. The stirrer was introduced on a sliding base, without a special seal. In the absence of sharp fluctuations of the voltage in the supply net, the accuracy of maintenance of the temperature was within ± 0.10 - 0.15°C.

The experiments staged showed the extraordinary ease with which parasites appear in the solution, owing to the volatilization of the alcohols through leaks in the cover.

The usual methods of sealing crystallizers used in the laboratory proved to be unsuitable for work with solutions of sorbitol hexaacetate in 96% alcohol.

It was decided to check the possibility of growing single crystals of sorbitol hexaacetate from solutions in 40% alcohol. During the course of the experiments, a new circumstance showed up, preventing us from obtaining results of full value. During the process of holding the working solutions at the temperatures used in industry, and necessary to assure the required reserve of substance to be crystallized, preferential evaporation of the alcohol was observed in the apparatus, resulting in a sharp fall of solubility of the sorbitol hexaacetate in the alcohol-depleted alcohol-water mixture. A peculiar "salting-out" of the sorbitol hexaacetate occurred, the more rapid the higher the experimental temperature. The irregular increase of the quantity of solid phase segregated from the solution resulted in a vigorous growth of defective crystals and the spontaneous formation of seeds throughout the entire bulk of the solution.

We then used large wide-mouthed flasks with an elongated extension at the bottom to trap the parasitic crystals. A crystal carrier was introduced into the

STAT

Declassified in Part - Sanitized Copy Approved for Release @ 50-Yr 2014/03/07 : CIA-RDP81-01043R004200090004-8

Declassified in Part - Sanitized Copy Approved for Release @ 50-Yr 2014/03/07 : CIA-RDP81-01043R004200090004-8

glass, in the form of a stainless steel rod with a cylindrical bulb at the end. A horizontal passage was drilled in this rod, in which a rubber or cork stopper was inserted, serving as a holder for the seed crystals forced into the depressions in the rod.

The neck of the flask was tightly closed with a rubber stopper through which the shaft of the crystal carrier was passed; to strengthen the neck, in some series, it was tightly wound with 00 thread, and afterwards BF-4 cement was again applied.

The flask was placed in the water thermostatic chamber and placed in reversing motion.

Using this method we succeeded in practically eliminating the losses of solvent due to evaporation through untight places, and in obtaining several pure single crystals weighing up to 7.0 gm, which were utilized for studying their piezoelectric and dielectric properties.

This work showed that it is possible in principle to prepare industrial single crystals of sorbitol hexaacetate, and at the same time revealed the very high sensitivity of these crystals to fluctuations of temperature and other disturbances of the conditions during their growth.

The work on the synthesis of sorbitol hexaacetate, the determination of the solubility and growing of the single crystals was performed by I.S.Rez and associates at the TsNILP, while the goniometric and X-ray studies were performed by L.I.Tsinober at Moscow State University.

BIBLIOGRAPHY

1. - Journ. of the Acoust.Soc.Amer., Vol.26,No.3 (1954),p.480

2. - Chemists Handbook, Vol.II,p.858

3. Vincent - Comptes Rendus, Vol.109 (1889),p.678

4. Nicholas,S.D. and Smith,F. - Nature, Vol.161 (1948),p.349

5. Weissberger,A. - Physical Methods of Organic Chemistry. (1938); Hill,A.E. - J.Am.Chem.Soc., Vol.45 (1923),p.1143

STAT

Declassified in Part - Sanitized Copy Approved for Release @ 50-Yr 2014/03/07 : CIA-RDP81-01043R004200090004-8

Declassified in Part - Sanitized Copy Approved for Release @ 50-Yr 2014/03/07 : CIA-RDP81-01043R004200090004-8

THE PREPARATION, DIELECTRIC AND OPTICAL PROPERTIES OF SINGLE CRYSTALS OF SOLID SOLUTIONS $(Ba - Sr)TiO_3$

by

A.L.Khodakov, M.L.Sholokhovich, Ye.G.Fesenko, and O.P.Kramarov

Much work has been devoted in recent years to the growing of single crystals of ferroelectric materials. Single crystals of barium titanate and lead titanate have been studied in particular detail (Bibl.1-7), and data on the growing and properties of single crystals of strontium titanate have also appeared (Bibl.8).

Single crystals of $BaTiO_3$ were first grown by us by their crystallization from a solution of polycrystalline barium titanate in a molten mixture of soda and potash, and also from a solution of $BaTiO_3$ in a melt of barium chloride. These salt solvents had been previously employed for the same purpose by Blattner, Kaenzing and Merz (Bibl.1). Subsequently, on the basis of the experimental material obtained by us on the interaction of barium titanate with various substances in melts (see Bibl.9), other solvents were also used for growing single crystals of $BaTiO_3$, and the methods of growing were modified in accordance with these other solvents. In particular, potassium fluoride was used as the salt solvent. It was found that single crystals of barium titanate, depending on the growing conditions, had a cubic, hexagonal or tetragonal cell, and the conditions of transformation of crystals of the cubic modification into tetragonal crystals were also found (Bibl.10).

Single crystals of ferroelectric substances are not only of theoretical in-

STAT

Declassified in Part - Sanitized Copy Approved for Release @ 50-Yr 2014/03/07 : CIA-RDP81-01043R004200090004-8

Declassified in Part - Sanitized Copy Approved for Release @ 50-Yr 2014/03/07 : CIA-RDP81-01043R004200090004-8

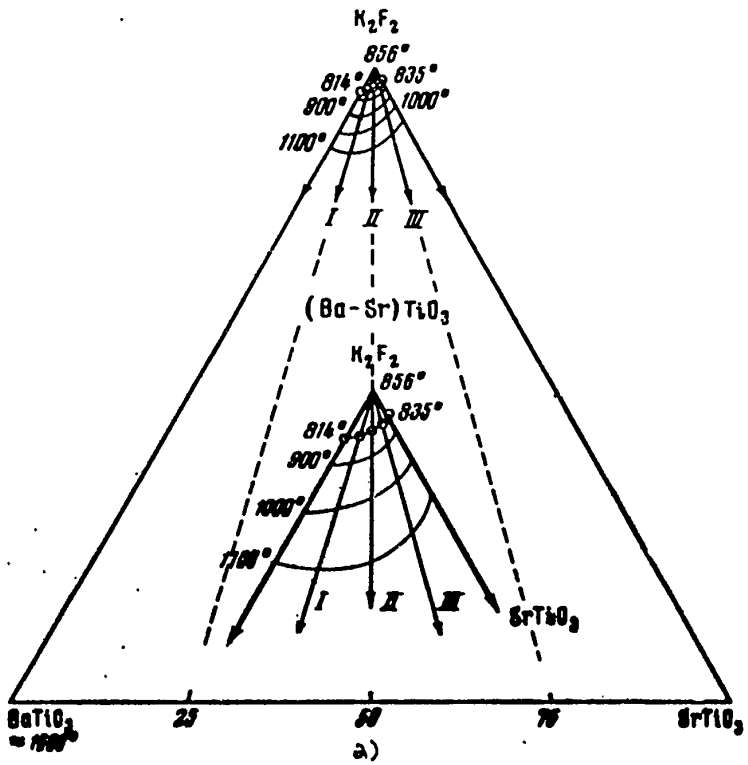

a)

Fig.1

a) Molecular percentage $SrTiO_3$

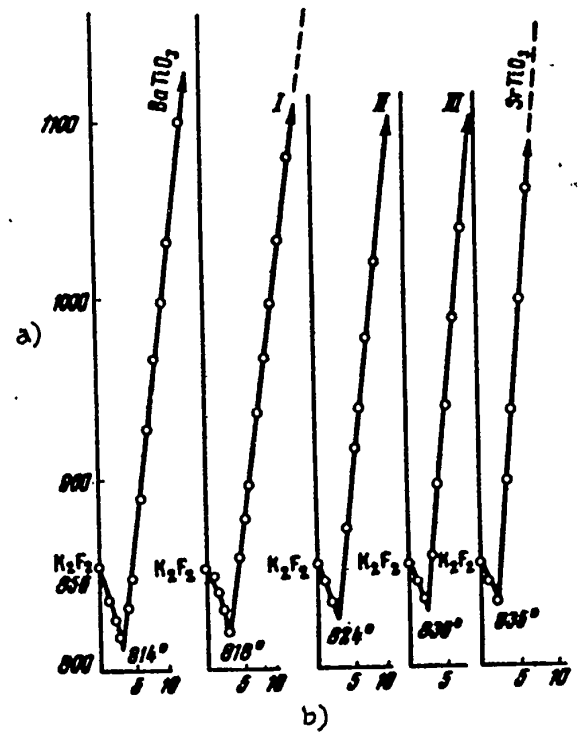

Fig.2

Curve I: section K_2F_2-[75% $BaTiO_3$+ 25% $SrTiO_3$];
Curve II: section K_2F_2-[50% $BaTiO_3$ + 50% $SrTiO_3$];
Curve III: section K_2F_2-[25% $BaTiO_3$ + 75% $SrTiO_3$]

a) Temperature, °C; b) Molecular percent

STAT

Declassified in Part - Sanitized Copy Approved for Release @ 50-Yr 2014/03/07 : CIA-RDP81-01043R004200090004-8

Declassified in Part - Sanitized Copy Approved for Release @ 50-Yr 2014/03/07 : CIA-RDP81-01043R004200090004-8

terest but are also of undoubted practical importance. In particular, they have found use in computers (Bibl.11). In this connection, it is exceedingly important to be able to vary the dielectric properties of the single crystals and to prepare single crystals with assigned parameters. Starting out from this, we staged work on

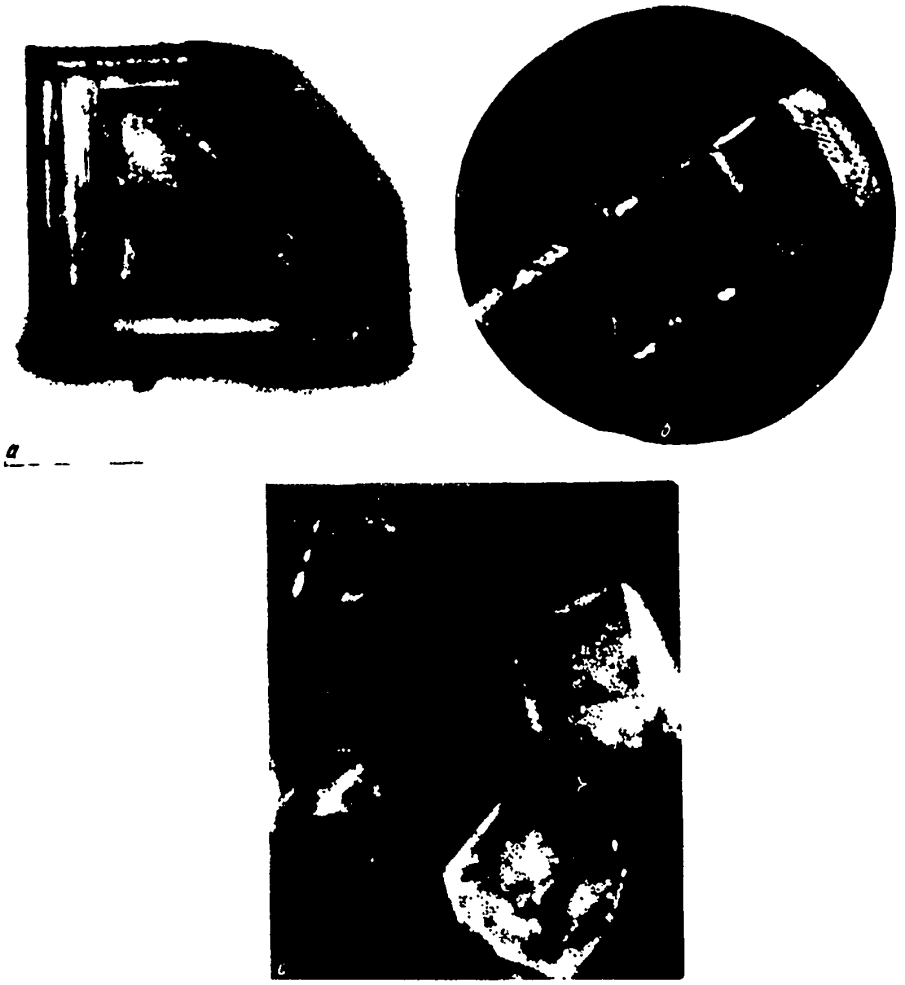

Fig.3 - Single Crystals

a - $BaTiO_3$; b - $(Ba - Sr)TiO_3$ (part of III); c - $SrTiO_3$

growing single crystals of solid solutions. The polycrystalline solid solutions $(Ba - Sr)TiO_3$ have been investigated in rather great detail by a number of authors (Bibl.12 - 16). In the present paper we shall describe the method of preparation of single crystals of solid solutions of $(Ba - Sr)TiO_3$, and of single crystals of

STAT

Declassified in Part - Sanitized Copy Approved for Release @ 50-Yr 2014/03/07 : CIA-RDP81-01043R004200090004-8

Declassified in Part - Sanitized Copy Approved for Release @ 50-Yr 2014/03/07 : CIA-RDP81-01043R004200090004-8

$BaTiO_3$ and $SrTiO_3$, as well as their dielectric, optical and structural properties.

Single crystals of $BaTiO_3$, of $SrTiO_3$ and of solid solutions of $(Ba - Sr)TiO_3$ were obtained by crystallization from solutions of strontium titanate and barium titanate and their mixtures in assigned proportions in a melt of potassium fluoride. The melt was held for a certain length of time at the crystallization temperature of the solid solutions, and was then slowly cooled until the system had completely solidified.

This method was based on the system $K_2F_2 - BaTiO_3 - SrTiO_3$, partially investigated by us (up to 1100°C) (visually by the polythermal fusibility method) (Fig.1). From the form of the surface of crystallization of the investigated part of the system, it follows that in this system a continuous series of solid solutions $(Ba - Sr)TiO_3$ must be formed. This was also confirmed by X-ray structural studies of the solid phases of the system. Figure 2 is a melting diagram of the binary systems $K_2F_2 - BaTiO_3$ and $K_2F_2 - SrTiO_3$ and internal cross sections of the system $K_2F_2 - SrTiO_3 - BaTiO_3$. On the basis of these data we established the conditions for growing single crystals of $BaTiO_3$, $SrTiO_3$ and their solid solutions.

Single Crystals of $BaTiO_3$

Single crystals were prepared by crystallization from a melt containing 95 molecular percent of K_2F_2 and 5 molecular percent of $BaTiO_3$. We obtained light yellow and completely transparent crystallites primarily of the forms {100} (Fig.3a). According to the dielectric measurements, their piezoelectric properties are not typically expressed. However, as shown by N.S.Novosil'tsev and A.L.Khodakov (Bibl.10), these crystals become typically piezoelectric after roasting at 1350°C. These crystals will be hereafter termed lot I crystals. The data of the chemical analysis of the crystals were as follows: Ba, 58.8%; Ti, 20.01%; remainder, oxygen and impurities.

STAT

Declassified in Part - Sanitized Copy Approved for Release @ 50-Yr 2014/03/07 : CIA-RDP81-01043R004200090004-8

Declassified in Part - Sanitized Copy Approved for Release @ 50-Yr 2014/03/07 : CIA-RDP81-01043R004200090004-8

Single Crystals of Solid Solutions of (Ba - Sr)TiO_3

We grew single crystals of solid solutions with varying proportions of the components as indicated in Table 1.

Table 1

a)	b)		e)	f)	g)
	c)	d)			
I	100	—	5,9	6,01	6,03
II	95	5	5,8	5,98	5,98
III	90	10	5,9	5,94	5,94
IV	90	10	—	5,94	5,94
V	85	15	—	5,92	5,92
VI	75	25	—	—	—
VII	50	50	5,4	5,54	5,63
VIII	—	100	4,9	5,14	5,12
IX	—	100	5,08	5,12	5,12

a) Number of crystal lot; b) Composition of starting mixtures of barium and strontium titanates; c) % mol. $BaTiO_3$; d) % mol. $SrTiO_3$; e) Density of crystals determined pycnometrically; f) Density of crystals from X-ray diffraction data; g) Density of polycrystalline specimens from X-ray diffraction data

A chemical analysis of the single crystals obtained indicates the close agreement of the composition of the single crystals with that of the initial mixture of barium and strontium titanates. In external habit the crystals obtained are a combination of {100} and {111} forms, the latter weakly developed, rarely encountered, and always in combination with {100}. The color of the crystals ranges from light yellow to brown, and the size up to 1.5 mm (Fig.3,b).

Single crystals of lot IV (Table 1) in contrast to the crystals of the other lots, were grown in a melt of potassium fluoride from a polycrystalline solid solution (95% Ba + 5% Sr)TiO_3, which had already been prepared by sintering. The crystals so obtained were found to be the same in structure and properties as the crys-

STAT

Declassified in Part - Sanitized Copy Approved for Release @ 50-Yr 2014/03/07 : CIA-RDP81-01043R004200090004-8

Declassified in Part - Sanitized Copy Approved for Release @ 50-Yr 2014/03/07 : CIA-RDP81-01043R004200090004-8

tals of solid solutions of the same composition (lot III), for the crystallization of which a mixture of $BaTiO_3$ and $SrTiO_3$ had been taken in the same proportions.

Single Crystals of $SrTiO_3$

Single crystals of $SrTiO_3$ were prepared by Merker directly from a melt of strontium titanate (Bibl.8). The single crystals of $SrTiO_3$ were obtained by us using two methods: (1) their crystallization from a solution of polycrystalline $SrTiO_3$ in a melt of potassium fluoride (lot VIII); (2) from a solution of $SrTiO_3$ in a melt of the mixture (50% of Na_2CO_3 + 50% of K_2CO_3) (lot IX). In the latter case, the crystals were grown in a screwed-down iron crucible.

Single crystals of $SrTiO_3$ (Fig.3,c), grown from a solution of strontium titanate in a solution of potassium fluoride, are completely transparent, refract light, and are confined to forms {100}. The data of the chemical analysis of the crystals were as follows: Sr, 47%; Ti, 25.9%; remainder oxygen and impurities. The crystals grown by the second method are less transparent and of a smoky color, with forms {100} and {111} prevalent. These crystallities are somewhat contaminated by iron (Fe content 0.7%).

Dielectric Properties of Crystals and Their Structure

The dielectric constant and tangent of dielectric loss angle of single crystals of (Ba - Sr)TiO_3 were measured over a wide range of temperatures from -180°C to +150°C. It was found that the dielectric parameters of the single crystals of solid solutions (Ba - Sr)TiO_3, obtained from fluorides, were strongly modified after heat treatment, according to the way this was observed for $BaTiO_3$ single crystals grown from fluorides (Bibl.10). The heat treatment consisted in heating the crystals for three hours at 1350°C. During this heating the crystals change their color and transparency several times. The same changes were observed after heating in crystals of $BaTiO_3$ as well.

STAT

Declassified in Part - Sanitized Copy Approved for Release @ 50-Yr 2014/03/07 : CIA-RDP81-01043R004200090004-8

Declassified in Part - Sanitized Copy Approved for Release @ 50-Yr 2014/03/07 : CIA-RDP81-01043R004200090004-8

Before heat treatment, the (Ba - Sr)TiO_3 crystals had weak ferroelectric properties and did not have the temperature dependence usual for ferroelectric substances. On Fig.4, curves 2 and 5 show respectively the temperature dependence, for crystals with 10% $SrTiO_3$ (lot III) and with 50% $SrTiO_3$ (lot VII), before the heat

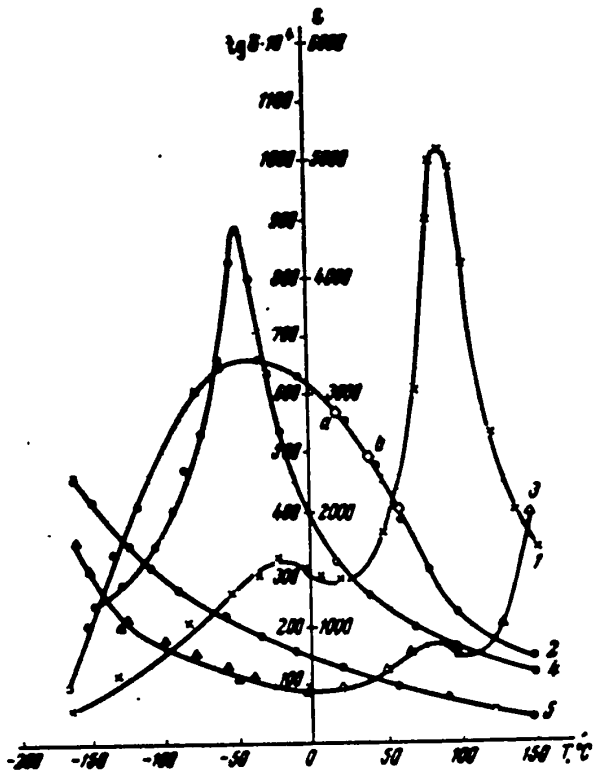

Fig.4

treatment. The temperature dependence ε after heating is shown by the corresponding curves 1 and 4. A pronounced maximum ε is observed close to the temperatures corresponding to the Curie points of polycrystalline solid solutions (Bibl.15, 16). A similar influence of heat treatment of (Ba - Sr)TiO_3 single crystals on other ratios between their components was also observed. The temperature dependence of tan δ for a single crystal of lot III (after heat treatment) is shown by curve 3. For the remaining crystals, tan δ at room temperature and $\nu = 10^6$ cycles, had values ranging from 50×10^{-4} to 500×10^{-4}, depending on the concentration of $SrTiO_3$.

STAT

Declassified in Part - Sanitized Copy Approved for Release @ 50-Yr 2014/03/07 : CIA-RDP81-01043R004200090004-8

Declassified in Part - Sanitized Copy Approved for Release @ 50-Yr 2014/03/07 : CIA-RDP81-01043R004200090004-8

Some single crystals had a dispersion in the frequency range from 50 to 10^6 cycles. Table 2 gives the values of ε for a single crystal of lot III (not given heat treatment) at various frequencies.

Table 2

ν, cycles	ε
50	6300
10^3	5000
$1{,}15 \cdot 10^6$	3600
$1{,}5 \cdot 10^6$	3000

Table 3

E, kv/cm	ε
1,5	1500
6,0	2100
1,5	3400

The dependence of ε on the electric field strength with this crystal is weakly expressed. After the crystal has been heated through, it acquires pronounced nonlinear properties (Table 3), and the frequency dependence of its dielectric constant now disappears.

Fig.5

Figure 5 give oscillograms of lot II taken at frequency 50 cycles. As will be seen from the photographs, the oscillograms of the hysteresis loops showed the weak nonlinear dependence of the polarization on the strength of the applied field. But crystals that had not been heat-treated had hysteresis loops of form close to that of the Rayleigh loops. After heat treatment, as will be seen from Fig.6, the hysteresis loops take the form usual for ferroelectric substances.

STAT

Declassified in Part - Sanitized Copy Approved for Release @ 50-Yr 2014/03/07 : CIA-RDP81-01043R004200090004-8

Declassified in Part - Sanitized Copy Approved for Release @ 50-Yr 2014/03/07 : CIA-RDP81-01043R004200090004-8

In crystals that have been heat-treated, the nonlinear properties are likewise manifested in the form of the dependence of the inverse dielectric constant on the strength of the displacing constant field.

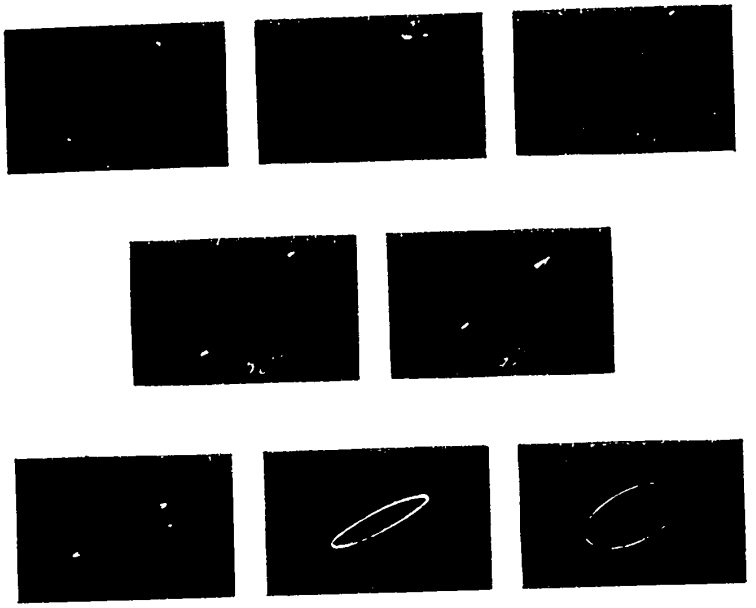

Fig.6

Single crystals of $SrTiO_3$ of lots VIII and IX differed somewhat in their dielectric properties. Figure 7 gives the temperature dependence of ε for crystals of both lots. Curve I relates to the crystals obtained from carbonates (lot IX), and curve II to $SrTiO_3$ from fluorides (lot VIII). Curve III corresponds to the temperature course of ε in polycrystalline $SrTiO_3$. The rise of ε at low temperatures is observed in all specimens of $SrTiO_3$, indicating the existence of a maximum dielectric constant in the low-temperature region, as, indeed, one should find in $SrTiO_3$. The value of ε at room temperature in the $SrTiO_3$ of lot IX corresponds to 340, but $\tan \delta = 3 - 5 \times 10^{-4}$, which is in agreement with the measurements of Merker (Bibl.8), who found $\varepsilon = 310$ and $\tan \delta = 3 \times 10^{-4}$. For $SrTiO_3$ prepared from fluorides before heat treatment, the value of ε is lower (curve II). After the heating, the temperature course of ε and the absolute value of the dielectric con-

STAT

Declassified in Part - Sanitized Copy Approved for Release @ 50-Yr 2014/03/07 : CIA-RDP81-01043R004200090004-8

Declassified in Part - Sanitized Copy Approved for Release @ 50-Yr 2014/03/07 : CIA-RDP81-01043R004200090004-8

stant approach the values of lot IX. The dielectric characteristics of single crys-

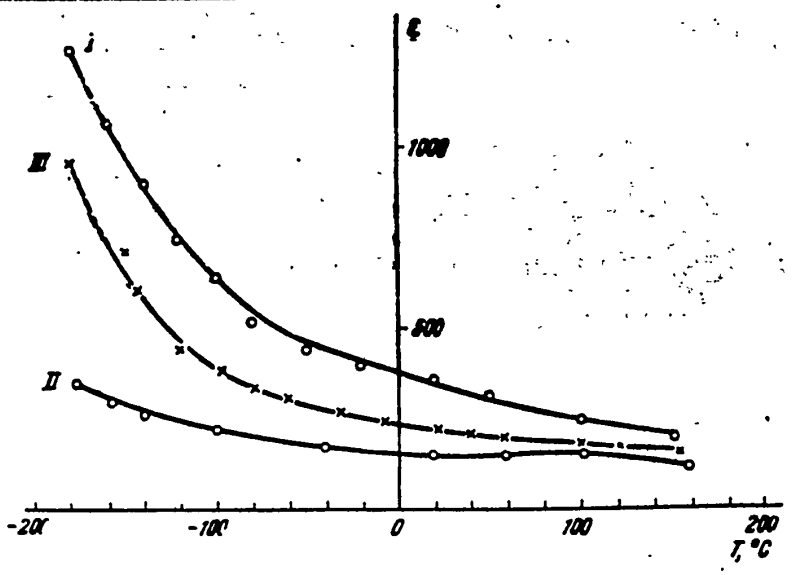

Fig.7

Table 4

Lot	Composition	θ, Degrees	ε
I	$BaTiO_3$	120	
II	$(Ba_{0.95}-Sr_{0.05})TiO_3$	94	1200
III	$(Ba_{0.90}-Sr_{0.10})TiO_3$	88	1500
V	$(Ba_{0.85}-Sr_{0.15})TiO_3$	56	2700
VII	$(Ba_{0.5}-Sr_{0.5})TiO_3$	—48	1550
VIII	$SrTiO_3$	—	340
IX	$SrTiO_3$	—	330

tals are given in Table 4 (the values of ε and the temperatures of the Curie point θ are shown for heat-treated crystals).

STAT

Declassified in Part - Sanitized Copy Approved for Release @ 50-Yr 2014/03/07 : CIA-RDP81-01043R004200090004-8

Declassified in Part - Sanitized Copy Approved for Release @ 50-Yr 2014/03/07 : CIA-RDP81-01043R004200090004-8

Structure and Optical Properties of the Crystals

The structural type, symmetry and cell dimensions of the above-described single crystals of solid solutions were determined by the powder method of X-ray structural analysis.

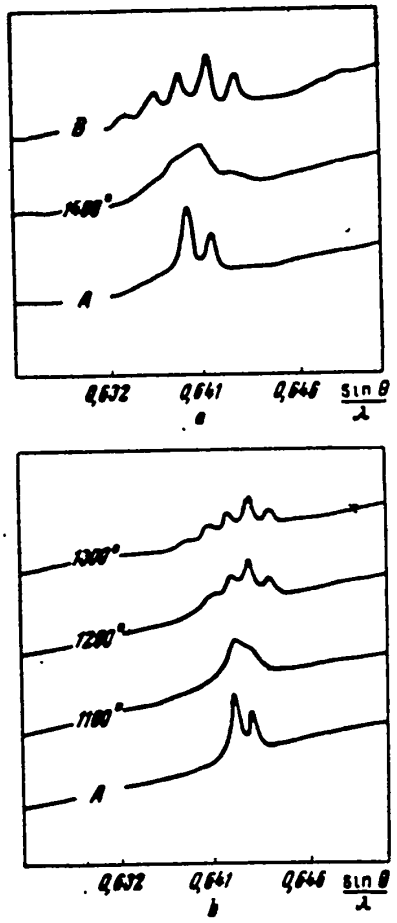

Fig.8 - Microphotometric Curves: a - $BaTiO_3$; b - $(Ba_{0.90}, Sr_{0.10})TiO_3$. The figures on the curves indicate the temperature of heat treatment; the upper curves on both figures relate to the polycrystalline specimens

On the diffraction patterns of all specimens, a more or less blurred but isolated $K\alpha_1\alpha_2$ doublet was found; the corresponding specimens are very close to being ideal cubic. The observed widening of the lines is naturally attributed to the microdistortions in the crystals.

The variation of the microsymmetry of single crystals of $BaTiO_3$ (prepared from fluorides) after heat treatment has been noted (Bibl.10). These variations are illustrated by Fig.8,b, showing the microphotometric curves of the group of line $\Sigma h_i^2 = 26$ for $BaTiO_3$ single crystals annealed 1 hr at various temperatures. Figure 8,a shows the effect of heat treatment on single crystals of $(Ba - Sr)TiO_3$. For comparison we give on Fig.8,a the microphotometric curve of the corresponding polycrystalline specimen. A comparison of the microphotometric curves shows that in spite of the duration (up to 10 hrs) and the high annealing (1400°) of the anneal given the $(Ba - Sr)TiO_3$ by us, results analogous to those obtained for $BaTiO_3$ single crystals were not completely attained.

STAT

Declassified in Part - Sanitized Copy Approved for Release @ 50-Yr 2014/03/07 : CIA-RDP81-01043R004200090004-8

Declassified in Part - Sanitized Copy Approved for Release @ 50-Yr 2014/03/07 : CIA-RDP81-01043R004200090004-8

Observations in polarized light showed that the crystals from all lots were optically anisotropic. On crystals that were not heat-treated, especially those of lot III, domains were observed. Characteristic was their localization in separate and predominantly external zones of the crystal. It was found that the crystal was anisotropic even at 250°C.

However, as will be seen from the photomicrograms, given on Fig.8,a, the crystals of this lot are cubic. The very fact of the presence of domains at room temperature in them therefore appeared strange. It was thought to be probable that during the process of crystallization of single crystals as solid solutions, crystals of varying symmetry were obtained, but that the number of tetragonal crystals (which regularly have a domain structure at room temperature) in the total number is small, so that on the X-ray photographs, in view of statistical averaging, their presence is not established.

To verify this hypothesis, we staged simultaneous observations of the variation of the domain structure and measurements of $\varepsilon = f(t)$. This experiment showed that, in the crystals studied, the disappearance of spontaneously polarized regions (domains) is not connected with the maximum of the dielectric constant that is usually observed in this case. Analogous results were obtained on cubic crystals of $BaTiO_3$ (lot I) as well.

Figure 9 shows photographs characterizing the temperature variations of the domains in crystals of lot III that were not heat-treated. The values of the dielectric constant corresponding to these states of the crystal are indicated by the letters a, b and c on Fig.4. On Fig.9, in addition, we show the breakdown of cubic $BaTiO_3$ into domains (lot I) on imposition of field.

Conclusions

1. The possibility of growing single crystals of a continuous series of solid solutions of $(Ba - Sr)TiO_3$ from a melt in potassium fluoride has been established;

STAT

Declassified in Part - Sanitized Copy Approved for Release @ 50-Yr 2014/03/07 : CIA-RDP81-01043R004200090004-8

Declassified in Part - Sanitized Copy Approved for Release @ 50-Yr 2014/03/07 : CIA-RDP81-01043R004200090004-8

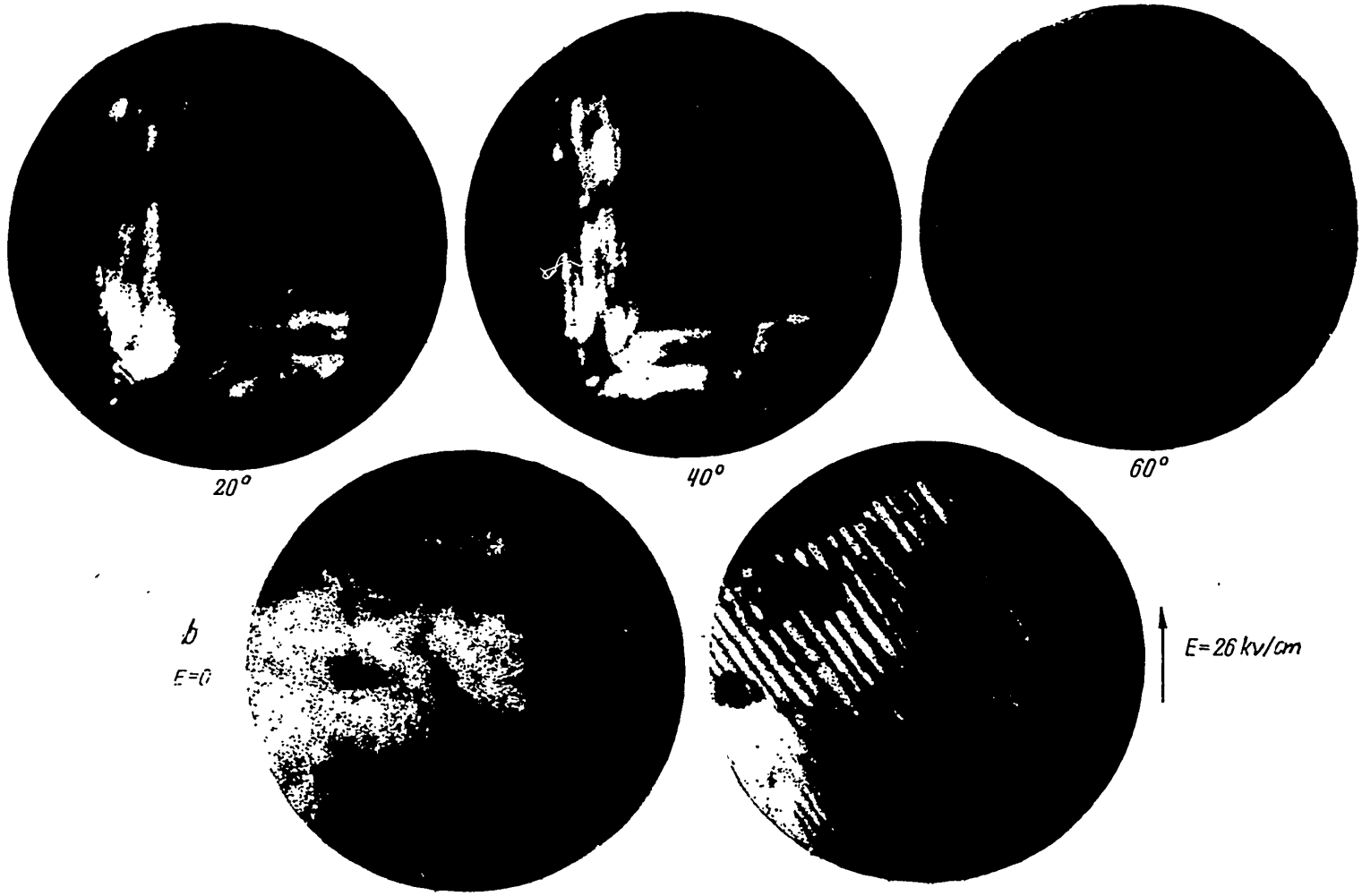

Fig.9 - Domain Structure of $(Ba_{0.90}, Sr_{0.10})TiO_3$

a - Temperature changes; b - Effect of a constant electric field

STAT

Declassified in Part - Sanitized Copy Approved for Release @ 50-Yr 2014/03/07 : CIA-RDP81-01043R004200090004-8

Declassified in Part - Sanitized Copy Approved for Release @ 50-Yr 2014/03/07 : CIA-RDP81-01043R004200090004-8

the proportions of the components and the temperature conditions for growing crystals from such melts are indicated.

2. Single crystals have been prepared for a series of solid solutions (Ba - Sr)TiO_3 and $SrTiO_3$ with dimensions sufficient for investigation of their properties.

3. X-ray structural analysis and the results of dielectric and optical measurements have confirmed the fact that the crystals so obtained are single crystals of solid solutions of (Ba - Sr)TiO_3.

4. It has been established that before heat treatment the single crystals of (Ba - Sr)TiO_3 prepared from fluorides possess only weak ferroelectric properties, but that after heating at 1350°C they become typical ferroelectric crystals. It is possible that this is due to microstresses arising during crystallization. The role of heat treatment apparently reduces down to the removal of the microstresses, the single crystals with higher $SrTiO_3$ content requiring higher temperatures to remove the stresses.

5. The existence of a domain structure (in crystals that have not been heat-treated) at temperatures considerably higher than the temperature of maximum dielectric constant, has been established both for $BaTiO_3$ single crystals and for certain solid solutions. With increasing temperature, the disappearance of the domains and the decrease of the dielectric constant is observed.

In conclusion the authors express their thanks to N.S.Novosil'tsev for his valuable suggestions and his interest in this work.

BIBLIOGRAPHY

1. Blattner,H., Kaenzing,W., and Merz,W. - Helv.Phys.Acta, Vol.22 (1949),p.35
2. Oxbrow,C. - Nature, Vol.174 (1954),p.1091
3. Nishioka,A. - Journ.Phys.Soc., Japan, Vol.VII (1955),p.535
4. Belyayev,I.N., Novosil'tsev,N.S., Khodakov,A.L., and Fesenko,Ye.G. - Dok.AN SSSR,

STAT

Declassified in Part - Sanitized Copy Approved for Release @ 50-Yr 2014/03/07 : CIA-RDP81-01043R004200090004-8

Declassified in Part - Sanitized Copy Approved for Release @ 50-Yr 2014/03/07 : CIA-RDP81-01043R004200090004-8

Vol.78 (1951),p.875

5. Belyayev,I.N., Novosil'tsev,N.S., Fesenko,Ye.G., and Khodakov,A.L. - Zhur.Eksp. Teor.Fiz., Vol.23 (1952),p.211

6. Belyayev,I.N., Novosil'tsev,N.S., Fesenko,Ye.G., and Khodakov,A.L. - Dok.AN SSSR, Vol.83 (1952),p.675

7. Belyayev,I.N. and Khodakov,I.L. - Zhur.Eksp.Teor.Fiz., Vol.22 (3), (1952),p.376

8. Merker,L. - Mining Eng., Vol.7 (1955),p.645

9. Sholokhovich,M.L. and Belyayev,I.N. - Zhur.Obshch.Khim., Vol.24 (1954),p.218; Belyayev,I.N. and Sholokhovich,M.L. - Tr.NIFMI RGU, Vol.4 (1955), 27(6),46

10. Novosil'tsev,N.S. and Khodakov,A.L. - Dok.AN SSSR, Vol.85 (1952),p.1263

11. Ferranti - Wireless World, Vol.60 (1954),p.392

12. Durst,Cr., Crotenhuis,M., and Barkon,A. - Journ.Amer.Ceram.Soc., Vol.33 (1933) (1950)

13. Elmer,W., Shelton,C., and Creamer,A. - Journ.Res.Nat.Bureau Stand.,Vol.38, (1947),p.337

14. Donley,H. - RCA Rev., Vol.8 (1947),p.539

15. Khodakov,A.L. and Shul'man,M.S. - Tr.NIFMI RGU, Vol.25 (1955),p.27

16. Ishkhneli,A.Kh. - Soobshch. AN GruzSSR, Vol.11 (1950),p.275

NIFMI, State University,

Rostov-on-Don

STAT

Declassified in Part - Sanitized Copy Approved for Release @ 50-Yr 2014/03/07 : CIA-RDP81-01043R004200090004-8

Declassified in Part - Sanitized Copy Approved for Release @ 50-Yr 2014/03/07 : CIA-RDP81-01043R004200090004-8

A NEW TECHNIQUE OF STUDYING THE PHASE TRANSFORMATIONS UNDER HIGH PRESSURES AND TEMPERATURES AND ITS APPLICATION TO THE STUDY OF THE POLYMORPHISM OF PHOSPHORUS

by

V.P.Butuzov and S.S.Boksha

An extreme-pressure multiplier has been developed at the Institute of Crystallography, Academy of Sciences USSR, permitting pressures up to 40,000 kg/cm^2 to be obtained, in a large volume, and the simultaneous production of rather high temperatures.

In the present report we shall set forth certain questions of the simultaneous production of extreme gaseous pressures and high temperatures, the technique of direct measurement of temperature and pressure inside an extreme-pressure vessel, and the application of this apparatus and technique to the study of the polymorphic transformation of phosphorus.

Up to now the allotropic transformations of substances taking place under the conditions of extreme pressure have been determined either by a method based on the variation of the electrical resistance of the substance under study or from the change of volume established by the method of the "displaced plunger". Both these methods have certain shortcomings. The former method does not permit a sufficiently reliable determination of the character of the polymorphic transformation, since there are considerable changes that take place in the electrical resistance of the specimen, frequently not of a regular character, during the process of variation

STAT

Declassified in Part - Sanitized Copy Approved for Release @ 50-Yr 2014/03/07 : CIA-RDP81-01043R004200090004-8

Declassified in Part - Sanitized Copy Approved for Release @ 50-Yr 2014/03/07 : CIA-RDP81-01043R004200090004-8

of temperature and pressure. The method of the "displaced plunger" likewise is unable to assure the exact registration of the beginning of transformation; owing to the high friction of the plunger against the walls of the high-pressure vessel, in the case where the polymorphic transformation is accompanied by a small change in volume, or in the case of the use of small weighed portions of the substance under study.

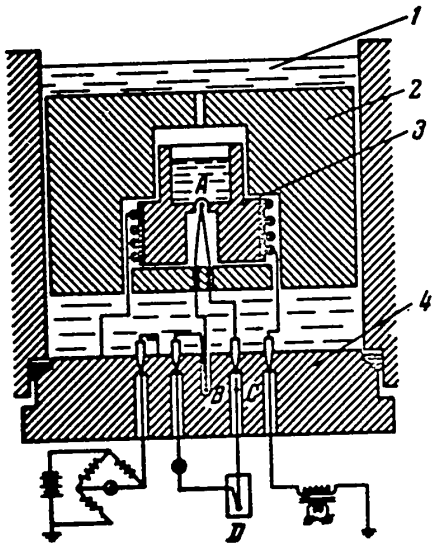

Fig.1 - System of Measuring Temperature Inside the Pressure Vessel

1 - Channel of pressure vessel; 2 - Thermal insulation; 3 - Crucible; 4 - Cylinder of electric lead

There are definite difficulties, too, in the way of the direct measurement of temperature inside extreme-pressure vessels. Two methods of measuring the temperature are in use today. The first method is based on the change of the electrical resistance of a copper or platinum wire with changing temperature. In this case, the mean temperature of some volume or other is determined, which gives considerable errors owing to the existence of a great temperature gradient inside the extreme-pressure vessel (Bibl.2). The second method is based on the use of thermo-

STAT

Declassified in Part - Sanitized Copy Approved for Release @ 50-Yr 2014/03/07 : CIA-RDP81-01043R004200090004-8

Declassified in Part - Sanitized Copy Approved for Release @ 50-Yr 2014/03/07 : CIA-RDP81-01043R004200090004-8

couples. In most cases one attempts to introduce the thermocouple wire directly into the pressure vessels, insulating them from the walls by a set of insulating disks and washers. In this case, the "cold" junction of the thermocouple is outside the pressure vessel, where it is easy to measure its temperature. But the design of such electric leads under high pressure is very troublesome and demands rather large volumes. At first we used the technique of measuring temperature (Bibl.3) in which both thermocouple junctions are located in the channel of the pressure vessel, while the temperature of the "cold" junction of the thermocouple was determined by the aid of a copper thermometer. But even this method of temperature measurement had its own shortcomings, and in particular, the cold junction showed the mean temperature of a certain volume, and it was hard to use the readings of such a thermocouple for automatic recording, owing to certain fluctuations in the temperature of the cold junction.

On subsequent work these shortcomings were eliminated, since we dispensed with the measurement of the temperature of the cold junction of the thermocouple, using a second differential thermocouple. Figure 1 gives the system for the temperature measurement inside the pressure vessels. It will be seen from this diagram that in this case a thermocouple consisting of four junctions A, B, C, D connected in series is used (hereafter we shall term it "combination thermocouple"). Two junctions of the combination thermocouple are located inside the pressure vessel - the junction A is at the point where the temperature is to be measured, and the second, junction B, is in a rather deep opening drilled in the electrical lead. The two other junctions are outside the pressure vessel. Junction C is likewise placed in an opening of the electric lead alongside of junction B. The fourth junction D is in a thermostat held at an assigned temperature. By virtue of the high thermal conductivity of metal, it may be considered that the points B and C lie on a single isothermal surface, and, consequently, that the temperatures at these points are equal, and therefore the measuring instrument shows the temperature difference of two junc-

STAT

Declassified in Part - Sanitized Copy Approved for Release @ 50-Yr 2014/03/07 : CIA-RDP81-01043R004200090004-8

Declassified in Part - Sanitized Copy Approved for Release @ 50-Yr 2014/03/07 : CIA-RDP81-01043R004200090004-8

tions, A and D. Knowing the temperature junction D, we shall determine with sufficient accuracy the temperature of point A. It must be said that in this case we do not take account of the influence of pressure on the emf of that part of the combination thermocouple that is inside the pressure vessel*. As pointed out by Birch (Bibl.4), the variation of emf with pressure is slight, and this variation may in

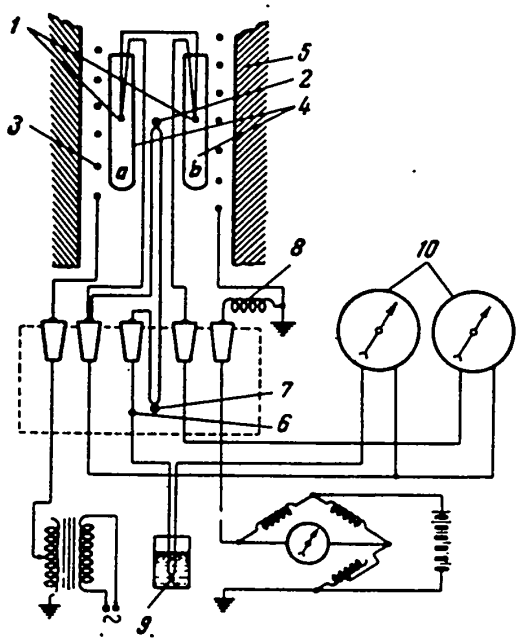

Fig.2 - Apparatus for Investigating Allotropic Transformations

1 - Junctions of differential thermocouple; 2, 6, 7, 9 - Junctions of combination thermocouple; 3 - Resistance furnace; 4 - Porcelain ampules; 5 - High pressure vessel (cone); 8 - Manganin pressure indicator; 10 - Mirror galvanometers of TsK-52 pyrometer; a - Reference standard; b - Substance under study

first approximation be neglected.

In measuring temperatures up to 600°C we used iron-nichrome thermocouples, and at higher temperatures, platinum-platinorhodium thermocouples.

* This effect is not taken into account, either, by all the above-described techniques of temperature measurement.

STAT

Declassified in Part - Sanitized Copy Approved for Release @ 50-Yr 2014/03/07 : CIA-RDP81-01043R004200090004-8

Declassified in Part - Sanitized Copy Approved for Release @ 50-Yr 2014/03/07 : CIA-RDP81-01043R004200090004-8

The subsequent improvement of the technique of temperature measurement under extreme pressure was the use of a photorecording pyrometer for automatic recording of the heating and cooling curves, and the use of two thermocouples.

Figure 2 shows the setup for the investigation of allotropic transformations in the pressure vessel, with the electrical circuit diagram of the measurement. For measuring the temperature of polymorphic transformation, the above-described combination thermocouple is used (represented by the junctions 2, 7, 6, 9), and for registration of the small thermal effects the separate differential thermocouple is used with its junctions 1 placed in the investigated substance and in a reference standard substance. The test substance a and the reference standard substance b are placed in the porcelain ampules 4. The emf of the combination and differential thermocouples is noted by the aid of a PK-52 Kurnakov pyrometer.

The measurement of pressure in the extreme-pressure multipliers is accomplished by the aid of manganin pressure indicators, which are secondary pressure indicators, and consequently require calibration. The calibration of the manganin pressure indicators is accomplished from the allotropic transformations of various substances, whose numerical values are taken from the works of P.W.Bridgman (Bibl.5). At pressures up to 30,000 kg/cm^2, bismuth is usually employed as reference standard. At room temperature bismuth undergoes two polymorphic transformations, at 25,650 kg/cm^2 and 27,080 kg/cm^2. For lower pressures, the melting or solidification of mercury is used. The allotropic transformations that have taken place are usually determined by the method of the displaced plunger.

We employed a more improved technique of calibration of the manganin pressure indicators, based on thermal analysis. Figure 3 gives a thermogram showing the process of solidification and melting of mercury, whose solidification temperature was utilized by us as one of the reference points for calibration. The figures above the curve correspond to the times of pressure rise by approximately equal amounts. The figures under the curve indicate the corresponding electrical resistances of the

STAT

Declassified in Part - Sanitized Copy Approved for Release @ 50-Yr 2014/03/07 : CIA-RDP81-01043R004200090004-8

Declassified in Part - Sanitized Copy Approved for Release @ 50-Yr 2014/03/07 : CIA-RDP81-01043R004200090004-8

manganin pressure indicator in ohms. The zero line corresponds to the temperature at the beginning of the experiment, 19.2°C. Taking the pressure of solidification of mercury at 19.2°C as 11,300 kg/cm^2, we find that the pressure at which melting at the same temperature begins is 10,600 kg/cm^2, and that it differs from the solidification pressure by 700 kg/cm^2. At the same time, according to the literature data (Bibl.6), the solidification and melting of mercury is noted at one and the same pressure.

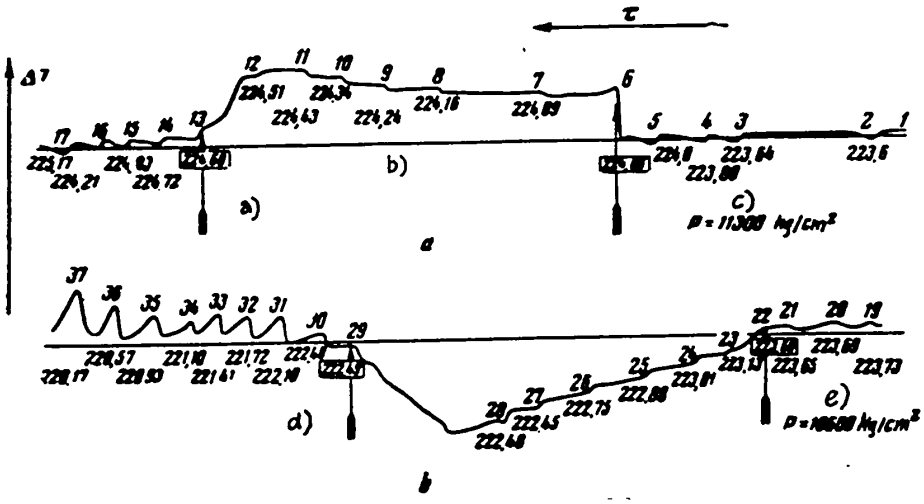

Fig.3 - Thermogram of Solidification (a) and Melting (b) of Mercury at 19.2°C (the Pressures are Represented by the Values of the Resistance of the Manganin Pressure Indicator) with R_0 = 217.27 ohms; ΔR = 0.01 ohm Corresponds to ΔP = 20 kg/cm^2

a) End of solidification; b) Zero line (T = 19.2°C); c) Beginning of solidification; d) End of melting; e) Beginning of melting

It is difficult to get temperatures over 600°C in the liquid phase under high pressures, since at high temperatures the compressed liquid decomposes, and thus the heating element goes out of commission. Recently we have developed an extreme-pressure apparatus in which gas can be compressed to a pressure of 30,000 kg/cm^2, but this demands a rather complex equipment (compressors or compressing devices);

STAT

Declassified in Part - Sanitized Copy Approved for Release @ 50-Yr 2014/03/07 : CIA-RDP81-01043R004200090004-8

Declassified in Part - Sanitized Copy Approved for Release @ 50-Yr 2014/03/07 : CIA-RDP81-01043R004200090004-8

while it is possible to produce gas pressure by using solid carbon dioxide for this purpose.

The experiments with carbon dioxide were staged as follows. In the high pressure vessel (cone), at its upper end, a sealing "mushroom" was stamped. Its sealing rings (copper and lead) were "melted in". The cone was then cooled to a temperature of -76°C, and solid carbon dioxide was packed into its channel, leaving space for the insertion of the heating element; the electric lead, likewise cooled to -76°C, was then rapidly inserted, and the entire extreme-pressure apparatus was assembled. The carbon dioxide gas remains for a rather long time in the channel of the vessel with motionless mushroom obturator, but if a higher pressure is desired, it is necessary to advance the mushroom obturator, and in this case it is difficult to maintain a pressure over 15,000 kg/cm^2, in spite of the most careful machining and fitting of the sealing parts. On the other hand, there was no particular trouble in obtaining pressure in the liquid phase. We therefore established liquid layers between the compressed gas and the sealing parts (the obturator and electric lead) and in this way the compressed gas was practically brought under the same conditions as in obtaining extreme pressure in a liquid. In work with carbon dioxide it must be borne in mind that, under a pressure of about 9000 kg/cm^2, carbon dioxide solidifies at room temperature, and it is therefore necessary to provide a certain temperature rise at the same time the pressure is increased over 9000 kg/cm^2.

The heating element for the production of rather high temperatures in our case consisted of selite rods, with an opening in the center sufficient for placing ampules with a test substance in it. Such a heating element is most reliable and assures a very wide temperature range.

The technique developed by us was applied to the study of the allotropic transformations of phosphorus over a wide range of pressures and temperatures. Before passing to the exposition of the results obtained, we shall set forth briefly the data in the literature on the polymorphism of phosphorus.

STAT

Declassified in Part - Sanitized Copy Approved for Release @ 50-Yr 2014/03/07 : CIA-RDP81-01043R004200090004-8

Declassified in Part - Sanitized Copy Approved for Release @ 50-Yr 2014/03/07 : CIA-RDP81-01043R004200090004-8

Three polymorphic modifications of phosphorus are distinguished, white, red and black, each of which has its own varieties. There are two such varieties in white phosphorus (I and II). Crystals of white phosphorus I are obtained from ordinary yellow phosphorus by heating to 200°C in an atmosphere of nitrogen or carbon dioxide gas under a pressure of 70 - 80 atm. White phosphorus II was first prepared by Bridgman (Bibl.7) under a pressure of 11,000 kg/cm^2 at a temperature of 60°C, who established the regions of stable existence of the two varieties and pointed out the existence of a reversible transition.

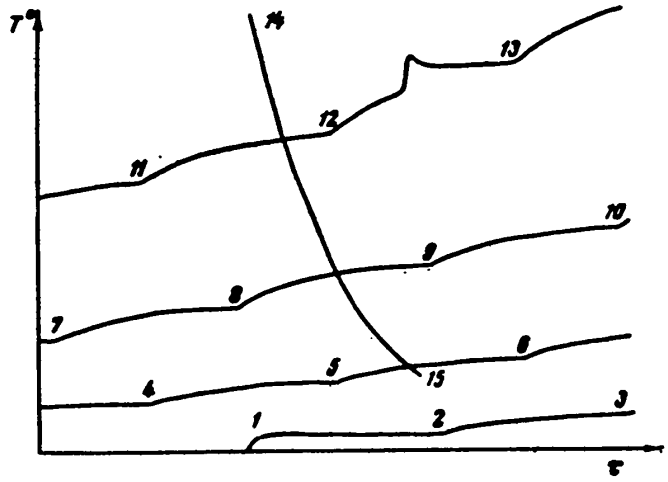

Fig.4 - Thermogram of Polymorphic Transformation of Yellow Phosphorus into Black Crystalline Phosphorus

Red phosphorus is obtained by heating yellow phosphorus above 200°C. Its varieties are distinguished mainly by density and color. Each form of red phosphorus has its own temperature of formation, and the violet variety is the highest-temperature form.

There are two varieties of black phosphorus, black crystalline phosphorus, first prepared by Bridgman under extreme pressures (12,000 kg/cm^2 and 200°C) and black amorphous phosphorus, prepared by Jacobs (Bibl.8), likewise under extreme pressure. The specific gravity of black crystalline phosphorus is 2.69 gm/cm^3,

STAT

Declassified in Part - Sanitized Copy Approved for Release @ 50-Yr 2014/03/07 : CIA-RDP81-01043R004200090004-8

Declassified in Part - Sanitized Copy Approved for Release @ 50-Yr 2014/03/07 : CIA-RDP81-01043R004200090004-8

which is considerably higher than for any other variety of phosphorus. It possesses metallic conductivity. Black amorphous phosphorus has the specific gravity of 2.25, and its heat content is 14 kilojoules higher than that of black crystalline phosphorus. During the transformation of white phosphorus into black phosphorus, Jacobs distinguishes two stages following one another. On the attainment of certain thermodynamic conditions, a slow transformation takes place, with a decrease in volume. This is the first stage of transformation. Then follows a sharp acceleration of the process of transformation, in which a more considerable change of volume is observed. This is the second stage of transformation. During the first stage, the volume decreases 10%, and during the second stage, 90%, of the total volume decrease during both stages of transformation. Jacobs has demonstrated experimentally that in the first, or preparatory stage, part of the white phosphorus is transformed into black amorphous phosphorus, which, during its formation, liberates a certain quantity of heat, warming the still untransformed white phosphorus to a temperature at which the formation of black crystalline phosphorus from yellow phosphorus is practically instantaneous.

In 1926, V.Ipat'yev and V.Nikolayev (Bibl.9), by heating white phosphorus in a silver tube at 265 - 278°C under a pressure of 140 - 165 atm, obtained red phosphorus, in which particles of black phosphorus were included, i.e., a small quantity of black phosphorus was obtained under conditions completely different from the experimental conditions used by other investigators. The specific gravity of the granules of black phosphorus so obtained was found to be 2.7.

All studies on the polymorphic transformation of phosphorus under high pressures were staged at low temperatures, since externally heated extreme-pressure apparatus was used in these investigations. The studies were staged in the solid phase, and the kinetics of transformation could not be followed through, since the polymorphic transformations were recorded by the method of the moving piston.

The formation of polymorphic modifications at higher temperatures and in a

STAT

Declassified in Part - Sanitized Copy Approved for Release @ 50-Yr 2014/03/07 : CIA-RDP81-01043R004200090004-8

Declassified in Part - Sanitized Copy Approved for Release @ 50-Yr 2014/03/07 : CIA-RDP81-01043R004200090004-8

wider pressure range is of considerable interest. On Fig.4 the polymorphic transformation of yellow phosphorus into black crystalline phosphorus is noted according to the system used in Fig.2. The curve between points 1 and 2 fixes the temperature of the apparatus before the beginning of the experiment. After turning on the

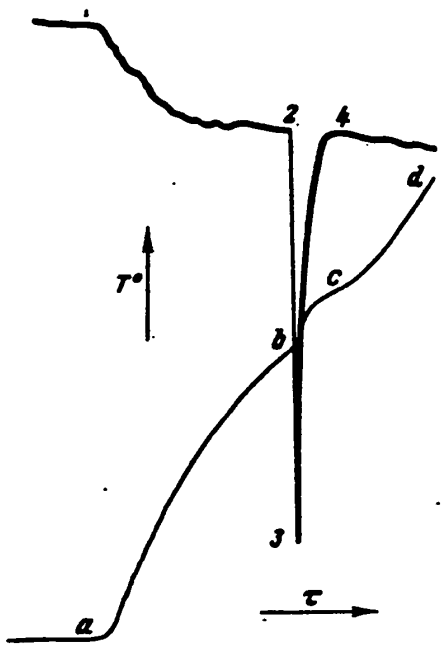

Fig.5 - Thermogram of Polymorphic Transformation of Yellow Phosphorus into Black Crystalline Phosphorus, Obtained with the Aid of a Differential Thermocouple and a Combination Thermocouple

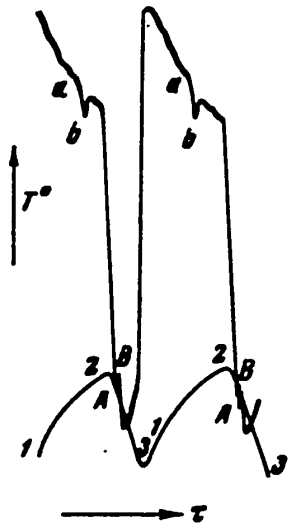

Fig.6 - Thermogram of Reversible Polymorphic Transformation of Red Phosphorus into a New Modification of Phosphorus

electric heat, the curve gradually rises, making small breaks at the points 2, 3, 4, ..., 12, 13, ..., which correspond to the times of equal increase in the strength of the current passed through the heater. A sharp temperature jump, not connected with a change in the furnace temperature, is observed between points 12 and 13. This jump indicates the occurrence of a polymorphic transformation of the phosphorus. After turning off the heat, the temperature sharply falls (points 14, 15), but the reverse transformation is not observed on the heating curve. After the ex-

STAT

Declassified in Part - Sanitized Copy Approved for Release @ 50-Yr 2014/03/07 : CIA-RDP81-01043R004200090004-8

Declassified in Part - Sanitized Copy Approved for Release @ 50-Yr 2014/03/07 : CIA-RDP81-01043R004200090004-8

periment black crystalline phosphorus was detected. Figure 5 is a thermogram of the polymorphic transformation of yellow phosphorus into the black crystalline form, obtained by the system given on Fig.2. The curve, denoted by the letters a, b, c, d, was recorded by the combination thermocouple and determines the temperature of the block. The furnace temperature was increased regularly during the course of the experiment by the aid of a special device. There is a certain inflection in the

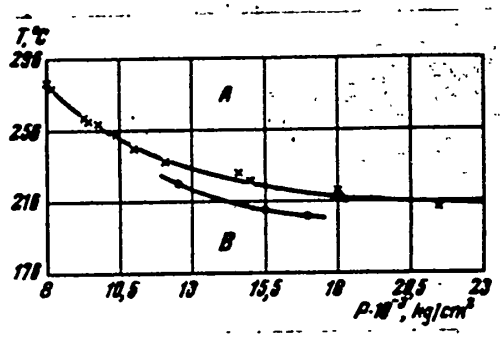

Fig.7 - Curves Separating the Region of Formation of Black Crystalline Phosphorus from Yellow Phosphorus without a Preliminary Stage from the Region with a Preliminary Stage

× - Our data; - Data of Jacobs

curves between the points b and c, which is explained by the additional heating of the block on account of the liberation of heat taking place at the time of the polymorphic transformation. The curve denoted by the figures 1, 2, 3, 4 relates to the differential thermocouple, which registers the temperature difference between the standard substance and the test substance, in the case of an allotropic transformation that has taken place. It is the segment of this curve between the points 2 and 4 that precisely corresponds to the allotropic transformation in the test substance. As will be clear from the thermograms presented, the technique employed by us of studying the allotropic transformations under extreme pressures has substantial advantages over those previously described and makes it possible to determine

STAT

Declassified in Part - Sanitized Copy Approved for Release @ 50-Yr 2014/03/07 : CIA-RDP81-01043R004200090004-8

Declassified in Part - Sanitized Copy Approved for Release @ 50-Yr 2014/03/07 : CIA-RDP81-01043R004200090004-8

small thermal effects which cannot be detected by other methods.

Studies of black crystalline phosphorus were made by this method under extreme pressures (20,000 kg/cm^2) and high temperatures (1200°C), but no new modifications of phosphorus were found. With increasing pressure, only a smooth rise of the melting point of black crystalline phosphorus takes place (at 18,000 kg/cm^2, the melting point of phosphorus reaches about 1000°C).

Fig.8 - Photograph of Polished Section of the Black Crystalline Phosphorus Obtained at P = 14,500 kg/cm^2 and T = 230°C

On investigating the behavior of red phosphorus, we did find that a new reversible modification of phosphorus was formed under a pressure of 4000 kg/cm^2 and a temperature of 600°C. Figure 6 gives a segment of the thermogram on which the temperature jump registered by the differential thermocouple (points a, b) is noted, indicating the occurrence of a polymorphic transformation, and which at the same time fixes the reverse transition (the points A, B) with decreasing specimen temperature. The curve from the combination thermocouple, which determines the transformation temperature, shows practically no temperature jump (points 1, 2, 3). To confirm the reversibility of the transition, the process shown on Fig.6 was repeated twice. Figure 7 gives the curve separating region A of formation of black crystal-

STAT

Declassified in Part - Sanitized Copy Approved for Release @ 50-Yr 2014/03/07 : CIA-RDP81-01043R004200090004-8

Declassified in Part - Sanitized Copy Approved for Release @ 50-Yr 2014/03/07 : CIA-RDP81-01043R004200090004-8

line phosphorus from yellow phosphorus, which has no preliminary stage, from the region B, which does have a preliminary stage (the upper curve, according to our data, and the lower curve according to the data of Jacobs). The lower transformation temperatures found by Jacobs are explained by the fact that he could not take account of the temperature rise due to the rapid compression of the phosphorus which took place in his experiments.

Figure 8 presents a photograph of a polished section of the black crystalline phosphorus obtained under a pressure of 14,500 kg/cm^2 and a temperature of 230°C. It can be seen on this photograph that the formation of black crystalline phosphorus begins at the walls of the ampule, which had a higher temperature than the inner parts of the ampule. The technique developed by us for producing extreme gas pressures, and our technique of temperature measurement, permitted us to obtain a melt of black crystalline phosphorus. With an appropriate ampule shape and under appropriate temperature conditions of cooling, the formation of a single crystal of black crystalline phosphorus may be expected.

Conclusions

1. A method of producing extreme gas pressures by the use of solid carbon dioxide and the employment of liquid layers between the sealing part of the apparatus and the compressed gas has been developed.

2. A technique of measuring temperatures in extreme-pressure vessels has been developed, and differential thermocouples have been employed, permitting detection of very small thermal effects.

3. We have studied the conditions of formation of black crystalline phosphorus over a wide range of pressures (up to 22,000 kg/cm^2). We have shown that black crystalline phosphorus, over a wide range of pressures (20,000 kg/cm^2) and up to its melting point (1000°C) does not form new modifications of phosphorus, while red phosphorus does form a new reversible modification of phosphorus.

STAT

Declassified in Part - Sanitized Copy Approved for Release @ 50-Yr 2014/03/07 : CIA-RDP81-01043R004200090004-8

Declassified in Part - Sanitized Copy Approved for Release @ 50-Yr 2014/03/07 : CIA-RDP81-01043R004200090004-8

BIBLIOGRAPHY

1. Butuzov,V.P., Shakhovskoy,G.P., and Gonikberg,M.G. - Trudy Inst. Kristallogr., No.11 (1955), p.233
2. Vereshchagin,L.F. and Kalashnikov - Dok. AN SSSR, Vol.99 (1954), p.745
3. Butuzov,V.P., and Gonikberg,N.G. - Dok. AN SSSR, Vol.89 (1953), p.651
4. Birch,F. - Rev.Sci.Instr., Vol.10 (1939), p.137
5. Bridzhmen,P.V. (Percy Bridgman) - Recent Work in the Field of High Pressures. State Publishing House for Foreign Literature (1948)
6. Zhokhovskiy,M.K. - Izmer.Tekh., No.5 (1955), p.3
7. Bridgman,P.W. - Journ.Amer.Chem.Soc., Vol.36 (1914), p.1344
8. Jacobs,R. - Journ.Chem.Phys., Vol.5 (1937), p.945
9. Ipat'yev,V. and Nikolayev,V. - Zhur.Russ.Fiz.Khim.Obshch., Chast' Khim., Vol.60 (1928), p.885

STAT

Declassified in Part - Sanitized Copy Approved for Release @ 50-Yr 2014/03/07 : CIA-RDP81-01043R004200090004-8

Declassified in Part - Sanitized Copy Approved for Release @ 50-Yr 2014/03/07 : CIA-RDP81-01043R004200090004-8

A NEW TYPE OF AUTOCLAVE FOR HYDROTHERMAL SYNTHESIS

by

V.P.Butuzov, G.P.Shakhovskoy and S.P.Smirnov

The hydrothermal synthesis of single crystals, which is conducted in a wide range of pressures and temperatures, is being more and more widely used today. The physicochemical study of systems with volatile components has also found rather wide popularity. Autoclaves capable of withstanding high pressures at high temperatures are necessary for such work.

Industry today is producing refractory steels capable of withstanding high mechanical stresses at high temperatures, and therefore the basic problem in the creation of these autoclaves is the development of a design for a reliable closure capable of withstanding the necessary pressure.

The closure must satisfy the following requirements: with an absolute and reliable seal, it must also be simple to manufacture, easily and rapidly assembled and disassembled, without undergoing damage. The assembly and disassembly of the closures for autoclaves of large diameter should be mechanized.

The closures used in autoclaves may be of two designs, without self-sealing and with self-sealing.

Figure 1 shows a typical construction of a closure without self-sealing. The unit pressure in the sealing gasket 1 before the closing of the autoclave is considerably greater than the possible pressure in the autoclave. This is accomplished by tightening the bolts 2 pressing against the autoclave cover. With increasing

STAT

Declassified in Part - Sanitized Copy Approved for Release @ 50-Yr 2014/03/07 : CIA-RDP81-01043R004200090004-8

Declassified in Part - Sanitized Copy Approved for Release @ 50-Yr 2014/03/07 : CIA-RDP81-01043R004200090004-8

internal pressure in the autoclave, the pressure of the gases of the cover also increases, the bolts become elongated and the unit pressure in the sealing gasket decreases. As soon as the unit pressure falls to the level of the gas pressure in the autoclave, the closure begins to pass gas.

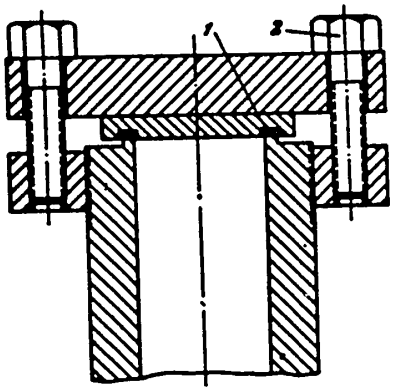

Fig.1 - Design of Closure without Self-Sealing

1 - Sealing gasket; 2 - Bolt

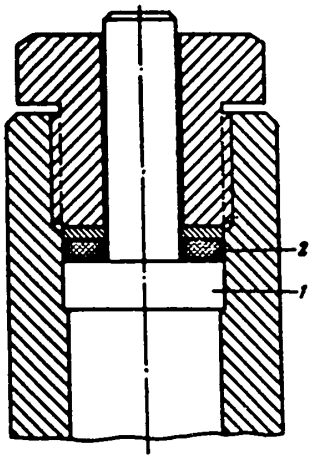

Fig.2 - Design of Closure with Self-Sealing

1 - Obturator; 2 - Sealing gasket

Closures with self-sealing make use of the principle of the "uncompensated area", which is that the pressure in a sealing gasket is always higher than the pressure produced in the autoclave. Figure 2 shows the system of such a closure. Here the pressure of the gases acting on the obturator 1 is transmitted to the sealing gasket 2, and the pressure in that gasket will be as many times greater as the area of the obturator exceeds the area of its support. Only the initial compression of the sealing gasket takes place in an autoclave with a self-sealing closure, and with increasing pressure in the autoclave, the unit pressure in the gasket automatically increases, always remaining higher than the pressure in the autoclave.

When closures built on the principle of the "uncompensated area" are used, the area of the gasket is so calculated that the pressure produced in it shall not exceed the yield point of its material.

STAT

Declassified in Part - Sanitized Copy Approved for Release @ 50-Yr 2014/03/07 : CIA-RDP81-01043R004200090004-8

Declassified in Part - Sanitized Copy Approved for Release @ 50-Yr 2014/03/07 : CIA-RDP81-01043R004200090004-8

A substantial shortcoming of a number of closure designs is the use of threaded connections in them. The pressures taken by the cover or obturator may reach tens of tons and sometimes even hundred of tons. Under the action of such a load, the threaded connections of a closure operating for a long time under high temperatures may be considerably deformed. This leads to seizing and elongation of the thread,

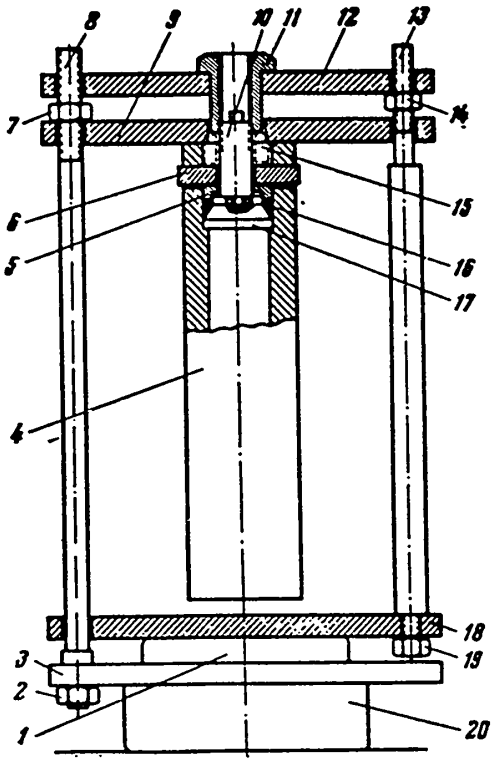

Fig.3 - Autoclave with Arrangement for Opening and Closing

which makes it very difficult to open the autoclave and may put it out of commission.

Moreover the production of a high degree of preliminary sealing with autoclave of large diameters demands considerable mechancial forces. We assume that an autoclave closure must satisfy the following requirements in order to assure reliable operation: (1) the seal must be designed on the principle of "the uncompensated area"; (2) the design of the closure must not have threaded connections; (3) the

STAT

Declassified in Part - Sanitized Copy Approved for Release @ 50-Yr 2014/03/07 : CIA-RDP81-01043R004200090004-8

Declassified in Part - Sanitized Copy Approved for Release @ 50-Yr 2014/03/07 : CIA-RDP81-01043R004200090004-8

closing and opening of the autoclave must be mechanized.

Such an autoclave, taking these requirements into account, has been built and tested at the Institute of Crystallography.

Figure 3 shows the design of the autoclave with the device for opening and closing it. The autoclave closure 4 consists of the obturator 17 with the tailpiece 10, the copper sealing ring 16, the stop bushing 5 and the lock plate 6.

When closing the autoclave, the obturator, with ring and bushing, is inserted in the socket of the autoclave, the locking plate is inserted in the slit in the upper part of the autoclave, and the tailpiece of the obturator is screwed into the obturator. To close the autoclave, the obturator must be pulled upward, applying the initial compressive force to the copper sealing ring.

To open the autoclave, the lock plate and obturator are pushed down, the tailpiece of the obturator is unscrewed, the lock plate is removed from the slit, and the obturator after the tailpiece is pulled out of the autoclave.

A hydraulic press is used to close and open the autoclave. On the cylinder 20 of this press is screwed the flange 3, in which the rod 8 attached by the nut 2 are inserted. On the piston of the press 1 is attached the flange 18 with the four posts 13 inserted in it, and fastened by the nuts 19. The four rods 8 pass freely through openings in the flange 18. The posts and rods are arranged alternately along the circumference of the flange.

To withdraw the obturator from the autoclave, the autoclave is attached by means of the bushing 11 to the upper flange 12 in such fashion as to leave a clearance of 30 - 40 mm between the bottom of the autoclave and a flange 18. The size of the clearance is adjusted by the four nuts 14. The flange 9 in this case rests in against the upper face of the autoclave and is likewise held in position by the four nuts 7. On displacement of the piston of the press 1, its force is transmitted by the flange 18 through the brace 13 and the flange 12 with the bushing 11 to the obturator, and pulls it, while the autoclave itself remains motionless, supported in

STAT

Declassified in Part - Sanitized Copy Approved for Release @ 50-Yr 2014/03/07 : CIA-RDP81-01043R004200090004-8

Declassified in Part - Sanitized Copy Approved for Release @ 50-Yr 2014/03/07 : CIA-RDP81-01043R004200090004-8

the flange 9. In this way, the initial pressure is applied to the copper sealing ring. The pressure in the autoclave, subsequently increasing during the course of the experiment, acting on the obturator, presses against and seals the copper ring, and the unit pressure in it is always higher than the pressure in the autoclave.

To open the autoclave, the lock plate and the obturator with the copper sealing ring must be pushed down, the supporting plate pulled out of the slot, and the obturator must then be pulled out of the autoclave. For this purpose, the autoclave is placed on the flange 18, and the bushing 15 (indicated by the dashed line) is seated on the tailpiece of the obturator. On it is placed the flange 9 which is fastened by the nut 7. Between the flange 9 and the upper face of the autoclave a gap of 10 - 12 mm remains. When the piston of the press with the autoclave moves upward, the bushing 15, resting on the motionless flange 9, lowers the plate with the obturator. After the lock plate has been removed, the obturator is withdrawn from the autoclave in the same way as was done in closing the autoclave.

As shown by long experience, this installation is simple and reliable in operation and requires only a single mechanic to operate it, while the opening of other designs of autoclaves of large inside diameter, and particularly their closing, is difficult to accomplish under laboratory conditions. An autoclave of this new arrangement has an inside diameter of 120 mm and has been operated at 1500 atm and 400°C. On this basis we believe that this construction may find application in work on the hydrothermal synthesis of minerals.

STAT

Declassified in Part - Sanitized Copy Approved for Release @ 50-Yr 2014/03/07 : CIA-RDP81-01043R004200090004-8

Declassified in Part - Sanitized Copy Approved for Release @ 50-Yr 2014/03/07 : CIA-RDP81-01043R004200090004-8

TECHNIQUE OF SYNTHESIS OF REFRACTORY CRYSTALS INSOLUBLE IN WATER

by

I.N.Anikin

Among the crystals with valuable properties employed in modern technology, there are many whose synthesis is very difficult owing to their insolubility in water and to the fact that on heating they either decompose or melt at a very high temperature. Such substances include potassium and cadmium tungstates, whose crystals, as has been recently found (Bibl.1, 2) are most sensitive for the registration of γ-radiation and may be used in scintillation counters. For this purpose it is necessary to have pure transparent crystals not less than 0.5 cm^2 in size.

As has been shown by foreign investigators (Bibl.3, 4) and by the work of the Institute of Crystallography, Academy of Sciences USSR, crystals of $CaWO_4$ and $CdWO_4$ may be prepared from a melt by the temperature gradient method and by the Verneuil method. These methods, although they do yield a certain favorable result, are still distinguished by great technical complexity - this is particularly true of the former method - since they involve the use of a high temperature.

In searching for a simpler technique, we turned our attention to a method which during the last Century was used to prepare crystals of most magmatogenic minerals (Bibl.5,6) (including also scheelite), namely the method of crystallization out of two-component systems, where the solvent is a melt of some low-melting and mobile salt. This method, which is purely empirical, has also begun to be used again in

STAT

Declassified in Part - Sanitized Copy Approved for Release @ 50-Yr 2014/03/07 : CIA-RDP81-01043R004200090004-8

Declassified in Part - Sanitized Copy Approved for Release @ 50-Yr 2014/03/07 : CIA-RDP81-01043R004200090004-8

recent years (Bibl.7, 8, 9, 10). The opinion is held, however, that such a method would hardly be applicable to the preparation of large single crystals; the maximum size of the crystals prepared by such a method was 1 - 3 mm (Bibl.11). B.V.Vitrovskiy proposed to me the use of this method for the crystallization of scheelite from the system NaCl - $CaWO_4$. I found, however, that the solubility of $CaWO_4$ in molten NaCl is slight, and the crystals obtained were very small. It was necessary to find a more suitable solvent, which is one of the principal difficulties, besides the determination of the conditions of crystallization, that confronted me in this work.

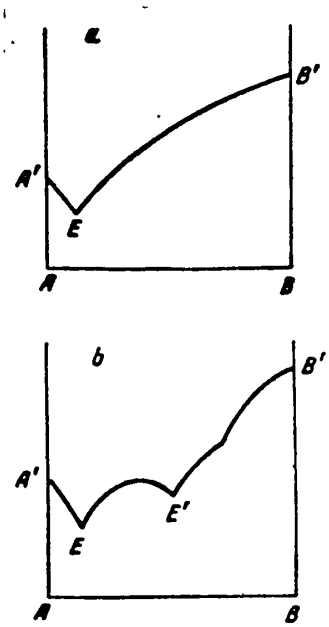

Fig.1

The following consideration must be taken into account in the selection of a solvent.

1. The solvent and the solute in the liquid state must be completely miscible, but they must not form solid solutions in the solid state (Fig.1,a). It is only in this case that the crystallization of the pure component B will occur over the entire curve B'E. It is undesirable that any compounds should be formed in this case (Fig.1,b), because if they are formed, there would be no sense in crystallizing the pure component B (since it may be found to crystallize in a narrow range of high temperatures), or its crystallization will be difficult. The intermediate compounds so formed might spoil the growing crystals by forming various types of inclusions in them. Thus, on the crystallization of nepheline ($NaAlSiO_4$) out of a melt of LiF - - $NaAlSiO_4$, vitreous inclusions of composition $Na_2Al_2(LiF_4)_3$ are formed in it (Bibl.12). It is more advantageous to use as the solvent that salt which forms with the solute the eutectic of lowest temperature and closest to the solvent ordinate on the phase diagram. The solubility of B in A (Fig.1,a) will be greatest

STAT

Declassified in Part - Sanitized Copy Approved for Release @ 50-Yr 2014/03/07 : CIA-RDP81-01043R004200090004-8

Declassified in Part - Sanitized Copy Approved for Release @ 50-Yr 2014/03/07 : CIA-RDP81-01043R004200090004-8

in this case.

2. The solvent must be such that its entrance in the form of an impurity into the growing crystals does not affect the properties of the crystal with which we are concerned. Thus, for example, for the crystallization of most luminescent crystals, including scheelite, compounds of the iron group and of certain other heavy metals which have the power of "quenching" luminescence, cannot be used. In this case those salts which are used as "fluxes" in the preparation of finely crystalline phosphors (Bibl.13) must be used: chlorides, fluorides, sulfates, phosphates and other compounds of the alkali and alkaline-earth metals.

3. To avoid the introduction of foreign ions into the system, the solvent must possess an ion in common with the substance to be crystallized. For example, to dissolve $CaWO_4$ it is better to use some calcium compound (for instance $CaCl_2$) or salt of tungstic acid (for instance Na_2WO_4). If it is impossible to realize this, then the radii of the solvent ions must differ as much as possible from the ionic radii of the solute. The closeness of the ionic radii of solvent and solute may lead to the isomorphous entry of undesirable impurities in the crystallized substance and to modification of its properties. Thus $CdCl_2$, $BaCl_2$, $MgCl_2$, $SrCl_2$, Na_2MoO_4, Li_2MoO_4 must not be used to dissolve scheelite.

4. The viscosity of the melt-solvent must be low: for instance, the alkali metal chlorides have about the same viscosity as water or even a lower viscosity.

5. The vapor pressure of the melt-solvent must be as low as possible, so that intense evaporation of the solvent does not take place during crystallization, thus changing the composition of the solvent, and causing crystallization from the surface. To assure this, the melting and boiling points of the solvent must differ greatly. Thus, for example, owing to the nearness of the melting and boiling points of beryllium chloride, it cannot be used as a solvent, or at any rate it is very difficult to use it, although for a number of other reasons (low melting point, low viscosity, and probably a high dielectric constant) it is rather tempting.

STAT

Declassified in Part - Sanitized Copy Approved for Release @ 50-Yr 2014/03/07 : CIA-RDP81-01043R004200090004-8

Declassified in Part - Sanitized Copy Approved for Release @ 50-Yr 2014/03/07 : CIA-RDP81-01043R004200090004-8

6. The solvent must have a considerably lower melting point than the crystallizate. The greater this difference, the more reason there is to use one of them as the solvent of the other, since in this case one can work at lower temperatures. For this reason, for instance, it is more advantageous to use sodium chloride for the synthesis of scheelite than calcium fluorite, while lithium chloride is still more

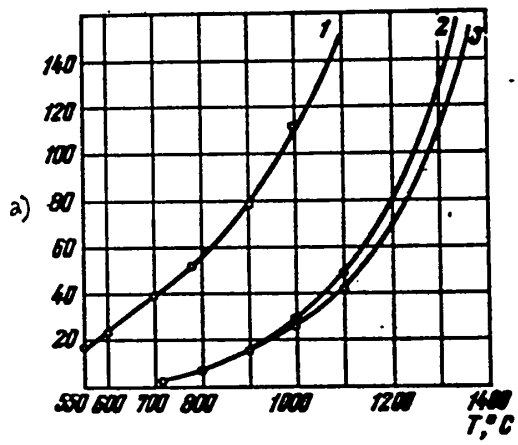

Fig.2 - Solubility of $CaWO_4$ in Grams per 100 gm of Solvent:

1 - LiCl; 2 - NaCl; 3 - KCl

a) Quantity of $CaWO_4$ per 100 gm of solvent, gm

advantageous than sodium chloride. For the crystallization of $CdWO_4$, for instance, the system NaCl - $CdWO_4$ cannot be used, although cadmium tungstate does dissolve very well in this system. In this case, at temperatures over 750 - 800°C the $CdCl_2$, m.p. 568°C, will rapidly volatilize from the melt, for its vapor pressure at this temperature is very high, and will leave Na_2WO_4 in the melt.

7. It is also desirable that the salt of the solvent shall be soluble in water (or in some other readily available solvent), while the crystals to be synthesized are insoluble, so that they can be easily separated, after crystallization has been completed, from the solidified melt, by merely washing it.

Of course, in selecting a solvent in each specific case, one must not blindly

STAT

Declassified in Part - Sanitized Copy Approved for Release @ 50-Yr 2014/03/07 : CIA-RDP81-01043R004200090004-8

Declassified in Part - Sanitized Copy Approved for Release @ 50-Yr 2014/03/07 : CIA-RDP81-01043R004200090004-8

follow this proposed system and demand that the solvent must necessarily possess all the properties indicated.

Taking account of the considerations above expressed, the chlorides of the group of alkali metals, LiCl, NaCl, KCl, and salts having one ion in common with $CaWO_4$, $CaCl_2$ and Na_2WO_4, were proposed as possible solvents for $CaWO_4$. In comparing the properties of these salts, lithium chloride attracts particular attention. This salt possesses the lowest melting point, the greatest ionic polarizability, and

Table

Solubility of $CaWO_4$ in Melts of Various Salts, Calculated in Grams per 100 gm of Solvent

a)	b)	c)	d)	e)	f)	g)
LiCl	112	16 } $t_1 = t_{eut}$	96	0,21	606	550
NaCl	28	3 } $t_1 = t_{eut}$	25	0,10	800	745
KCl	26	3 } $t_1 = t_{eut}$	23	0,09	772	730
$CaCl_2$	35	9 } $t_1 = t_{melt}$	26	0,11	770	—
Na_2WO_4	25	11 } $t_1 = t_{melt}$	14	0,04	680	—

a) Solvent; b) Solubility at 1000°C, gm; c) Solubility at t_1, gm; d) Quantity of $CaWO_4$ (Δm), segregated on cooling from 1000°C to t_1, gm; e) Mean quantity of $CaWO_4$ $\left(\frac{\Delta m}{1000 - t_1}\right)$ segregated during cooling per °C; f) m.p. of solvent, °C; g) t_{eut}, °C

probably also a very high dielectric constant in the molten state. For the final choice of a working solvent, I determined the solubility of scheelite in a melt of each salt, together with its temperature dependence. This was established by quantitative analysis of samples of the test melt, heated at a definite temperature, and also by the visual-polythermic method. I found (Fig.2 and Table) that the solubility of scheelite is greatest in a melt of lithium chloride. Even higher is the solubility of $CdWO_4$ in molten LiCl, 250 gm in 100 gm of solvent at 600°C, eutectic

STAT

Declassified in Part - Sanitized Copy Approved for Release @ 50-Yr 2014/03/07 : CIA-RDP81-01043R004200090004-8

Declassified in Part - Sanitized Copy Approved for Release @ 50-Yr 2014/03/07 : CIA-RDP81-01043R004200090004-8

at 480°C. The high solubility of such compounds as CaF_2 and $CaCO_3$ is also shown in a melt of lithium chloride, although their solubility in other solvents is only slight. Lithium chloride was therefore chosen as the principal working solvent for the crystallization of calcium tungstate.

Preliminary studies of the crystallization of scheelite in a small volume (up to 1.5 gm of solvent) staged by the aid of a special microscope (Bibl.14), yielded the following results.

1. It is rational to conduct crystallization from the system LiCl - $CaWO_4$ at temperatures below 700°C, since, at higher temperatures, the evaporation of the solvent is too great.

Fig.3 - Well Demarcated Transparent Crystals of Scheelite Prepared by Slow Cooling of a Homogeneous Solution. 1.8 ×

2. The melt must be superheated by 100 - 150°C to dissolve the foreign impurities and destroy the centers of crystallization.

3. The following cases of preparation of the individual large single crystals are possible: (a) slow cooling of a saturated solution with "spontaneous" formation of individual crystals; (b) formation and growth of crystals at sites with artificial removal of heat; (c) growth of crystal on a seed placed in the solution with the lowering of the solution temperature according to an established system;

STAT

Declassified in Part - Sanitized Copy Approved for Release @ 50-Yr 2014/03/07 : CIA-RDP81-01043R004200090004-8

Declassified in Part - Sanitized Copy Approved for Release @ 50-Yr 2014/03/07 : CIA-RDP81-01043R004200090004-8

(d) growth of the crystal on a seed suspended in the upper part of the crystallizer, on account of the transport of feed material from the bottom under a certain temperature gradient.

4. The velocity of growth of a transparent $CaWO_4$ crystal along the c axis, without mechanical agitation of the solution, is 0.2 - 0.3 mm/hr. The knowledge of the rate of growth permitted me to calculate the rate of cooling of the various volumes of solution under the conditions of the growth of a single crystal without agitation of the solution.

Fig.4 - Skeletal Crystals of Scheelite Obtained on Rapid Cooling of the Melt. 12 ×

After ascertaining the necessary conditions of crystallization, experiments with a larger quantity of solution were staged. Since only platinum is suitable for work with lithium chloride, I had to confine myself to the available standard crucibles Nos.8 and 9 and run my experiments with 40 - 50 gm of solvent. Most of the experiments were run under slow cooling of a homogeneous solution and "spontaneous" formation of crystals. In this case, the crucible, with the solution saturated at 700°C, in a crucible furnace, was tightly covered with a cover, and the furnace was

STAT

Declassified in Part - Sanitized Copy Approved for Release @ 50-Yr 2014/03/07 : CIA-RDP81-01043R004200090004-8

Declassified in Part - Sanitized Copy Approved for Release @ 50-Yr 2014/03/07 : CIA-RDP81-01043R004200090004-8

covered with preheated sand. The temperature was measured by a platinum-platinorhodium thermocouple resting on the crucible cover; the temperature was lowered according to an assigned program during a period of 4 - 5 days. Three to eight seeds were formed in the melt, and grew, mostly located on the bottom of the crucible; especially perfect crystals grew on the crucible walls. The crystals acquired well demarcated tetragonal pyramidal shapes (Fig.3) and were for the larger part transparent, and 8 - 12 mm in size. Often the central part of the crystal was cloudy, indicating intense growth at the time of nucleation from a highly supersaturated solution. If the rate of cooling did not correspond to the rate of growth of the transparent crystal, i.e., if the solution was cooled too rapidly, zonal, skeletal and dendritic crystals were formed (Figs.4, 5).

Fig.5 - Zonal Crystal of Scheelite

10 ×

To obtain larger and more perfect crystals, the use of a larger volume of charge (up to 300 - 400 gm) in special crystallizers, and with a finer temperature adjustment, is recommended. In my experiments the temperature was stabilized with accuracy of ± 3°C. Crystallization should be on a seed, out of a continuously agitated melt, with the temperature lowered according to an assigned program, or at constant temperature, in presence of an excess of feed substance on the bottom of the crystallizer, and with a definite vertical temperature gradient in the melt. Such experiments in a small volume when the crystallization was conducted under the microscope yielded very satisfactory results.

The morphology of the scheelite crystals produced is an aspect of the study that is of independent interest, but in this exposition I shall elucidate only certain identifying features of the crystals. The measurement of transparent crystals

STAT

Declassified in Part - Sanitized Copy Approved for Release @ 50-Yr 2014/03/07 : CIA-RDP81-01043R004200090004-8

Declassified in Part - Sanitized Copy Approved for Release @ 50-Yr 2014/03/07 : CIA-RDP81-01043R004200090004-8

on the goniometer showed (Fig.6) the presence of three well developed forms: p (011), e (112) and β(013). The less transparent crystals or the cloudy ones are characterized by the presence only of p and e faces, or even only of p faces.

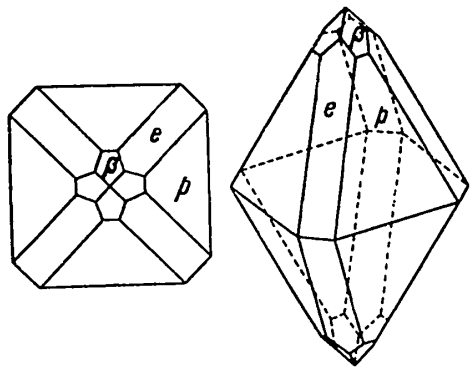

Fig.6 - Drawing of Scheelite Crystal; Developed Faces

p (011), e (112), β(013)

Various figures of growth are distinctly visible on the crystal face: rings, spirals, dendrites, polygons, and all possible types of complex figures (Fig.7). The

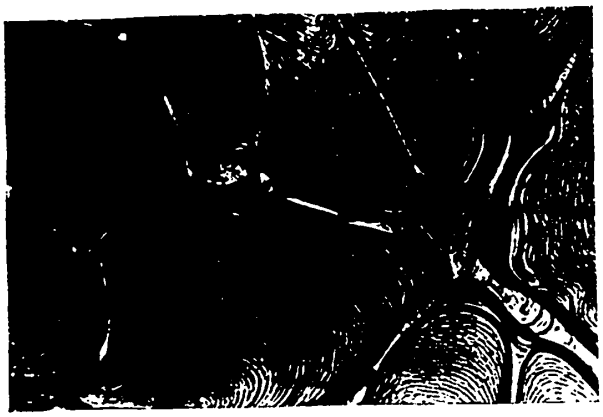

Fig.7 - Topography of Part of a p Face. 230 ×

more transparent the crystal, and the more perfect it is, the finer the designs on its faces.

The density of the crystals obtained, measured by the pycnometric method, was

STAT

Declassified in Part - Sanitized Copy Approved for Release @ 50-Yr 2014/03/07 : CIA-RDP81-01043R004200090004-8

Declassified in Part - Sanitized Copy Approved for Release @ 50-Yr 2014/03/07 : CIA-RDP81-01043R004200090004-8

6.065.

The refractive index, measured by the aid of high-refracting liquids prepared by S.S.Batsanov, likewise agreed with the literature data.

The luminescence of scheelite crystals is characterized by a blue and blue-azure color under excitation by short ultraviolet, cathode, and X-rays. Tests of the synthesized crystals showed that they are completely suitable for use in ultraviolet microscopy for separating the shortwave part of the specimen, and if their sizes are increased, for registration of γ-radiation in scintillation counters.

In conclusion I express my appreciation and gratitude to those who have helped me at various stages of this work, and especially to G.B.Bokiy, B.V.Vitovskiy, G.G.Lemmleyn, and L.M.Belyayev.

BIBLIOGRAPHY

1. Moon,R.J. - Phys.Rev., Vol.73,10 (1948),p.1210
2. Klick,C.C. and Schulman,J.H. - Phys.Rev., Vol.75,10 (1949),pp.1606-07
3. Zerfross,S., Johnson,L.R., and Imber,O. - Phys.Rev., Vol.75,2 (1949),p.320
4. Gillette,R.H. - Rev.Sci.Instr., Vol.21,4 (1950),pp.294-301
5. Chirvinskiy,P.K. - Artificial Preparation of Minerals in the 19th Century. Kiev, 1903 - 1906
6. Brauns,R. - Chemical Mineralogy. St.Petersburg, 1904
7. Matthias,B. - Phys.Rev., Vol.73 (1948),p.808
8. Mergault,P. and Brauche,G. - C.r.Acad.Sci., Vol.238,8 (1954),pp.914-916
9. Khristoforov,B.S., Grosman,L.I., and Kalashnikova,S.N. - Zap.Vses.Min.Obshch., Vol.81,3 (1952),pp.205-207
10. Jona,F., Schiranea,G., and Pepinsky,R. - Phys.Rev., Vol.97,6 (1955),pp.1584-1590
11. - New Studies on Cristallography and Crystal Chemistry. Symposium 1. The Growth of Crystals. State Publishing House for Foreign Lit., 1950
12. Winkler,Helmut - Amer.Min., Vol.32,(1947),pp.3-4, 131-136

STAT

Declassified in Part - Sanitized Copy Approved for Release @ 50-Yr 2014/03/07 : CIA-RDP81-01043R004200090004-8

Declassified in Part - Sanitized Copy Approved for Release @ 50-Yr 2014/03/07 : CIA-RDP81-01043R004200090004-8

13. Zhirov,N.F. - Luminophores. Moscow (1940)

14. Anikin,I.N. - Zavod.Lab., Vol.7 (1956),p.805

STAT

Declassified in Part - Sanitized Copy Approved for Release @ 50-Yr 2014/03/07 : CIA-RDP81-01043R004200090004-8

Declassified in Part - Sanitized Copy Approved for Release @ 50-Yr 2014/03/07 : CIA-RDP81-01043R004200090004-8

A PRECISION METHOD OF DETERMINING THE SATURATION TEMPERATURE OF TRANSPARENT SOLUTIONS

by

A.N.Kovalevskiy

In the practice of laboratory and plant growing of crystals from solutions, the sufficiently rapid and accurate determination of the saturation temperature of the working solution is of substantial importance. For this purpose the "concentration current method" proposed by A.A.Shternberg is ordinarily used (Bibl.1).

Together with certain advantages, simplicity and relative speed, this method also has shortcomings. It is difficult to distinguish the currents in the solution, their observation by the naked eye is tiring and demands a certain amount of practice from the observer. This introduces the element of subjectivity into the estimate of the saturation temperature. The saturation temperatures found by this method are also, as a rule, 0.5 - 1°C too low, especially at high rates of cooling of the solution (over 2 - 3°C/hr) or in working with solutions of marked viscosity.

The method of determining the saturation temperature, from the gate of crystallization, or diffusion boundary layer, is free from these shortcomings.

A crystal immersed in its mother liquor and not in equilibrium with it (i.e., growing or dissolving in it), is surrounded by a thin layer of solution through which the diffusion of the matter from the solution to the crystal, or from the crystal to the solution, takes place. This layer, called the film or gate of crystallization, is a region of the solution with a nonzero concentration gradient. By

STAT

Declassified in Part - Sanitized Copy Approved for Release @ 50-Yr 2014/03/07 : CIA-RDP81-01043R004200090004-8

Declassified in Part - Sanitized Copy Approved for Release @ 50-Yr 2014/03/07 : CIA-RDP81-01043R004200090004-8

energetic mixing of the solution, practically all of its temperature and concentration inhomogeneity can be eliminated, except for the film of crystallization. The film of crystallization becomes thinner, but the concentration gradient in it, other conditions being equal, increases in inverse proportion to its thickness. The concentration gradient in the film of crystallization decreases as the solution ap-

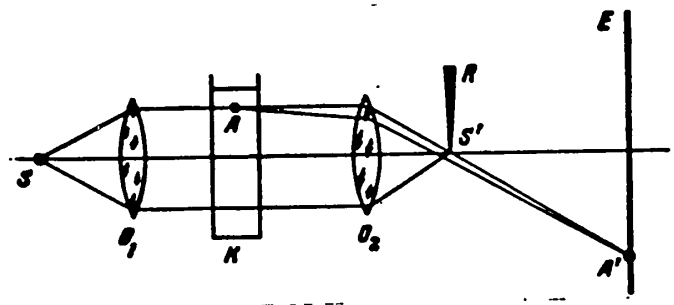

Fig.1

proaches saturation, and becomes equal to zero at the final saturation of the solution, when the film of crystallization disappears completely.

By noting the moment of disappearance of the film of crystallization, the saturation temperature of a solution may be measured with an accuracy limited only by the accuracy of the thermometer or thermocouple used, and the sensitivity of the optical system of the apparatus.

The film of crystallization, being a region of concentration gradient (meaning also a region of gradient of refractive index), constitutes an optical inhomogeneity in the solution. Thanks to this fact, the film may be observed and photographed by the aid of one of the well known solution-optical systems used to observe the optical inhomogeneities of transparent media (Bibl.2).

Use of the elementary grating or raster scheme, known under the name of Tepler system, already yields results sufficient for estimating the saturation temperature with an accuracy not less than 0.05°C, which exceeds the accuracy of the mercury thermometers in general use.

Figure 1 shows a somewhat more complex system which gives, with a shorter op-

STAT

Declassified in Part - Sanitized Copy Approved for Release @ 50-Yr 2014/03/07 : CIA-RDP81-01043R004200090004-8

Declassified in Part - Sanitized Copy Approved for Release @ 50-Yr 2014/03/07 : CIA-RDP81-01043R004200090004-8

tical length, a considerably larger field of vision, whose angular diameter remains constant while the image is being focused and the magnification is changing.

Light from the point source S, located at the principal focus of the lens O_1, falls in a parallel beam on the lens O_2, giving the image S_1' of the source at its

Fig.2 - Crystal of Ammonium Dihydrophosphate in Supersaturated Solution. The image of the film of crystallization is visible only to the left of the crystal; the concentration current directed upward is visible. 3 ×

Fig.3 - Photograph Obtained Using Star-Shaped Gratings. The film is visible on all sides of the crystal, and its laminar structure is also visible. 4 ×

principal focus. This image is covered by the sharp edge of the blackened screen R, so that the white screen E remains darkened. If any optical inhomogeneity is encountered on the path of the light from S to S^1, for example at the point A, then the light, being deflected at this point from its original path, will pass the edge R and yield the image A' of this inhomogeneity on the screen E, which is placed in the conjugate focal plane. By placing the transparent cell K with the solution and crystal between the lenses O_1 and O_2, a bright image of the crystallization

STAT

Declassified in Part - Sanitized Copy Approved for Release @ 50-Yr 2014/03/07 : CIA-RDP81-01043R004200090004-8

Declassified in Part - Sanitized Copy Approved for Release @ 50-Yr 2014/03/07 : CIA-RDP81-01043R004200090004-8

film against the dark background may be obtained on the screen E. The image is formed only by rays deflected to one side of the edge R, and the film of only about half of the faces of the crystal parallel to the edge R (or almost parallel to it) is visible on the screen (Fig.2).

When the solution passes through the state of saturation, the sign of the gradient of the film is reversed, and on the screen there appears the image of the film around the opposite half of the crystal, which makes a supersaturated solution readily distinguishable from an undersaturated one (this may be used, in particular, for the purpose of automatically holding a solution at the saturation temperature by the aid of a photorelay device, even if the concentration of the solution varies).

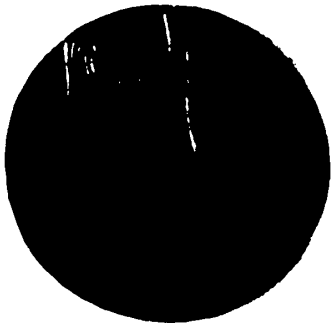

Fig.4 - Photograph Obtained Using a Slit and Band. The image contrast is less, but the film is visible from all sides. 3 ×

The use of optical gratings in this system makes it possible to observe the film simultaneously from all sides of the crystal (Figs.3, 4), increases the accuracy of determination of the instant of saturation, permits determination of the difference in saturation temperatures for the various faces of the crystal (i.e., their solubility), increases the brightness of the image, and lowers the requirements for lens quality. At the same time, the use of solutions considerably complicates the adjustment of the system, which is necessary in working with solutions of different substances, concentrations and temperatures, and even with slight changes in the position of the cell. This may be avoided by using star-shaped or spiral gratings , or by using as the first grating R_1 (Fig.5) a slit of adjustable width illuminated by the condenser O_1, and a narrow and finely outlined strip 0.5 - 1 mm wide and about 0.1 mm thick as the

STAT

Declassified in Part - Sanitized Copy Approved for Release @ 50-Yr 2014/03/07 : CIA-RDP81-01043R004200090004-8

Declassified in Part - Sanitized Copy Approved for Release @ 50-Yr 2014/03/07 : CIA-RDP81-01043R004200090004-8

second grating R_2.

The adjustment in this case is accomplished by changing the width of the slit and moving the band in two directions, along the optical axis and perpendicular to the optical axis and the length of the strip.

The sign of the gradient of the film may be determined by placing the pair of light filters C_1 and C_2 between the white screen E and the strip (as close as possible to it) in such a way that the line from the junction shall pass through the optical axis of the instrument parallel to the band. To obtain the maximum light contrast, light filters of complementary colors should be used. With a change of sign of the gradient of the film, the rays are deflected in it in the opposite direction, pass on the other side of the strip, and the color of the film on the screen will change to the complementary color.

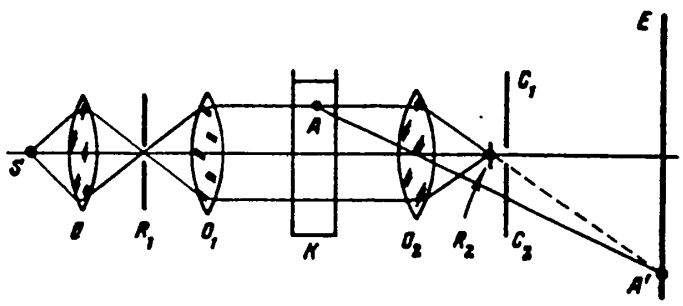

Fig.5

It must be borne in mind that the sign of gradient of the film also depends on the position of the crystal face. If the slit and the band are in vertical positions, then the films on the right and left sides of the crystal have a different color, other conditions being equal. When the state of the solution changes from undersaturated to supersaturated, their color changes in the reverse sequence.

The accuracy of determination of the saturation temperature from the film of crystallization without mixing the solution exceeds 0.05°C with a focal length of not less than 20 cm for the lens O_2 and a rate of change of the solution tempera- STAT

Declassified in Part - Sanitized Copy Approved for Release @ 50-Yr 2014/03/07 : CIA-RDP81-01043R004200090004-8

Declassified in Part - Sanitized Copy Approved for Release @ 50-Yr 2014/03/07 : CIA-RDP81-01043R004200090004-8

ture not over 0.2°C/min. By mixing the solution and using a longer focus optical system, the accuracy may be increased.

This method makes it possible rapidly to measure the saturation temperature of a solution for the crystal as a whole and for its faces, to determine the temperature coefficient of solubility, and construct a solubility curve, to maintain a solution automatically in a state of saturation, etc. The image of the film on the screen is sufficiently bright, and its contrast is sufficiently high, to assure convenience and objectivity of observation and to permit still and motion picture photography of the processes taking place.

The shortcomings of this method include the necessity of having a special optical installation, but this is made up by the convenience, accuracy and speed of the measurements.

BIBLIOGRAPHY

1. Shternberg,A.A. - Uch.Zap.Leningrad State University, Ser.Geol.Pochv.Nauk, No.13 (1945)

2. Valyus,N.A. - A Grating Optical System. Gostekhizdat, 1949

STAT

Declassified in Part - Sanitized Copy Approved for Release @ 50-Yr 2014/03/07 : CIA-RDP81-01043R004200090004-8

Declassified in Part - Sanitized Copy Approved for Release @ 50-Yr 2014/03/07 : CIA-RDP81-01043R004200090004-8

V. MISCELLANEOUS

CRYSTALLIZATION OF VIRUSES

by

V.L.Ryzhkov

The structural elements of virus crystals are not their ions, not their molecules and not their micelles, but living individuals. This puts virus crystals in a most peculiar position, but there is no internal contradiction in the fact that biological individuals form crystalline aggregates. It has been shown that, under certain conditions, even motile rod-like bacteria may associate to form crystal-like formations, reaching 100 μ in length and 20 μ in thickness, and externally similar to the para-crystals of the virus of tobacco mosaic disease. In such crystal-like bacterial aggregates, the distance between the separate individuals reaches tens of thousands of angstroms, and the diffraction of a ray of visible light passed through such crystalline aggregates of bacteria may be observed (Bibl.1).

The individuals of which the crystals of viruses are composed are more complex than molecules, as is clear from crystallographic studies, at the very beginning of which it was noted that these individuals "are more analogous to protein crystals than to protein molecules, and their internal order is very considerable" (Bibl.2).

The virus particles of which virus crystals are built up, will be considered by us as the resting forms of the virus, analogous to the spores, and may be called virospores (Bibl.3). The structure of at least some viruses in the virospore stage has been rather well studied. The virus particles of tobacco mosaic disease have been investigated in particularly great detail (Fig.1). They are hexagonal prisms,

STAT

Declassified in Part - Sanitized Copy Approved for Release @ 50-Yr 2014/03/07 : CIA-RDP81-01043R004200090004-8

Declassified in Part - Sanitized Copy Approved for Release @ 50-Yr 2014/03/07 : CIA-RDP81-01043R004200090004-8

about 3000 Å in length and 150 Å in diameter. Such a particle consists of hexagonal platelets 68 Å thick, the total number of which reaches 40 in each individual particle. Each such platelets consists of three rhomboprismatic particles; the side of a rhombus is 87 Å long. The molecular weight of these elementary units is about 370,000. It was found subsequently, however, that elementary units with a molecular weight of about 30,000 are disposed spirally around the axis of the hexagonal prism (Bibl.4, 5). It must be borne in mind that we are here discussing the hyperfine structure discovered by the aid of X-ray analysis. The data on the spiral structure of virus particles discovered by observation under the electron microscope are extremely doubtful (Bibl.6, 7). Studies have shown that the particles of tobacco mosaic virus look like hexagonal prisms under the electron microscope, and it has also been possible to observe them in cross-section.

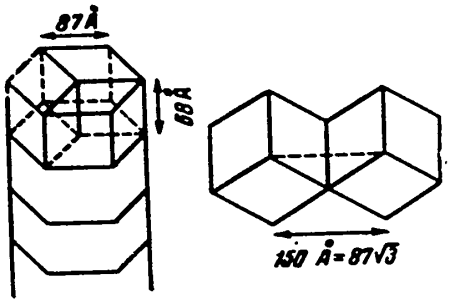

Fig.1 - Structure of a Particle of the Virus of Tobacco Mosaic Disease (Bibl.2)

About 20 years ago, studies of the products of decomposition of the rods of the tobacco mosaic virus under the action of alkalies were initiated. These studies showed that the rods break down into smaller particles which, on acidification, can again assemble into rods of the original size, which, however, are no longer infectious. It has been established as a result of recent electron microscopic studies (Bibl.8) that the rod of the virus of tobacco mosaic disease has a cavity in the center, containing the nucleic acid of yeast (Fig.2). The data of X-ray analysis are not inconsistent with the idea that the nucleic acid is at the center of the bacillus of the virus of tobacco mosaic. Thus it may be said that the nucleic acid of tobacco mosaic virus is clad in a crystalline protein sheath. This type of structure is characteristic of other virus particles as well. The virus of yellow STAT

Declassified in Part - Sanitized Copy Approved for Release @ 50-Yr 2014/03/07 : CIA-RDP81-01043R004200090004-8

Declassified in Part - Sanitized Copy Approved for Release @ 50-Yr 2014/03/07 : CIA-RDP81-01043R004200090004-8

turnip mosaic is about 190 Å in diameter. Under the electron microscope these particles appear spherical, but, judging from the data of X-ray analysis, they have tetrahedral configurations (Bibl.9). The nucleic acid of this virus, which is of the ribose type, is located at the center of the particle. It is surrounded by a crystalline protein sheath (Bibl.10). The bacterial viruses (phages) contain thymonucleic acid, which is also enclosed inside a rather thick protein sheath.

Fig.2 - Rods Formed by the Protein Sheath of Tobacco Mosaic Virus (Under the Electron Microscope); in Some of the Fragments We See the Cavities in which the Filament of Nucleic Acid in the Active Particle Is Located (Bibl.2)

These studies show that the greater part of the virus protein goes for the construction of its sheath, the crystalline structure of which apparently helps to increase the resistance of this sheath against the unfavorable influences of the environment. The structure of the resting forms of viruses here described forces us to recall how widely monocellular organisms, as well as the more highly organized animals, utilize crystalline structures, consisting of either organic or mineral molecules, to form various types of protective sheaths and armor. In this connection one might recall the metaphorical remark of Engels that "protein surrounds itself, so to say, with its own crystalline mold" (Bibl.11,p.248). Applying this to STAT

Declassified in Part - Sanitized Copy Approved for Release @ 50-Yr 2014/03/07 : CIA-RDP81-01043R004200090004-8

Declassified in Part - Sanitized Copy Approved for Release @ 50-Yr 2014/03/07 : CIA-RDP81-01043R004200090004-8

viruses, one might put it in this way: nucleic acid surrounds itself with its own protein crystalline mold. So or otherwise, life utilizes the crystalline structure, already at the molecular level, for protection against unfavorable external influences.

The crystallography of the protein sheath of the virus has been worked out far better than that of the contents of virus particles, which are rich in nucleic acid. But the data of a crystallographic study of thymonucleic acid are also of great scientific importance, which we cannot fail to mention here (Bibl.12). In the dry state, thymonucleic acid has a true crystalline structure, but in its moist state, its structure becomes paracrystalline. Research has shown that thymonucleic acid consists of two spirally coiled filaments, as schematically shown on Fig.3. Perpendicular to the axis of the entire structure are the purine and pyrimidine bases, the adenine of one filament always being connected with the thymine of the other filament by a hydrogen bridge, while the guanine is connected with the cytosine by the aid of the same bridge. Two purine bases cannot be located opposite each other for the simple reason that they would not fit into the space made available to them by this structure. If two pyrimidine bases were opposite each other, then the distance would be too great for any connection by means of a hydrogen bridge to be possible. The most remarkable peculiarity of this structure is that it is always coiled in a right-hand direction. Both high-polymer preparations of thymonucleic acid and the thymonucleic acid of human and animal sperm, as well as the filaments of thymonucleic acid which are present in the coiled state in the

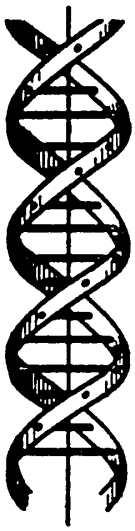

Fig.3 - Diagram of the Structure of Thymonucleic Acid. The hydrogen bridges, connecting the purine and pyrimidine bases of the two filaments, are represented in the form of transverse bridges (Bibl.12)

STAT

Declassified in Part - Sanitized Copy Approved for Release @ 50-Yr 2014/03/07 : CIA-RDP81-01043R004200090004-8

Declassified in Part - Sanitized Copy Approved for Release @ 50-Yr 2014/03/07 : CIA-RDP81-01043R004200090004-8

heads of bacteriophages, have a similar structure.

According to a very probable hypothesis, the structure here described, built up of nucleic acid, is responsible for the synthesis of the polypeptide chains which are characteristic for a given form of proteins. This appears with particular clarity with respect to the phage. Phage attaches itself to the bacterial cell by means of a process, its protein sheath remaining outside the bacterium, and only the content of the phage particle, consisting primarily of thymonucleic acid, penetrates into the bacterium. By end of the period of multiplication, mature phage particles provided with dense protein sheaths, are formed in the bacterial cell.

Considering the questions of virus crystallography, one cannot but direct one's attention to a very important circumstance, which has until now been disregarded. The origin of the optical asymmetry of living bodies remains unknown, and is very abstractly explained by the role of some asymmetric space. And yet it is the submicroscopic structures of nucleic acid of which this asymmetric space apparently consists. Pasteur, who first expounded the theory of the asymmetric structure of living bodies, made wide use of screw structures as an example. It is well known that he distinguished two forms of optical asymmetry, molecular, where each molecule is asymmetric, and the asymmetry of supermolecular structures which may be the result of the combination of optically symmetric molecules (Bibl.13). The spiral formed by thymonucleic acid, as it were, belongs to this second category. Here it is not the individual component elementary units that are asymmetric (if we do not consider the optical asymmetry of the desoxyriboses in the composition of the individual nucleotides), but the entire structure, as a whole, is asymmetric.

It might be postulated that it is precisely the asymmetric structures here considered that assure the selection of molecules of amino acids of some definite optical activity. The amino acids of the opposite optical activity, even if they were synthesized by the organism, could have been rapidly destroyed by the ferments. It is well known that ferments destroying nonnatural amino acids are widely dis-

STAT

Declassified in Part - Sanitized Copy Approved for Release @ 50-Yr 2014/03/07 : CIA-RDP81-01043R004200090004-8

Declassified in Part - Sanitized Copy Approved for Release @ 50-Yr 2014/03/07 : CIA-RDP81-01043R004200090004-8

tributed in living bodies. Their presence in the organism up to now remains a well-known enigma for biochemists.

Let us return to the conditions of crystallization. The question as to these conditions must first of all be considered with respect to the virus particles themselves, for which, as we have seen, a crystalline structure has been demonstrated in a number of cases. The entire process of formation (or, if one prefers, crystallization) of these particles takes place within the cell, and therefore we know very little about how it proceeds. It is essential that together with the active virus particles, inactive virus particles are also isolated from the tissues of a diseased plant or from bacteria invaded by phages, and also from the tissues of an animal suffering from a virus disease. These inactive particles differ from the active particles by not containing nucleic acid. This is a sheath without its contents, or so to say vacancies. Such vacancies of tobacco mosaic virus, and of yellow turnip mosaic virus, have been subjected to crystallographic investigations. X-ray analysis has shown each inactive virus particle to have a cavity inside it, which collapses when the particles are dried. The size of this inactive particle depends on the quantity of water absorbed by it, which, naturally, is not observed in active particles, in which the cavity is occupied by nucleic acid (Bibl.14, 15). We do not know how the sheaths without contents are formed. Perhaps they originate when the multiplication of the virus stops, but the "packing mechanism", for some reason or the other, still continues to operate. Here we must, however, recall that, if we are speaking of nucleic acid, then it is not excluded (and we think, it may even be supposed) that a small quantity of the protein of the virus itself, not the protein of its sheath, is connected with this nucleic acid. Our idea of the role of the protein compounds in life is so firmly grounded that we cannot imagine life in the form of nucleic acid alone. If we are always thinking of nucleic acid, it is only because we are still unable precisely to demonstrate the presense of protein in the structures within the virus particle. One should obviously speak of a nucleoprotein,

STAT

Declassified in Part - Sanitized Copy Approved for Release @ 50-Yr 2014/03/07 : CIA-RDP81-01043R004200090004-8

Declassified in Part - Sanitized Copy Approved for Release @ 50-Yr 2014/03/07 : CIA-RDP81-01043R004200090004-8

very rich in nucleic acid.

A large number of attempts to recrystallize virus particles (Bibl.16, 17) are known, and we have already mentioned some of them. Both the products of the disintegration of the bacilli of tobacco mosaic virus under the influence of caustic alkali or ultrasonic waves, and particles of inert protein, or "vacuoles", may aggregate, under the action of a shift in the pH toward the acid side, into rods of length corresponding to that of active virus particles. It has recently been possible apparently also to restore active virus particles. The scheme of the experiment leading to such resynthesis, was as follows. By the aid of weak solutions of caustic alkali, a virus protein without nucleic acid is prepared, and then the nucleic acid is isolated by the aid of dodecyl sulfate. These two preparations, separately, have no virulence whatsoever. But if the two preparations are combined, and the mixture is acidified, then polymerization of the protein is observed, and a small percentage of the original activity of the virus is restored. The results of this experiment are usually interpreted to mean that in a small percentage of cases it is possible to resynthesize the virus particles with nucleic acid, surrounded by a crystalline protein sheath. Such a resynthesis is not particularly understandable, and has not been rigorously proved, since the polymerization of the "vacuoles" proceeds, even without the presence of nucleic acid, and it is not entirely clear how the filament of nucleic acid penetrates into these vacuoles. It seems to us that these experiments also admit of a different interpretation, according to which it is necessary for infection that both the protein sheath and the filament of nucleic acid shall be in one and the same cell. It is possible that the infectiousness may be restored if the two components, independently of each other, meet by chance in a single cell, and perhaps this may be assured by the adhesion of the nucleic acid filament to the outside of the protein "vacuole". It has recently been demonstrated that if the crystalline protein sheath is removed from the particles of tobacco mosaic virus, then their contents (mainly consisting of filaments of yeast nucleic

STAT

Declassified in Part - Sanitized Copy Approved for Release @ 50-Yr 2014/03/07 : CIA-RDP81-01043R004200090004-8

Declassified in Part - Sanitized Copy Approved for Release @ 50-Yr 2014/03/07 : CIA-RDP81-01043R004200090004-8

acid) retain a certain infectiousness even without the sheath. This infectiousness, however, is rapidly lost by filaments of yeast nucleic acid without sheaths, which once again confirms the protective role of the protein sheaths (Bibl.16, 17).

Table

Change of Interparticle Distance in Virus Crystals

Virus	Size of Particles Å	Distance between Particles, Å	
		In Dry State	In Moist State
Shrub dwarfing	255-270	272	332
Yellow mosaic of turnip	193-220	228	306
Tobacco necrosis	130-166	157	179
Tobacco mosaic disease	2800-3000	152	175

The conditions of formation of crystalline aggregates out of virus particles have been studied somewhat better. Only well purified viruses usually crystallize; and often the purification of viruses from the pigments in the plant tissue involves great difficulties. For the crystallization of the viruses, the attainment of a certain degree of concentration of the suspension of virus particles is also necessary. Crystallization is usually conducted under the conditions of addition of ammonium sulfate and acidification of the liquid to a pH which still remains somewhat higher than the isoelectric point of the virus. For various viruses, the conditions of crystallization are different. It may be said in general that the precipitation of phytopathogenic viruses requires the attainment of about 0.2 of saturation with ammonium sulfate.

Bernel has developed methods permitting the X-ray analysis of individual virus crystals in their mother liquor. The virus of tobacco mosaic disease forms spindle-shaped paracrystals reaching 40μ in length. They are anisotropic. The paracrystals of the virus of orange mosaic disease of the cucumber (Cucumis virus 2) are entirel

STAT

Declassified in Part - Sanitized Copy Approved for Release @ 50-Yr 2014/03/07 : CIA-RDP81-01043R004200090004-8

Declassified in Part - Sanitized Copy Approved for Release @ 50-Yr 2014/03/07 : CIA-RDP81-01043R004200090004-8

similar to them. The crystals of yellow turnip mosaic virus are isotropic and consist of octahedra reaching a diameter of 0.1 mm. The crystals of virus of the dwarf tomato shrub (Lucopersicum virus 4) are dodecahedra, and are isotropic. The forms of the crystals of tobacco necrosis virus are highly polymorphic (Fig.4). Its virus forms prisms, hexagonal and pseudohexagonal plates (Bibl.18). As a result of a year-long process of growing, it was possible to obtain crystals of this virus 4.5 mm in size. They may be called the giants among virus crystals (Bibl.19).

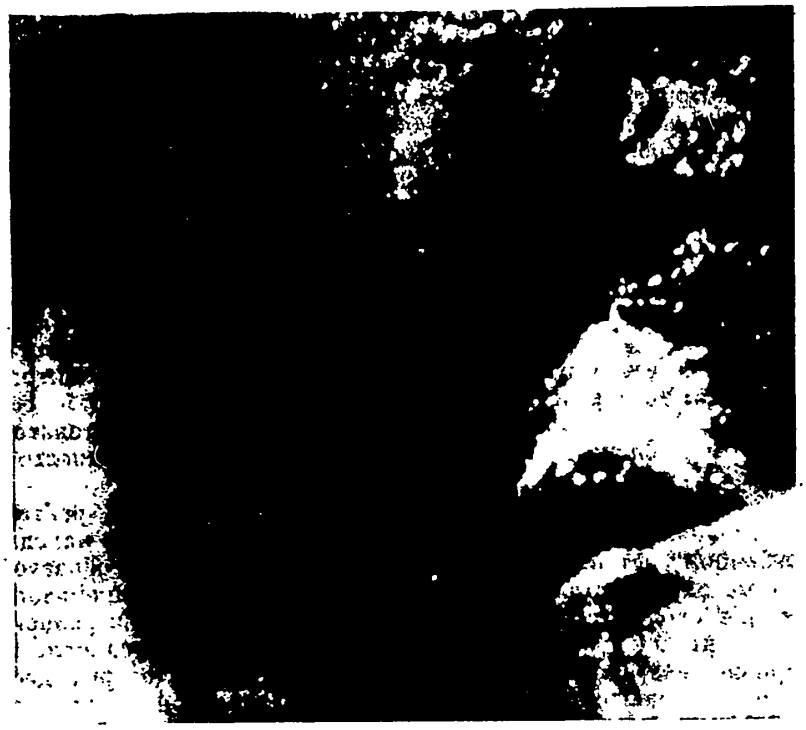

Fig.4 - Crystals of Tobacco Necrosis Virus under the Electron Microscope; the Packing of the Individual Virus Particles Will Be Seen (Bibl.10, 19)

X-ray analysis has shown that all virus crystals contain water of crystallization, as will be seen from the Table of Hodgkin (Bibl.20).

It will be seen from this table that the crystals of yellow turnip mosaic are richest in water. On drying, the distance between the particles decreases by 78 Å,

STAT

Declassified in Part - Sanitized Copy Approved for Release @ 50-Yr 2014/03/07 : CIA-RDP81-01043R004200090004-8

Declassified in Part - Sanitized Copy Approved for Release @ 50-Yr 2014/03/07 : CIA-RDP81-01043R004200090004-8

while the crystals of tobacco necrosis, which are poorest in water, show a decrease of only 22 Å in this distance on drying.

The polyhedral corpuscles encountered in the virus diseases of insects, for instance in the jaundice of the silk worm, are of great interest in this respect. The polyhedral corpuscles in silk worm jaundice were the first virus formations studied crystallographically. Panabianco studied them in detail as far back as 1895. The rather complex structure of these crystalloid formations is rather well known to us today. They have a thin protein sheath and a crystalline protein matrix, containing inclusions of rod-like particles of virus. These particles are about 3000 Å long and about 400 Å in diameter. The amino-acid composition of the proteins of the sheath, the matrix, and of the virus particles is different (Bibl.21). The relatively large size of the polyhedral particles make them fairly available for investigation, although they do consist of rather complex formations. The principle of their structure, however, is the same as that of the smallest resting forms of virus. The virus particles are encrusted in the protein crystal. These structures are so plainly of biological advantage that their very existence makes the hypothesis of the non-living nature of the viruses improbable. Panabianco wrote that he had succeeded in precipitating a polyhedral protein in the crystalline form by acidifying its solutions in sodium acetate. No one has yet succeeded in repeating the Panabianco experiments.

The crystallization of viruses, as we have described it, proceeds under biological conditions. In the protoplasm, one does not encounter either such high concentrations of salts or such an acid reaction of the medium, as when the crystallization of viruses takes place in vitro. In the cells of plants affected by various diseases, however, one does encounter viruses in the crystalline form, and this raises the problem of the conditions of crystallization of viruses within the protoplasm. The virus crystals of tobacco mosaic disease have been extracted from the cells in the frozen state, after which they were fixed and studied under the elec-

STAT

Declassified in Part - Sanitized Copy Approved for Release @ 50-Yr 2014/03/07 : CIA-RDP81-01043R004200090004-8

Declassified in Part - Sanitized Copy Approved for Release @ 50-Yr 2014/03/07 : CIA-RDP81-01043R004200090004-8

tron microscope (Bibl.22). It was shown by this method that about a third of the volume of the crystal consists of water, while the remaining part consists of virus particles. In vitro we observe only paracrystals of tobacco mosaic virus, while in protoplasm it forms true crystals.

Our work, and that of our associates (Bibl.23, 24, 25), throws a certain amount of light on the conditions of crystallization of viruses in the protoplasm. We have shown, for instance, that if a tomato is grown in solutions of red soluble streptocide, then the streptocide is deposited in the form of crystals in the protein clumps of the protoplasm of the cells of the root hairs of the tomato. With the slightest damage to the cells, the crystals of streptocide dissolve just as the cells of the Ivanovskiy cells (crystals of tobacco mosaic virus) dissolve when they are damaged. It is well known that the crystallization of a virus is often connected with amorphous formations (for example, ameboid corpuscles in tobacco mosaic disease). These amorphous formations apparently contain not only the virus, but also protein substances of the protoplasm of the plant itself. The formation of gels in the protoplasm under the influence of the virus creates centers of attraction of the virus particles and of crystallization of the virus.

It was shown, further, that the paracrystalline structures of tobacco mosaic virus easily arise in solutions of hydrophyl colloids (starch paste, water glass, etc.). In the protoplasm, the virus particles interact with the hydrophyl colloids, and this may favor their segregation, leading to the aggregation of virus particles. Finally, we have observed that if a drop of a suspension of virus particles is in a stream, then liquid crystals of virus easily arise in it. Protoplasm is in constant motion, and the currents of protoplasm may favor the regular orientation of the virus particles and thereby create foci of crystallization.

We have given a brief survey of the conditions of formation of crystalline virus particles, and also of their crystalline aggregates. We have glanced at the world of exceedingly peculiar relations, to which it will hardly be easy to apply

STAT

Declassified in Part - Sanitized Copy Approved for Release @ 50-Yr 2014/03/07 : CIA-RDP81-01043R004200090004-8

Declassified in Part - Sanitized Copy Approved for Release @ 50-Yr 2014/03/07 : CIA-RDP81-01043R004200090004-8

our concepts of living and nonliving, developed before the discovery of the world of viruses. The problem of viruses occupies the center of the attention of biologists, and is an important problem in natural science. Virus particles are used not only for studying the problems of variability, reproduction and ontogenesis on the molecular level, but also for the solution of such purely physical problems as the question of the attraction and repulsions of particles at a distance. Viruses still remain the simplest forms of life, morphologically and chemically, which are known to biology, but at the same time they form the most peculiar crystals the crystallographer has ever encountered. Perhaps, although only for this reason, they deserve more attention from crystallographers than they have been given up to now.

BIBLIOGRAPHY

1. Goldacre,R. - Nature, Vol.174,4433 (1954),pp.732-734
2. Bernala,I.D. and Fan-Kuchen,I. - Journ.Gener.Physiol., Vol.25,No.1 (1941),p.111
3. Ryzhkov,V.L. - Zhurn.Obshch.Biolog., Vol.16,No.3,pp.238-247
4. Franklin,R.E. - Nature, Vol.175,4452 (1955),pp.379-381
5. Franklin,R.E. and Klug,A. - Biochim.Biophys.Acta, Vol.19,No.3 (1956),pp.403-418
6. Koehler,E. and Bode,B. - Electron Microscope Study of Tobacco Mosaic Virus. Naturwiss., Vol.38,No.18 (1951),p.431
7. Sukhov,K.S. and Nikiforov,G.S. - Dok. AN SSSR, Vol.90,No.4 (1954),pp.671-672
8. Schramm,G. - Advance Enzymology, Vol.15 (1954),pp.449-484
9. Bernala,I.D. and Carlisle,C.H. - Nature, Vol.162 (1948),p.139
10. Markham,R. - Chemistry of Some Functional Component of Viruses. Cold Spring Harbor Symposia on Quant.Biol., V. XVIII (1953), Viruses pp.141-148
11. Engels,F. - The Dialectics of Nature. Gospolitizdat (1948)
12. Watson,J.D. and Crick,F. - The Structure of DMA. Cold Spring Harbor Symposium on Quant.Biol., V, XVIII (1953), Viruses,pp.141-148
13. Pasteur,L. - Tartaric Acid, and Its Significance for the Study of the Structure

STAT

Declassified in Part - Sanitized Copy Approved for Release @ 50-Yr 2014/03/07 : CIA-RDP81-01043R004200090004-8

Declassified in Part - Sanitized Copy Approved for Release @ 50-Yr 2014/03/07 : CIA-RDP81-01043R004200090004-8

of Matter. St.Petersburg (1894)

14. Rich,A. and Dunitz,J. - Nature, Vol.175,4468 (1955),pp.1074-1075
15. Franklin,R. - Nature, Vol.175,4468 (1955),pp.676-677
16. Fraenkel-Conrad,H. and Williams,R. - Proc.Nat.Ac.Sc., Vol.41,No.10 (1955), pp.690-698
17. Lippincott,I. and Commoner,B. - Biochimica et Biophysica Acta, Vol.19,No.1, pp.198-199
18. Ryzhkov,V.L. - Principles of the Study of Virus Plant Diseases. Moscow (1944)
19. Crowfoot,D. and Schmidt,G. - Nature, Vol.155,3939 (1945),pp.504-505
20. Hodgkin,D.C. - X-ray Analysis and Protein Structure. Cold Spring Harbor Symposia on Quant.Biol., Vol.XIV (1950)
21. Ryzhkov,V.L. - The First Crystallographic Work on Viruses. Mikrobiol., Vol.25, No.1,pp.125-127
22. Sterrea,R. and Williams,R. - Identification of Crystalline Inclusion Bodies Extracted Intact from Plant Cells Infected with Tobacco Mosaic Virus. Amer. Journ.Bot., Vol.40,No.2 (1953),pp.81-84
23. Ryzhkov,V.L. and Smirnova,V.A. - Dok. AN SSSR, Vol.31,No.9 (1941)
24. Ryzhkov,V.L. and Smirnova,V.A. - Zhurn.Obshch.Biologii, No.3 (1942)
25. Ryzhkov,V.L. - Dok. AN SSSR, Vol.47,No.7 (1945)

STAT

Declassified in Part - Sanitized Copy Approved for Release @ 50-Yr 2014/03/07 : CIA-RDP81-01043R004200090004-8

Declassified in Part - Sanitized Copy Approved for Release @ 50-Yr 2014/03/07 : CIA-RDP81-01043R004200090004-8

SOME QUESTIONS ON THE KINETICS OF CRYSTAL GROWTH

by

V.A.Koptsik

1. The Introduction of the Linear Parameters of Crystallization

We shall term linear parameters of crystallization certain quantities of dimension of length l_i, in terms of which the total surface, volume and mass of the crystal at any time t may be expressed:

$$S = S[l_i(t)], \quad V = V[l_i(t)], \quad m = m[l_i(t)]. \tag{1}$$

After the initial period of regeneration of the crystal seed, a time usually arrives when the crystal grows in the form of a convex polyhedron with a relatively small number of faces.

For such a crystal the form of the functions (1) can be obtained with relative ease by using the crystallographic data obtained on the basis of the law of constant angles.

Thus, for the case of crystals of potassium orthophosphate, KH_2PO_4, the usual form of which is composed of a combination of the faces of a tetragonal prism and a dipyramid (Fig.1), we get:

$$\left.\begin{aligned} S &= 5{,}44\,ah - a^2, \\ m &= \rho\,(1{,}36\,a^2h - 0{,}62\,a^3), \\ \frac{dm}{dt} &= \rho\left(2{,}72\,ah\,\frac{da}{dt} + 1{,}36\,a^2\frac{dh}{dt} - 1{,}86\,a^2\frac{da}{dt}\right), \end{aligned}\right\} \tag{2}$$

STAT

Declassified in Part - Sanitized Copy Approved for Release @ 50-Yr 2014/03/07 : CIA-RDP81-01043R004200090004-8

Declassified in Part - Sanitized Copy Approved for Release @ 50-Yr 2014/03/07 : CIA-RDP81-01043R004200090004-8

For crystals of resorcinol, $C_6H_4(OH)_2$, the form of which is composed of a combination of rhombic prisms and two dihedra (Fig.2), we have

$$\left.\begin{aligned} S &= 2{,}60\,ac + 9{,}97\,a^2, \\ m &= \rho\,(0{,}59\,a^2c - 0{,}14\,a^3), \\ \frac{dm}{dt} &= \rho\,(1{,}18\,ac - 0{,}42\,a^2)\frac{da}{dt} + 0{,}59\,\rho a^2\frac{dc}{dt} \end{aligned}\right\} \qquad (3)$$

For crystals of rochelle salt, $KNaC_4H_4O_6 \cdot 4H_2O$, formed by a combination of rhombic prisms and three pinacoids (Fig.3) we obtain in the same way:

$$\left.\begin{aligned} S &= 0{,}53\,b^2 + 2{,}85\,bc, \\ m &= 0{,}53\,\rho b^2c, \\ \frac{dm}{dt} &= 0{,}53\,\rho b^2\frac{dc}{dt} + 1{,}06\,\rho bc\frac{db}{dt}. \end{aligned}\right\} \qquad (4)$$

Figure 4 shows the apparatus used by us for growing rochelle salt crystals under dynamic conditions (see also Fig.2, page 259). A substantial part of the apparatus is the cathetometer with a vertical scale and a horizontal scale; the accuracy of the readings with both verniers is 0.02 mm. This cathetometer permitted the measurement of the parameters l_i without disturbing the crystallization conditions. Similar apparatus was used by us for growing crystals of potassium orthophosphate and resorcinol as well.

The sizes of the KH_2PO_4 crystals, in view of the short duration of the experiments (several minutes) were measured by a micrometer with accuracy of 0.01 mm only twice, at the beginning and end of the experiment. The sizes of the resorcinol crystals were determined by comparing the crystals with scales placed close to them. A graphic correction of the data so obtained at two points (results of measurements of crystals by the micrometer before and after the conclusion of the experiment) permits their accuracy to be estimated at 0.5 mm.

2. Some Experimental Results

The experiments on the crystallization of rochelle salt were staged with a

STAT

Declassified in Part - Sanitized Copy Approved for Release @ 50-Yr 2014/03/07 : CIA-RDP81-01043R004200090004-8

Declassified in Part - Sanitized Copy Approved for Release @ 50-Yr 2014/03/07 : CIA-RDP81-01043R004200090004-8

methodological object in a student special practical course given by the Department of Crystal Physics at Moscow State University. The crystallization was conducted in the temperature range of 20 - 35°C on the apparatus described in the preceding Sec-

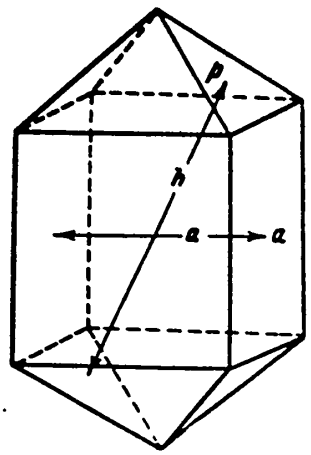

Fig.1 - Crystal of KH_2PO_4. The angles between the normals to the faces of the tetragonal prism a {100} and the dipyramid p {101} : $(\widehat{a,p}) = 46°56'$

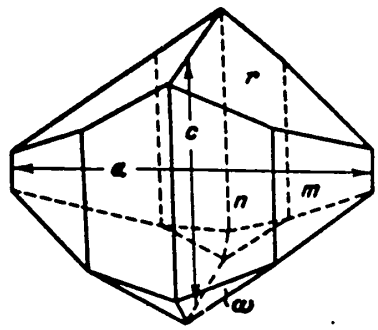

Fig.2 - Crystal of Resorcinol. The angles between the normals to the faces of the dihedron r {101} , the rhombic prisms m {110} , n {120} and the axis a; $(\widehat{m,a}) = 42°19'$; $(\widehat{n,a}) = 61°31'$; $(\widehat{r,a}) = 59°17'$

tion. The seed crystals used were well-shaped crystals attached to a stationary platform; the mean rate of mixing of the solution with the stirrer was 80 - 100 rpm.

On the conclusion of the period of regeneration, the linear dimensions b and c of the crystals were measured every half hour by the aid of the cathetometer, and the surface and mass of the crystal were calculated by eq.(4). Figures 5 and 6 give the results of the measurements and calculations for five experiments; the subscripts of the corresponding letters denote the experiment number. The mean relative supersaturation in experiments 1 - 5 (0.014; 0.020; 0.006; 0.010 and 0.006 respectively) were maintained during the time of growth by appropriate lowering of the temperature.

Analyses of these data show that the velocities λ_b, λ_c and dm/dt, according to

STAT

Declassified in Part - Sanitized Copy Approved for Release @ 50-Yr 2014/03/07 : CIA-RDP81-01043R004200090004-8

Declassified in Part - Sanitized Copy Approved for Release @ 50-Yr 2014/03/07 : CIA-RDP81-01043R004200090004-8

the theory, depend linearly on the supersaturation. At low relative supersaturations (< 0.01) the velocities λ_b and λ_c are practically equal; at elevated super-

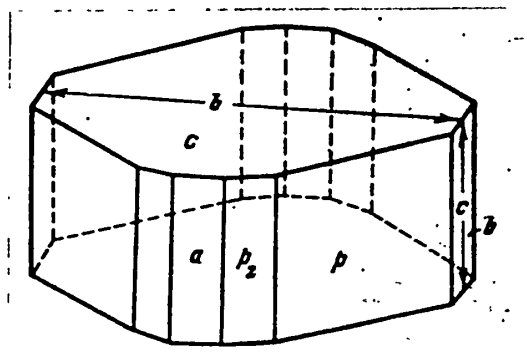

Fig.3 - Crystal of Rochelle Salt. Angles between the normals to the faces of the pinacoids a {100} , b {010} , c {001} and the rhombic prisms p {110} , p_2 {210} : $(\widehat{p,a}) = 39^\circ 43'$

$(\widehat{p_2 a}) = 22^\circ 35'$

saturations, a distinct tendency to the more rapid growth of the velocity λ_b is noted; in experiments 1 and 2, the mean velocities λ_b (1.0 and 1.8 mm/hr) are 2.5 times as great as the mean velocities λ_c.

If the graphs we have presented are available, it is possible, by controlling the supersaturation, to realize crystallization conditions at constant linear velocities of growth of the faces, which best correspond to the conditions for obtaining uniform crystals. In this case one may assure considerably higher velocities of crystal growth than those used in technology under similar conditions (Bibl.1,2). In our experiments, the mean relative supersaturation calculated per square centimeter of growing surface (0.002 - 0.004 cm^{-2}) was two or three times as great as the recommended value (Bibl.1). It likewise proved possible, in order to accelerate the initial period of regeneration and growth of the crystal, to permit for a short time (about an hour) even considerably higher relative supersaturations (0.007 and 0.013 cm^{-2} in experiments 1 and 2).

Let us evaluate the sensitivity of this method of control of the linear par-

STAT

Declassified in Part - Sanitized Copy Approved for Release @ 50-Yr 2014/03/07 : CIA-RDP81-01043R004200090004-8

Declassified in Part - Sanitized Copy Approved for Release @ 50-Yr 2014/03/07 : CIA-RDP81-01043R004200090004-8

ameters of crystallization. The curve of dm_2/dt given on Fig.6, constructed by graphic differentiation of the curve of $m_2(t)$, has a characteristic stepped form. Constant velocity dm/dt is reached under the condition $\sum_i S_i(t)\,\lambda_i(t) = \text{const}$, i.e., under the condition of the monotone decline of the velocities $\lambda_i(t)$.

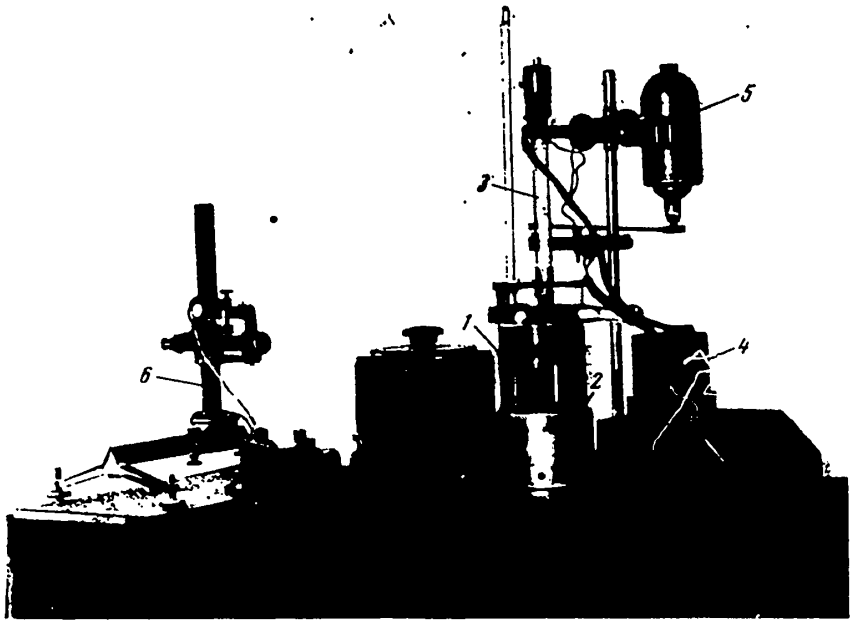

Fig.4 - Automatic Laboratory Apparatus for Rapid Growing of Crystals from Solutions:

1 - Crystallizer; 2 - Heater; 3 - Contact thermometer; 4 - Relay; 5 - Electric motor; 6 - Cathetometer

To the first flat part of the curve there corresponds a sharp fall in the velocity λ_b (see Fig.5), connected with the removal of the excess supersaturation, assigned during the initial period of growth; to the second flat region corresponds the natural removal of supersaturation on account of the growth of the crystal. The two rises with which the curve ends correspond to an increase in the relative supersaturation of the solution by 0.004, due to the twice repeated lowering of the temperature by 0.1°C (after five hours and six and a half hours of growth). Experi-

STAT

Declassified in Part - Sanitized Copy Approved for Release @ 50-Yr 2014/03/07 : CIA-RDP81-01043R004200090004-8

Declassified in Part - Sanitized Copy Approved for Release @ 50-Yr 2014/03/07 : CIA-RDP81-01043R004200090004-8

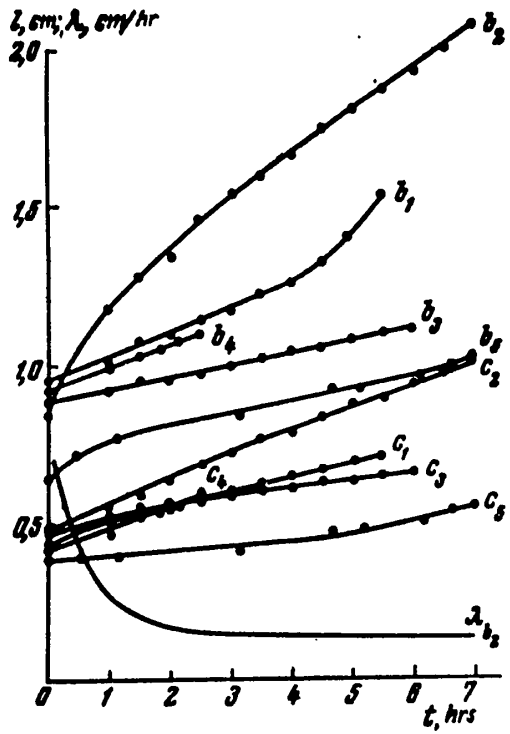

Fig.5 - Variation of Linear Parameters p, b, c on Growth of a Rochelle Salt Crystal in Experiments No.1-5; the Curve $\lambda b_2(t)$ Was Constructed by Graphic Differentiation of the Curve $b_2(t)$

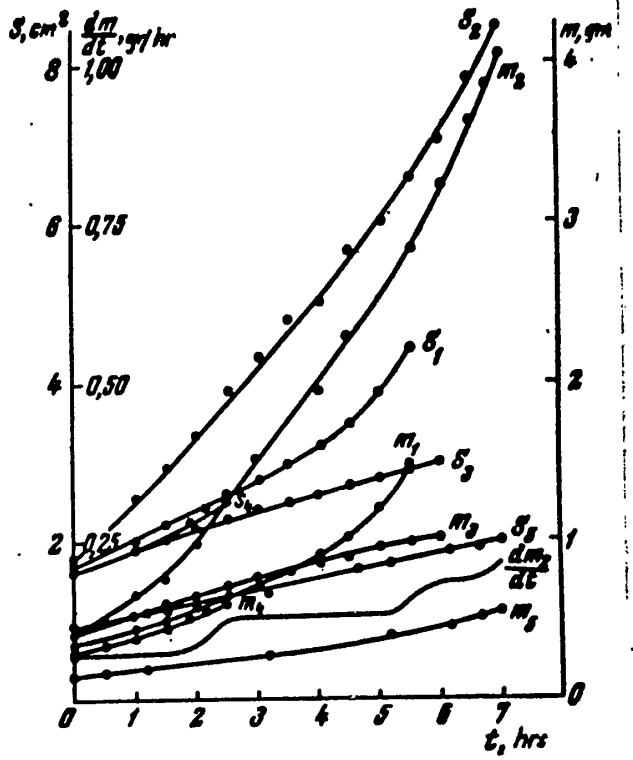

Fig.6 - Variation of Surface and Mass during Growth of Rochelle Salts Crystal in Experiments No.1-5; the Curve dm_2/dt Was Constructed by Graphic Differentiation of the Curve $m_2(t)$

STAT

Declassified in Part - Sanitized Copy Approved for Release @ 50-Yr 2014/03/07 : CIA-RDP81-01043R004200090004-8

Declassified in Part - Sanitized Copy Approved for Release @ 50-Yr 2014/03/07 : CIA-RDP81-01043R004200090004-8

ence shows that a half-hour time interval is entirely sufficient to determine, from the character of the kinetic curves, the variations that have taken place in the system and to introduce the necessary corrections if required.

Let us pass to a description of the results in growing single crystals of potassium orthophosphate. With the object of studying the influence of various factors under kinetic crystallization, we staged a series of experiments in which we varied, as far as possible, only a single parameter, holding the others constant. Table 1 presents the necessary information.

In experiments 1 - 8', the crystal seeds used were crystalline spheres, while in experiments 9 - 13', they were shaped crystals. The seeds were introduced into a system with already assigned supersaturation. In the experiments not denoted by a prime, the crystals were given a planetary rotation, in the others, an axial rotation, and in experiment 10*, the crystal was not rotated. In the last two columns of the table we give the mean velocities $\Delta m/\Delta t$, determined experimentally from the known difference of weight Δm and difference of the crystallization time Δt, and those calculated theoretically by eq.(2), for the case of the growth of a crystal on a full-face crystal seed, and by the formula

$$\frac{dm}{dt} = \rho\left(1{,}36\, a^2 \frac{dh}{dt} + 0{,}86\, a^2 \frac{da}{dt} + 3{,}14\, a^2 \frac{dc}{dt}\right) \qquad (5)$$

for the case of growth on a spherical seed, where dc/dt is a certain mean linear velocity of regeneration of the sphere. The good agreement between the two series of figures permits us to hold that formulas of the type of eq.(2) or eq.(5) respectively, are suitable for describing the kinetics of crystal growth at any stage.

Analysis of the data of the table shows that the most powerful factors influencing the kinetics of crystallization are the structural facts determining the form of the surface of the phase transition, and its free surface energy in the given solution. Indeed, the velocities of growth of the crystal during the period

STAT

Declassified in Part - Sanitized Copy Approved for Release @ 50-Yr 2014/03/07 : CIA-RDP81-01043R004200090004-8

Declassified in Part - Sanitized Copy Approved for Release @ 50-Yr 2014/03/07 : CIA-RDP81-01043R004200090004-8

of regeneration are tens of times greater than the velocities of growth of a shaped crystal (Fig.7). The decrease in growth with time is connected with the growth of

Table 1

Data on the Kinetics of Growth of KH_2PO_4 Crystals

a)	T, °C	b)	c)	Δt, min.	d)		e)		f)		g)	
					a, cm	h, cm	Δa, cm	Δh, cm	Δa/Δt, cm/min 10⁶	Δh/Δt, cm/min 10⁶	h)	i)
1	57	0,12	78	1	0,427		0,010	0,016	1000	1600	9025	8100
2				3	0,400		0,018	0,037	600	1230	1970	1873
3				8	0,362		0,013	0,057	160	700	637	633
4				15	0,392		0,021	0,111	140	740	640	611
1'				1	0,430		0,010	0,013	1000	1300	9170	8700
2'				3	0,395		0,014	0,033	470	1110	1700	1730
3'				8	0,301		0,006	0,040	76	500	338	335
4'				15	0,393		0,011	0,069	70	460	424	453
5	19	0,15	78	5	0,478		0,001	0,020	0	400	1420	1400
6				30	0,454		0,016	0,088	54	290	384	369
7	30	0,15	78	5	0,334		0,001	0,020	20	400	670	542
8				15	0,346		0	0,067	0	450	300	310
7'				5	0,323		0,002	0,017	20	340	520	524
8'				15	0,396		0	0,046	0	307	334	351
9			48	10	0,465	0,533	0	0,035	0	350	200	238
10*			0	30	0,465	0,568	0,002	0,056	6	187	127	131
11	25	0,27	78	15	0,398	0,464	0,046	0,094	300	625	534	446
11'				15	0,397	0,425	0,025	0,052	170	350	273	239
12			0	15	0,449	0,533	0,036	0,070	240	470	494	449
13				15	0,444	0,558	0,043	0,081	286	540	587	540
12'				15	0,440	0,478	0,007	0,060	50	400	266	268
13'				15	0,422	0,477	0,001	0,075	7	500	247	284

a) Experiment No.; b) Relative supersaturation; c) Rate of rotation, rpm; d) Initial dimensions of crystal; e) Growth by end of experiment; f) Mean velocity of growth; g) Mean velocity of growth of mass, $\Delta m/\Delta t$, gm/min; h) $10^5 \times$ Experimental value; i) $10^5 \times$ Theoretical value

the faces, with the greater surface energy, and with the decrease, in this connection, of the total surface of the growing crystal and of its free energy calculated

STAT

Declassified in Part - Sanitized Copy Approved for Release @ 50-Yr 2014/03/07 : CIA-RDP81-01043R004200090004-8

Declassified in Part - Sanitized Copy Approved for Release @ 50-Yr 2014/03/07 : CIA-RDP81-01043R004200090004-8

per unit mass (the total form of the KH_2PO_4 crystal consists only of the combination of a tetragonal prism and a dipyramid). It is interesting to note that the linear velocity of growth of the faces of the dipyramid is several times greater than the velocities of growth of the faces of the prisms. In a number of cases, after 10 - 15 min from the beginning of crystallization, the faces of the prisms practically stop growing, in spite of the existence of a finite supersaturation of the solution.

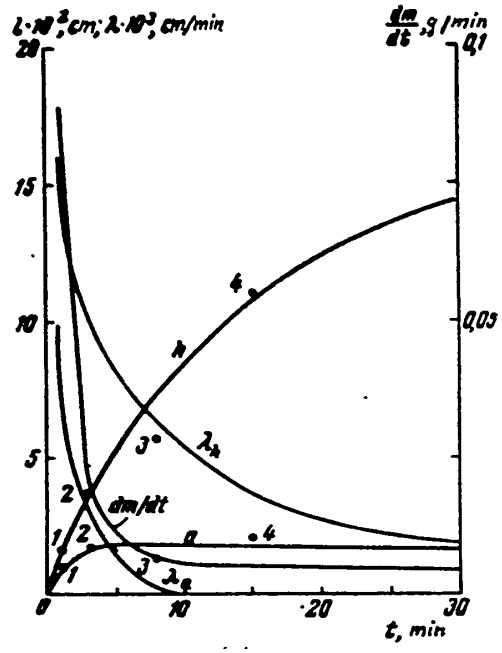

Fig.7 - Variation of Linear Parameters a, h during Growth of KH_2PO_4 Crystal in Experiments No.1-4; the Curves of λ_h and λ_a Were Constructed by the Graphic Differentiation of the Curves h(t) and a(t); the Curve of dm/dt Was Constructed from Table 1

As will be easily seen, the strong influence of the structural factors on crystallization masks the expected linear dependence of the velocities of growth on the supersaturation. At the same time, the existence of a dependence of the velocities of growth on the rate of mixing of the solution (compare the data of experiments 1 -

STAT

Declassified in Part - Sanitized Copy Approved for Release @ 50-Yr 2014/03/07 : CIA-RDP81-01043R004200090004-8

Declassified in Part - Sanitized Copy Approved for Release @ 50-Yr 2014/03/07 : CIA-RDP81-01043R004200090004-8

- 4 and 1' - 4', 9 and 10*, 8 and 9, 11 and 12) confirms the fact that crystallization is accomplished in the kinetic region. It is interesting to note that this dependence is not observed during the initial period of regeneration.

Thus, in the kinetic experiments, the only quantities that are fully comparable are the statistical mean values or results relating to one and the same crystal, provided the measurements are made without disturbing the crystallization conditions.

In the case of resorcinol, an extremely strong dependence of the kinetics of crystal growth on structural factors is observed. The experiments on growing resorcinol from aqueous solutions, each lasting from 10 to 158 hrs, were run at temperatures from 42 to 22°C at relative supersaturations of the solution ranging from 0.005 to 0.15. The crystal seeds, of mean size 0.5 - 1.0 cm, were rigidly attached to the platform or crystal carrier; the solution was mixed by a stirrer at a speed of 60 - 80 rpm.

Under these conditions we found that the linear velocities λ_c, measured in opposite directions along the c axis, differ by one order of magnitude; sometimes the crystallization in one of these directions stops completely, in spite of the existence of a finite supersaturation of the solution. At small relative supersaturations (< 0.02), the velocities λ_a and the maximum velocity λ_c are approximately equal (about 0.5 mm/hr). At elevated supersaturations, there is a vigorous growth of the crystal along one of the directions of the c axis, accompanied by absorption of the mother liquor, at a velocity of 1.5 - 2.5 mm/hr. Under the same conditions, however, the pyramids of growth of the faces of the prismatic belt remain pure, since the velocities λ_a, of the order of 0.7 mm/hr, show almost no increase.

We note that the data here presented makes no claim to being an exhaustive description of the entire group of phenomena that accompany the growth of crystals. They are intended rather to illustrate the character of the conclusions that may be drawn on the basis of a control of the linear velocities of crystal growth, and to appraise the possibilities of this method. Additional material on this question

STAT

Declassified in Part - Sanitized Copy Approved for Release @ 50-Yr 2014/03/07 : CIA-RDP81-01043R004200090004-8

Declassified in Part - Sanitized Copy Approved for Release @ 50-Yr 2014/03/07 : CIA-RDP81-01043R004200090004-8

will be presented in other papers of this series.

BIBLIOGRAPHY

1. Vitovskiy,B.V. - Rochelle Salt Crystals (Properties, Technology of Growing the Crystals, and of Manufacture of Piezo Elements). Dissertation. Institute of Crystallography, Academy of Sciences USSR, Moscow (1948)

2. Ansheles,O.M., Tatarskiy,V.B., and Shternberg,A.A. - The Rapid Growing of Crystals from Solutions. The Crystallization of Rochelle Salt, Lenizdat (1945)

STAT

Declassified in Part - Sanitized Copy Approved for Release @ 50-Yr 2014/03/07 : CIA-RDP81-01043R004200090004-8

Declassified in Part - Sanitized Copy Approved for Release @ 50-Yr 2014/03/07 : CIA-RDP81-01043R004200090004-8

EXPERIENCE OF THE WORK OF THE STUDENT PRACTICAL COURSE IN THE TECHNOLOGY OF ARTIFICIAL CRYSTAL GROWING

by

N.L.Pokrovskiy

In connection with the necessity of training specialists in crystal physics, who are also acquainted with the technique of artificial crystal growing, a special practical course on crystal growth was organized in the department of crystallography, which was organized in 1953 under the Faculty of Physics, Moscow State University. This article is devoted to a description of its work.

The practical course consists of two groups of problems, the first connected directly with the technology of artificial growing of crystals from solutions and melts, and the second devoted to the study of phase transformations.

In organizing the practical course, we attempted, on the one hand, to utilize the principles and procedures of industrial methods of producing crystals, and on the other hand we also attempted to have the students accumulate new experimental data which might be the object of short scientific papers.

Tasks of the First Group. Let us consider the problem in which the technique of construction of a solubility curve is expounded. As applied to this problem, the method of shadow projection is very lucid and graphic, and makes it possible to get a clear idea of the conditions under which the growth of crystals is possible. This method allows the observation, in definite sequence, of the so-called concentration currents of dissolution and crystal growth; their disappearance, consequently, cor-

STAT

Declassified in Part - Sanitized Copy Approved for Release @ 50-Yr 2014/03/07 : CIA-RDP81-01043R004200090004-8

Declassified in Part - Sanitized Copy Approved for Release @ 50-Yr 2014/03/07 : CIA-RDP81-01043R004200090004-8

responds to the condition of dynamic equilibrium, when the velocity of dissolution and the velocity of growth of the crystal are equal.

Figure 1 shows a schematic diagram of apparatus on which the concentration currents are observed. It is extremely simple and may be accomplished by ordinary means. The ray from the point light source S, passing through the lens L_1, forms a homogeneous beam. On its path is placed the plane-parallel cell G with the test

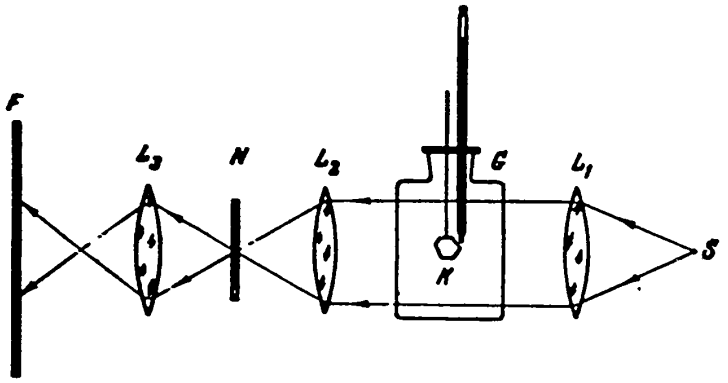

Fig.1 - Optical Diagram of Method of Shadow Projection

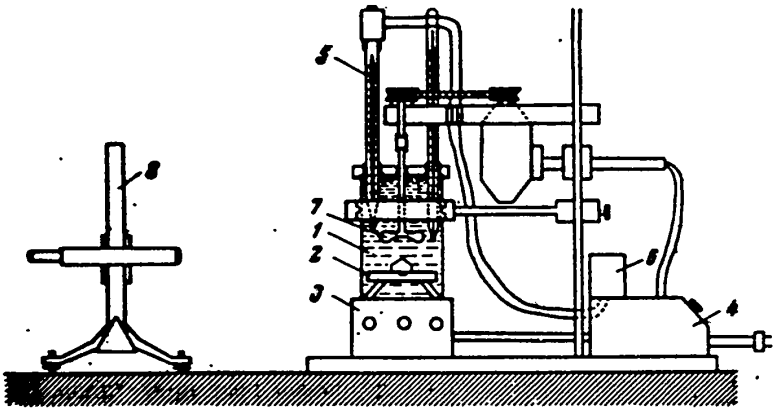

Fig.2 — Schematic Diagram of Crystallization Apparatus for Growing Crystals from a Solution

solution. In the solution is submerged a crystal of the salt, whose solubility is determined. The lens L_2 forms an image of the lamp filament in the plane of the slit N. Under this condition, any inhomogeneities in the test solution, and, in

STAT

Declassified in Part - Sanitized Copy Approved for Release @ 50-Yr 2014/03/07 : CIA-RDP81-01043R004200090004-8

Declassified in Part - Sanitized Copy Approved for Release @ 50-Yr 2014/03/07 : CIA-RDP81-01043R004200090004-8

particular, any concentration currents around the crystal placed in the solution, will cause a bending of the rays of light, which are focused by the lens L_3 on the screen F. As a result we get on the screen F an image of the crystal and of the inhomogeneities of the medium around it in the form of concentration currents.

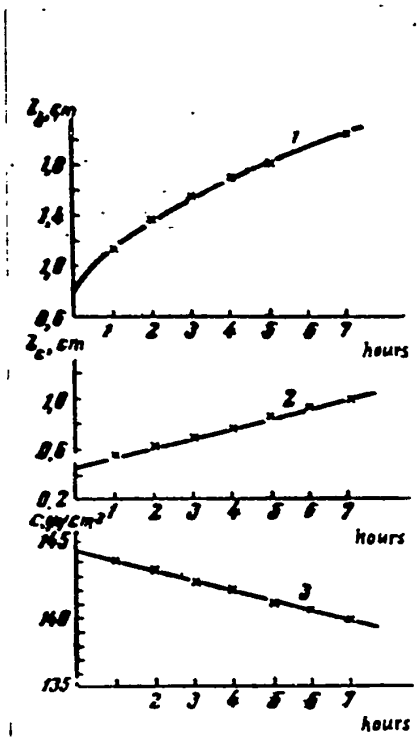

Fig.3 - Kinetic Curves of Growth of a Rochelle Salt Crystal; 1,2 - Variation of Linear Dimensions of Crystal Along b and c axes; 3 - Variation of Concentration of Rochelle Salt Solution with Time

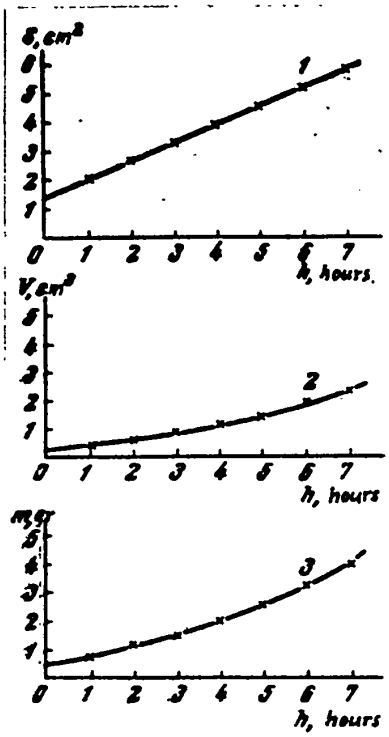

Fig.4 - Kinetic Curves of Growth of Rochelle Salt Crystal; Increase of Its Surface 1, Volume 2, and Weight 3

The saturation temperature is determined more sharply from the extinction of the crystallization "film". By this method the saturation temperature is determined with accuracy ± 0.2°C.

If data on the solubility of the salt under study are available, we proceed to

STAT

Declassified in Part - Sanitized Copy Approved for Release @ 50-Yr 2014/03/07 : CIA-RDP81-01043R004200090004-8

Declassified in Part - Sanitized Copy Approved for Release @ 50-Yr 2014/03/07 : CIA-RDP81-01043R004200090004-8

the growing of the single crystal. In this case we take the kinetic curve of its growth. Figure 2 schematically represents the crystallization apparatus. Its design is not original, but represents on a small scale one of the modern crystallization plants with "isothermal" insulation. Such installations (Bibl.1, 2) which appeared 10 or 15 years ago, are not built on the principle of adiabatic insulation of the system, but on the principle of the constant relation between the heat flows brought into the system and those taken out of it.

The principal parts of our apparatus are as follows: the crystallizer 1 with the platform for attaching the crystal 2, the heater 3, the block for feeding the entire apparatus and regulating the temperature 4, connected with the contact thermometer 5 and the relay 6, and the electrically driven stirrer 7. The cathetometer 8 performs very substantial functions in our crystallization apparatus. By its aid we take the dimensions of the growing crystal. The presence of a cathetometer in the apparatus permits us to depart from the usual qualitative observations of the growth of crystals and to pass to quantitative measurements. Figures 3 and 4 show kinetic characteristics of the growth of a single crystal of rochelle salt, plotted from the data of one of the student projects. From these curves definite conclusions can be drawn on the linear velocity of crystal growth, and one can judge the quantity of substance passing out of solution into the crystalline phase, the total surface in weight of the crystal, and the variations in the concentration of the solution. Our attention is struck by the difference in the linear velocities of growth along the c and b axes. While the linear velocity of growth in the direction $\bar{c}$ is constant (Fig.3, curve 2), on the b axis it is, in the first place, somewhat greater, and in the second place it is not constant (Fig.3, curve 1). On our apparatus a series of experiments on the crystallization of rochelle salt was run by the students. The experimental results obtained were worked up and have been presented at this Conference*.

* See in this symposium the paper: V.A.Koptsik. Some questions (Cont'd on next page)

STAT

Declassified in Part - Sanitized Copy Approved for Release @ 50-Yr 2014/03/07 : CIA-RDP81-01043R004200090004-8

Declassified in Part - Sanitized Copy Approved for Release @ 50-Yr 2014/03/07 : CIA-RDP81-01043R004200090004-8

To familiarize the student with the technology of growing single crystals from a melt, the practical course disposes of apparatus based on the Kyropoulos method (Bibl.2). In a relatively simple experimental shape, this method assures the production of very perfect crystals of large size. As in the first problem, we attempted to bring our apparatus close to the most modern prototype. We succeeded in

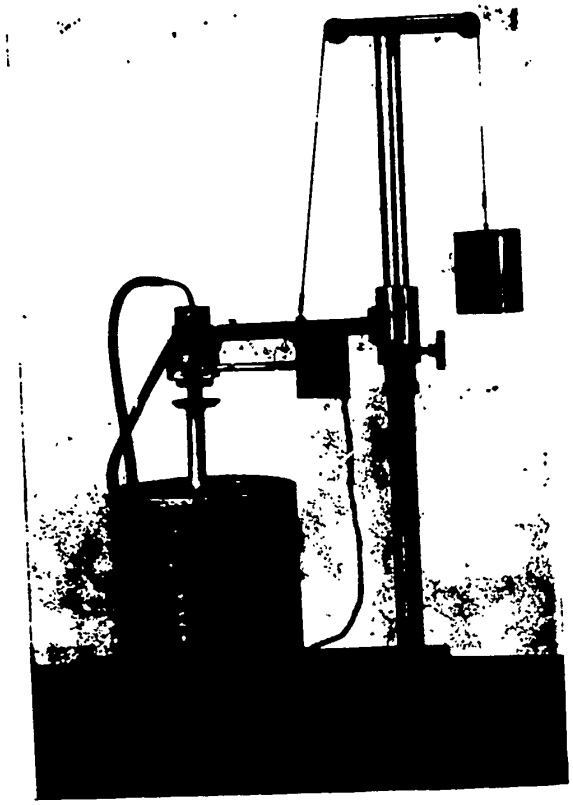

Fig.5 - Apparatus for Growing Crystals from a Melt by the Kyropoulos Method

constructing such an apparatus, based on a design developed at the Institute of Crystallography. The photograph of the apparatus (Fig.5) will give a sufficiently complete idea of it. The apparatus has a device for rotating the cooler together with the growing crystal. Under this condition the irregularities of the tempera-

* (Cont'd) of the kinetics of crystal growth.

STAT

Declassified in Part - Sanitized Copy Approved for Release @ 50-Yr 2014/03/07 : CIA-RDP81-01043R004200090004-8

Declassified in Part - Sanitized Copy Approved for Release @ 50-Yr 2014/03/07 : CIA-RDP81-01043R004200090004-8

ture field around the growing crystal have less of an effect. The temperature is maintained by an automatic electronic heat regulator with an accuracy of ± 2 - 3°C. The clockwork mechanism adopted by us to the heat regulator permits a programmed lowering of temperature during the process of crystal growth. On this installation the alkali halide crystals of KCl and KBr are grown.

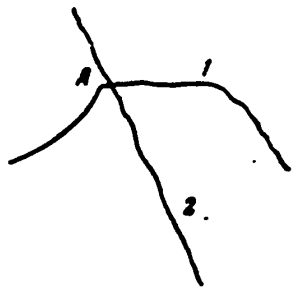

Fig.6 - On the Question of the Study of Phase Transition of the Second Kind

1 - Heating curve of nickel and copper specimens, measured by a differential thermocouple;

2 - Heating curve of a nickel specimen measured by a simple thermocouple. Point A corresponds to the beginning of the transition of nickel to the paramagnetic state (Curie point)

Besides these installations, the practical course also disposes of an extremely simple apparatus according to the Obreimov-Shubnikov method for preparing single crystals of the low-melting metals Zn, Sn, etc.

The problems on growing crystals include the preparation by the A.V.Shubnikov method (Bibl.3) of piezoelectric textures on a metal base. The preparation of this type of piezo elements requires no special apparatus whatever. But only the careful performance of the corresponding operations will assure the experimenter of obtaining piezo elements of the required quality. The final part of this problem, after the texture has matured, consists in testing the piezo elements so produced.

For studying certain features of crystal growth the students are instructed to stage experiments on microcrystallization. Using the microscope for this purpose, the processes of crystallization in a drop are observed under ordinary and polarized light. In these experiments the process of formation of solitary crystals can be observed, the influence of undercooling on the shape of the crystals can be fol-

STAT

Declassified in Part - Sanitized Copy Approved for Release @ 50-Yr 2014/03/07 : CIA-RDP81-01043R004200090004-8

Declassified in Part - Sanitized Copy Approved for Release @ 50-Yr 2014/03/07 : CIA-RDP81-01043R004200090004-8

lowed, the formation of the textures there arising as a result of the action of the "law of geometrical selection" can be seen, and the student can become familiarized with the phenomena of polymorphism from the example of ammonium nitrate. The number of such extremely instructive experiments is very great and varied (Bibl.1, 4, 5). Here we have indicated only some of them. As objects of study for these purposes, many low-melting organic substances may be used (thymol, salol, paratoluidine, coumarin, resorcinol, naphthalene, and many others). Salol can be particularly recommended for these experiments.

The problems of the second group begin with the study of the technique of constructing phase diagrams from the example of a system phenol-water. In spite of the simplicity of the technique of doing this problem, this system combines very important elements of the phase diagrams, such as, for instance, the presence of a eutectic, the limited solubility of the participating components, and other important details.

In the next problem the students become acquainted with the method of taking heating and cooling curves by the aid of a Kurnakov pyrometer. The phenomena accompanying the process of transition from the liquid state to the solid state, are particularly clear and striking in studying the heating and cooling curves. These curves distinctly show breaks corresponding to the temperatures at which the various phase transitions take place.

In recent years the method of taking heating and cooling curves has become an independent field of scientific research, which is known as thermography (Bibl.6). The Kurnakov pyrometer (Bibl.7) has played an important part in its development, and the constant improvement of this instrument over the course of more than 15 yrs led in 1952 to the creation of a small PK-52 apparatus which does not require a special darkened room (Bibl.8).

We have used the Kurnakov pyrometer for the solution of the simplest problems of phase analysis. They include the taking of heating and cooling curves on tran-

STAT

Declassified in Part - Sanitized Copy Approved for Release @ 50-Yr 2014/03/07 : CIA-RDP81-01043R004200090004-8

Declassified in Part - Sanitized Copy Approved for Release @ 50-Yr 2014/03/07 : CIA-RDP81-01043R004200090004-8

sition from a liquid state to the solid, and a study of the polymorphic transformations during the processes of dehydration.

Of interest is the attempt to utilize the Kurnakov pyrometer for investigating what are called phase transitions of the second kind, which, in contrast to phase transition of the first kind, are not accompanied by thermal effects. They include, for example, the transition of a ferromagnetic substance to the paramagnetic state, of ferroelectric substances to dielectric substances, and a number of other phenomena.

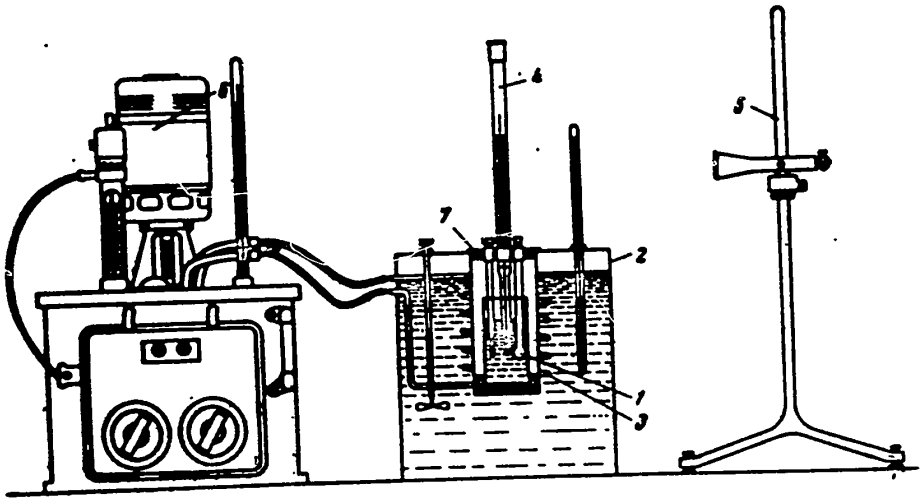

Fig.7 - Schematic Diagram of Calorimetric Installation

To elucidate this type of possibilities, we made use of the data of Sykes and Moser (Bibl.9), who found that, in the region of the Curie point, the heat capacity of nickel actually does pass through a distinct maximum. Thus, if we take two specimens, one of which is nickel, and the other, for instance, is copper, and their masses are so selected that the rates of heating shall be as equal as possible, then in the region of the Curie point (357°C), the rate of heating of the specimen should decrease sharply owing to the increase of its heat capacity. This change in the rate of heating of the nickel specimen was registered by us by the aid of a differential thermocouple (Fig.6). Any desired metal may be used as the standard speci-

STAT

Declassified in Part - Sanitized Copy Approved for Release @ 50-Yr 2014/03/07 : CIA-RDP81-01043R004200090004-8

Declassified in Part - Sanitized Copy Approved for Release @ 50-Yr 2014/03/07 : CIA-RDP81-01043R004200090004-8

men, provided that it does not itself undergo any transformations in this temperature region. One of the exercises in the problem with the Kurnakov pyrometer is precisely the determination of the Curie point for nickel.

The thermographic method makes it possible with considerable accuracy to determine, in most cases, the temperatures at which one phase transformation or another will take place. As for the quantitative determination of the values of the heat effects, this may be most reliably done in a calorimeter. One of the problems of our practical course is devoted precisely to this technique. Of the existing types of calorimeters (Bibl.10), the calorimeter with isothermal shell (Fig.7) is the most suitable for our purposes.

The calorimeter consists of a thin-walled copper cylinder 1 which is placed on a heat-insulating base on the bottom of the cylindrical shell 2, which has double walls. To decrease the heat exchange with the surrounding medium, the calorimeter shell is filled with water the temperature of which is held constant during the experiment (25°C). To satisfy this condition, the worm 3 is provided inside the thermostat, and water is circulated through it. The temperature of this water is likewise held at about 25°C, with accuracy ± 0.01°C, by the aid of the thermostat 6. In addition, to decrease the heat exchange, the calorimeter is provided with the hard rubber cover 7, and its outer surface is given additional protection by a wooden shell. The Beckmann thermometer 4 is used to measure the temperature of the calorimetric liquid. By the aid of the optical reading tube 5, the variations of temperature may be evaluated with an accuracy of ± 0.005°C. The students do two exercises, determination of the integral heat of solution corresponding to the condition of an extremely dilute solution, and determination of the heat of crystallization of hyposulfite.

A number of members of the Department of Crystallography took part in the establishment of the practical course. Valuable suggestions were made by G.G.Lemmleyn and V.A.Koptsik. A.T.Izrailenko, M.M.Prokhorova, V.I.Stepanova, D.I.Tissen, and

STAT

Declassified in Part - Sanitized Copy Approved for Release @ 50-Yr 2014/03/07 : CIA-RDP81-01043R004200090004-8

Declassified in Part - Sanitized Copy Approved for Release @ 50-Yr 2014/03/07 : CIA-RDP81-01043R004200090004-8

V.N.Fetisova directly formulated the problems under my supervision.

BIBLIOGRAPHY

1. Shubnikov,A.V. - Formation of Crystals. Publishing Dept., Academy of Sciences USSR (1947)
2. Bakli,G. [H.Buckley] - Crystal Growth. State Pub.House for Foreign Lit., 1954
3. Shubnikov,A.V. - Piezoelectric Textures. Publishing Dept., Academy of Sciences USSR (1946)
4. Lemmleyn,G.G. - Sectorial Structure of Crystals. Publishing Dept., Academy of Sciences USSR, Moscow (1948)
5. Mlodzeyevskiy,A.B. - Lecture Demonstrations in Physics, No.5. Molecular Physics and Thermodynamics. Gostekhizdat (1948)
6. Berg,L.G., Nikolayev,A.V., and Rode,Ye.Ya. - Thermography. Publishing Dept., Academy of Sciences USSR, Moscow-Leningrad (1944)
7. Kurnakov,N.S. - Zhur.Russk.Fiz.Khim.Obshch., Vol.1,No.36 (1904),pp.841-856
8. Tsurinov,G. - The Kurnakov Pyrometer. Publishing Dept., Academy of Sciences USSR (1953)
9. Kubashevskiy,O. and Evans,E. - Thermochemistry in Metallurgy. State Publishing House for Foreign Literature (1954),p.54
10. Popov,M.M. - Thermometry and Calorimetry. Publishing Department, Moscow State University, Moscow (1954)

STAT

Declassified in Part - Sanitized Copy Approved for Release @ 50-Yr 2014/03/07 : CIA-RDP81-01043R004200090004-8

Declassified in Part - Sanitized Copy Approved for Release @ 50-Yr 2014/03/07 : CIA-RDP81-01043R004200090004-8

PART II

Abstract Translation Of Foreign Pages

110-127

138-158

205-211

320-325

STAT

Declassified in Part - Sanitized Copy Approved for Release @ 50-Yr 2014/03/07 : CIA-RDP81-01043R004200090004-8

Declassified in Part - Sanitized Copy Approved for Release @ 50-Yr 2014/03/07 : CIA-RDP81-01043R004200090004-8

TABLE OF CONTENTS

		Page
1.	Crystallization of Admixtures on the Surface of a Crystal Investigated by Means of an Electron and Ion Projectors, by A. P. Komar and Yu. N. Talanin	270
2.	Certain Characteristics of the Growth of Crystals of New Phase in Solid Metal Solutions Observed by Means of an Electron Microscope, by N. N. Buynov	273
3.	Mechanism of Crystallization and the Structure of Alloys of Eutectic Composition, by P. S. Vadilo	275
4.	New Data on the Reaction of an Organic Admixtures with Inorganic Crystals, by Ye. N. Slavnova	277
5.	On the Mechanism of Formation of Spheroidal Graphite in Cast Iron, by I. Ye. Bolotov, V. I. Syreyshchikova and S. G. Guterman	279
6.	Installation for Obtaining and Cleaning High Melting Monocrystals by the Zonal Melting Method, by V. P. Butuzov and V. V. Dobrovenskiy	281

STAT

Declassified in Part - Sanitized Copy Approved for Release @ 50-Yr 2014/03/07 : CIA-RDP81-01043R004200090004-8

Declassified in Part - Sanitized Copy Approved for Release @ 50-Yr 2014/03/07 : CIA-RDP81-01043R004200090004-8

CRYSTALLIZATION OF ADMIXTURES ON THE SURFACE OF A CRYSTAL INVESTIGATED BY MEANS OF AN ELECTRON AND ION PROJECTORS

By
A. P. Komar and Yu. N. Talanin

The electron microscope projector is described as an instrument, in which the object investigated, is a monocrystal point of any given metal. In front of and at a certain distance from the point is situated a spherical screen which also acts in the capacity of an anode. If a comparatively low voltage is applied between the anode and the point it produces a strong heterogeneous field on the surface of the point. The strong electric field promotes cold emissinn of electrons from the point. The field at the surface of the point is similar to the field of a spherical capacitor and the electrons migrate from the point to the screen over a radius projecting on it an image of the surface of the point in a highly magnified form. The magnification is determined by a certain ratio and the radius of the point by the peak. The resolving power is determined basically by the presence of a field component in the electrons, which is tangent to the surface of the point.

The electron microscope-projector represents a perspective instrument for studying certain properties of crystals - surface migration, adsorption, crystallization and recrystallization, phase conversions etc.

In the case of the ion microscope-projector the polarity of the voltage applied between point and anode changes into reverse (reversed polarity). The image of the surface of the point is obtained with the aid of the ions which form as a result of the severance of bonds in the

STAT

Declassified in Part - Sanitized Copy Approved for Release @ 50-Yr 2014/03/07 : CIA-RDP81-01043R004200090004-8

Declassified in Part - Sanitized Copy Approved for Release @ 50-Yr 2014/03/07 : CIA-RDP81-01043R004200090004-8

hydrogen molecules and the ionization of atoms in a highly heterogeneous field at the surface of the point. The picture appearing on the screen of the electron or ion microscope-projector reflects the electron or ion emission over the surface of the point. The emission distribution depends upon the output from the surface and upon the intensity of the local electric field which depends (the intensity) upon the contour of the surface.

An alternate investigation of one and the same crystal in the electron and ion microscope projectors allows to reveal the cause for increased emission in any one of the zones and to determine more reliably the form and changes of the crystal. The image obtained in the ion projector has a very weak luminescence making photographing of the image highly difficult. In a majority of cases the study has to be limited to visual observation.

The electron projector often shows an anisotropic spreading of an impurity in the form of mobile films on the surface of a monocrystal. The migration of the films is usually in direction of the tetrad or triad axis of the crystal. The migration of the film begins at the periphery and ends in the center of the face; the migration of the film is due to its partial evaporation and contraction by the surface tension forces. The presence of impurities brings about a characteristic change in the form of the crystal. It was established that the presence of oxygen changes the form of the crystal mainly in the zone of the hexahedron plane and is characterized by the appearance of fine faces bordering the edges. The contamination of crystal surfaces with carbon converts the rounded crystal into finned shape which is accompanied by

STAT

Declassified in Part - Sanitized Copy Approved for Release @ 50-Yr 2014/03/07 : CIA-RDP81-01043R004200090004-8

Declassified in Part - Sanitized Copy Approved for Release @ 50-Yr 2014/03/07 : CIA-RDP81-01043R004200090004-8

the appearance of additional faces near the triad axis. These faces are highly unstable and highly sensitive to impurity concentrations and surface temperature. If the amount of the impurity on the surface is particularly high one can observe during the heating of a longer period of time how the films slide off in layers one after the other. Purification of the surface retards the migration of the films. The rapid movements of the films can be photographed by means of a motion picture camera but not with an ordinary still camera.

The numerous examples listed in this report illustrate the broad possibilities of employing electron and ion microscope-projectors for studying the structural changes occurring on the surface of crystals.

STAT

Declassified in Part - Sanitized Copy Approved for Release @ 50-Yr 2014/03/07 : CIA-RDP81-01043R004200090004-8

Declassified in Part - Sanitized Copy Approved for Release @ 50-Yr 2014/03/07 : CIA-RDP81-01043R004200090004-8

CERTAIN CHARACTERISTICS OF THE GROWTH OF CRYSTALS, OF NEW PHASE IN SOLID METAL SOLUTIONS OBSERVED BY MEANS OF AN ELECTRON MICROSCOPE

By
N. N. Buynov

Using an electron microscope the author discovered that aging Al - Cu and Al - Ag alloys, hardened at a temperature above the solubility curve, have a heterogeneous structure. The existence in hardened alloys of zones enriched with alloying components indicates the beginning of phase conversions. During the crystallization in solid state it is necessary to take into consideration, not the probability of the formation of crystal nuclei, but rather the probability of the development of already existing zones enriched with alloying components. The zones forming in the alloys at the beginning of decomposition are not very enriched with alloying components. The dimensions of depleted zones of a solid solution, around the zones and particles of metastable phases can be determined from the electron-microscopic photos. Even if such zones are completely depleted by the alloying components, the number of alloying atoms is insufficient to form zones or particles of phases of certain dimensions and composition.

The contention, prior to introducing electronmicroscopic investigations, was that aging in a fusion begins with the formation of zones or crystal nuclei of metastable or stable phases of specific composition having the form of very thin plates. Electronmicroscopic investigations showed that in many alloys the aging process begins with the formation of equiaxial zones or zones slightly differing from equiaxial. The existence of the equiaxial form can be explained by the fact that the

STAT

Declassified in Part - Sanitized Copy Approved for Release @ 50-Yr 2014/03/07 : CIA-RDP81-01043R004200090004-8

Declassified in Part - Sanitized Copy Approved for Release @ 50-Yr 2014/03/07 : CIA-RDP81-01043R004200090004-8

originally formed zones were still relatively low in alloying components. The enrichment of the zones with the alloying components takes place during the aging and this determines the nature of the aging. The enrichment determines the magnitude of the stresses in the alloys and also the method and sequency of formation: zones ⟶ metastable phases ⟶ stable phase.

The zones and particles of metastable phases appearing in form of plates and rods do not have monolithic structure, they consist of individual elements which often have the same form as in the initial zone. Practical experiments with Al-Cu and Al-Zn alloys as well as x-ray analyses showed that the formation of zones and phases takes place by allotropic conversion which also determines their sequence. Such a successive formation of metastable zones followed by the formation of stable phases does not exclude their solution. The solution of these formations is brought about by the continuous change in stress distribution in the alloy during the aging.

It was established that recrystallization in supersaturated solid solutions with a tendency for decomposition takes place not by the formation of new phase crystal nuclei, but by the development of already existing (in hardened alloys) submicro zones enriched by the atoms of the alloying components. The nature of the development of crystallization in solid state is determined by the process of enriching zones and particles of metastable phases by the alloying components. The crystallization in solution is described as: zones ⟶ metastable phase particles ⟶ Stable phase particles. The conversion of zones into particles of metastable and stable phases is allotropic.

STAT

Declassified in Part - Sanitized Copy Approved for Release @ 50-Yr 2014/03/07 : CIA-RDP81-01043R004200090004-8

Declassified in Part - Sanitized Copy Approved for Release @ 50-Yr 2014/03/07 : CIA-RDP81-01043R004200090004-8

MECHANISM OF CRYSTALLIZATION AND THE STRUCTURE OF ALLOYS OF EUTECTIC COMPOSITION

By

P. S. Vadilo

A study of the crystallization process and structure of an eutectic melt showed that the eutectic alloy consists of greater crystals of the master component forming as result of amalgamation of dendrite branches of this component. Since the components of the eutectic melt are epitaxic substances (the epitaxy phenomenon is observed during their crystallization) fine oriented crystals of the slave component originate on the surface of the dendrite branches of the master component. The slave component does not form a continuously oriented layer on the dendrite branch or on the crystal of the master component. This is explained by the fact that a continuous growth requires a strong oversaturation of the solution by the slave component. It was found that crystallization of the slave component begins only on these sections of homologous facets or poles of the dendrite branches of the master component, where the solution is considerably supersaturated as result of fluctuation. The deposition of the master component occurs only on its oriented crystals because the crystallization continues even at the slightest supersaturation. Only at a certain distance from the growing oriented crystal of the slave component, where the reduction in the supersaturation of the solution as result of liberation of crystallization heat and extraction of elementary particles from the solution has no effect, is the origination of another oriented crystal of the slave component possible. This distance depends upon the degree of supersaturation of the total mass of the solution (melt) by the slave component and upon the difference in the parameters of the flat crystal lattices of the

STAT

Declassified in Part - Sanitized Copy Approved for Release @ 50-Yr 2014/03/07 : CIA-RDP81-01043R004200090004-8

Declassified in Part - Sanitized Copy Approved for Release @ 50-Yr 2014/03/07 : CIA-RDP81-01043R004200090004-8

master and slave components of the melt.

Since the crystals of the slave component and the dendrite branch of the master component, on which crystallographically lawful oriented crystals of the slave component have formed, grow simultaneously then the latter ones grow into them.

Only the crystal peaks of the slave component remain on the surface of the dendrite branch of the master component. Only the surface of the dendrite branch (of the crystal) of the master component spreads tangentially. As this surface spreads new finely oriented crystals of the slave component originate on the dendrite branch of the master component for the very same reasons which led to the origination of the first oriented crystals. The master component crystals cannot spread perpendicularly with respect to their peaks because they are enveloped on the sides by the growing dendrite branch, i. e. by the crystal of the master component. Then the dendrite branches of the master component are grown together by their sides the crystals of the slave component, which are situated on these sides, stop growing. The crystallization of the eutectic melt leads to the formation of large crystals of the master component representing an adhesion in crystallographically parallel position of its dendrite branches. These branches contain fine crystallographically proper oriented slave component crystals spread in direction of the normal growth of the branch surface.

STAT

Declassified in Part - Sanitized Copy Approved for Release @ 50-Yr 2014/03/07 : CIA-RDP81-01043R004200090004-8

Declassified in Part - Sanitized Copy Approved for Release @ 50-Yr 2014/03/07 : CIA-RDP81-01043R004200090004-8

NEW DATA ON THE REACTION OF AN ORGANIC ADMIXTURE WITH INORGANIC CRYSTALS

By

Ye. N. Slavnova

A study of the crystallization of lead and barium nitrates in the presence of methylene blue showed that the organic admixture in the form of a structurally complex ion may be included in a different way in crystals of uniform structure. The dye in the lead nitrate crystals is preferably in molecular state and the pyramids of the cube face growth solid solutions of special type are being formed. Lead nitrate extracts methylene blue only from solution in which the dye is in a state of monomer, i. e., at concentrations not exceeding a certain percentage. Higher dye concentrations lead to the formation of colorless crystals which indicates absence of dye absorption (dye in a state of a dimer). Very high dye concentrations in the solution result in a slight ingrowing of the latter into the crystals; this ingrowing process bears a different nature is not typical for lead nitrate. The extraction of the dye by barium nitrate is possible from solutions in which the dimer predominates i. e., at much higher dye concentrations. A noticeable absorption of the dye by $Ba(NO_3)_2$ begins at certain concentrations i. e. at conditions at which the dye extraction by $Pb(NO_3)_2$ is at a maximum. The dye grows-in into the barium nitrate crystals forming submicroscopic, differently oriented small crystals thus forming a microheterogeneous system. The orientation of the small dye crystals with respect to the crystallographic direction of the master-crystal, and with respect to each other, depends, at other conditions being equal, upon the dye concentration in the basic solution. The formation of a microheterogeneous system in the case of $Ba(NO_3)_2$ coincides well with the relatively large dye content in the barium nitrate

STAT

Declassified in Part - Sanitized Copy Approved for Release @ 50-Yr 2014/03/07 : CIA-RDP81-01043R004200090004-8

Declassified in Part - Sanitized Copy Approved for Release @ 50-Yr 2014/03/07 : CIA-RDP81-01043R004200090004-8

crystals at weak adsorption properties of their facets (poor absorption of the dye in monomeric state).

The zones of concentration at which the nitrates do extract the dye differ by almost a full order. Also the specific content of the dye in the nitrates differs by an order. Barium nitrate can absorb up to 0.4% of the methylene blue while lead nitrate only 0.04%. A study of the dichroism properties of barium nitrate crystals cultivated a relatively low and at much higher dye concentrations showed that the dye concentration affects the degree of selective absorption of the dye by the nitrate and the nature of dichroism as well. In the presence of a structural homology between the components the nature of introducing a methylene blue admixture will be determined by the adsorption properties of the surface, especially by its ability to doubly fix the ions of a given admixture, state of this admixture in the basic solution and the tendency of admixtures toward the formation of associated particles. During relatively low dye concentrations its small crystals are oriented by the elongation axes which are almost perpendicular to the facets on which they are formed. At much higher dye concentrations its small crystals are oriented in such a way that the molecules appear either on the "rib" or on the "end". It was concluded that the crystal of the nitrates investigated have structural prerequisites for the formation of a solid methylene blue solution when the latter grows in through the cube faces.

STAT

Declassified in Part - Sanitized Copy Approved for Release @ 50-Yr 2014/03/07 : CIA-RDP81-01043R004200090004-8

Declassified in Part - Sanitized Copy Approved for Release @ 50-Yr 2014/03/07 : CIA-RDP81-01043R004200090004-8

ON THE MECHANISM OF FORMATION OF SPEROIDAL GRAPHITE CRYSTALS IN CAST IRON

By

I. Ye. Bolotov; V. I. Syreyshchikova; S. G. Guterman

Experiments were conducted to check the existing data regarding the mechanism of the least investigated initial stage of formation of spheroidal graphite. It was observed that if the modifier is confined to the role of cleaning the cast iron from sulfur and oxygen the cast iron melted out in vacuum from pure basic materials should have spheroidal graphite crystals. The microstructure of cast iron melted-out in vacuo indicates that a part of the graphite crystallizes in the cast iron in the form of globules - ferrolites. These globules have a radical structure characteristic for spheroidal graphite in a cast iron treated with a modifier. It was established that the necessary condition for the crystallization of graphite in the form of spherulites is a considerable supercooling of the cast iron. The mechanism of formation of spheriodal graphite is analogous with the mechanism of formation of radial spherulites which takes place during the crystallization of other strongly supercooled systems.

The autoradiography of the cast iron proves that lamellar graphite is enriched with sulfur as result of sulfur adsorption on the graphite and crystallization of the graphite by sulfurous inclusions exist in the graphite because they act as crystallization centers for the graphite. Since sulfur is a surface active element, it reduces the surface tension on the graphite-melt boundary, the enrichment of graphite plates with S can also take place as result of adsorption on the melt-graphite boundary and consequent entrapment of S in the crystalline lattices of the graphite. Both these factors make considerable supercooling of the cast iron impossible. The absence of S in spheroidal graphite leads to the belief that

STAT

Declassified in Part - Sanitized Copy Approved for Release @ 50-Yr 2014/03/07 : CIA-RDP81-01043R004200090004-8

Declassified in Part - Sanitized Copy Approved for Release @ 50-Yr 2014/03/07 : CIA-RDP81-01043R004200090004-8

during the treatment with the modifier the smelt cleanses itself from the sulfur dissolved in it which would otherwise become adsorbed on the graphite.

The sulfur existing in the smelt in form of inclusion passes over into other compounds (CaS, MgS, etc.) which are not crystallization centers for graphite. The role of the modifier consists in cleansing the smelt from sulfur and oxygen dissolved in the smelt and in the destruction of the impurities. This cleansing process makes supercooling, necessary for the crystallization of spheroidal graphite, possible. There is also a possibility that the modifier aids in the supercooling of the cast iron (in addition to cleansing) because the cast iron being adsorbed on the graphite hampers the access of carbon atoms striving to reach the cast iron.

Supercooling, warranting the formation of spheroidal graphite crystals, was attained not only as result of increasing the surface tension of the melted cast iron or elimination of crystallization centers but also as result of rapid cooling the liquid cast iron.

The process of spheroidal graphite crystallization is extremely analogous with the crystallization of many smelts and solutions which leads to the formation of spherulites with the very same radial structure as in the case of spheroidal graphite.

STAT

Declassified in Part - Sanitized Copy Approved for Release @ 50-Yr 2014/03/07 : CIA-RDP81-01043R004200090004-8

Declassified in Part - Sanitized Copy Approved for Release @ 50-Yr 2014/03/07 : CIA-RDP81-01043R004200090004-8

INSTALLATION FOR OBTAINING AND CLEANING HIGH MELTING MONOCRYSTALS BY THE ZONAL MELTING METHOD

By

V. P. Butuzov and V. V. Dobrovenskiy

The new, so-called zonal melting method, was developed for the purpose of obtaining ultra-pure monocrystals. The zonal purification method, like the method of cleaning by ordinary "directed" crystallization, is based on the fact that the admixtures have a different solubility in solid and liquid phases of the substance crystallized. Whereas during the cleaning by ordinary directed crystallization repeated cleaning is possible only after the removal of the contaminated part of the sample, in the case of the zonal melting method all these separate operations can be combined into one. This is accomplished by shifting several melted zones along the ingot. Each consecutive zone secures additional cleansing of the material.

The zonal melting method is employed in two ways - vertical (without the crucible) and horizontal zonal melting. In both cases, the obtainment of a melted zone requires either the employment of a resistance furnace or induction heating. The vertical zonal melting method is quite complex and the employment of same is advisable only in the case when it becomes impossible to select a crucible material which would not react with the substance being crystallized.

The horizontal zonal melting method is much simpler and has, therefore, attained much wider application. The latter method is employed for multiple zonal purification of straight line samples placed in the crucible prepared in the form of a small skiff and for repeated zonal purification of ring-shaped samples placed in a crucible prepared in the form of a split ring. In the case of purifying a straight line sample the number of passes of the melted zones per each single operation

STAT

Declassified in Part - Sanitized Copy Approved for Release @ 50-Yr 2014/03/07 : CIA-RDP81-01043R004200090004-8

Declassified in Part - Sanitized Copy Approved for Release @ 50-Yr 2014/03/07 : CIA-RDP81-01043R004200090004-8

depends upon the number of heating elements set up for the operation, but in the case of cleansing a ring-shaped sample the number of passes per single operation is unlimited.

The heating elements are the most important components of such cleansing installation. The first heating elements developed for this purpose were of the low temperature type prepared in the form of slotted resistances furnaces made of nichrome wire drawn over a ceramic body covered with chamotte clay. An installation using such type of heating elements made it possible to obtain a number of mono-crystals of low melting point. Next were developed high temperature heating elements, also in the form of slotted wire resistance furnaces with tungsten spiral. The latter ones appeared to be unsuitable for the simple reason that the tungsten spiral had to be heated by individual sections which changed their positions from time to time and in addition the spiral became deformed after intensive heating.

A brief description is given of a high temperature heating element with graphite heater part of which has a spherical shape for the purpose of focusing the liberated thermal energy toward a small section of the specimen. The slots made in the spherical section of the heater are for the purpose of increasing the resistance of the heater and to reduce the necessary current intensity and the profile of the copper current feeders. The arrangement of the installation and mode of operation are explained.

STAT

Declassified in Part - Sanitized Copy Approved for Release @ 50-Yr 2014/03/07 : CIA-RDP81-01043R004200090004-8